UNCLASSIFIED

A COMPILATION OF PAPERS PRESENTED AT
THE FOURTH JOINT AFMTC - RANGE USER
DATA CONFERENCE

THEME: NEW DATA REDUCTION METHODS TO IMPROVE RANGE DATA

AIR FORCE CONFERENCE FACILITY
ORLANDO AIR FORCE BASE, FLORIDA
26-28 FEBRUARY 1963

UNCLASSIFIED

TABLE OF CONTENTS

FOREWORD

The 1963 Joint AFMTC/Range User Data Conference, the fourth in a series of annual meetings between the AFMTC and Range User data analysts, was held at the Air Force Conference Facility, Orlando Air Force Base, Florida. The theme of the conference was "New Data Reduction Methods to Improve Range Data" which included a description of both the new mathematical methods being developed and the data reduction procedures for new instrumentation systems.

Certain types of problems, such as the determination of improved filters, refraction correction methods, and techniques for developing error models are common to all analysis efforts. Since this suggests that something is to be gained by pooling our knowledge and experience in working on these problems, several of the other AFSC Centers were invited to participate in the conference program. Inclusion of these papers is believed to have broadened the scope of the conference.

Once again we are including all of the papers in a report as a means of documenting the current status of the AFMTC efforts in data reduction and analysis. This report will be furnished to the attendees who have requested it, but will not be available for a general distribution. Also, it should be noted, that the collection of papers is disseminated by way of providing information and does not represent an official AFMTC or Air Force document.

The 1963 conference was the most successful to date in terms of attendance. Tentative plans call for a continuation of this endeavor as long as it appears fruitful. Again we would like to invite comments from all who attended the meeting as to any suggested improvements. These comments should be addressed to:

Director, Data Acquisition & Processing (MTOE)
Air Force Missile Test Center
Patrick Air Force Base, Fla.

INTRODUCTORY REMARKS

DR. GEORGE K. HESS, JR.

Good morning, ladies and gentlemen.

Welcome to the Fourth Joint AFMTC/Range User Data Conference. Our theme this year is "New Data Reduction Methods to Improve Range Data".

To some people, statistics are something to lie with. However, to those of us here today statistics is the body of principles and methods that have been developed for collecting, analyzing, presenting and interpreting large masses of numerical data. Statistical treatment cannot in any way improve the basic validity or accuracy of the raw data. The basic information must be collected in such a way that it is accurate, representative and as comprehensive as possible.

As you know, the general purpose of science is to predict and control what will happen in a series of events. The scientist himself must be a careful and tireless worker. He must experiment and he must be extremely honest in recording what he observes. He must be willing to do things over and over tunil he is sure of his results. You are going to hear today about a wide variety of measurement and data reduction techniques. The scientific honesty which is the root of this work is of utmost importance. I might add that this forum has no place for the scientific swindler. The data reduction methods to be reported here are complex and sophisticated. You will not find the material easy.

If you will look over your conference agenda you will see that the heavy emphasis is on the technical subject of trajectory measurements. Our national missile strategy calls for accurate shots. Guidance and tracking

technology are in a close race. This state of measurement accuracy has been achieved by painstaking care in gyroscope and accelerometer manufacture and by corresponding advances in radar systems. But dominating the entire picture is our scientific integrity. It is professionally embarassing to me to see so much science hocus-pocus advertised in the technical and public press. But, in the end, it will be your efforts and interests in keeping the measurement sciences honest that will save this golden age of science.

INTRODUCTORY REMARKS

G. DENTON CLARK

Once again it is my pleasure to be the official spokesman for the Air Force Missile Test Center Range Contractor and the Radio Corporation of America.

In my area of interest, the RCA Missile Test Project, contributions are in the technical operating, and scientific fields. We are very proud of the role we have been playing in the gathering of data - on the Range - The reduction of data, and its analysis.

As each year passes you, who represent the Range Users, are bringing to reality an ever increasing number of feats which, only a few years ago, were considered science fiction. Last year, to mention a couple of these feats, we saw manned orbital flights and real-time television programs relayed between two continents. This coming year we will see the fruition of much that has been in the laboratories and shops; and the future will unfold that which is on paper and in the fertile minds of our devoted people.

This rapid advancement in technology has placed great demands on: 1) the accuracy and precision of data collection, 2) data reduction and data analysis techniques and, ultimately, timely delivery of data to you the Range User. [See Figure (1)]

Our work starts the moment Range User requirements are placed on the Range; which is usually well in advance of hardware delivery. As launch day is reached we are in high gear at our battle stations for the acquisition of your data. Next follows its processing, reduction and, finally, delivery.

In order to fulfill this full loop of responsibility to PAA and the Air Force we are organized as shown in Figure (2).

We not only hope that our data product is useful to you but that joint meetings such as this will promote a flow of ideas and useful information. I encourage you to discuss with us, not only during the next few days but at any time, subjects which may be of particular interest to you. We sincerely hope you will enjoy your stay.

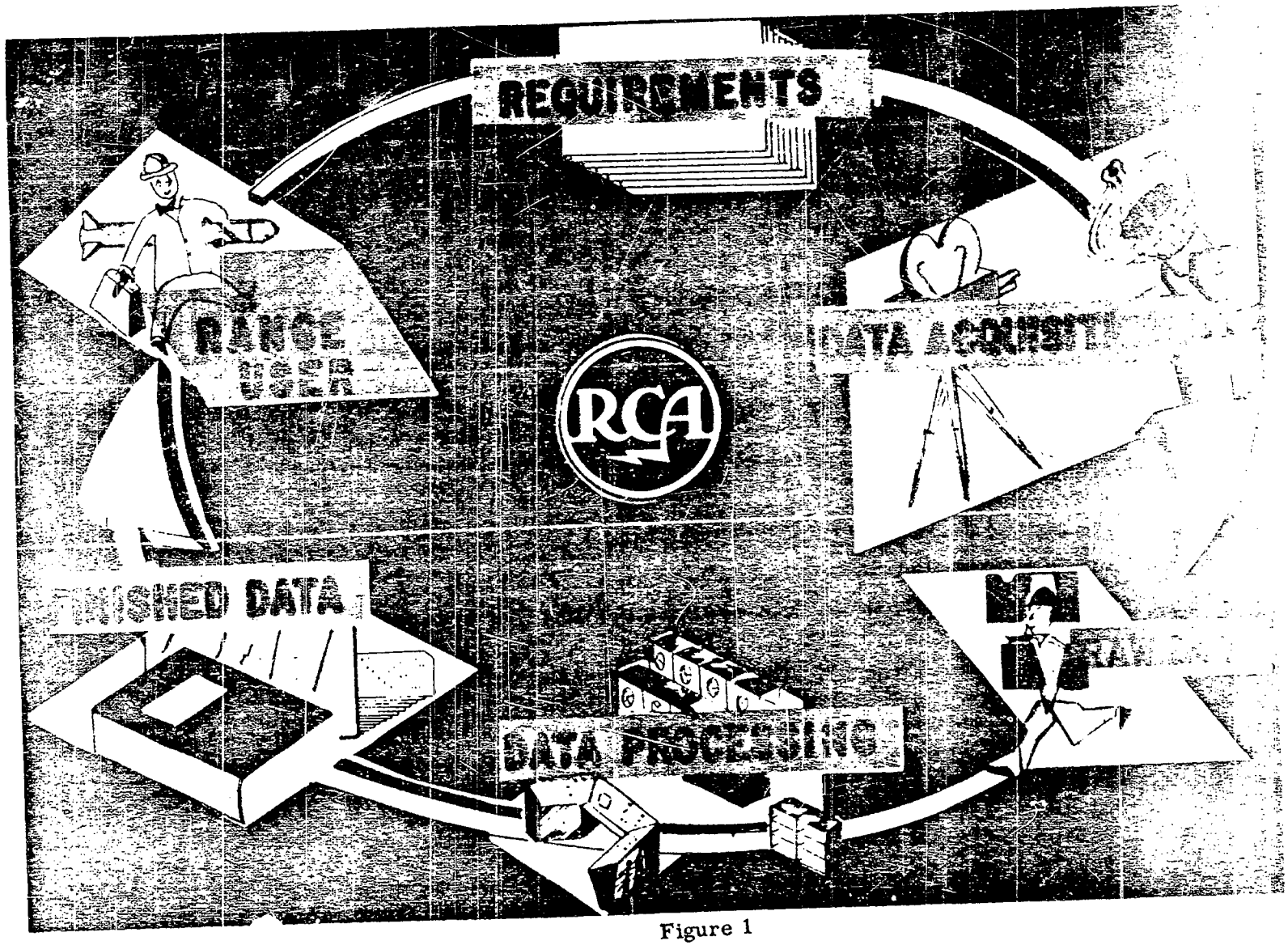

Figure 1

RCA MISSILE TEST PROJECT

(DATA ORGANIZATION)

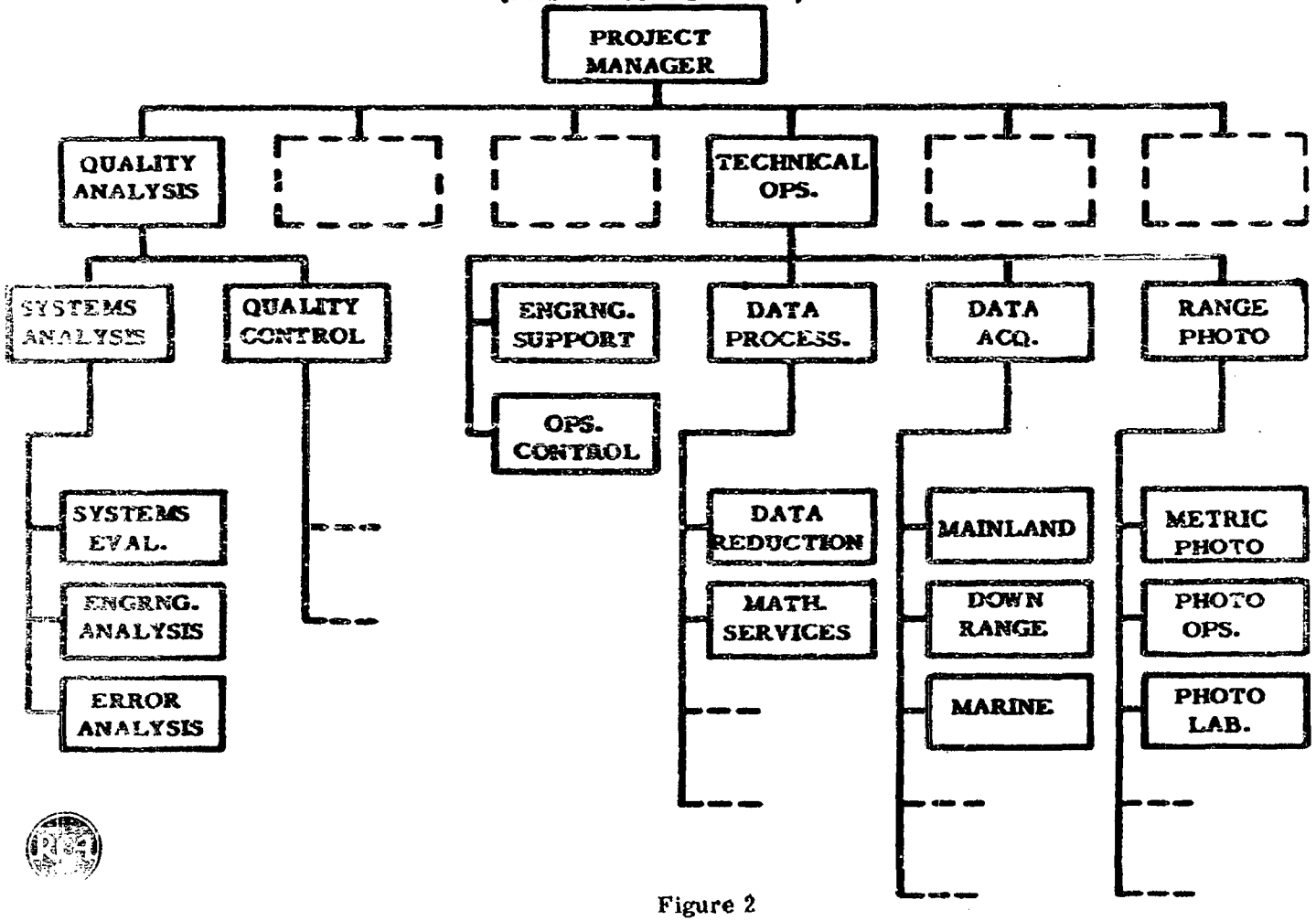

Figure 2

ERROR PROPAGATION

by:
James N. Jamieson
RCA Missile Test Project
Patrick Air Force Base, Florida

Presented at:
FOURTH JOINT AFMTC RANGE USER DATA CONFERENCE
Orlando Air Force Base, Florida
26-28 February 1963

ERROR PROPAGATION

ABSTRACT

The random errors known to exist in a measuring device are propagated through the mathematical model of the device to the final measurements, so that we can obtain estimates of the errors in the data to be expected when future measurements are taken. This is commonly referred to as Geometric Dilution of Precision (GDOP).

A description of the theory and the methods of computation will be given.

INTRODUCTION

GDOP, or Geometric Dilution of Precision, is the title given at AMR to the covariance propagation arising from the maximum likelihood, or least squares adjustments, of tracking data. It is a measure of the accuracy of an instrument or combination of instruments to be used for a particular tracking assignment. It is utilized by those who plan the instrumentation to be used in future tests. Given a theoretical trajectory of some missile program it is necessary to prove that the proposed tracking instrumentation can deliver the accuracy demanded by the Missile Contractor on the particular flight in which he is interested.

COORDINATE TRANSFORMATIONS

Before computing the GDOP of an array of tracking devices, it is necessary to transform the trajectory from the given coordinate system to each of the tracking stations.

If a point in space is represented by

$$\hat{\underline{x}} = (\hat{x}, \hat{y}, \hat{z}) \tag{1}$$

in some coordinate system and by

$$\underline{x} = (x, y, z) \tag{2}$$

in some other coordinate system, then there exist an orthogonal matrix A, of order 3, and a 3-dimensional vector $\underline{b}$, such that

$$\underline{x} = A\hat{\underline{x}} + \underline{b} \tag{3}$$

"A" represents the rotation of the original system to one parallel with that of the second coordinate system, and $\underline{b}$ represents the translation from one location to the other to complete the coordinate transformation.

The time derivative of (3) gives

$$\dot{\underline{x}} = \dot{A}\underline{\hat{x}} + A\dot{\underline{\hat{x}}} + \dot{\underline{b}} \tag{4}$$

where in all cases the dots denote time derivatvies. $\dot{A}$ is the matrix resulting from the time derivatives of each term of A, as is $\dot{\underline{b}}$, the vector of derivatives of elements of $\underline{b}$. Equations (3) and (4) may be combined into one matrix equation.

$$\begin{pmatrix} \underline{x} \\ \dot{\underline{x}} \end{pmatrix} = \begin{pmatrix} A & 0 \\ \dot{A} & A \end{pmatrix} \begin{pmatrix} \hat{\underline{x}} \\ \dot{\hat{\underline{x}}} \end{pmatrix} + \begin{pmatrix} \underline{b} \\ \dot{\underline{b}} \end{pmatrix} \tag{5}$$

In the event the two coordinate systems are stationary with respect to one another, $\dot{A}$ and $\dot{\underline{b}}$ will contain zeros only. An example of this would be two earth-fixed systems, say, one at the launch pad and the other at some tracking station. On the other hand, an inertial transformation, say, from some system fixed with reference to the sun to an earth-bound tracking station would produce non-zero terms in $\dot{A}$ and $\dot{\underline{b}}$.

COVARIANCE PROPAGATION

Covariance propagation arises from the need to know certain quantities that we cannot measure directly. Cartesian coordinates are sensible and easy to visualize, but electronic tracking devices don't measure x, y, and z directly. They measure ranges, range differences, range sums, angles, direction cosines; quantities that are not quite as easy to visualize in space. These measurements are then transformed to "easy-to-see" coordinates. Included in these transformations are the errors in measurement that these tracking devices, being machines, must have.

When a measurement is made there is a difference, however small, between the measurement and the true value of the quantity being measured. Let this difference be called Δx. If the measurement is repeated several times it is hoped that $\bar{x}$ the average or arithmetic mean of all the measurements, defined by

$$\bar{x} = \frac{1}{n} \sum_{i=1}^{n} x_i \tag{6}$$

is close to the true value, say, x_t. Since each measured value x_i is made up of the true value plus the error

$$x_i = x_t + (\Delta x)_i \tag{7}$$

the average of n measurements is from Equations (6) and (7)

$$\bar{x} = \frac{1}{n} \sum_{i=1}^{n} \left[x_t + (\Delta x)_i \right] \tag{8}$$

$$\overline{x} = \frac{1}{n} \sum_{i=1}^{n} x_t + \frac{1}{n} \sum_{i=1}^{n} (\Delta x)_i \qquad (9)$$

$$\overline{x} = x_t + \overline{\Delta x} \qquad (10)$$

The first term on the right of Equation (10) comes from the corresponding term in Equation (9) where the true value is added n times to itself and the sum divided by n to give the x_t or true value again. The second term is the average of the n errors which suggests the $\overline{\Delta x}$ notation.

If as is hoped the average measurement is in fact close to the true value, then the average of the errors is very nearly zero. Ideally, when the average error is zero, the average of the squares of the errors shown in

$$\overline{(\Delta x)^2} = \frac{1}{n} \sum_{i=1}^{n} (\Delta x)_i^2 \qquad (11)$$

equals a value known as the estimate of the variance of x.

In our application we, of course, do not have the ideal case to work with, but the average of the errors can indeed be considered to be zero for if it were not it would indicate a bias in the measurements which, once identified, could be subtracted to leave a zero mean once again. It is further known that the distribution of the errors is not necessarily Gaussian, however, we blithely proceed with the optimistic assumption that it is for two reasons:

1. It is believed that the approximation is a close enough one, and

2. We have no other means of attacking the problem.

As the number of terms taken in the determination of the average grows larger, $\overline{(\Delta x)^2}$ begins to settle down to the variance. This can be symbolized

$$\sigma_x^2 = \lim_{n \to \infty} \frac{1}{n} \sum_{i=1}^{n} (\Delta x)^2_i \qquad (12)$$

Where σ_x^2 is called the variance of x. The square root of the variance is σ_x, the standard deviation about the mean, which is associated with the bell-shaped curve of the normal probability distribution.

Closely associated with the variance is the covariance. If, each time x is measured, another variable, y, is also measured, then as in Equation (12) for x the variance of y can be calculated, along with a "cross" variance or covariance

$$\sigma_{xy} = \lim_{n \to \infty} \frac{1}{n} \sum_{i=1}^{u} (\Delta x)_i \ (\Delta y)_i \qquad (13)$$

between the variable x and y.

The variance is a measure of the size of the error to be expected in the measurements. The standard deviation bounds some 68.26% of the expected errors. The covariance i a measure of the dependence of the errors of one variable upon the errors of another variable.

Suppose that there is a group of ℓ quantities $(x_1, x_2, x_3 \ldots, x_\ell)$ to be measured. The covariance of any pair of them can be written

$$\sigma_{x_j x_k} = \lim_{n\to\infty} \frac{1}{n} \sum_{i=1}^{n} (\Delta x_j)_i \, (\Delta x_k)_i \tag{14}$$

Now, if the x's are each functions of a list of variables u; i.e.

$$\begin{aligned} x_1 &= x_1 (u_1, u_2, \ldots, u_p) \\ x_2 &= x_2 (u_1, u_2, \ldots, u_p) \\ &\vdots \\ x_\ell &= x_\ell (u_1, u_2, \ldots, u_p) \end{aligned} \tag{15}$$

then small errors in x_j may be approximated by the differential expression

$$\Delta x_j = \sum_{q=1}^{p} \frac{\partial x_j}{\partial u_q} \Delta u_q \tag{16}$$

Substituting Equation (16) into (14) we get

$$\sigma_{x_j x_k} = \lim_{n\to\infty} \frac{1}{n} \sum_{i=1}^{n} \sum_{q=1}^{p} \frac{\partial x_j}{\partial u_q} (\Delta u_q)_i \sum_{r=1}^{p} \frac{\partial x_k}{\partial u_r} (\Delta u_r)_i \tag{17}$$

$$\sigma_{x_j x_k} = \lim_{n\to\infty} \frac{1}{n} \sum_{i=1}^{n} \sum_{q=1}^{p} \sum_{r=1}^{p} \frac{\partial x_j}{\partial u_q} \frac{\partial x_k}{\partial u_r} (\Delta u_q)_i \, (\Delta u_r)_i \tag{18}$$

Now, because the partial derivatives are independent of the observations, we can again change the order to

$$\sigma_{x_j x_k} = \sum_{q=1}^{p} \sum_{r=1}^{p} \frac{\partial x_j}{\partial u_q} \frac{\partial x_k}{\partial u_r} \lim_{n\to\infty} \frac{1}{n} \sum_{i=1}^{n} (\Delta u_q)_i \, (\Delta u_r)_i \tag{19}$$

and by applying (14) to the limit in (19) we have

$$\sigma_{x_j x_k} = \sum_{q=1}^{p} \sum_{r=1}^{p} \frac{\partial x_j}{\partial u_q} \frac{\partial x_k}{\partial u_r} \sigma_{u_q u_r} \tag{20}$$

The generalized law of covariance propagation.

THE PRINCIPLE OF LEAST SQUARES

Let us think of the variances and covariances set down in a matrix

$$\sum = \begin{pmatrix} \sigma_{x_1x_1} & \sigma_{x_1x_2} & \sigma_{x_1x_3} \cdots \sigma_{x_1x_\ell} \\ \sigma_{x_2x_1} & \sigma_{x_2x_2} & \sigma_{x_2x_3} \cdots \sigma_{x_2x_\ell} \\ \sigma_{x_3x_1} & \sigma_{x_3x_2} & \sigma_{x_3x_3} \cdots \sigma_{x_3x_\ell} \\ \vdots & & \\ \sigma_{x_\ell x_1} & \sigma_{x_\ell x_2} & \sigma_{x_\ell x_3} \cdots \sigma_{x_\ell x_\ell} \end{pmatrix} \tag{21}$$

It is a good picture of the errors to be expected when measuring the ℓ variables $x_1, x_2, \ldots, x_\ell$. Notice that $\sum$ is an ℓ x ℓ array. This is the covariance matrix of ℓ variables. Associated with the covariance matrix $\sum$ is another ℓ x ℓ matrix W.

$$W = \begin{pmatrix} w_{x_1x_1} & w_{x_1x_2} \cdots w_{x_1x_\ell} \\ w_{x_2x_1} & w_{x_2x_2} \cdots w_{x_2x_\ell} \\ \vdots & \\ w_{x_\ell x_1} & w_{x_\ell x_2} \cdots w_{x_\ell x_\ell} \end{pmatrix} \tag{22}$$

which is the inverse of the $\sum$ matrix, or

$$W = \sum^{-1} \tag{23}$$

We shall refer to W as the weight matrix. The generalized method of least squares shows that W is propagated in much the same manner as $\sum$. Corresponding to Equation (20), the generalized law of covariance propagation, is the propagation of weight.

$$w_{x_jx_k} = \sum_{q=1}^{p} \sum_{r=1}^{p} \frac{\partial u_\ell}{\partial x_j} \frac{\partial u_r}{\partial x_k} w_{u_q u_r} \tag{24}$$

Note that the partial derivatives are taken in an inverted manner from those in Equation (20). As the covariance matrix gives a picture of the errors of a system the weight matrix gives a picture of its accuracy. If a term in the weight matrix is large the corresponding variable can be measured accurately, if the weight is small so is the expected accuracy of measurement.

If we are considering measurements from several devices which may be supposed completely independent of one another, such as radars, etc., then, if their measurements are all properly taken into account to solve for the best estimate of the set of Cartesian coordinates, the weight matrix of this set of coordinates is the sum of the weight matrices of all the stations in the solution. This additivity of W can be shown for the so called least squares method.

$$W_{total} = W_1 + W_2 + W_3 + \ldots + W_m \tag{25}$$

If this were written in terms of covariance matrices we would have

$$\Sigma_{\text{total}} = (\Sigma_1^{-1} + \Sigma_2^{-1} + \Sigma_3^{-1} + \ldots + \Sigma_m^{-1})^{-1} \tag{26}$$

However, Equation (26) brings up a problem which Equation (25) solves immediately, the covariance matrix in many cases for a single instrument **does not exist** while the weight matrix always exists.

Recall from Equation (15) that in order to generate the covariance matrix of an instrument it was necessary to solve for the Cartesian coordinates in terms of the measured parameters alone. At times this is impossible. For instance, if the instrument under consideration measures range only, the relationship between the measured quantity and the Cartesian coordinates can be written:

$$R^2 = x^2 + y^2 + z^2 \tag{27}$$

but one cannot solve for the Cartesian quantities in terms of R alone. Another example would be a camera which cannot measure range. Azimuth and elevation are all that can be obtained. The relation here may be written

$$\sin A = x/(x^2 + y^2)^{1/2} \tag{28}$$

$$\sin E = z/(x^2 + y^2 + z^2)^{1/2} \tag{29}$$

but again, one cannot solve for x, y, and z in terms of A and E alone. The partials of the terms on the left of each of the three preceding equations can be evaluated with respect to x, y, and z so that Equation (24) can be written for any system. That is, one can always write the weight matrix for any system.

Let us combine Equations (23), (25), and (26)

$$\Sigma_{\text{total}} = (W_1 + W_2 + W_3 + \ldots + W_m)^{-1} \tag{30}$$

so that with Equation (24) we have all the mathematics we need to compute GDOPs.

For convenience we will convert Equation (24) to a matrix equation and then give an example for clarification. Suppose that there are ℓ x's and p u's so that all of the partial derivatives of the u's with respect to the x's may be listed thus:

$$B = \begin{pmatrix} \frac{\partial u_1}{\partial x_1} & \frac{\partial u_1}{\partial x_2} & \cdots & \frac{\partial u_1}{\partial x_\ell} \\ \frac{\partial u_2}{\partial x_1} & \frac{\partial u_2}{\partial x_2} & \cdots & \frac{\partial u_2}{\partial x_\ell} \\ \vdots & & & \\ \frac{\partial u_p}{\partial x_1} & \frac{\partial u_p}{\partial x_2} & \cdots & \frac{\partial u_p}{\partial x_\ell} \end{pmatrix} \tag{31}$$

If B^T means the transpose of the matrix B then Equation (24) can be written

$$W_x = B^T W_u B \tag{32}$$

Let us consider the example of a range measuring device. The manner in which it determines range is of no concern here (it may even be a foot rule); all we need to know is the variance σ_r^2 of the measured parameter. The covariance matrix Σ of this instrument is a 1 x 1 matrix consisting of the single number

$$\Sigma = (\sigma_R^2) \tag{33}$$

The inverse of a 1 x 1 matrix is easy to find. It is the reciprocal of its element.

$$W = \left(\frac{1}{\sigma_R^2}\right) = (w_{RR}) \tag{34}$$

Let us now solve for the matrix B associated with this instrument. From Equation (27) we have the relation between coordinates and

$$\frac{\partial R}{\partial x} = \frac{x}{R} \; ; \quad \frac{\partial R}{\partial y} = \frac{y}{R} \; ; \quad \frac{\partial R}{\partial z} = \frac{z}{R} \tag{35}$$

and Equation (31) give

$$B = \left(\frac{x}{R} \; \frac{y}{R} \; \frac{z}{R}\right) \tag{36}$$

From Equation (32) we find

$$W_{xyz} = \begin{pmatrix} \frac{x}{R} \\ \frac{y}{R} \\ \frac{z}{R} \end{pmatrix} (w_{RR}) \left(\frac{x}{R} \; \frac{y}{R} \; \frac{z}{R}\right) \tag{37}$$

or

$$W_{xyz} = \begin{pmatrix} \frac{x^2}{R^2} W_{RR} & \frac{xy}{R^2} W_{RR} & \frac{xz}{R^2} W_{RR} \\ \frac{xy}{R^2} W_{RR} & \frac{y^2}{R^2} W_{RR} & \frac{yz}{R^2} W_{RR} \\ \frac{xz}{R^2} W_{RR} & \frac{yz}{R^2} W_{RR} & \frac{z^2}{R^2} W_{RR} \end{pmatrix} \tag{38}$$

The inverse of the matrix in Equation (38) does not exist for the reasons stated earlier, however, if two more range-only measuring devices were introduced and their matrices added to the matrix in Equation (38), then the theory predicts that there will be a solution to Equation (30) and a covariance matrix can be computed. The diagonal elements of the covariance matrix are the variances of the Cartesian coordinates.

SUMMARY

The procedure just outlined is what is now in our regularly used IBM 7094 GDOP Program ZAAR. The program is capable of estimating the combined GDOP of up to ten separate instruments in any combination of all the tracking devices on the range or now anticipated.

The ability to propagate the error in geodetic location of the tracking station is available as well as the ability to refer the GDOP to any earth-fixed coordinate system desired.

Another feature in the program is the ability to increase the error due to refraction at lower elevations.

ZAAR will process from one thousand to two thousand trajectory points per hour per tracking device depending upon how much information is requested. It is a large scale program which requires most of the core storage in the 32K memory available. The program was written to be able to process any instrument on the range and is arranged for easy modification to include new instrumentation when required.

The program requires the location and orientation of the tracking instrumentation. It must have a trajectory along which to compute GDOP's. Of course, this means that the origin of the trajectory and its orientation are required. Finally, the independent errors in the tracking devices themselves must be entered. These are the errors which are to be propagated.

The program then produces the transformation matrices it uses. As it processes points along the trajectory it lists those that can be measured by any instrument. It then lists the transformed trajectory or at least that part of it which can be seen by each instrument. Following this information are the look angles from each instrument, i.e., A, E, R, l, and m. Finally, the GDOP, the errors, in any Cartesian coordinate system desired, the standard deviations of the individual coordinates and the total position and velocity errors to be expected are listed.

The program assumes that the parameters measured by a tracker are independent of one another. It is realized that a certain amount of error is introduced by this assumption but estimates of the covariances between these parameters are not presently possible.

BALLISTIC CAMERA ACCURACY REVIEW

B

8-9-2

Presented by:

G. H. Rosenfield

Prepared by:

The BACAR Committee
(C.R. Scott, Chairman; A.E. Glei, Sub-Chairman
G.H. Rosenfield, Sub-Chairman)

RCA-Missile Test Project

PAFB, Florida

Presented at:

FOURTH JOINT AFMTC-RANGE USER DATA CONFERENCE

Orlando Air Force Base, Florida

26-28 February 1963

BALLISTIC CAMERA ACCURACY REVIEW

Abstract

PHASE I

(Preparation for MISTRAM Calibration)

809 (C)

This report is a compilation of the separate final reports from each of the major areas of activity concerned with the determination and the correction of errors of the AMR Ballistic Camera systems required for calibration of the MISTRAM System.

The history of the Ballistic Camera Accuracy Review project (BACAR) is described. The reasons for, the objectives, and the methods of the project are discussed in detail. An indication of the amount of effort expended to evaluate and calibrate the Ballistic Camera System is given. Discussion of the major accomplishments to date, as well as the limiting problem areas for the future is also presented. The project will result in better data for the Range User and in increased credence in the accuracy of the Ballistic Camera System. The results of this phase will be used to determine the present accuracy of the Ballistic Camera Systems.

AUTHOR

Preface

In order to establish the improvement resulting from Phase I, it was necessary to first evaluate the accuracy of the earlier Ballistic Camera data. Data were already on hand from 38 plates and 20 tests from the AZUSA MK II evaluation of the summer of 1959. In addition, data were accumulated from 103 plates and 36 tests from 1961. The measure of the accuracy of the systems can be obtained from analysis of the standard errors of unit weight from the orientations and also from the triangulations. These data are summarized in Table I. Equivalent data are to be continuously accumulated on all future plates and tests using the BACAR computer routines.

TABLE I

	focal length	orientation 115	210	300	Cumulative	Triangulation
1959:	s_o	3.5	3.7	4.3	3.8	4.5
	s	-	-	-	0.9	2.0
1961:	s_o	3.5	4.0	4.5	4.2	4.8
	s	0.7	0.6	0.8	0.8	1.8

s_o = standard error of unit weight

s = standard deviation of data about the standard error of unit weight.

All values are in microns.

The total errors computed from actual data were then subdivided into component errors as shown in the following table:

Error budget for BC-300 Camera (from actual data)

Estimated: before BACAR

Orientation	s	s^2	s_o
Setting error	1.5mu	2.25	
Comparator error (STK1)	2.7	7.29	
Emulsion error	3.0	9.0	
Star catalogue error 0.7 sec	1.0	1.0	
Refraction error (stars) 0.2 sec	0.3	0.09	
		$[19.63]^{\frac{1}{2}}$	= 4.4mu 2".93
Triangulation			
Orientation error	4.4	19.63	
Setting error	1.5	2.25	
Refraction error (atmosphere) 1.5 sec	2.0	4.0	
		$[25.88]^{\frac{1}{2}}$	= 5.1mu 3".40

s = estimated standard deviation or standard error
s_o = standard error of unit weight

The improvements brought about by Phase I of the BACAR work are expected to reduce the component errors as shown below. The data estimates are being validated by evaluation of actual data.

Expected: after BACAR Phase I

Orientation	s	s^2	s_o
Setting error	1.5mu	2.25	
Comparator error (STK1)	1.0	1.0	
Emulsion error	1.0	1.0	
Star catalogue error 0.7 sec.	1.0	1.0	
Refraction error (stars) 0.2 sec.	0.3	0.09	
		$[5.34]^{\frac{1}{2}}$	= 2.3mu 1".54
Triangulation			
Orientation error	2.3	5.29	
Setting error	1.5	2.25	
Refraction error (atmosphere) 1.5 sec.	2.0	4.0	
		$[11.54]^{\frac{1}{2}}$	= 3.4mu 2".27

Section I - Scope of Work

This section discusses the founding of the original BACAR Committee and the tentative outline of work to be performed under the BACAR Project.

In any system of precision instrumentation, the equipment is designed, engineered and manufactured to produce a particular level of geometric quality. When the system is operated in accordance with the manufacturer's specifications, the user is justified in expecting the geometric quality requirements for the system to be fulfilled. The certification of the manufacturer is, of course, not sufficient to assure the operational goemetric quality of the instrumentation system. Thus, the necessity exists for evaluation by the user. When a higher level of geometric quality, over and above the design requirements, is needed it becomes necessary to calibrate the equipment; and to use the calibration coefficients in the data reduction process to remove systematic errors. The major question in both evaluation and calibration is what to use as a standard. These concepts may be applied to any system of measuring equipment.

During past years, the Ballistic Camera System has been considered to be the accuracy standard at AMR with a prime mission of evaluation and calibration of other instrumentation systems, both optical and electronic. The state-of-the-art of electronic measuring has now reached the point where the geometric quality required of the Ballistic Camera System now becomes a function of the focal length - the lever arm. Thus the geometric quality of a 1,000 mm focal length camera will be represented by the ratio of 2 parts per million. A two-camera reduction with good geometry will transform this geometric quality to the spatial position point. Additional cameras with good geometry will increase the geometric quality of the position data by approximately the square root of the number of cameras added.

A working committee was established in September 1961 to review the present status of the Ballistic Camera System on the AMR and to develop and implement a plan capable of meeting the objectives defined below:

Specific: Phase I

1. To improve the AMR Ballistic Camera System geometric quality capability in order to meet the MISTRAM evaluation requirements.
2. Determine the maximum theoretical geometric quality capability of the system in its present configuration on the AMR today.
3. Evaluate the geometric quality of the present system as it performs today.

Release date by Committee - 15 July 1962

Broad: Phase II

Having reached the practical maximum geometric quality capability of the present system, to establish a program to preserve this maximum geometric quality as well as developing on a continuing basis refinements to the system compatible with the state-of-the-art capable of leading to improved system geometric quality.

Plan of Attack

The technical elements of the Ballistic Camera System have been broken down into four major areas with each major area further sub-divided into more detailed parts, as outlined below. Because of the complex inter-weaving of the technical elements and their dependence one upon the other, it has not been feasible to establish one or more elements as being the most critical area affecting system accuracy.

Acquisition Instrumentation Considerations

- Camera
- Timing

Photographic Considerations

- Plate
- Emulsion
- Processing
- Storage
- Plate Performance

Operational Considerations (Acquisition)

- Pedestal Stability
- Environmental Conditions
- Procedures
- Personnel

Data Reduction Considerations

- Mathematical Error Model
- Statistical Estimation
- Equipment
- Procedures
- Personnel

Method of Operation

The Ballistic Camera Accuracy Review project is, thus, a two-phase operation:

1) the evaluation of the geometric quality of the Ballistic Camera System as it is engineered at the present time, and

2) the calibration of this system so that increased geometric quality may be obtained. In doing this, the entire BC System has been considered by its various components, such as:

a) the photogrammetric aspects, which include the theory and operation of the system for measuring;

b) the photometric aspects, which include the ability of the system to record and measure the light which passes through the optics and impinges onto the photo-receptive elements. The extension of photometrics concerns all aspects of type of photographic environment, to the care, handling, processing, and storage of the emulsion and plate;

c) the optical aspects, which concern the actual glass which makes up the lens itself and tie in with the photometric characteristics;

d) the mechanical aspects, which concern the shutter, operation and vibration, and the camera mounting technique and stability;

e) the electronic aspects which concern the timing requirements of the system, the delays of the timing impulses between Central Control and the camera station. All of these: photogrammetric, photometric, optical, mechanical, and electronic, have been investigated from a calibration standpoint, because of the higher geometric quality now required of the Ballistic Camera System.

Restrictions

Because of the late delivery for operational use of the BC-600 and BC-1000 cameras, the BACAR Phase I effort was primarily directed to the Wild BC-4 type cameras. The Vero Beach BC-600, however, was evaluated because of its planned use with the MISTRAM calibration.

Section II - Summary of Results

This section summarizes the results and conclusions of the BACAR Committee's work during the period 1 November 1961 to 1 July 1962.

A. Acquisition Instrumentation

1. Camera and Associated Equipment

a. Training

Engineering and Shops personnel received factory-type training on the Wild BC-4 cameras which have focal lengths of 115, 210 and 310 mm, and the Wild Goniometer. From this training, information was collected for the preparation of a complete operations, maintenance and overhaul manual.

Calibration procedures were developed from the training course.

b. Goniometer
During the training course it was learned that Wild produces a new model goniometer which eliminates many deficiencies in their first model. The new goniometer provides greater accuracy, performs some measurements beyond the capability of the old goniometer and permits quicker set-up for tests, thus saving many hours of set-up time for each camera.

c. Vibration and Stability
Preliminary results of a study of Wild BC-4 cameras and camera pedestals indicated a need to evaluate the significance of camera vibration and pedestal stability on the geometric quality of the data.
(1) Tilt Angle Transducer: A tilt angle transducer was procured for pedestal stability tests.
(2) Vibration Measuring and Recording Equipment: New items were procured and other items modified for these specialized problems. A special pulse-operated camera recording system was made up from surplus equipment.

In measuring the performance of the Ballistic Cameras, oscillations of the optical axis were found of a comparatively high frequency (18-20 cps). These oscillations were caused by shutter vibration, motor vibration, and wind disturbances. A second type of axis motion was encountered wherein the camera shifted its elevation axis in response to the shock transmitted to the elevation assembly by the action of the shutter. Such a shift introduced a constant bias. Wind screens are being designed to eliminate vibration from wind disturbances. The camera mounting is being modified to reduce elevation axis shifting.

d. Camera Calibration
The geometric quality of the BC-210 and BC-300 cameras was inadequate for MISTRAM prior to the BACAR program. Even though the best geometric quality obtainable from the cameras, when in peak operating condition, may be short of that necessary to evaluate and calibrate MISTRAM, these are the best available equipments for this task. It was necessary to overhaul seven BC-300 and four BC-210 cameras before they could be calibrated. It was necessary to fine-adjust all components to minimize or eliminate systematic errors and to calibrate the remaining systematic errors. Techniques were devised to: provide the best over-all results for the entire photographic plate area;

improve lens centering; re-align fiducials for greater precision; align the principle axis to the camera fiducials more precisely; square the focal plane with the principle axis. Fixtures were designed and fabricated to achieve this calibration. The calibration data were published. The remaining BC-210 and BC-115 cameras will be overhauled and calibrated.

BC-600 Cameras

Two BC-600 cameras were analyzed in the Optics Laboratory and tested for maximum resolution. Analysis of the focal plane setting was made in order to evaluate factory data. Two cameras have been installed on the Range.

e. Optical Laboratory Collimator

A precision-type flash unit was procured installed and evaluated. The results of subsequent tests have shown great accuracy and high resolution. The uniformity of exposure across the field is excellent.

2. Timing and Associated Equipment

a. Photomultiplier

Prior to the BACAR program, an improved photomultiplier was being developed because:

(1) requests for a reliable photomultiplier (the old units are so unreliable that four units might be used to insure collecting data);
(2) request for better quality data for greater accuracy and ease of data reduction;
(3) requirements for accuracy of 0.0001second.

The BACAR program priority accelerated the development of a new photomultiplier head. A prototype unit was developed, tested and found to be acceptable. A total of eight units have been fabricated and two more will be fabricated. Units have been successfully used on aircraft and live missile tests. Accuracy is expected to run about 0.0001to 0.0002 second.

b. Timing Magnetic Tape Recorders

The original tape recorders which were used with the old photomultipliers were portable, light weight and easily damaged. Their reliability had deteriorated with age and continuous handling throughout the Range. The accuracy was inadequate to fulfill the present requirements. Surplus tape recorders with sufficient accuracy were located and earmarked for use with the improved photomultipliers.

A system which will permit the photomultiplier tape to be used with TARE III results in a 32 manhour/test savings in the reduction of photomultiplier data.

c. Timing Communications
A major problem in the communications area was in the area of measurement of timing delays and in obtaining adequate communications to all of the Ballistic Camera sites that were assigned for MISTRAM checkout. As a result of tests it was concluded that the communication system must be replaced by a new VHF system.
Measurements of time delays in all field equipment have been satisfactorily recorded. Measurements of time delays in the communication links will be accomplished upon completion of the VHF installation.

d. BC Shutter Time Delay
BC shutter delay measurements were measured and found to be different for each camera. The studies associated with these measurements showed that the delay is varied by adjustment of the shutter, or by changing the belts on the shutter drive. Procedures were set up to re-measure shutter delays after each adjustment or repair. The measured delays are used in Data Reduction to remove the timing errors.

e. Terminal Timing Unit Time Delay
TTUs Models 9605 and 36770 were measured. It was found that changing the level of the activating tone burst varied the delay from 40 to 80 milliseconds. Relays in the unit varied from 15 to 35 milliseconds in delay time. As a result, these units were replaced by modified Dynatronic's TTUs for all future tests. The delay of these units is within limits of 0.007 seconds and is constant.

B. Photographic Considerations

Each component of the Ballistic Camera Plate has certain important characteristics that are evaluated. The final performance of the plate is dependent on the interrelated functions of its components. Component and performance characteristics for best AMR use were defined as follows:

1. Plate

a. Support - flatness, stability
The ¼" glass plate was selected as a support to provide the greatest temperature and humidity stability available as a support for the light sensitive emulsion. The plate provides a coating surface with a flatness which is not to exceed 0.00002 in. per linear inch.

b. Emulsion - spectral sensitivity
The present emulsion (103-F) is light sensitive over the entire visible range. For routine usage

there is no need for an additional spectral sensitivity capability. Extension of the sensitivity into the infrared region is not needed for our general purpose work and would tend to increase the plate handling problems due to the influence of heat.
- photographic sensitivity vs. spread function -
The 103-F emulsion is able, with ½ sec. exposure and good weather conditions, to record more stars than can be utilized due to the star catalog limitations. This sensitivity is needed to record stars of the required magnitude under optimum and unfavorable weather conditions and is the logical selection as the workhorse of the Ballistic Camera System.
-dimensional stability -
The inherent emulsion dimensional stability is established during the manufacturing process and this inherent stability is influenced by the chemical and physical reactions during the developing process. Experiment (local and Eastman Kodak) show that the dimensional stability of emulsion prior to processing is satisfactory.

2. Developing

a. Chemical Process
The chemical process used for developing the exposed ballistic plate is based on the manufacturer's recommendations. Gas burst agitation is used to obtain process uniformity. Sensitometry, a controlled exposure on photographic material, is used to sample the developing process to verify the process position and uniformity.

b. Dimension Instability
Dimensional instability occurs because of the swelling of the emulsion, the chemical reactions and the shrinkage of the emulsion during the drying cycle. The most critical portion of this process occurs during the drying stage. It is imperative that the emulsion be uniformly dried with no water spotting. The effect of dimensional instability or emulsion creep on the acquired data is being determined from the emulsion creep experiments now being completed.

3. Storage and Handling

The vendor has provided a protective packing that protects the plate from breakage, heat and high relative humidity. The shelf-life of the packaged 103-F plate is approximately one year under our bulk storage conditions of 50°F, 50% RH. The field handling procedures for ballistic plates appear to be adequate. The most important steps are to be sure that the moisture seal is kept intact as long as possible prior to use and the plate should not be

subjected to elevated temperatures (above 80°F) for long periods of time.

4. Plate Performance

a. Receptor Capability
The 103-F plate used in the Ballistic Camera System as the image receptor has sufficient recording capability to acquire data with present camera systems under the varied Range conditions of weather and flare or strobe characteristics.

b. Image Formation
The minimum image diameter produced from a point source light of the 103-F emulsion is the limiting factor for image size when used in the BC-300, BC-210 and BC-115 cameras, but the lens is the limiting factor when the 103-F plate is used in the BC-600 camera. An improvement in the emulsion for imaging capability with no loss in sensitivity would require a state-of-the-art advancement in emulsion making.

c. Image Position
The position of the recorded image must not change from the time the image is recorded to the time the image position is determined by the plate reader. This means the emulsion must not swell, move or shrink. The image position instability due to emulsion movement of 3.7 to 4.2 microns RMS is becoming better understood through the emulsion creep experiment. On completion of the emulsion creep experiment we should know how to apply exact corrections for the image position movement.
It is expected that use of a reseau will allow a 2 to 3 micron mean correction to be applied during the data reduction process. A residual error of 1.0 to 1.2 microns will be left. Further investigations will be made to find methods for reducing the residual error to 0.7 microns.

C. Operational Considerations

1. Pedestal Stability (MISTRAM Required Pedestals only)

Among the factors found to affect the stability of pedestals are:

a. Differential absorption of heat from the sun with consequent bending of the structure.

b. Mechanical coupling between the operator's working platform and the pedestal, causing the operator's movements to be transmitted to the pedestal.

c. Exposure of the pedestals to wind which disturbs both camera and pedestal.

d. Possible shifting of the earth caused by the passage of heavy vehicles or tidal shifts.

As a result of these findings all mechanical couplings have been removed. Three of the four concrete pedestals have been wrapped with a double layer of approved insulation as a temporary solution to reduce thermal shifts. Provisions have been made to shade all exposed sites for at least two hours prior to each test. A prototype wind shield has been designed. Operational procedures have been published to prevent shifting of the soil caused by heavy weights or vehicles during a test. Land tidal effects are still being measured and evaluated.

2. Environmental Conditions

In addition to the environmental effects described the effects of wind and temperature on the cameras set up for a test were studied. Air condition of existing BC domes was found to be unsatisfactory for several reasons. Primarily, the existing systems were not designed to handle the heat problem without creating air drafts or turbulence that could affect the quality of the recorded image. Prototype portable domes have been designed to shield the camera and pedestal from wind where the sites are not protected by permanent domes.

3. Procedures

Procedures were written for:

a. Shop calibration of all Ballistic Cameras.
b. Field operation and maintenance of the BC systems.

4. Personnel (Training)

Training was requested on all new Ballistic Camera equipment. Eight men attended classes and will train the remainder of the Ballistic Camera personnel. Of the items left to be covered, the most important is the electronic system to be used with all cameras. A training program on this subject is being prepared.

All personnel have received complete training on the Wild BC-4 Camera Systems. Along with this, they have received training in Astronomy, Meteorology, Transistor and Timing Circuits, Radio Transmitter and Receivers. It was realized at the beginning of the Ballistic Camera System that full training was necessary to assure good data. The person manning a Wild BC-4 site is normally operating alone or without support that can be reached in reasonable time; therefore, he must be capable of making his own decisions based on his training and experience.

D. Data Reduction Considerations

1. Mathematical Error Model and Statistical Estimation

Investigation into the error parameters of the Ballistic Camera System revealed that existing error data was not of sufficient quality needed to construct a mathematical model that would provide a basis for meeting the new, stringent MISTRAM accuracies. The following specific areas were investigated:

a. Plate reading error.
b. Random and systematic emulsion creep.
c. Random and systematic accuracy of star catalogs.
d. The location of the center of perspective in object space.

Computation tools for performing the necessary systematic error studies did not exist. It was, therefore, necessary to develop the analysis for such problems as calibration of the measuring comparators, calibration of the systematic errors of the emulsion and base, and investigation of the residual lens distortion.

Finally, it was necessary to combine all the analysis knowledge into the working data reduction computer routines so that knowledge and correction of the errors, both systematic and random, could be properly considered. Therefore, analysis for new programs, and for revisions to existing programs had to be performed. This analysis had to include: perform the necessary object space computation of the perspective center; accept the repeated readings on the image points and correct the observations for 1) temperature fluctuations during the measuring process, 2) for the comparator calibrations, and 3) for the systematic errors of the emulsion and base.

The following RCA Technical Memos have been published as a result of the BACAR Project:

TM 62-2: Computation of a Mathematical Model to Describe the Systematic Errors of a Photographic Emulsion and Base, G. H. Rosenfield, 19 March 1962.

TM 62-4: A Summary of a Study of Star Catalogues and Their Accuracies, H. K. Eichhorn, 20 March 1962.

TM 62-5: On the Relation Between the Catalogued Mean Positions of the Stars and the Coordinates of Their Photographic Images, H. K. Eichhorn, 20 March 1962.

TM 28: Redesign of BC-4 Elevation Arm Lock, R. A. Brown, 16 November 1962.

The following RCA Data Processing Technical Reports have been published as a result of the BACAR Project:

TR 62-2: Calibration of a Precision Coordinate Comparator, G. H. Rosenfield

TR 62-3: Monitoring Photogrammetric Plate Observations, G. H. Rosenfield

The following computer programs were prepared:

(1) BACEC, Emulsion Creep Calibration
(2) BACSC, Secular Screw Calibration (comparator calibration)
(3) BOMB3, Computation of Standard Deviation
(4) BACPE, Periodic Error
(5) BACHA, Polynomial and Harmonic Analysis
(6) BACWW, Weave of the Ways Calibration
(7) BACPP, Misperpendicularity of the Comparator Axes
(8) BACMR, Ballistic Camera Data Monitor
(9) BACDR, Ballistic Camera Distortion Calibration
(10) BACPO, Double Precision Ballistic Camera Position

2. Equipment

The MANN and Wild Comparators were calibrated for periodic error, longer period leadscrew errors, curvature and weave of the ways, and misperpendicularity of the comparator axes. These errors were reduced as follows:

Wild Comparator - from 2.7 microns to 1.0 microns;

Mann Comparator - from 5.8 microns to 1.1 microns.

3. Procedures

Reading errors were reduced by incorporation of new reading techniques to the range of 0.1 to 0.5 microns. These errors are now computed in the data reduction programs and will be propagated through the estimates of error in the position data.

Procedures have been developed to compensate for emulsion creep on a plate-by-plate basis by the use of a reseau grid exposed on the plate (superimposed with the star and flare images). As an interim procedure, a lens distortion calibration will be performed to absorb these errors as well as refraction errors.

4. Personnel

A rigorous training program and reading error tests have been initiated to enable selection of personnel for the reading of Ballistic Camera plates.

Section III - Conclusion

The results of the BACAR effort to date serve to indicate the magnitude and direction for future investigations. The major amount of future effort is to be expended in reducing those factors which were found to be limiting the accuracy of the Ballistic Camera Systems. Future work includes but is not restricted to: optimum camera operational site facilities, a certified initial standard of accuracy, sufficient corrections for atmospheric refraction and knowledge of refraction anomalies, errors in the star catalogues, and finally, manufactured cameras which approach the ideal optical instrument. Statistically correct and photogrammetrically rigorous data reduction procedures are being developed and implemented. Further applications of the results of the BACAR work will appear in future developments of range equipment.

The results of the BACAR project will give better data for the Range User. The evaluation of the Ballistic Camera System will allow reliance on the range standard of known accuracy. The calibration of the System will allow for improving the accuracy of the range standard. Also, problem areas have been pinpointed, and the needs for future research indicated.

Section IV - Results of Ballistic Camera Operation for MISTRAM Evaluation of October 1962.

A total of 127 Ballistic Camera plates were evaluated to determine the operational capability of the Ballistic Camera system as used on the MISTRAM evaluation of October 1962. The plates were distributed as follows:

BC 1000- 57 plates,
BC 600 - 8 plates,
BC 300 - 62 plates.

The plates were evaluated for the factors of:

1. emulsion creep: setting error on images and standard error of the emulsion calibration adjustment. The emulsion calibration was performed on only 28 plates;
2. setting error on star images;
3. setting error on flash data point images;
4. standard error of unit weight for camera orientation.

Except for emulsion creep, the data were evaluated independently for each type of camera system. No attempt was made to separate triangulation error into components for the individual cameras, or camera types, since the present triangulation routine does not properly weight the stations used in the adjustment. Because of the improper weights, the residuals have no valid meaning for the individual cameras. A triangulation

routine with a more statistically valid weighting procedure will shortly be released. Consideration of the proper weighting in the triangulation was not possible until all errors in the system had been recognized and evaluated (results of the BACAR effort).

The following definitions are used in the evaluation:

$\bar{s}$ average setting error (standard deviation of one setting) computed as the arithmetic average of the individual setting errors for all the plates considered.

s standard deviation of the individual setting errors about the average value.

SDM standard deviation of the mean for the setting error. Since the value of each measurement is the average of 4 readings, this value is determined by $\bar{s}$ divided by $\sqrt{3}$.

$\bar{s}_e$ the average standard error of unit weight from the emulsion creep adjustment computed from the reseau residuals following a 2nd degree calibration fit.

$\bar{s}_o$ the average standard error of unit weight for the orientation adjustment of the plates. Computed as an arithmetic average; since each plate had sufficient degrees of freedom for a satisfactory orientation and is therefore considered as a separate unit.

$\bar{s}_t$ the pooled standard error of unit weight for triangulation of all images on all plates.

N the number of plates used in the analysis.

The following tabulated results are presented (all values are in microns unless otherwise indicated):

Emulsion creep:	N	26
standard error:	$\bar{s}_e$	1.53
	s	0.21
reseau images:		
setting error:	$\bar{s}$	2.37
	s	0.55
	SDM	1.08

		BC100	BC600	BC300
number of plates	N	57	8	62
Star images:	$\bar{s}$	3.23	3.63	3.04
setting error:	s	0.64	0.54	0.53
	SDM	1.86	2.10	1.76
Orientation				
standard error:	s_o	5.29	4.51	3.68
	s	0.61	0.68	0.78
arc sec:	$\bar{s}_o$	1".06	1".50	2".45
pooled:	$\bar{s}_o$	4.52		
Flash images:				
setting error:	$\bar{s}$	4.05	4.11	4.13
	s	0.65	0.78	0.66
	SDM	2.34	2.37	2.38
Triangulation				
pooled standard error:	$\bar{s}_o$	5.23		
arc sec:		1".04		

Conclusions:

The Ballistic Camera system lends itself to complete analysis of the major sources of contributing errors. The individual major errors can be evaluated and/or calibrated, and the geometric quality of the reduced data can be statistically estimated. Thus, it is realized, the least squares adjustment is not a magic procedure by which good results can be obtained from poor data. The results can be no better than the data entering the adjustment. It is therefore highly mandatory that the best possible measurements (lowest standard deviations) be obtained, and that all known sources of systematic error in the data be eliminated.

Thus, in order to obtain Ballistic Camera data of high geometric quality it is necessary that proper consideration be given to the data procurement and data reduction. The field operation should be performed utilizing stable mountings and pedestals, and the cameras should be protected by atmospherically conditioned shelters. It is mandatory that the emulsion be calibrated in order to correct the developed photographic image to the position on the plate of the latent optical image. The plates must be measured in an atmospherically controlled environment which is vibration isolated from disturbing influences. An accurate

method of recording temperature and humidity should be available during the measuring process. The measuring equipment must be protected from accumulation of oxidized oil and settling of dust and lint on the ways, bearing, and screws. The mathematics utilized in the computer processing of the data should be photogrammetrically and statistically correct.

Recommendations:

1. The data acquisition and data processing operations should be re-examined to correct any existing deficiencies.

2. It is mandatory that all sources of systematic error be calibrated or eliminated on all Ballistic Camera plates for which data of high geometric quality is desired.

3. Selected plates from the MISTRAM evaluation will be re-measured and re-reduced with tender loving care, in order to determine how much improvement in the data could have been achieved.

Section V - Editorial Comments

The BACAR effort has resulted in Ballistic Camera data of known and improved geometric quality. Each of the major sources of error in the Ballistic Camera system has been evaluated and where possible calibrated or eliminated so that the resulting data is of high geometric quality, as evidenced by the low standard error of unit weight resulting from the least squares adjustment. The error budget indicates that the cumulated standard error is equivalent to the standard error of unit weight resulting from the least squares adjustment of the data. We can now state that we have a true range standard for evaluation or calibration of other range instrumentation.

However, let us consider some newer types of range instrumentation: specifically, the electronic trajectory measuring equipment. These newer instruments are manufactured to meet a particular design requirement, which in some cases calls for a higher level than the present geometric quality of the Ballistic Camera used as a standard. But this is a design requirement only, and does not automatically indicate that the delivered instrument meets this design requirement. The instrument must be evaluated against some existing standard, which at the present time is the Ballistic Camera system. If it is not desired to accept an evaluation of electronic equipment against the Ballistic Camera standard, then the geometric quality of the electronic instrument must be established by an independent statistical determination of the standard error of unit weight for the reduced data. This independent evaluation must be performed by analyzing the various component errors of the equipment, in the same manner that has

been done for the Ballistic Camera system. The standard errors for each of the major components of the equipment must be established, and it must be proven that the total standard error of all the components are statistically equivalent to the standard error of unit weight for the reduced data.

There is another important topic upon which I would like to comment. This concerns the different philosophies of data reduction: the pure mathematical-statistical approach versus the technological approach. The mathematical-statistical approach is based upon the error model. It considers that all the instrumentation problems can be solved in the data reduction process, if only a good enough mathematical error model can be formulated. The technological approach is based upon a more involved philosophy. First, that the instrument system is designed, manufactured and adjusted to the highest possible degree. Second, that each contributing error of the system is isolated, analyzed, and corrected before the major data reduction adjustment takes place. Personally, I am a proponent of the technological approach to instrumentation systems. The results of the BACAR effort with the Ballistic Camera system indicates the improvements in geometric quality of the reduced data, and the advances in the state-of-the-art of instrumentation, that can be obtained by following this technological philosophy. In summation, and in support, I should like to quote from Hald, "Statistical Theory with Engineering Applications," John Wiley and Sons, New York, 1955, pg. 758:

"The formulation of a mathematical-statistical model which gives a satisfactory description of the data, is not in principle a statistical task, but belongs within the professional subject from which the observations have been derived. In practical work, however, we often find that professional knowledge is so small that it is not possible to formulate a proper (theoretical) model, i.e., a description based on general laws regarding the process which has generated the observations. In such cases the specification becomes merely a phenomenological description, i.e., a purely empirical description of the observed phenomenon without any attempt at linking this description up with theoretical reasoning based on professional knowledge.

"... It should, however, be born in mind that in the long run it does not pay to be satisfied with a phenomenological description; this should be resorted to only when all attempts at giving a theoretical description have proved impractical."

ERROR BUDGET

BC-300 (From Actual Data)

Estimated: Before BACAR

	S	S^2	S_o
Orientation			
Setting error	1.5mu	2.25	
Comparator error (STKI)	2.7	7.29	
Emulsion error	3.0	9.0	
Star catalogue error 0.7 sec	1.0	1.0	
Refraction error (stars) 0.2 sec	0.3	0.09	
		$[19.63]^{1/2}$ =	4.4mu
Triangulation			
Orientation	4.4	19.63	
Setting error	1.5	2.25	
Refraction (atmosphere) 1.5 sec	2.0	4.00	
		$[25.88]^{1/2}$ =	5.1mu

4.4 = 2".93
5.1 = 3".40

S = estimated standard deviation or standard error

S_o = standard error of unit weight

LENS DISTORTION

SC4 [illegible]229
210 mm

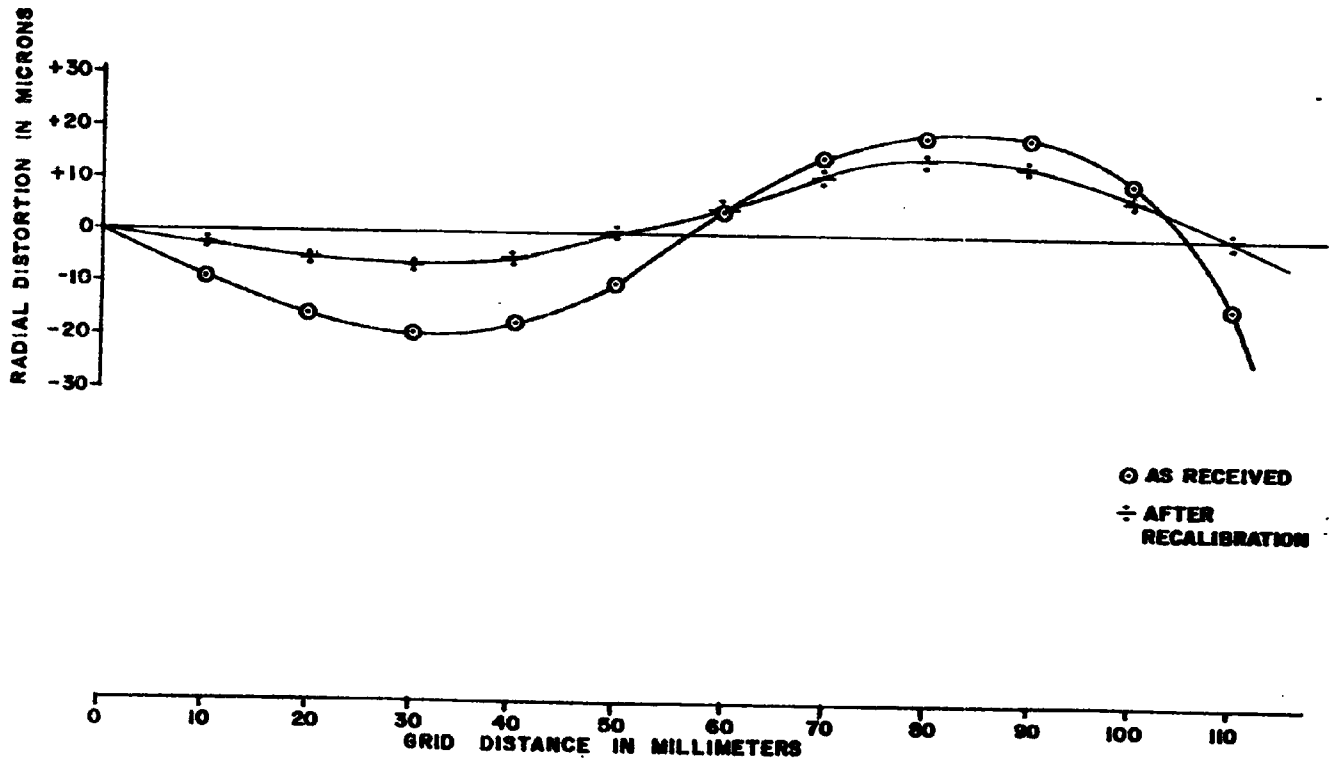

BC4 SHUTTER VIBRATION

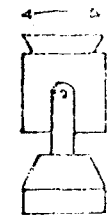

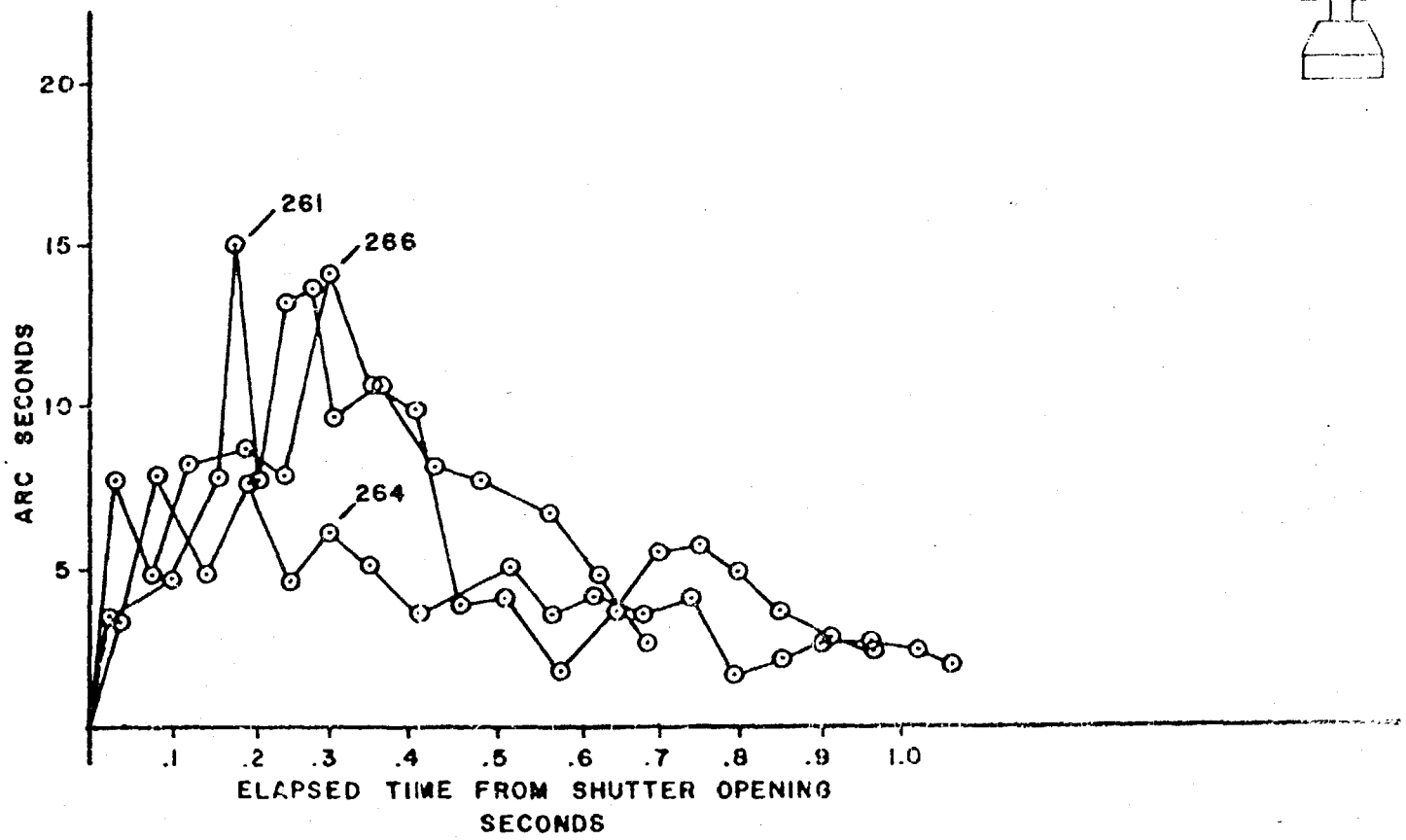

BC-4 ELEVATION ARM CLAMP

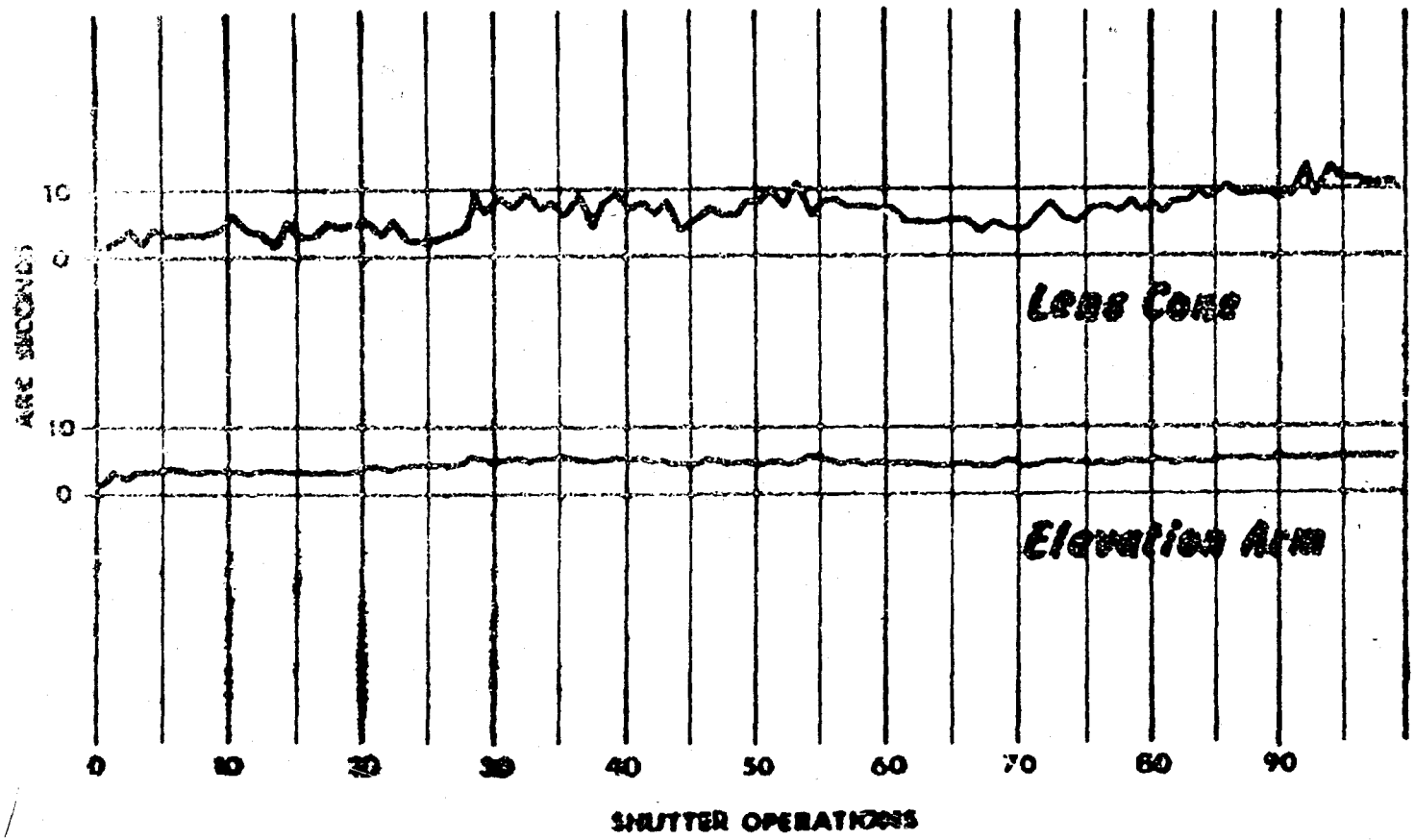

BC4 MOTOR VIBRATION

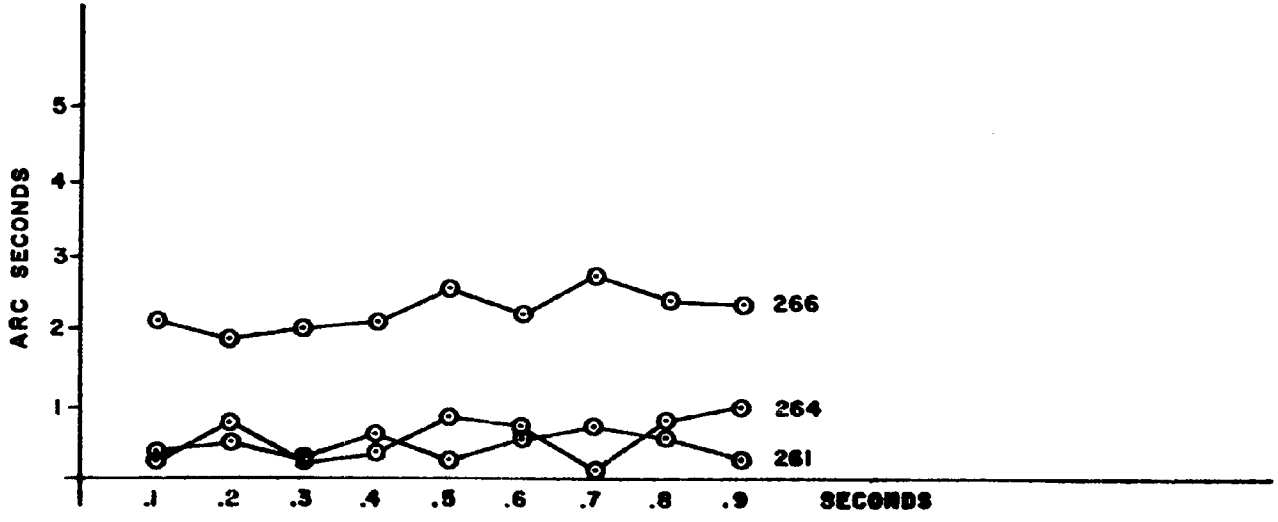

BC-4 Shutter Delay

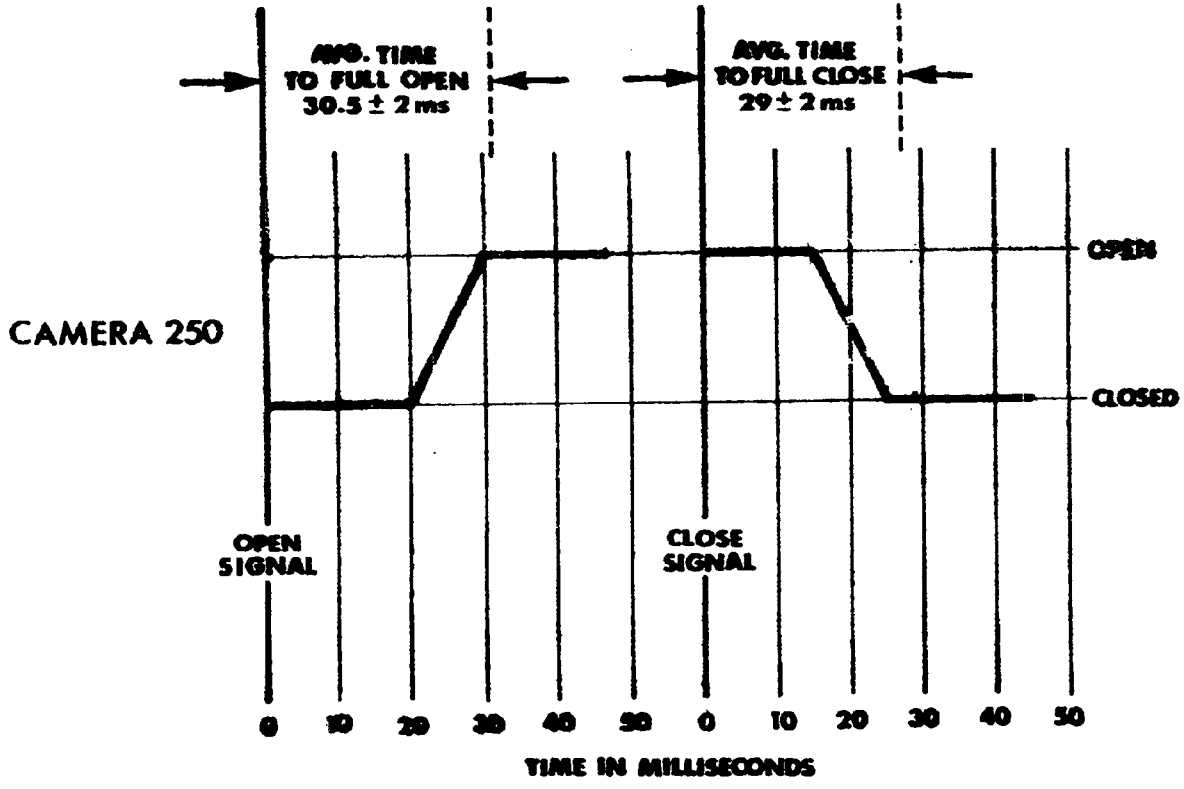

THERMAL STABILITY
15' CONCRETE PIER

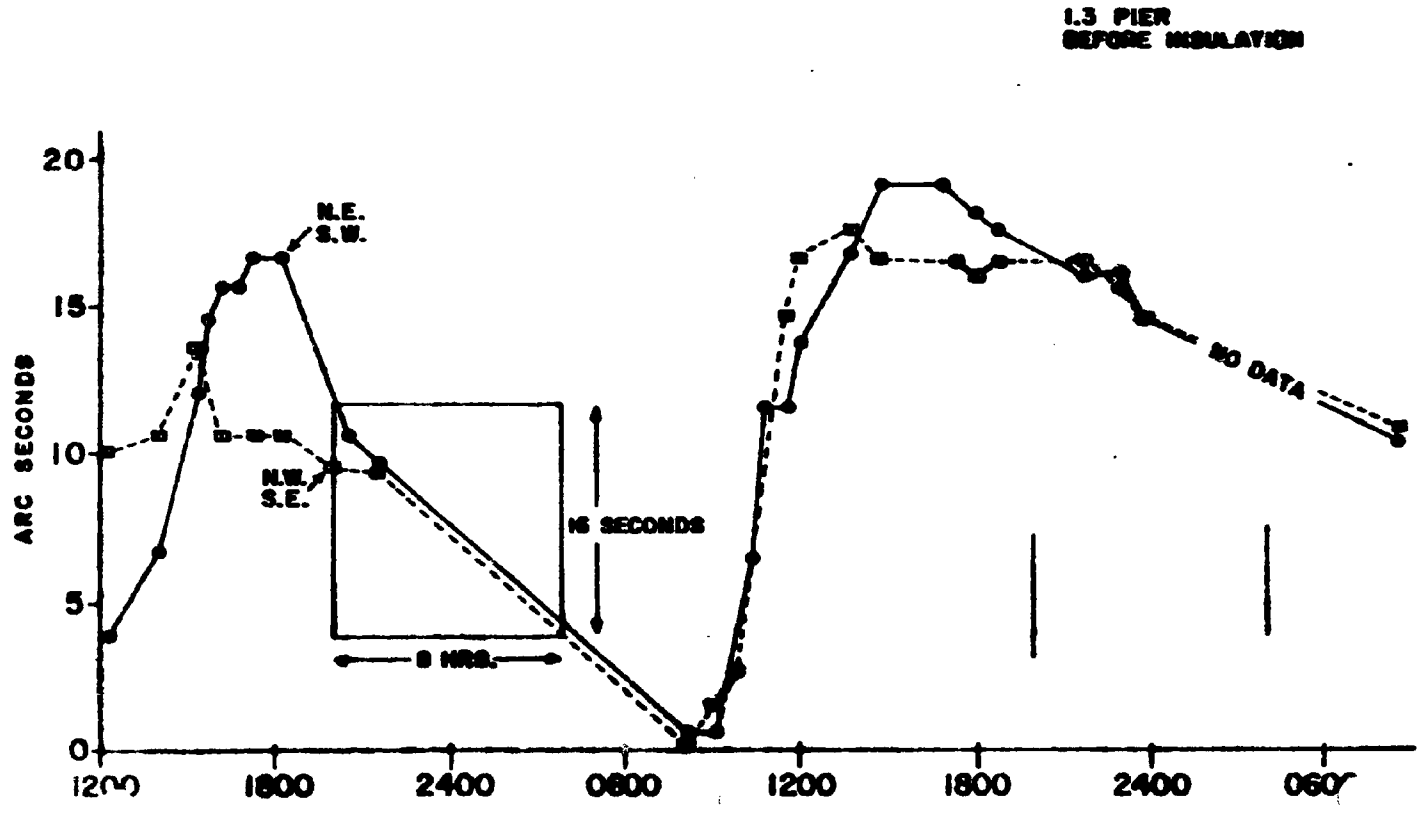

RESEAU PLATE

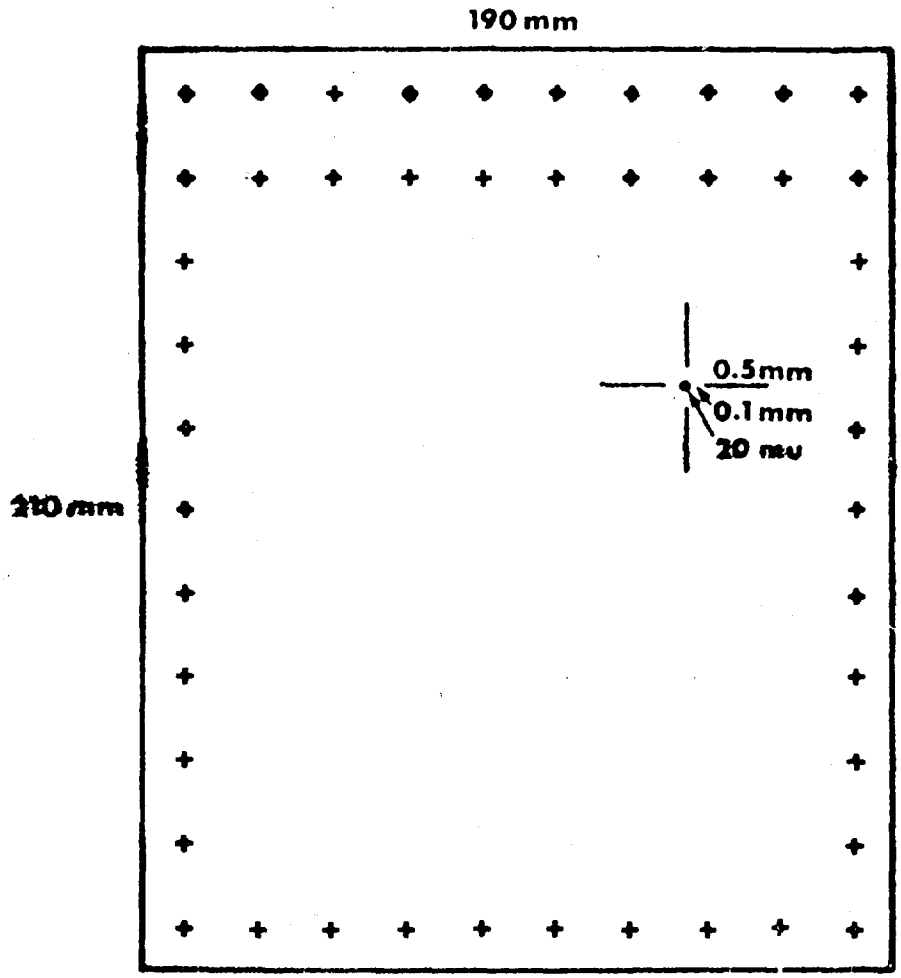

Camera Calibration Residuals

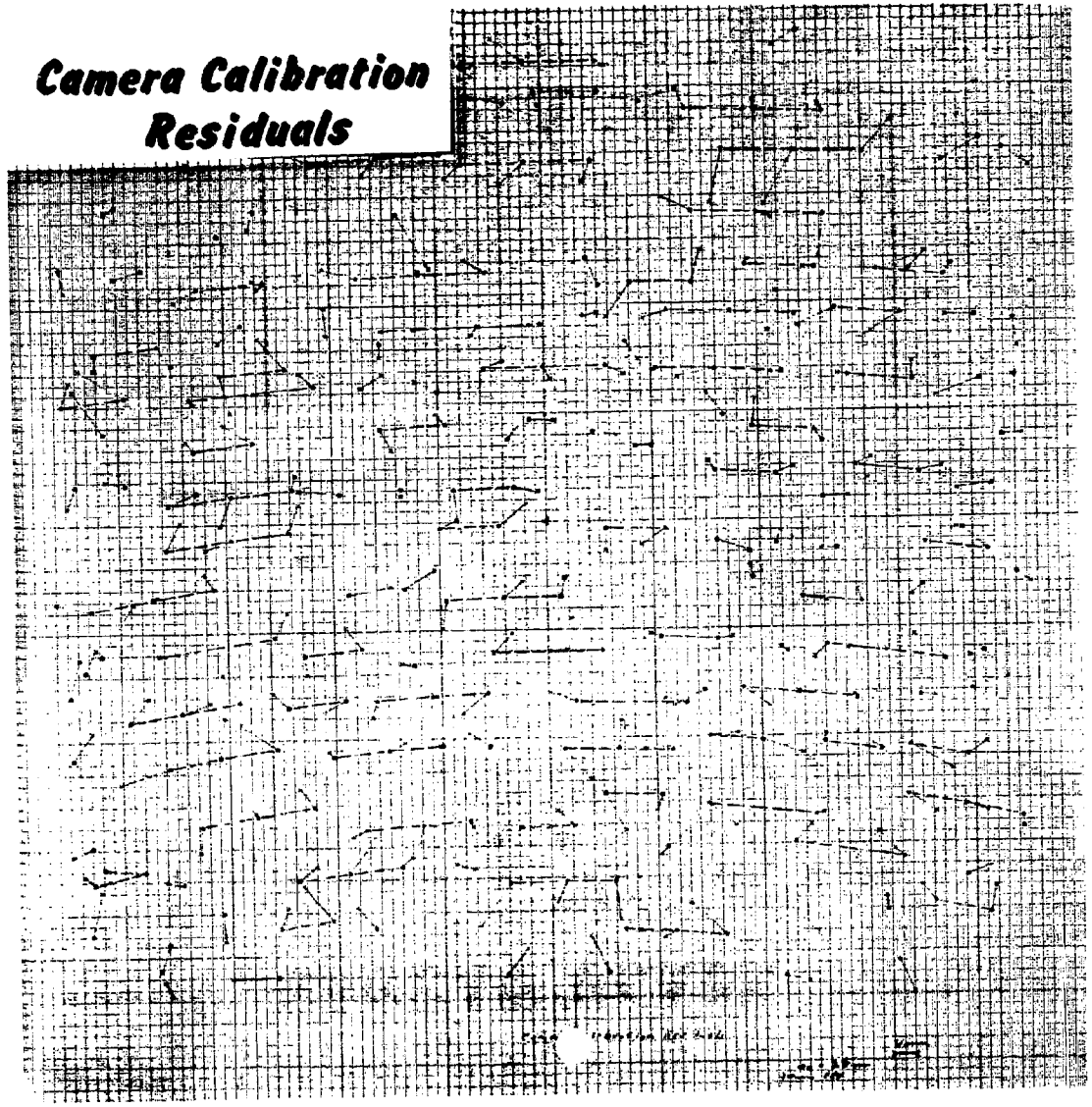

STEREO
PERIODIC ERROR

X

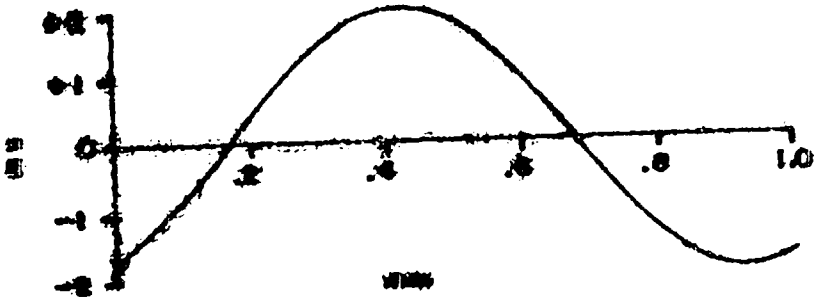

Y

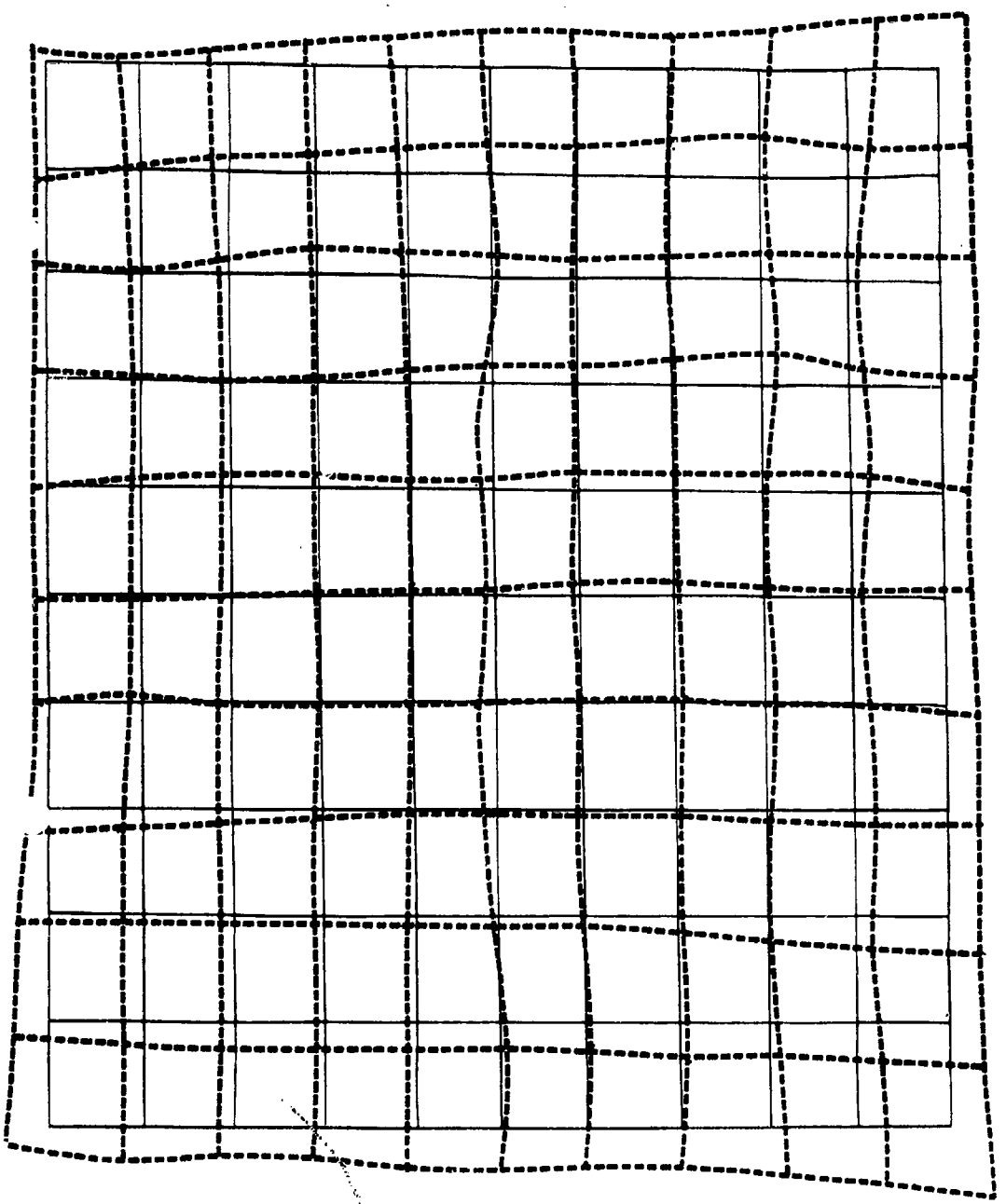

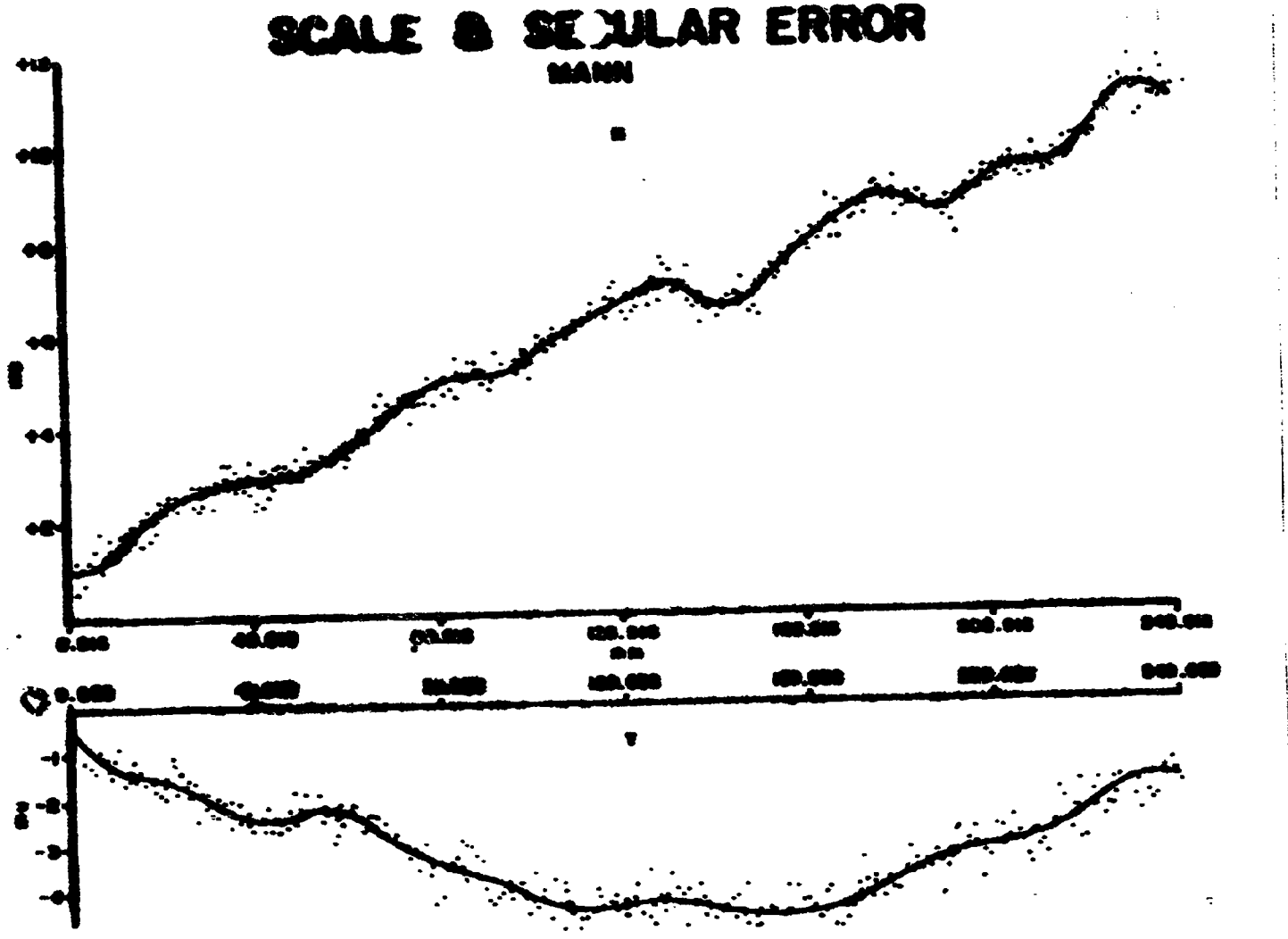
SCALE & SECULAR ERROR
MAIN

SCALE & SECULAR ERROR

STEREO

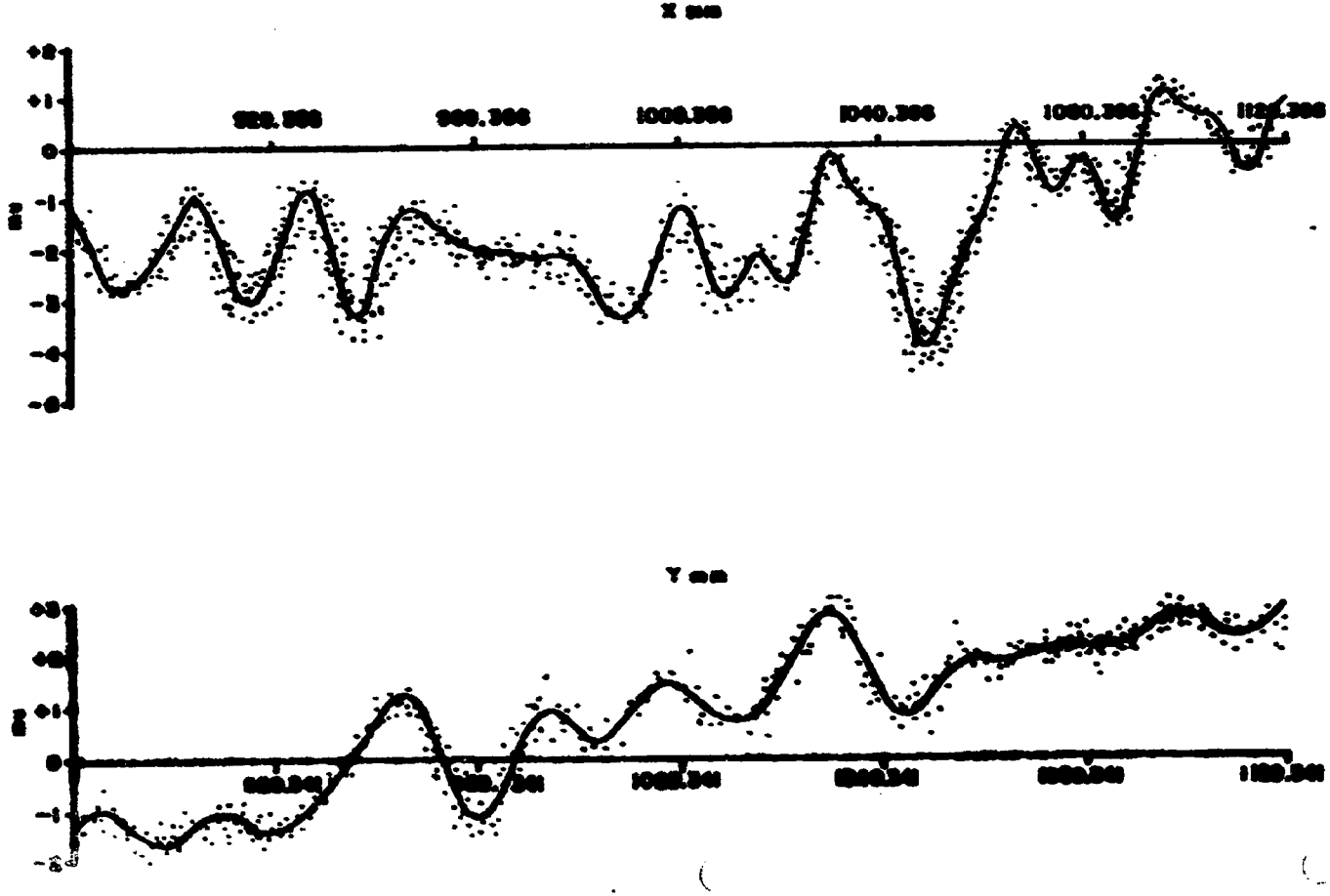

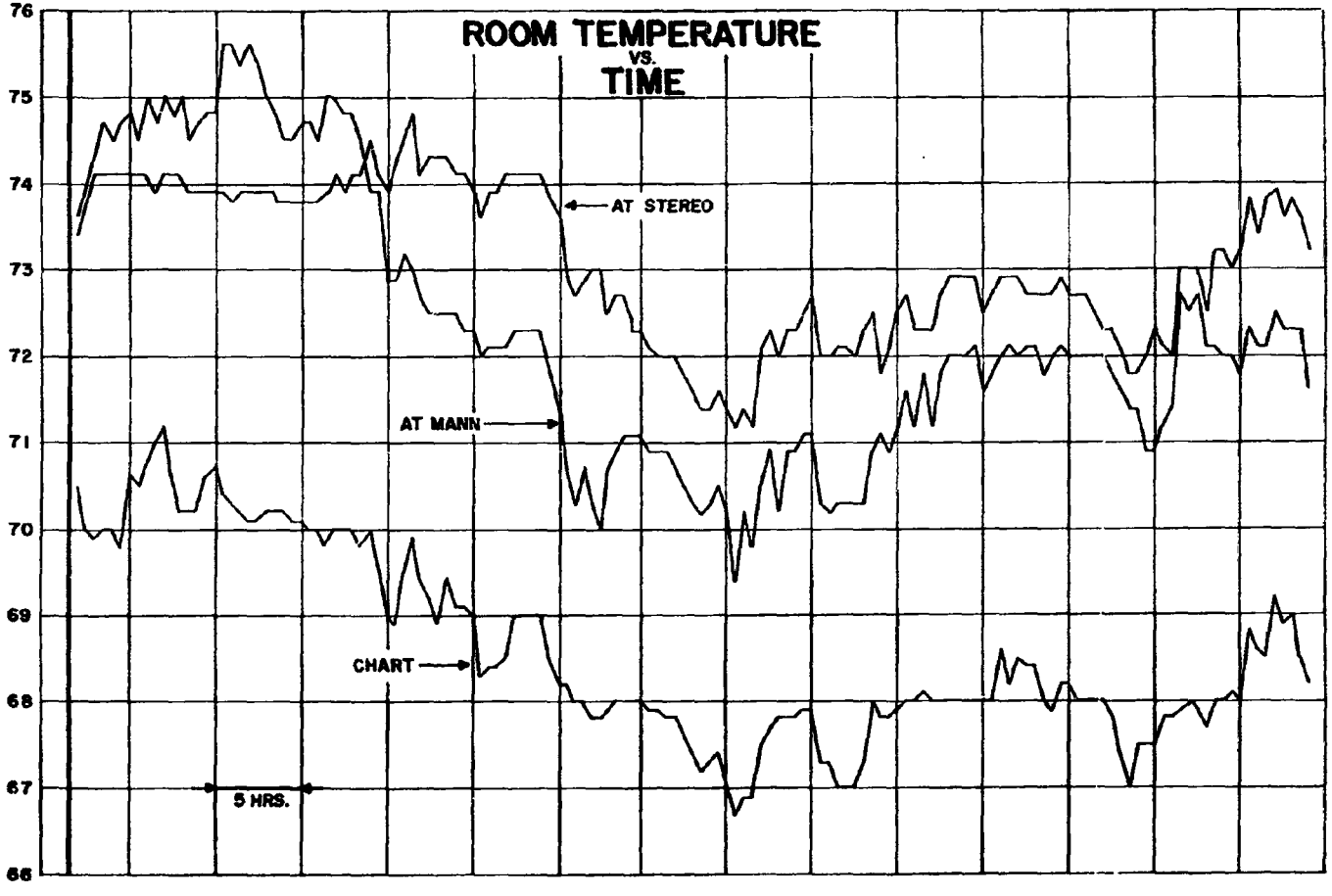
ROOM TEMPERATURE
VS.
TIME
76
75
74
73
72
71
70
69
68
67
66
AT STEREO
AT MANN
CHART
5 HRS.

CURVATURE & WEAVE ERROR

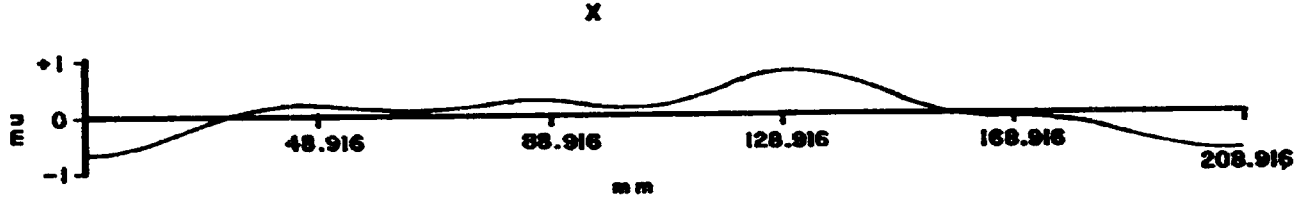

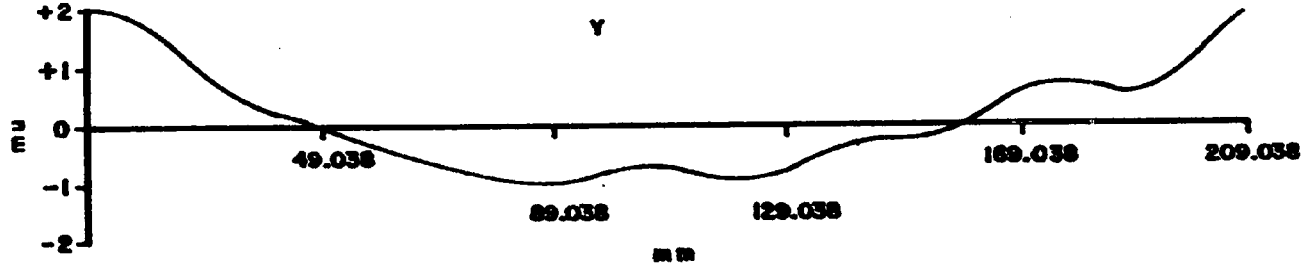

ERROR BUDGET

Expected: After BACAR Phase I

Orientation	S	S^2	S_o
Setting error	1.5mu	2.25	
Comparator error (STK1)	1.0	1.0	
Emulsion error	1.0	1.0	
Star catalogue error 0.7 sec	1.0	1.0	
Refraction error (stars) 0.2 sec	0.3	0.09	
		$[5.34]^{1/2}$ = 2.3mu	

Triangulation	S	S^2
Orientation	2.3	5.29
Setting error	1.5	2.25
Refraction (atmosphere) 1.5 sec	2.0	4.0
		$[11.54]^{1/2}$ = 3.4mu

2.3 = 1".54

3.4 = 2".27

OPERATIONAL RESULTS
MISTRAM BC TESTS

		BC 1000	BC 600	BC 300
SETTING ERROR				
Reseau	2.37			
Stars		3.23	3.63	3.04
Flashes		4.05	4.11	4.13
ORIENTATION ERROR		5.29	4.51	3.68
		1".06	1".50	2".45
Pooled	4.52			
TRIANGULATION ERROR				
Pooled	5.23			
	1".04			

C

TC4-2

M I S T R A M

BY

Dr. K. E. Relf
RCA Missile Test Project
PAFB, Florida

Presented at:
Fourth Joint AFMTC Range User Data Conference
Orlando AFB, Florida
26-28 February 1963

INTRODUCTION

MISTRAM is one of the latest and potentially most accurate electronic tracking systems to be acquired by the Atlantic Missile Range. The System was designed and built by the General Electric Company. Two systems have been installed, one at Valkaria, Florida about thirty miles south of Cape Canaveral and one at Eleuthera, about 350 miles down range.

This paper is devoted to a general description of the MISTRAM system, a more detailed description of the Precision Measuring Sub-System, an outline of the data reduction process and a discussion of the accuracy performance of the system.

GENERAL DESCRIPTION

The physical description of the system is taken directly from one or more of the documents published by the General Electric Company and enumerated as references.

A. The seven (7) Subsystems of MISTRAM as shown in Figure 1

The Mistram System is composed of eight major parts: seven subsystems and a systems components group. They are as follows:

1. Precision Measuring Subsystem (PMSS)

   The PMSS is an X-band c-w radar that uses interferometer techniques to measure the position of a vehicle.

2. Airborne Transponder Subsystem

   The Airborne Transponder Subsystem consists of a transponder, a filter, and suitable antennas, all of which are aboard the vehicle. The airborne transponder receives, amplifies, frequency-offsets, and re-transmits the two c-w X-band signals from the central station with a very

• MISTRAM •

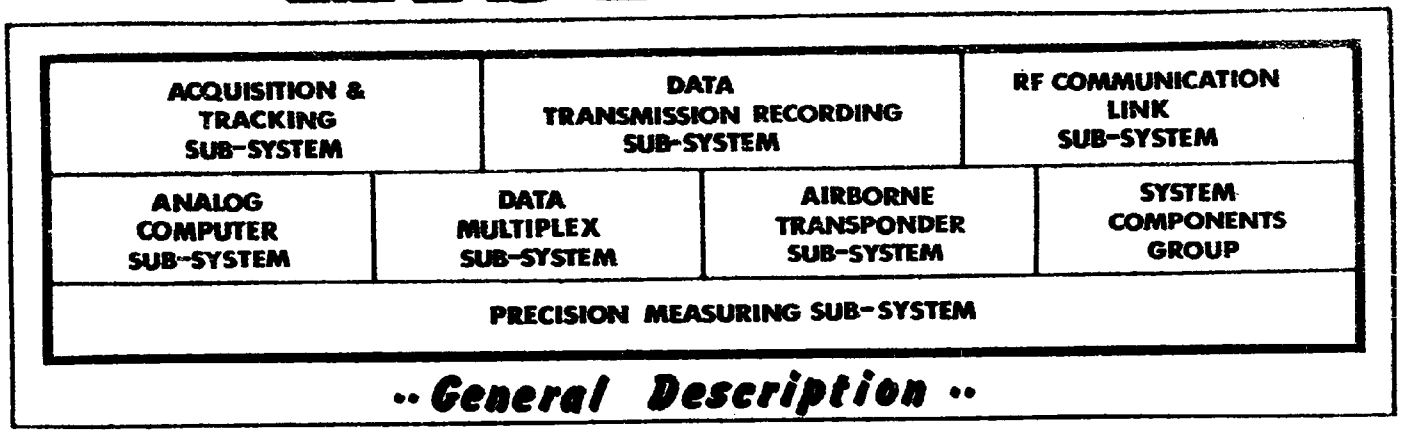

Figure 1

low uncertainty in the phase shift between the received and transmitted frequencies.

3. Acquisition and Tracking Subsystem

The Acquisition and Tracking Subsystem acquires the transponder and automatically tracks the incoming signal in azimuth, elevation, and polarization. The ATSS antenna supplies pointing information to the central PMSS antenna and to the Analog Computer Subsystem. The ATSS antenna is used as the transmitting antenna for the PMSS as well as the receiving antenna for the ATSS.

4. Analog Computer Subsystem

The Analog Computer Subsystem directs the four remote receiving antennas of the Precision Measurement Subsystem. Normally, it obtains the angle data of the ATSS antenna and the target range from the PMSS. This information then is transmitted to each of the receiving antennas by the Data Multiplex Subsystem and the Communication Link Subsystem where correction for parallax is inserted. It also has the capability of receiving slaving data from the range, correcting for parallax, and directing the transmitting antenna. In addition, slaving data can be supplied to the range.

5. Data Transmission and Recording Subsystem

The Data Transmission and Recording Subsystem includes the necessary equipment for encoding the five primary data words generated by the PMSS, the three words generated by the data multiplex equipment in response to input signals from a refractometer at each station, and the time codes generated in the PMSS; this data is encoded into a form suitable for transmitting over the R-F Communication Link Subsystem to Cape Canaveral. In addition, this subsystem provides for the

4

decoding of the signals in a form suitable for insertion into the IBM 7094 real time computer located at Cape Canaveral and provides a capability for recording these signals for later playback for post-flight data reduction.

6. R-F Communication Link Subsystem

The Communication Link Subsystem consists of the following two major groups:

(1) Baseline communication group, a microwave system which contains the necessary equipment for transmitting all signals between the central station and the 100,000 foot stations, with the exception of those coherent signals transmitted within the PMSS link.

(2) External Communication group, a microwave link which contains the necessary equipment for transmitting all signals between the central station and Cape Canaveral, including the special Data Transmission and Recording Subsystem signals and the timing synchronization.

7. Data Multiplex Subsystem

The Data Multiplex Subsystem is used for encoding and decoding, in the correct format, data required for transmission between the central station and the 100,000 foot, remote stations via the baseline communication link, and for data required for transmission between the central station and the 10,000 foot remote stations via wire lines.

In addition to the seven subsystems there is a Systems Components Group which includes all the miscellaneous equipment required for proper operation of the subsystems described in 1 through 7. It includes the intercommunication equipment, real time refractometers, optical tracker, power equipment for primary power generation and transmission, and installation material that is not supplied as a part of any of the above subsystems or as part of the facilities.

B. Location of the Equipment (Figure 2)

The major elements of MISTRAM are arranged in an L-shaped configuration of a central station and four remote stations spaced along 10,000 foot and 100,000 foot baselines. Three microwave antenna towers are located, one each, near the corner and two extremities of the configuration. Ideally, the baselines subtend an angle of exactly 90° and the remote stations are located on these baselines 10,000 feet and 100,000 feet from the central station. In practice, however, the relative positions of the stations with respect to each other are not critical as long as the distances and angles are known to extreme accuracy.

The central station equipment includes the ATSS tracking antenna and receiver, the PMSS transmitter and receiving antenna, ten receivers, data extraction circuits, communication and recording equipment, refractometer, optical tracker, simulator, operator and coordinator consoles plus miscellaneous power equipment and normal utilities. Of the ten receivers at the central station, one is used for beacon signals arriving direct from the vehicle, five for return signals arriving via the central station and four remote stations, and four are used for phase stabilization purposes.

Each remote station houses a simple receiving antenna slaved to the central station PMSS antenna, a receiver for beacon signals, a receiver for phase stabilization purposes, a refractometer, communication equipment, power supplies and normal utilities. The receivers at the remote stations and those at the central station are nearly identical.

Communication between the central station and the four remote stations

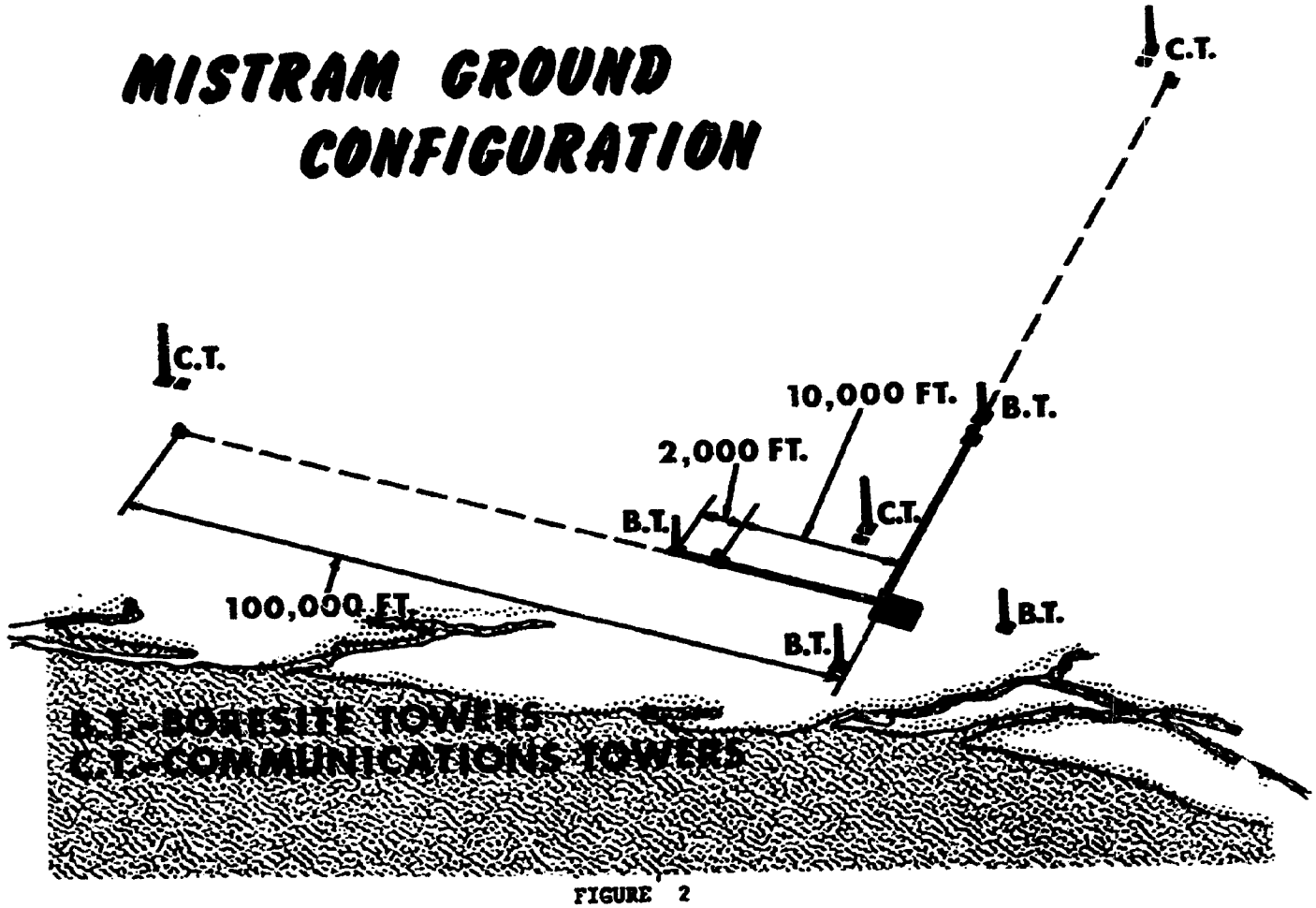
MISTRAM GROUND CONFIGURATION
C.T.
C.T.
10,000 FT.
B.T.
2,000 FT.
B.T.
C.T.
100,000 FT.
B.T.
B.T.
B.T.- BORESITE TOWERS
C.T.-COMMUNICATIONS TOWERS

FIGURE 2

is accomplished via waveguide over the 10,000 foot baselines and via microwave link over the 100,000 foot baselines. Communication between the central station and Cape Canaveral and Patrick Air Force Base is by microwave relay.

The MISTRAM central station is located approximately 30 miles south of Cape Canaveral. One baseline extends approximately twenty miles in a western direction from the central station and the other baseline approximately twenty miles south from the central station.

C. Theory of Operation

1. General

Position of a vehicle is determined by triangulation techniques involving measurements of range and range differences. Velocity of the vehicle is determined by comparing the rates at which range and range difference measurements are changing. The trajectory data available from MISTRAM are one range and four range differences.

2. Position Determination

Position is determined as shown in Figure 3 Range is measured from the central station by measuring the time required for radar signals to travel from the central station to the transponder in the vehicle and back to the central station. From this measurement the range of the vehicle from the central station can be computed but its angular position relative to the station is not defined. It will be known only that the vehicle lies on the surface of an imaginary hemisphere whose center lies at the central station and whose radius is equal to the range.

At the instant of the above measurement, the difference in distance

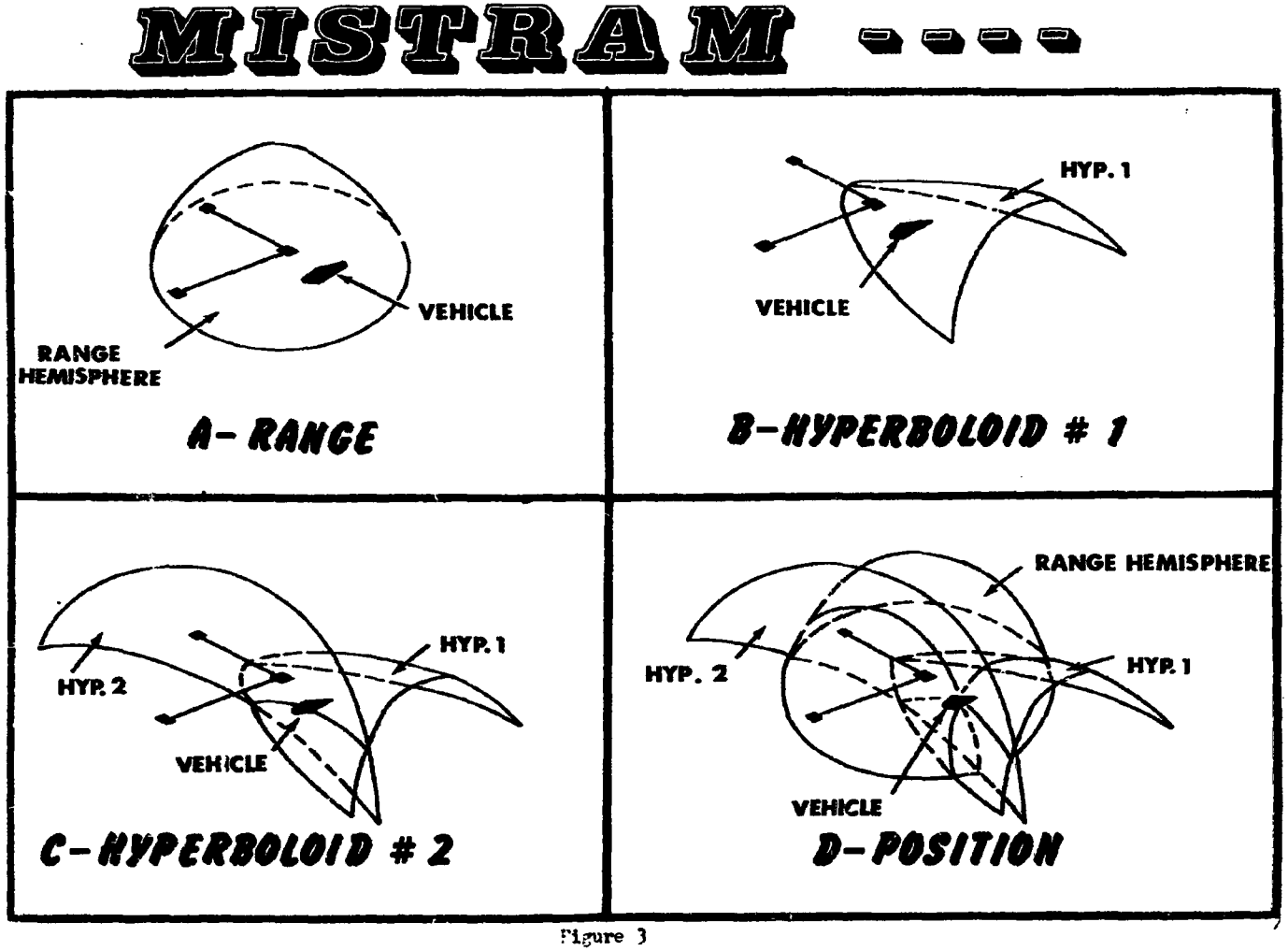
MISTRAM
RANGE HEMISPHERE
VEHICLE
A- RANGE
HYP. 1
VEHICLE
B-HYPERBOLOID # 1
HYP. 2
HYP. 1
VEHICLE
C-HYPERBOLOID # 2
RANGE HEMISPHERE
HYP. 2
HYP. 1
VEHICLE
D-POSITION

Figure 3

between the vehicle and the central station, and between the vehicle and one of MISTRAM's 10,000 foot remote stations, is measured to obtain a range difference. From this difference measurement it is known that the vehicle, regardless of its range from either station, must lie on the surface of an imaginary hyperboloid whose axis passes through both stations.

At this same instant, the difference in distance between the vehicle and the central station, and between the vehicle and the other 10,000 foot remote station, is measured to obtain a second range difference. From this second difference measurement it is known, as before, that the vehicle must lie on the surface of another hyperboloid whose axis passes through the central station and this second remote station. It is now known that the vehicle lies on the surface of both hyperboloids and the hyperboloids intersect in space, consequently, the vehicle will lie somewhere along this line of intersection. Since the vehicle's range from the central station describes a hemisphere, the intersection of this hemisphere with the above hyperbolic intersection is a point which defines the vehicle's position in space relative to the ground stations.

3. Velocity Determination

Velocity is determined in the MISTRAM system by comparing the rates at which the range and four range differences are changing. Range rate is extracted from the central station range measurement while range difference rates are extracted from the four range differences as measured between the central station and each of the four remote stations.

THE PRECISION MEASURING SUBSYSTEM

A. Two Channel Concept

The detailed operation of the MISTRAM system is very complex; only the basic principles upon which the system is designed will be discussed in this paper. Comprehensive descriptions of the circuitry can be found in the documents published by the General Electric Company some of which are enumerated in the references.

For purposes of explanation it is sometimes convenient to consider MISTRAM as consisting of two separate channels: (a) a continuous channel and (b) a calibrate channel. Since the calibrate and continuous channel signals are separate (except for phase reference circuits) from the time they leave the transmitter until they enter the data extraction circuits, the MISTRAM system behaves much like two c-w radar systems operating simultaneously. Consider first the fundamental behavior of the continuous channel.

1. Operation of the continuous channel.

The Continuous channel consists of electronic equipment designed to utilize the Doppler effect to produce range-type measurements. The MISTRAM transmitter emits a continuous X-band signal of 8,148 megacycles which is received by the missile transponder, offset by 68 megacycles and retransmitted to the ground receiver. The outputs of the ground transmitter and ground receiver are compared in phase and the phase difference produced by the Doppler effect is digitized and read out.

The continuous channel provides coarse and fine range data which is calibrated by the calibrate channel as well as fine rate data which

is not calibrated. The coarse range data are accurate to 64 feet; the fine range data, to 0.12 foot. The least significant bit in the fine rate data is 0.004 foot and it is not calibrated.

The continuous channel, therefore, utilizes the Doppler principle to provide range and range difference data the validity of which must be determined by comparison to other independent measurements of the same quantities. These are made by the calibrate channel which is described next.

2. Operation of the Calibrate Channel

The calibrate channel is designed around a pre-determined real change in frequency of a continuous wave signal. A Counter records the number of cycles change between the received and transmitted signal.

The principle is illustrated in Figure 4

Consider the following sequence of events:

TIME	EVENT
T_1	The ground transmitter is radiating a signal of frequency f_1 and the ground receiver is tuned to frequency f_1.
T_2	The ground transmitter changes frequency and radiates a signal of frequency f_2.
T_3	The transponder receives frequency f_2 and re-radiates a signal of the same frequency.
T_4	The ground receiver receives the new frequency f_2 and hence realizes the ground transmitter has shifted frequency.

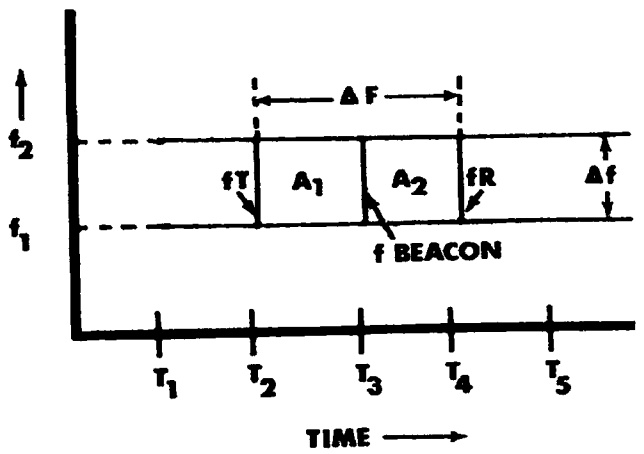

$$\text{Area } A (\equiv A_1 + A_2) = (f_2 - f_1)(T_4 - T_2)$$

$$T_4 - T_2 = \frac{2R}{C}$$

$$R = \frac{CA}{2(f_2 - f_1)}$$

Figure 4

The area indicated by A is given by the following expression:

$$A(\text{area}) = (f_2 - f_1)\ (T_4 - T_2) \text{ cycles}$$

The time interval $T_4 - T_2$ is the round trip transit time of the ground-radiated signal and is represented by τ. If the speed of propagation is taken to be that of the speed of light, the following expression can be written relating the area A, the change in frequency Δf ($= f_2 - f_1$), the round trip transit time τ ($= T_4 - T_2$), and range, R:

$$\tau = \frac{A}{\Delta f} = \frac{2R}{c}$$

and

$$R = \frac{cA}{2\Delta f}$$

The calibrate channel of the MISTRAM system provides circuitry to measure the area A and record it in cycles in a counter; it also provides an oscillator and sweep generator to produce a change in frequency, Δf, of exactly eight megacycles. The Calibrate channel, therefore, furnishes an unambiguous determination of range.

The actual implementation of this principle involves the generation and transmission of a continuous X-band signal which is swept between 7,892 and 7,884 megacycles, the eight megacycle change in frequency just described. A sweep change frequency is actually used instead of the abrupt change illustrated in Figure 4. Counting the cycles produced in the calibrate channel of the receivers during the 8 megacycle sweep of the X-band calibration signal provides an unambiguous range measurement to an accuracy of one wavelength at 8 megacycles or about 64 feet in the coarse-range calibration data Counter. The continuous channel range measurement, however, is made with an accuracy

PRINCIPLE OF BASELINE STABILIZATION

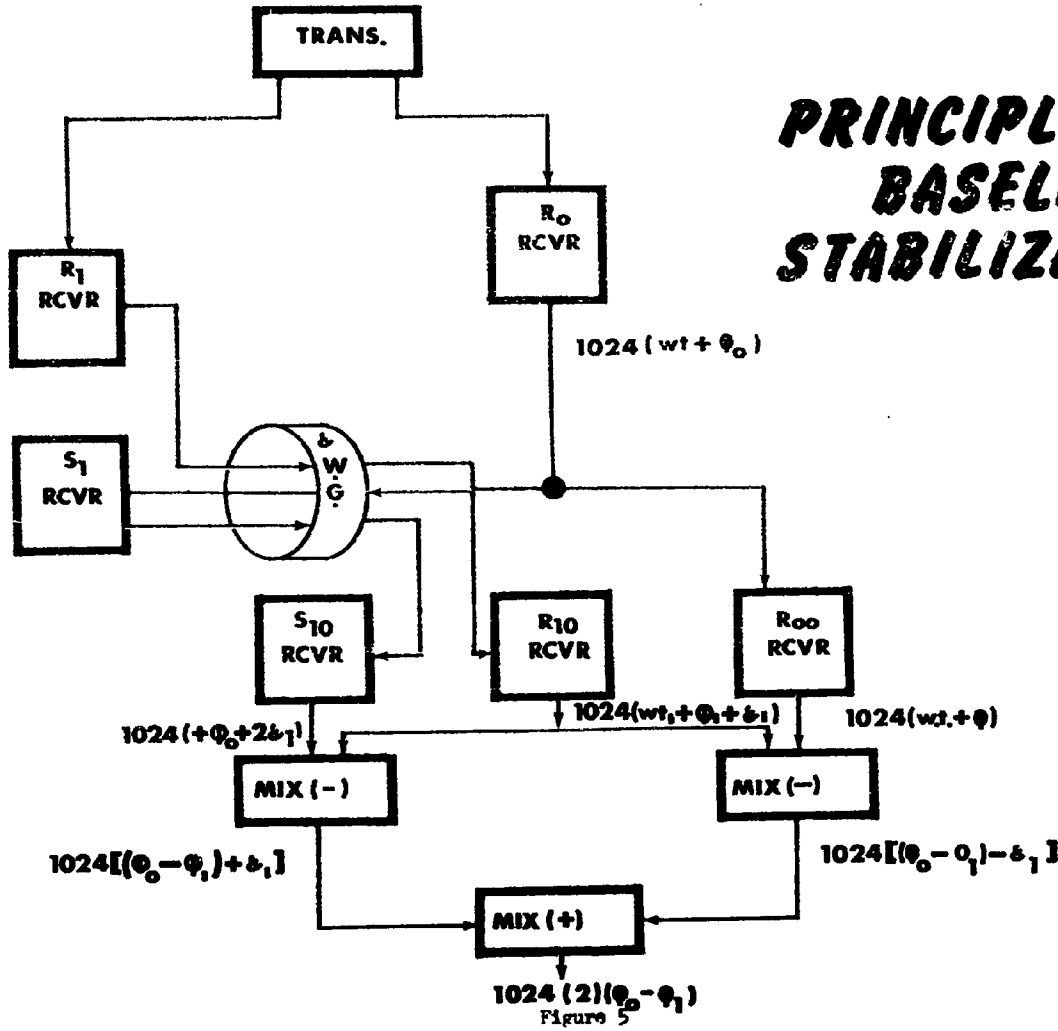

Figure 5

of one cycle of an x-band frequency which is approximately 0.128 feet. Initializing and checking the continuous-range reading to this degree of accuracy is accomplished by measuring the phase shift of the 256 megacycle beat frequency which exists between the x-band signals in the continuous and calibrate channels at one end of the sweep. Measurement of every 22.5 degrees of phase shift at 256 megacycles provides the required accuracy of 0.128 feet.

B. PRINCIPLE OF BASELINE STABILIZATION

One of the features of the MISTRAM system not common to other interferometer systems on the range is the automatic compensation of phase-shift produced by the transit time of signals traveling from the outlying sites to the central site. The principle is illustrated in Figure 5. The wave emitted by the transponder is detected in the Central receiver R_0 and carries on it the phase information ϕ_0 representing the transit time. The same wave is detected by an outlying receiver R_1 and carries on it the phase information ϕ_1 representing the transit time to the outlying site. To make a phase comparison this signal must be forwarded to the Central site and, therefore, incurs a phase shift δ representing the transit time from the remote to the Central site.

The method of removing this unwanted phase shift consists of four steps:

1. Transmit the signal received at the Central site to the remote site and return it. This signal now has superimposed upon it twice the phase shift of the one-way trip.
2. At the Central site, subtract from the returned signal [1024 $(\omega t+\phi_o+2\delta)$] the signal from the remote site [1024 $(\omega t + \phi_1 + \delta_1)$] to yield [1024 $(\phi_o-\phi_1+\delta_1)$].
3. At the Central site, subtract from the signal received at the Central site [1024 $(\omega t + \phi_o)$] the signal received at the outlying site [1024 $(\omega t + \phi_1 + \delta_1)$] to yield [1024 $(\phi_o-\phi_1-\delta_1)$].
4. At the Central site, add the two signals generated in steps 2 and 3:

   [1024 $(\phi_o-\phi_1+\delta_1)$] + [1024 $(\phi_o-\phi_1-\delta_1)$] = 1024 (2)$(\phi_o-\phi_1)$.

   The baseline phase shift has, therefore, been eliminated.

GENERAL DESCRIPTION OF THE DATA REDUCTION PROCESS Figure 6

The Mistram system at Valkaria transmits via a microwave relay link the tracking information produced by the Precision Measuring Subsystem. This is received by antennas on top of the Technical Laboratory located at Patrick Air Force Base. The data are relayed to the Cape by another microwave relay link and also recorded on a 729 low density tape to produce another raw data tape. This tape provides the input data to the IBM 7090 computer and is operated on by two programs (MTMA 1 and MTMC) which convert the raw data from counts to feet, apply corrections and transform

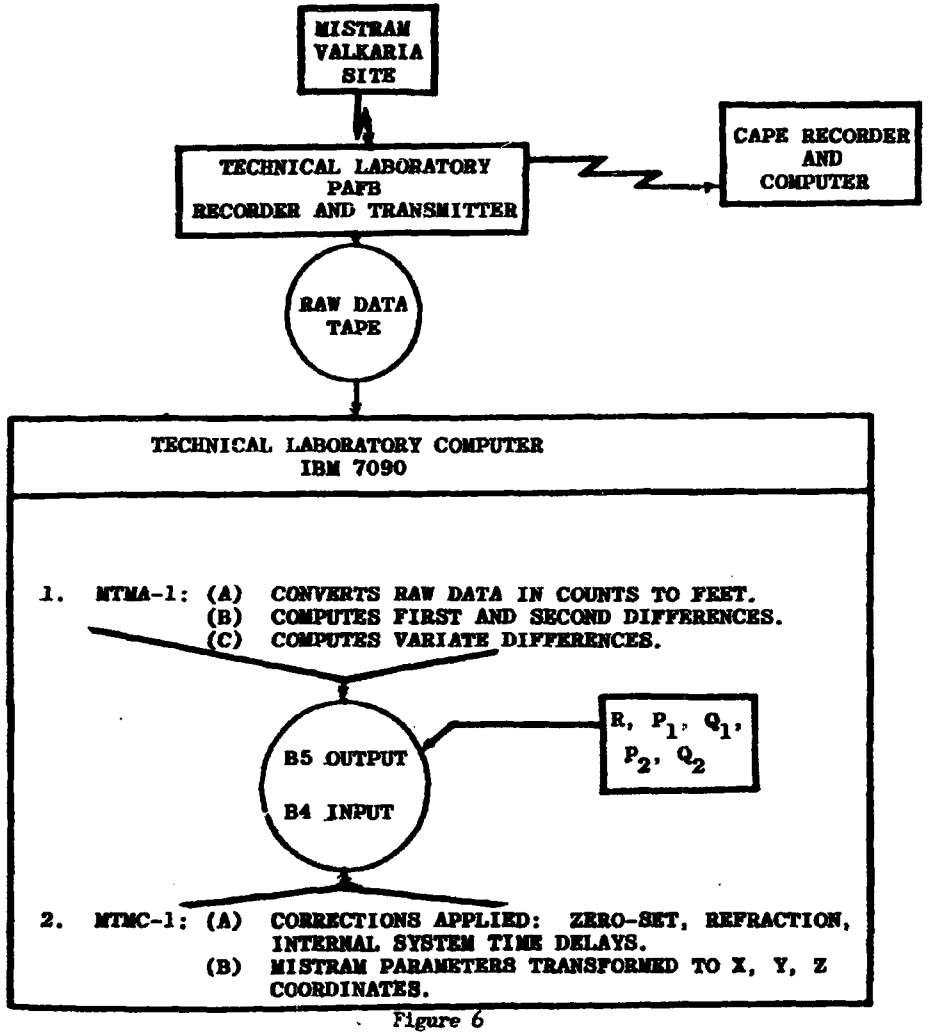
MISTRAM
VALKARIA
SITE
TECHNICAL LABORATORY
PAFB
RECORDER AND TRANSMITTER
CAPE RECORDER
AND
COMPUTER
RAW DATA
TAPE
TECHNICAL LABORATORY COMPUTER
IBM 7090
1. MTMA-1: (A) CONVERTS RAW DATA IN COUNTS TO FEET.
(B) COMPUTES FIRST AND SECOND DIFFERENCES.
(C) COMPUTES VARIATE DIFFERENCES.
B5 OUTPUT
B4 INPUT
R, P_1, Q_1,
P_2, Q_2
2. MTMC-1: (A) CORRECTIONS APPLIED: ZERO-SET, REFRACTION,
INTERNAL SYSTEM TIME DELAYS.
(B) MISTRAM PARAMETERS TRANSFORMED TO X, Y, Z
COORDINATES.

Figure 6

the MISTRAM parameters into X, Y, Z Coordinates. More detailed descriptions of these two programs taken from the program description documents are as follows:

MTMA-1:

"The purpose of this program is to process data from raw MISTRAM tapes. Each tape record consists of data quantities packed into an eight-word record as specified in the mathematics section. This program unpacks and processes these quantities. Range and range differences are converted from binary integers to scaled floating point values in double precision. Time is converted to seconds as either generated time with increments of .05 seconds or raw time. First, second, and variate differences are computed for range and range differences. Refractive index data is converted to floating point values in single precision.

Three channels of output are provided.

(1) Time, range, range differences, refractive indexes to floating binary tape.

(2) Time, range, range differences, 1st and 2nd differences, refractive indexes, and variate differences to CD tape.

(3) One file of the raw MISTRAM input is copies on an output tape as an optional feature.

MTMB-1:

"This program accepts as input a binary tape written by MTMA-1 containing the basic Mistram output, R, P_1, Q_1, R_2, and Q_2, in

double precision floating point along with time, flags, refractometer readings, signal strength, and spares.

Corrections found to be necessary through editing are read from cards and applied. All internal system time delays are corrected by the program according to the error model provided by the manufacturer relative to such delays. The program computes and applies a refraction correction to each basic measurement. This correction accounts for the apparent bending and shortening of the actual ray path due to an index of refraction profile described by a set of points connected by an exponential through each two points and asymptotic to unity. The set of points mentioned is the profile read from cards.

The output contains fully corrected R, P_1, Q_1, P_2, and Q_2 data (in feet) in double precision floating point form as well as the indicated cartesian data from the 10K ft. and 100K ft. baseline systems. Also ℓ, m, R data from each system is produced for use as input into an AZAR4 like program or into the existing quick-look programs.

"This program is specifically designed for use in the initial Mistram evaluation program and operates almost completely with double precision arithmetic in order to insure against loss of precision."

THE ACCURACY EVALUATION OF THE MISTRAM SYSTEM

A. The Design Performance

Before proceeding to the discussion of the observed performance of the Mistram System, the expected design performance will be reviewed.

The General Electric Company conducted an intensive error analysis study on the Mistram System and published their results in 1959 in a five-volume report. At that time, the five Mistram parameters were expected to be measured with the accuracy shown in Table 1. These numbers included propagation effects, but specifically excluded the uncertainty in the free-space speed of light. They were based upon a data recording rate of twenty points per second and a smoothing time of 1/2 second. These error estimates were the result of combining equipment errors, referencing errors, propagation errors, and survey errors.

Further studies were conducted by the General Electric Company and, in July of 1962, the results of additional study were published with an error budget illustrated in Table 2. These errors were then propagated into the trajectory defined in Table 3, a nominal trajectory of a liquid fuel missile. For this particular trajectory, the errors produced by the uncertainties in the speed of light and refraction were computed and are shown in Table 4.

PREDICTED MISTRAM STANDARD ERRORS, 1959

GENERAL ELECTRIC COMPANY

POSITION		VELOCITY	
$\hat{\sigma}_R$	= 0.4 FOOT	$\hat{\sigma}_{\dot{R}}$	= 0.02 FOOT/SECOND
$\hat{\sigma}_{P_1}$	= 0.03 FOOT	$\hat{\sigma}_{\dot{P}_1}$	= 0.001 FOOT/SECOND
$\hat{\sigma}_{Q_1}$	= 0.03 FOOT	$\hat{\sigma}_{\dot{Q}_1}$	= 0.001 FOOT/SECOND
$\hat{\sigma}_{P_2}$	= 0.3 FOOT	$\hat{\sigma}_{\dot{P}_2}$	= 0.002 FOOT/SECOND
$\hat{\sigma}_{Q_2}$	= 0.3 FOOT	$\hat{\sigma}_{\dot{Q}_2}$	= 0.002 FOOT/SECOND

INCLUDES: PROPAGATION, ZERO-REFERENCING, EQUIPMENT AND SURVEY ERRORS.

EXCLUDES: UNCERTAINTY IN FREE-SPACE SPEED OF LIGHT.

Table 1

ERROR BUDGET FOR VALKARIA MISTRAM SYSTEM

PREPARED BY

THE GENERAL ELECTRIC COMPANY

JULY, 1962

Survey Errors

	one sigma error
a) external angles	1.48 sec of arc
b) internal angles	1.04 sec of arc
c) 10K baselines	1.48 ppm
d) 100K baselines	2.96 ppm
e) external lengths	2.96 ppm

Timing Errors

$$\Delta R = \dot{R}\Delta t \qquad \Delta \dot{R} = \ddot{R}\Delta t$$
$$\Delta P = \dot{P}\Delta t \qquad \Delta \dot{P} = \ddot{P}\Delta t$$
$$\Delta Q = \dot{Q}\Delta t \qquad \Delta \dot{Q} = \ddot{Q}\Delta t$$

where $\Delta t = \pm$ 5 microseconds

Speed of Light Errors

$$\Delta R = R\frac{\Delta c}{c} = .667 \times 10^{-6}(R) \text{ ft.}$$
$$\Delta \dot{R} = \dot{R}\frac{\Delta c}{c} = .667 \times 10^{-6}(\dot{R}) \text{ ft/sec}$$

MISTRAM Error

$\sigma(R) = .4$ ft $\qquad \sigma(\dot{R}) = .02$ ft/sec

$\sigma(P_1, Q_1) = .03$ ft $\qquad \sigma(\dot{P}_1, \dot{Q}_1) = .001$ ft/sec

$\sigma(P_2, Q_2) = .3$ ft $\qquad \sigma(\dot{P}_2, \dot{Q}_2) = .002$ ft/sec

Refraction Errors

Refraction errors are interpolated from graphs of range error vs. apparent range for various target altitudes.

TABLE 2

NOMINAL TRAJECTORY OF A LIQUID FUELED MISSILE

GENERAL ELECTRIC COMPANY

TRAJECTORY (REFERENCED TO MISTRAM)

x - east y - north z - normal to spheroid

POINT	Coordinate	Position	Velocity
1.	x	8501.3	602.358
	y	199867.75	-180.623
	z	28568.3	1111.7908
2.	x	69688.7	2791.290
	y	181028.36	-867.3304
	z	91970.6	2120.4505
3.	x	409310.1	7821.070
	y	74038.01	-2478.7114
	z	275831.5	3383.0281
4.	x	972954.6	11183.098
	y	-133870.24	-4793.9729
	z	468030.7	2941.3943
5.	x	1807397.3	17490.518
	y	-537091.89	-9179.3539
	z	626431.3	2295.7690
6.	x	3154516.5	20625.795
	y	1267683.34	-11302.856
	z	726596.6	663.2224

TABLE 3

ERRORS CAUSED BY REFRACTION AND SPEED OF LIGHT

PREPARED BY

THE GENERAL ELECTRIC COMPANY

JULY, 1962

REFRACTION ERRORS

IN FEET

POINT	R	P_1	Q_1	P_2	Q_2	$\dot{R}$	$\dot{P}_1$	$\dot{Q}_1$	$\dot{P}_2$	$\dot{Q}_2$
1.	.787	1.14	1.16	1.31	1.48	-	-	-	-	-
2.	.3	.424	.424	.557	.578	-	-	-	-	-
3.	.239	.338	.338	.38	.362	-	-	-	-	-
4.	.312	.441	.441	.344	.312	-	-	-	-	-
5.	.443	.626	.626	.638	.619	-	-	-	-	-
6.	.707	1.0	1.0	1.01	1.0	-	-	-	-	-

SPEED OF LIGHT ERRORS

	FEET					FEET PER SECOND				
POINT	R	P_1	Q_1	P_2	Q_2	$\dot{R}$	$\dot{P}_1$	$\dot{Q}_1$	$\dot{P}_2$	$\dot{Q}_2$
1.	.131	-	-	-	-	-	-	-	-	-
2.	.139	-	-	-	-	-	-	-	-	-
3.	.324	-	-	-	-	-	-	-	-	.003
4.	.706	-	-	-	-	-	-	-	-	-
5.	1.29	-	-	-	-	.012	-	-	-	
6.	2.259	-	-	-	.066	.009	-	-	-	

Errors due to refraction and speed of light uncertainty are functions of position. Listed are the significant values calculated for the sample trajectory. Quantities which have negligible effect on the total error are deleted.

TABLE 4

The standard errors in position are illustrated in Figures 7, 8 and 9. The lower curve is the error introduced by equipment errors only and the top curve is the total of all errors. These curves indicate that the standard error in X and Y referenced to the launch pad for this typical trajectory varies from approximately 2.0 feet (minimum) near acquisition to approximately 40 feet maximum near burnout with all errors considered. In the Z-component the error extends from 4 feet (minimum) just past acquisition to approximately 190 feet at burnout. The velocity accuracies are illustrated in Figures 10, 11 and 12 When the total errors are propagated, $\sigma_{\dot{x}}$ and $\sigma_{\dot{y}}$ vary from approximately 0.01 foot per second to 0.2 foot per second; $\sigma_{\dot{z}}$ varies from as little as 0.1 foot per second to as high as 2 feet per second near burnout.

These accuracy capabilities are, by design, to extend over the following volume of coverage and range of velocity and acceleration.

Volume of Coverage

Azimuth:	360 degrees
Elevation:	1. 5 to 85 degrees
	2. zero to 90 degrees, decreased accuracy.
Range:	1. 20 to 600 nautical miles, full accuracy.
	2. 20 to 1000 + nautical miles, decreased accuracy. (Range is signal-level

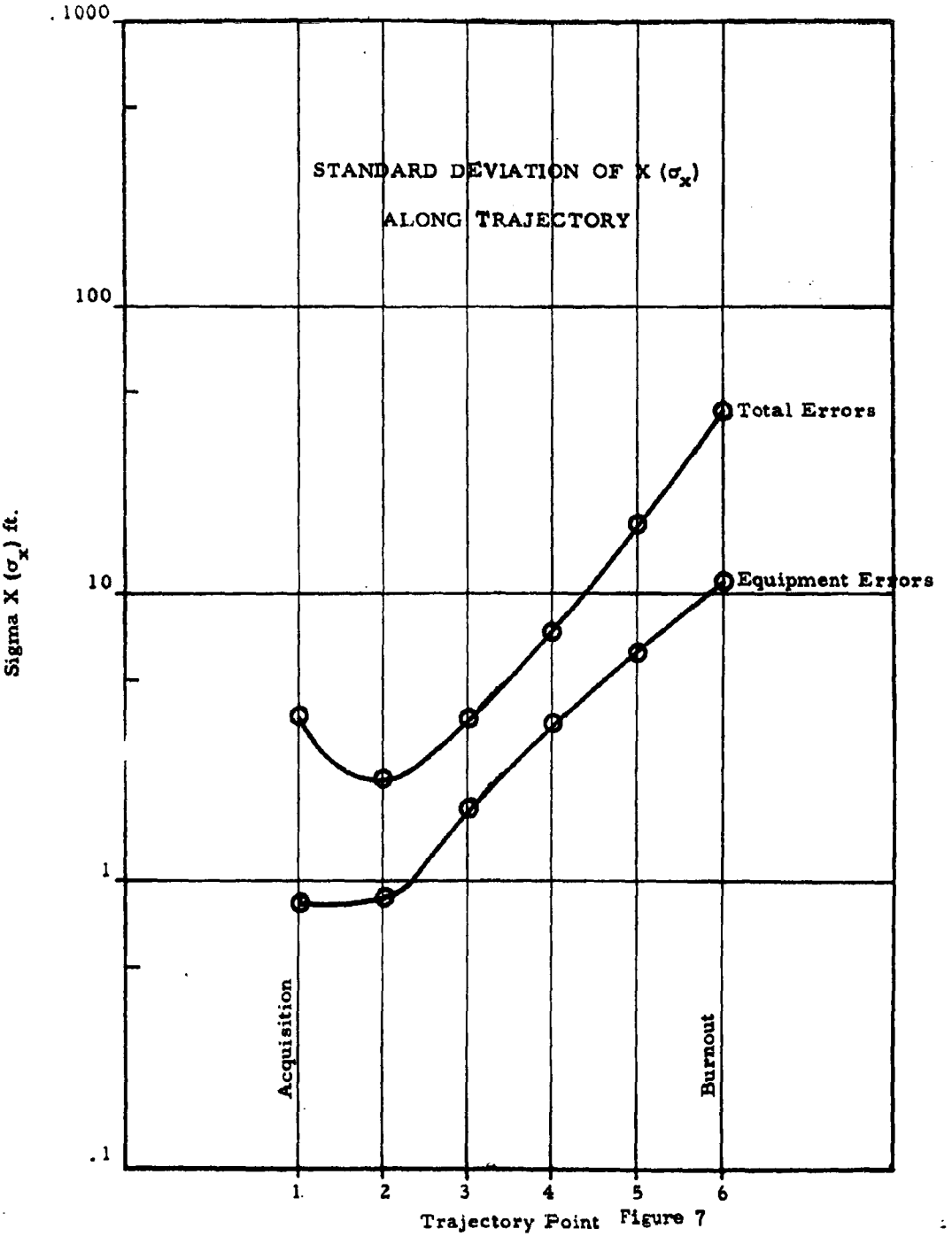
STANDARD DEVIATION OF X (σ_x)
ALONG TRAJECTORY
Sigma X (σ_x) ft.
1000
100
10
1
.1
Total Errors
Equipment Errors
Acquisition
Burnout
1
2
3
4
5
6
Trajectory Point

Figure 7

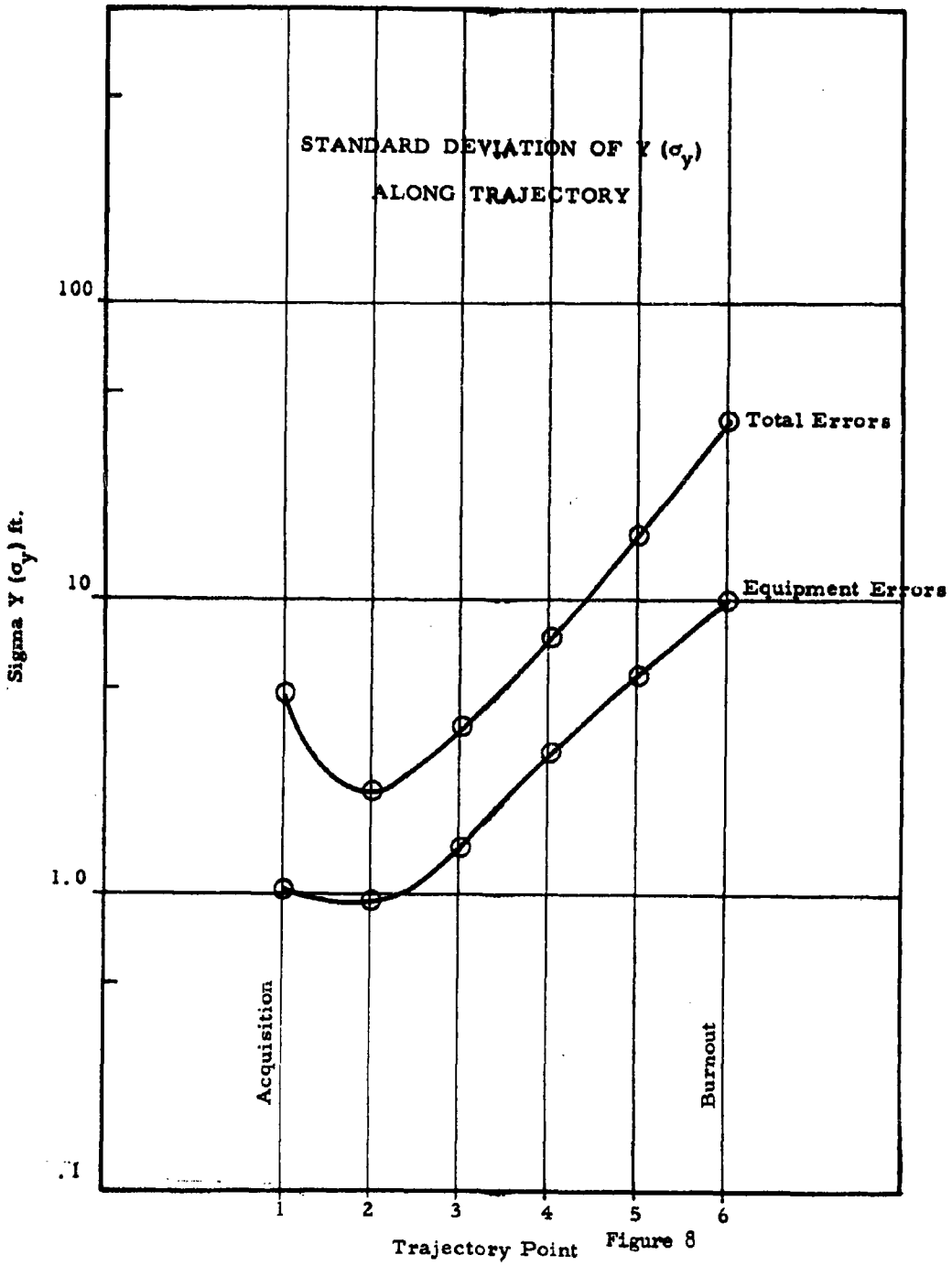
STANDARD DEVIATION OF Y (σ_y)
ALONG TRAJECTORY
100
10
1.0
.1
Sigma Y (σ_y) ft.
Total Errors
Equipment Errors
Acquisition
Burnout
1
2
3
4
5
6
Trajectory Point

Figure 8

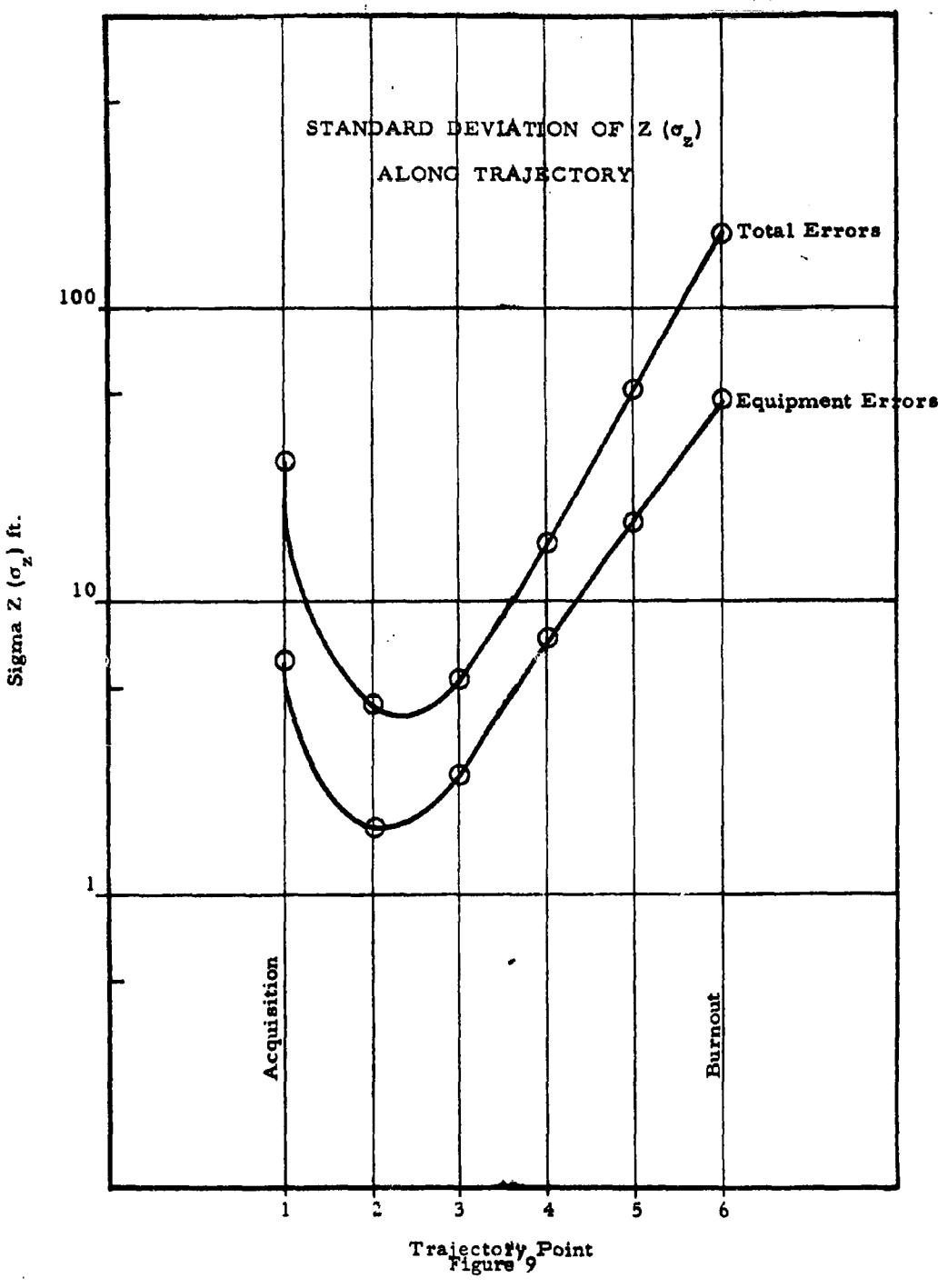
STANDARD DEVIATION OF Z (σ_z)
ALONG TRAJECTORY
Total Errors
Equipment Errors
100
10
1
Sigma Z (σ_z) ft.
Acquisition
Burnout
1
2
3
4
5
6
Trajectory Point

Figure 9

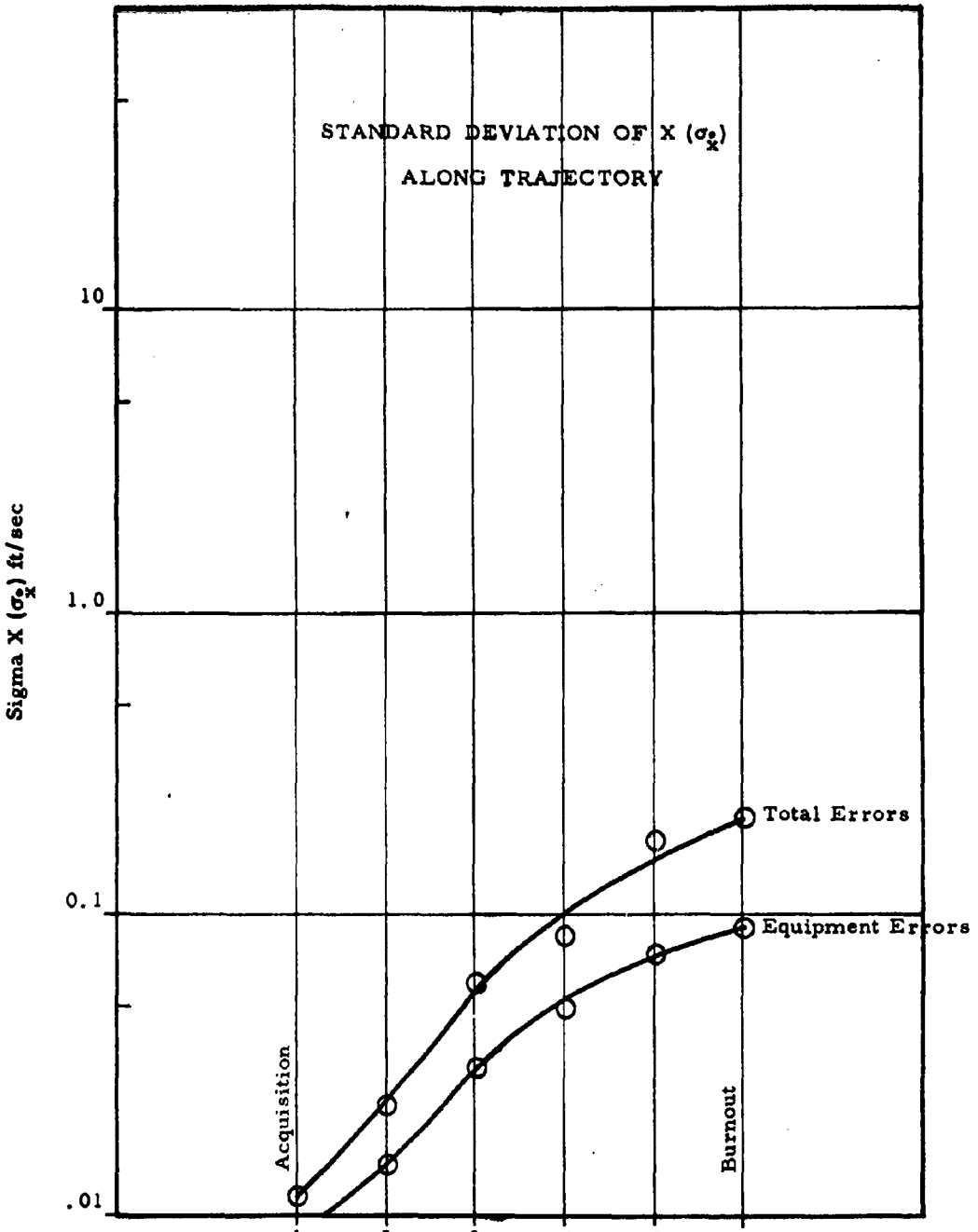
STANDARD DEVIATION OF X ($\sigma_{\dot{x}}$)
ALONG TRAJECTORY
Sigma X ($\sigma_{\dot{x}}$) ft/sec
10
1.0
0.1
.01
Total Errors
Equipment Errors
Acquisition
Burnout
1
2
3
4
5
6
Trajectory Point

Figure 10

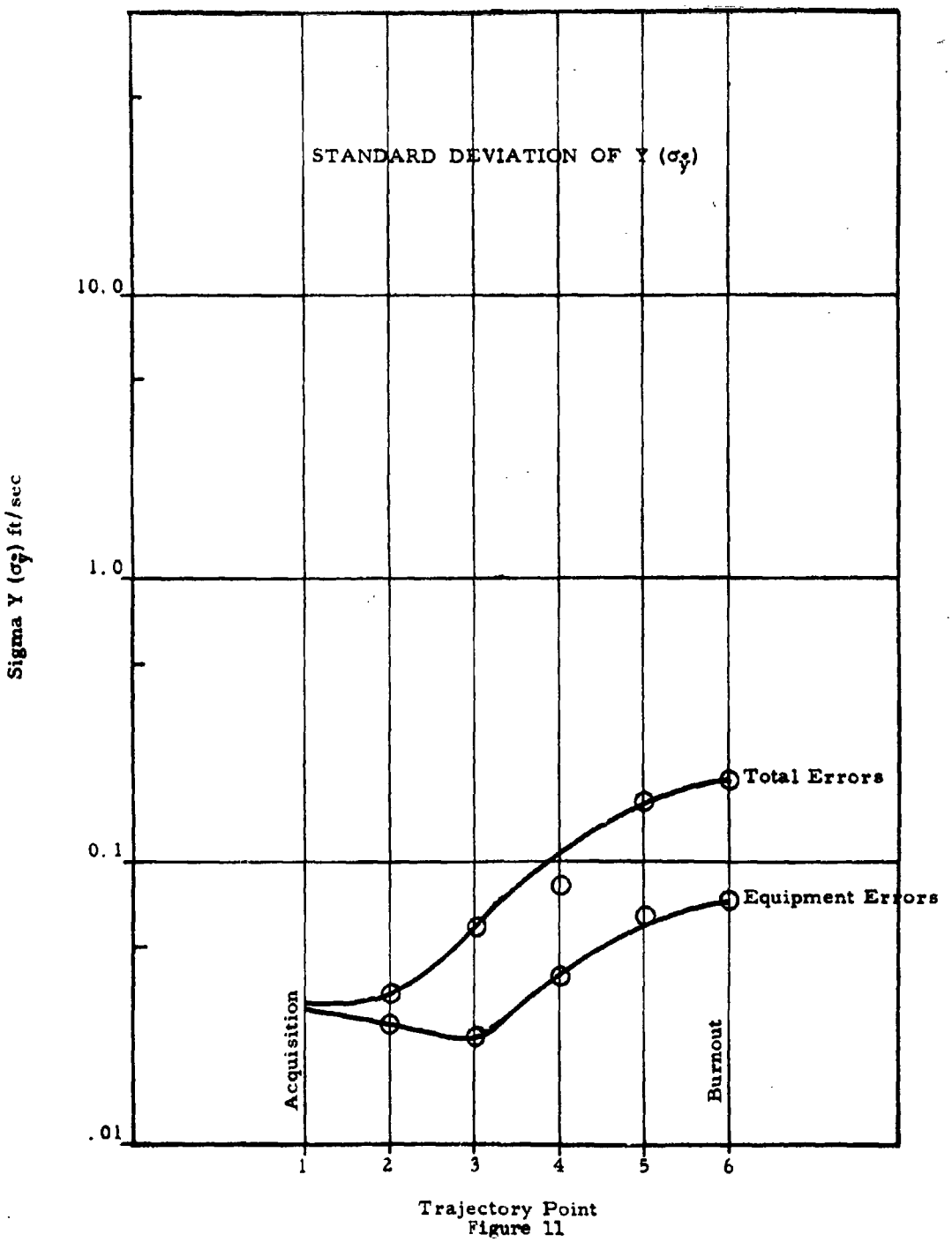
STANDARD DEVIATION OF Y ($\sigma_{\dot{y}}$)
Sigma Y ($\sigma_{\dot{y}}$) ft/sec
10.0
1.0
0.1
.01
Total Errors
Equipment Errors
Acquisition
Burnout
1
2
3
4
5
6
Trajectory Point

Figure 11

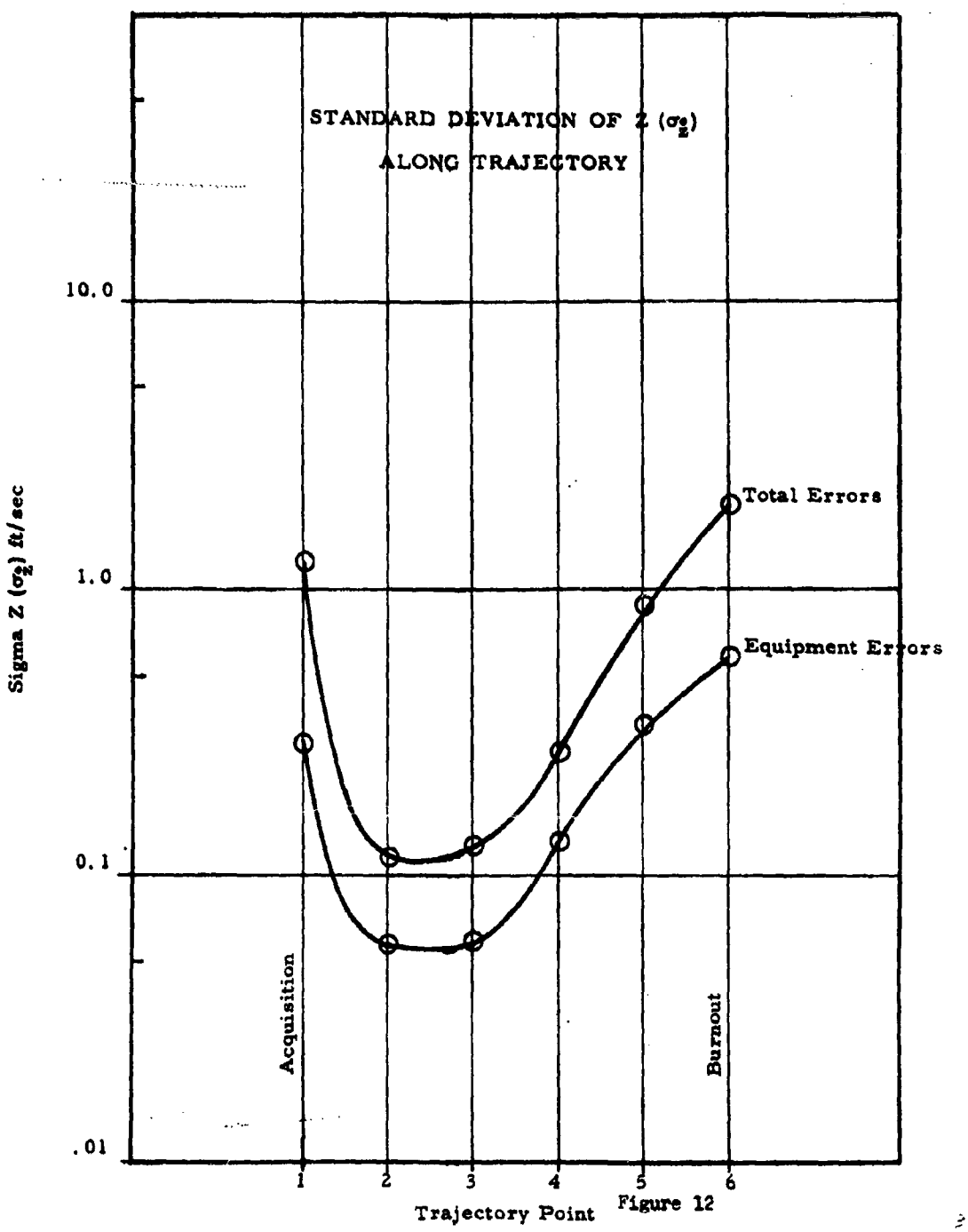
STANDARD DEVIATION OF Z ($\sigma_{\ddot{z}}$)
ALONG TRAJECTORY
10.0
1.0
0.1
.01
Sigma Z ($\sigma_{\ddot{z}}$) ft/sec
Total Errors
Equipment Errors
Acquisition
Burnout
1
2
3
4
5
6
Trajectory Point

Figure 12

limited, and full range depends upon the application.)

Velocity and Acceleration

Range velocity:	zero to 50,000 ft/sec.
Range acceleration:	zero to 750 ft/sec^2.
Rate of change of range acceleration:	zero to 80 ft/sec^2 per second.
Range difference velocity:	zero to 45 degrees/sec.
Azimuth and elevation tracking rate:	zero to 45 degrees/sec.
Azimuth and elevation acceleration:	zero to 250 degrees/sec^2.

B. The Observed Accuracy Performance

The Mistram system was originally intended to be subjected to an orderly evaluation based primarily upon aircraft tests before it was committed to tracking live missiles. Unavoidable delays, however, created the situation in which the system tracked several missile tests before the aircraft tests were flown. The evaluation, therefore, has been that of appraising system performance on both missile and aircraft tests concurrently.

The summarized results appear in Table 5.

The estimated accuracies of the system parameters are within a factor of two of the predicted values except for the range

PRELIMINARY ESTIMATES OF VALKARIA MISTRAM ACCURACY

10 JANUARY 1963

	POSITION			VELOCITY **	
	PREDICTED 1959 (G. E.)	ESTIMATED * 1963		PREDICTED 1959 (G. E.)	ESTIMATED * 1963
σ_R	- 0.4 FOOT	1.45 FOOT	$\sigma_{\dot{R}}$	0.02 FOOT/SEC.	0.03 FOOT/SEC.
σ_{P_1,Q_1}	- 0.03 FOOT	0.05 FOOT	$\sigma_{\dot{P}_1,\dot{Q}_1}$	0.001 FOOT/SEC.	0.001 FOOT/SEC.
σ_{P_2,Q_2}	- 0.3 FOOT	0.5 FOOT	$\sigma_{\dot{P}_2,\dot{Q}_2}$	0.002 FOOT/SEC.	0.004 FOOT/SEC.

* BASED UPON FIVE TITAN FLIGHTS AND 21 AIRCRAFT FLIGHTS OVER 36 CAMERA FIELDS; KNOWN AMBIGUITIES HAVE BEEN REMOVED.

** 13 POINT SMOOTHING.

Table 5

parameter which is about 3 1/2 times the predicted value. When these errors are propagated into a nominal trajectory, the results are as shown in Figures 13 and 14. The observed accuracy estimates are not too different from the predicted values.

In addition to the accuracy performance of the system, some information has been compiled concerning the length of time the system provides data useful for post-flight analysis. The number of seconds of data characterized by the accuracy figures just presented is illustrated in Figure 15 for five missile tests. The loss of data in the last two tests was caused by loss of the transponder signal, though the transponder itself may not have been at fault.

C. BRIEF DESCRIPTION OF THE AIRCRAFT EVALUATION

1. Statistical Design of the Experiments

Last year I had the privilege of presenting a paper at this meeting whose title was "System Evaluation Philosophy and Its Application". This paper discussed the statistical design of experiments. Two general types of experiments were described; (1) those in which the factors believed to be producing deviations (errors) in the data can be controlled and (2) those in which they cannot be (or, at least, are not) controlled. The analysis of variance was presented for an example of the first type, and the basic principles of regression analysis which are used to extract results from the second type were set forth. The current aircraft tests

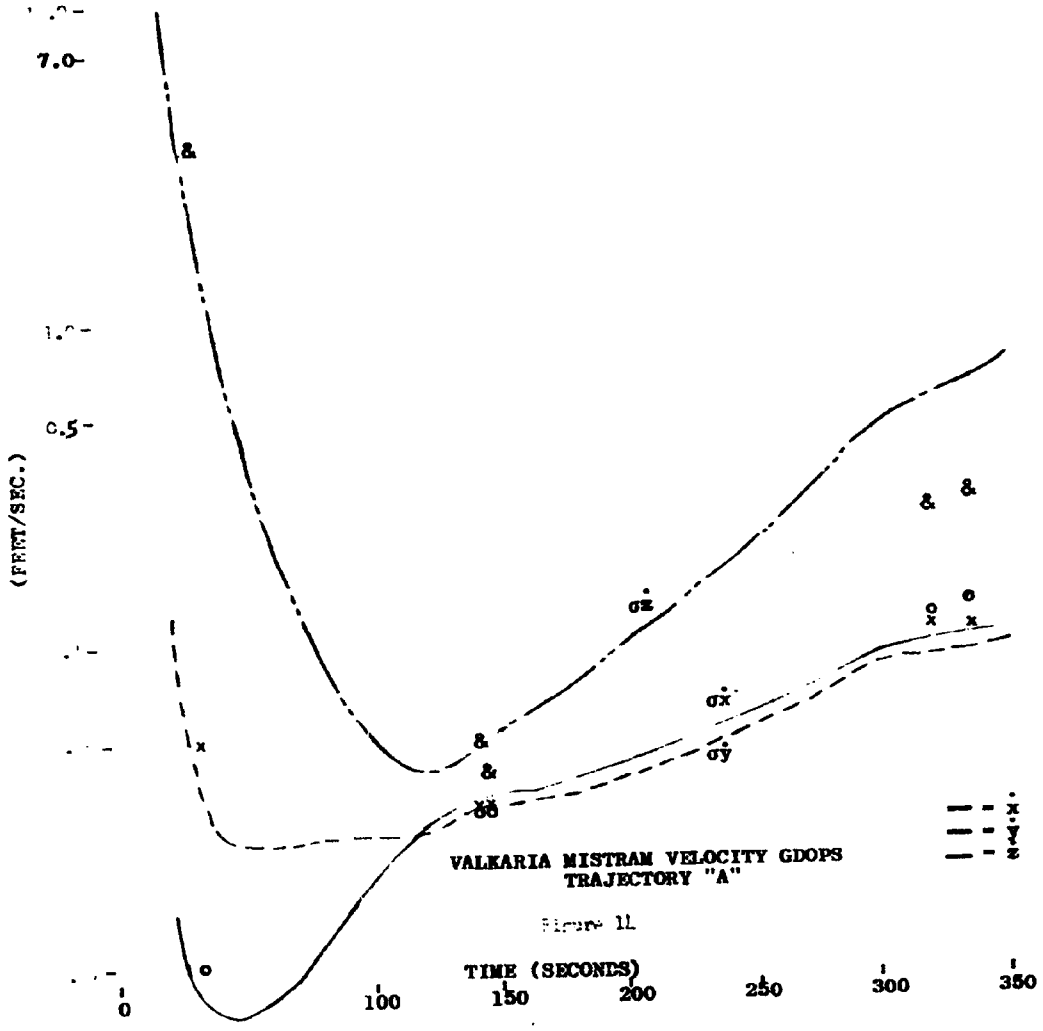
7.0
0.5
(FEET/SEC.)
TIME (SECONDS)
0
100
150
200
250
300
350
VALKARIA MISTRAM VELOCITY GDOPS
TRAJECTORY "A"

Figure 11

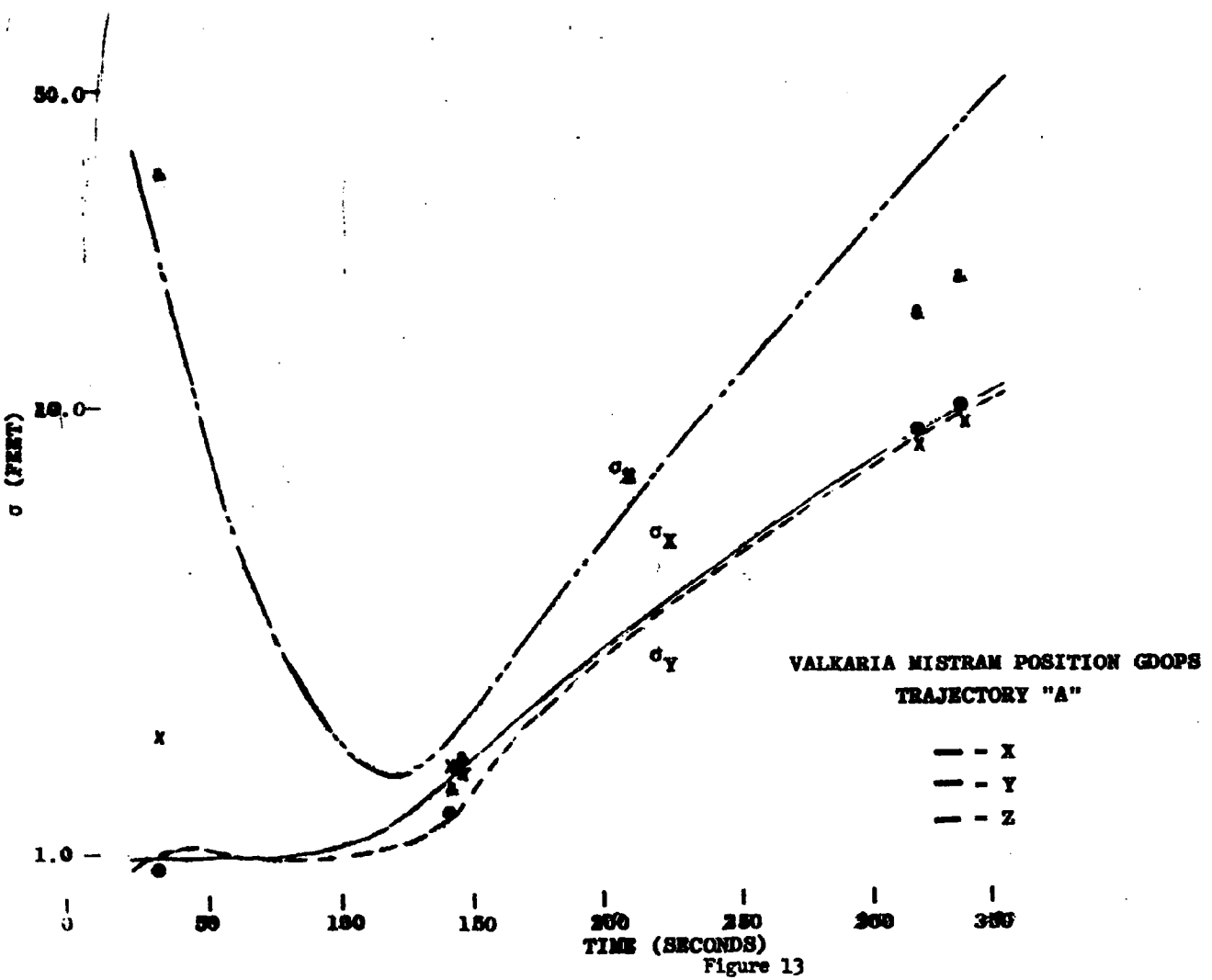
50.0
10.0
1.0
σ (FEET)
σ_Z
σ_X
σ_Y
VALKARIA MISTRAM POSITION GDOPS
TRAJECTORY "A"
X
Y
Z
0
50
100
150
200
250
300
350
TIME (SECONDS)
Figure 13

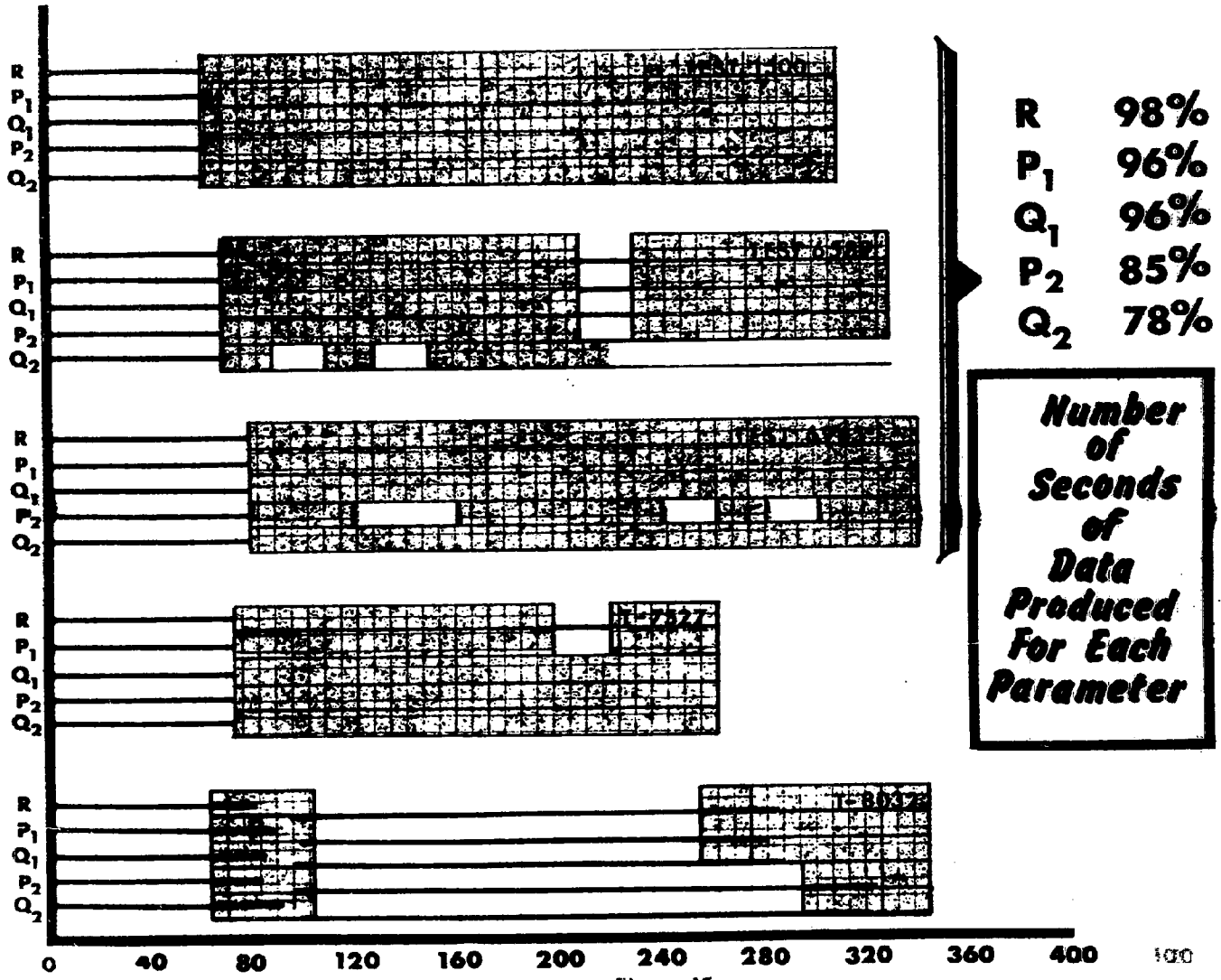
R
P1
Q1
P2
Q2
0
40
80
120
160
200
240
280
320
360
400
R 98%
P1 96%
Q1 96%
P2 85%
Q2 78%
Number of Seconds of Data Produced For Each Parameter

Figure 15

are based upon these principles.

The original experimental design concept for the MISTRAM aircraft evaluation is shown in Table 6. This is a factorial arrangement in which the effects of each of four factors [camera complex, flight direction, target (beacon plus aircraft), and test (night)] as well as their interactions can be quantitatively assessed for statistical significance. This design required sixteen aircraft runs each night to achieve complete orthogonality, and this was considered to be too expensive from both the financial and time points of view.

The design finally agreed upon is shown in Table 7. It is based upon the characteristics of a Latin square, but it is not a pure Latin square design. The indepedent variables to be assessed for their significance in producing unwanted deviations in the output data were camera complexes (not shown), flight directions, signal levels, and altitudes. The effect of different beacons cannot be dete-rmined from this design because only one beacon is used during each test (i.e., each night). The flight plans are shown in Figure 17.

The orthogonality shown in either of these tests was not realized in the results which are to be discussed. The reason for this is, of course, the many practical

GENERAL ELECTRIC PROPOSAL ARRANGED IN A FOUR-FACTOR RANDOMIZED BLOCK EXPERIMENT. COMPLEX NO. 5 AND RUN NO. 3 HAVE BEEN OMITTED.

(D) COMPLEX	(C) DIRECTION	NIGHT 1 (B)		NIGHT 2 (B)			NIGHT k (B)	
		(A) TARGET 1	(A) TARGET 2	(A) TARGET 1	(A) TARGET 2		(A) TARGET 1	(A) TARGET 2
1	(1) Cl 157° (5) Cl 48.5°							
	(6) Ccl 337° (9) Ccl 228.5°							
2	(1) Cl 157° (4) Cl 239°							
	(6) Ccl 337° (8) Ccl 50°							
3	(4) Cl 230° (2) Cl 314°							
	(8) Ccl 50° (7) Ccl 134°							
4	(2) Cl 314° (5) Cl 48.5°							
	(7) Ccl 134° 228.5°							

Table 6

STATISTICAL TEST DESIGN BASED UPON A LATIN SQUARE

GENERAL ELECTRIC COMPANY

TEST NUMBER	LOOP NUMBER	RUNS	DIRECTION C-CLOCKWISE CC-COUNTER-CLOCKWISE	SIGNAL LEVEL	ALTITUDE (THOUSANDS OF FEET)	BEACON
1	1	5 and 4	C	HIGH	25	1
	2	6 and 7	CC	LOW	40	1
2	1	8 and 9	CC	HIGH	25	2
	2	1 and 2	C	LOW	40	2
3	1	4 and 5	C	HIGH	40	3
	2	7 and 6	CC	LOW	25	3
4	1	9 and 8	CC	HIGH	40	4
	2	2 and 1	C	LOW	25	4

Table 7

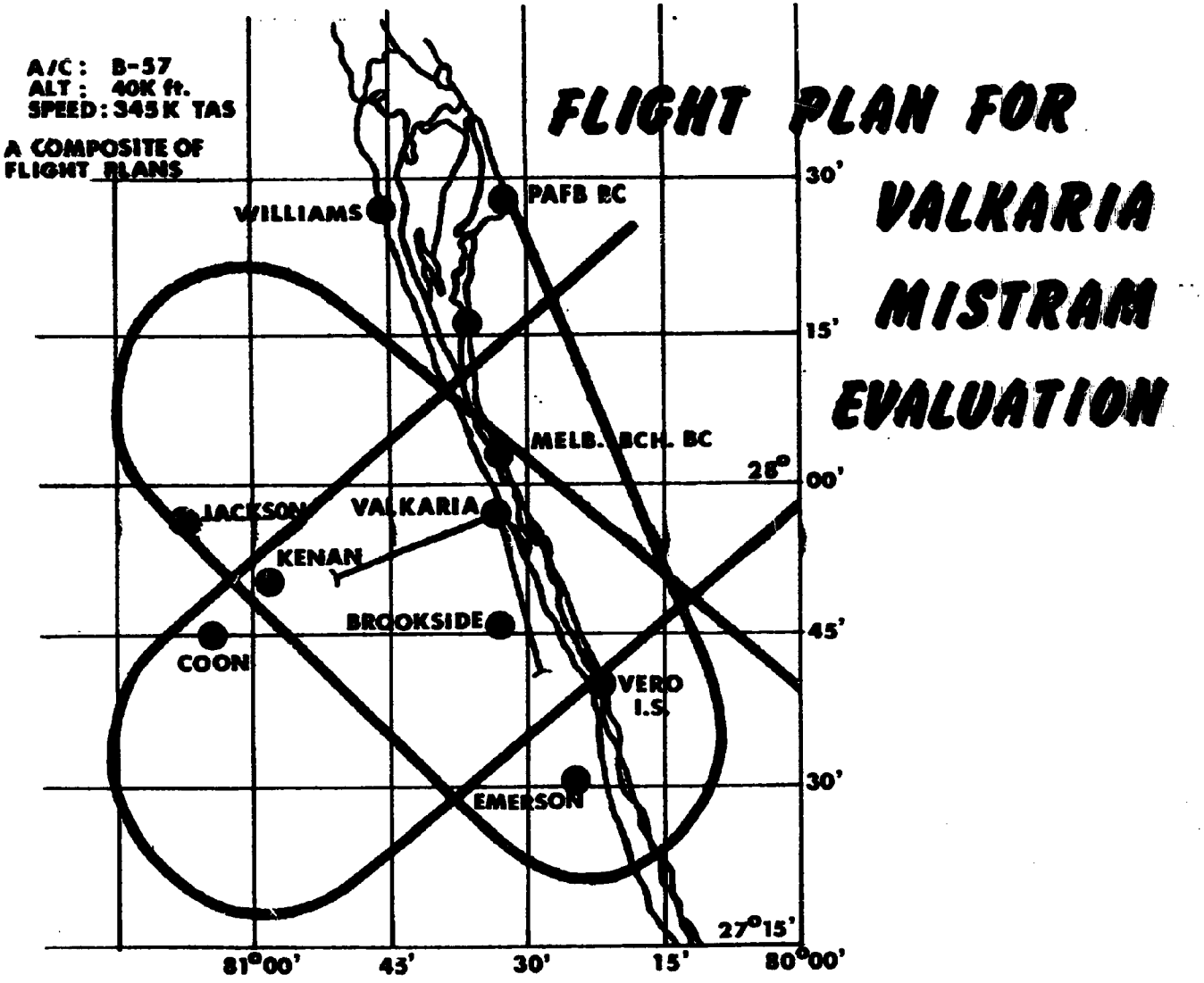
A/C : B-57
ALT : 40K ft.
SPEED: 345 K TAS
A COMPOSITE OF FLIGHT PLANS
FLIGHT PLAN FOR
VALKARIA
MISTRAM
EVALUATION
WILLIAMS
PAFB BC
MELB. BCH. BC
JACKSON
VALKARIA
KENAN
BROOKSIDE
COON
VERO I.S.
EMERSON
30'
15'
28° 00'
45'
30'
27°15'
81°00'
43'
30'
15'
80°00'

Figure 17

difficulties of conducting a test. The factors of weather, equipment operation, and coordination of all personnel and equipment almost precludes the successful conduct of such a design. It is for this reason that one finally resorts to the method of analysis called regression analysis. The exercise of designing an experiment as shown in the previous slides, however, is of great benefit because it brings out those factors that are likely to be most significant, the manner in which the test might be conducted to the greatest advantage from the point of view of obtaining orthogonality, and allows estimates to be made of the nature and number of flights necessary to estimate a given number of parameters with a desired confidence.

The degree of success in attaining the planned design is shown in Table 8. No variation in signal level or altitude was introduced so there is no information on the effects of these factors. Of the 21 runs producing usable data, 12 fit the concept of the original design (with exceptions noted above) and represent three tests, two camera complexes, two directions, and three beacons. The data from the remaining nine runs combined with those of these 12 provide other possible comparisons.

DEGREE OF SUCCESS IN ATTAINING PLANNED EXPERIMENTAL DESIGN

Test No.	Camera Complex	Loop No.	Runs	Direction	Signal Level	Altitude	Beacon
6365	I	1	F1	C	↑	40K	No. 7
		2	F6	CC	NO	40K	No. 7
	II	1	F4	C		40K	No. 7
		2	F8	CC		40K	No. 7
6433	I	1	F5	C		40K	No. 8
		2	F6	CC		40K	No. 8
	II	1	F4	C	CHANGE	40K	No. 8
		2	F6	CC		40K	No. 8
6434	I	1	F1	C		40K	No. 2
		2	F6	CC		40K	No. 2
	II	1	F1	C		40K	No. 2
		2	F6	CC	↓	40K	No. 2

Table 8

The principle method of analysis, however, is that of regression which allows all of the data to be used whether or not orthogonality exists. The results of this analysis are not complete at the time of writing, but they are expected to be available by the time of the meeting and will be presented.

2. The Error Model

In order to conduct a regression analysis on a set of data one must decide upon a set of independent variables which are believed to contribute to the deviations in the data. Each of these independent variables is multiplied by a constant and it is these constants that must be determined from the data.

Before a choice of independent variables can be made one must have some degree of understanding of the nature of the system producing the data and the possible sources of error. It is for this reason that it is highly desirable to have what is often referred to as an error model for the system under investigation. The term "error model" means different things to different people. I specifically refer to an equation which relates the deviation in a system parameter (range, for example) to the parameters of the system that enter into its determination. On a system as complex as Mistram this equation can be extremely complex if all factors are taken into consideration. We do not have this equation at this time. We do have,

however, a regression equation that is based upon physical considerations of the system behavior. The five major sources of error and the form of their appearance in range, range differences, and range rate differences are illustrated in Figure 18. The represent timing, both internal and external, propagation (this is, refraction), the uncertainty in the speed of light, the change in frequency of the master oscillator, and the zero-set,

The regression equations for R, P, and Q are as follows:

$$\Delta R = a_o + a_1 \dot{R}_o + a_2 \left[\tilde{R}_o \csc^2 E_o\right]$$

$$\Delta P_1 = b_o + b_1 \dot{P}_1 + b_2 \dot{R}_o + b_3 \left[\tilde{R}_o \ (\csc^2 E_o) - \tilde{R}_2 \ (\csc^2 E_2)\right]$$

$$\Delta Q_1 = c_o + c_1 \dot{Q}_1 + c_2 \dot{R}_o + c_3 \left[\tilde{R}_o \ (\csc^2 E_o) \ - \tilde{R}_1 \ (\csc^2 E_1)\right]$$

$$\Delta P_2 = d_o + d_1 \dot{P}_2 + d_2 \dot{R}_o + d_3 \left[\tilde{R}_o \ (\csc^2 E_o) - \tilde{R}_4 \ (\csc^2 E_4)\right]$$

$$\Delta Q_2 = e_o + e_1 \dot{Q}_2 + e_2 \dot{R}_o + e_3 \left[\tilde{R}_o \ (\csc^2 E_o) - \tilde{R}_3 \ (\csc^2 E_3)\right]$$

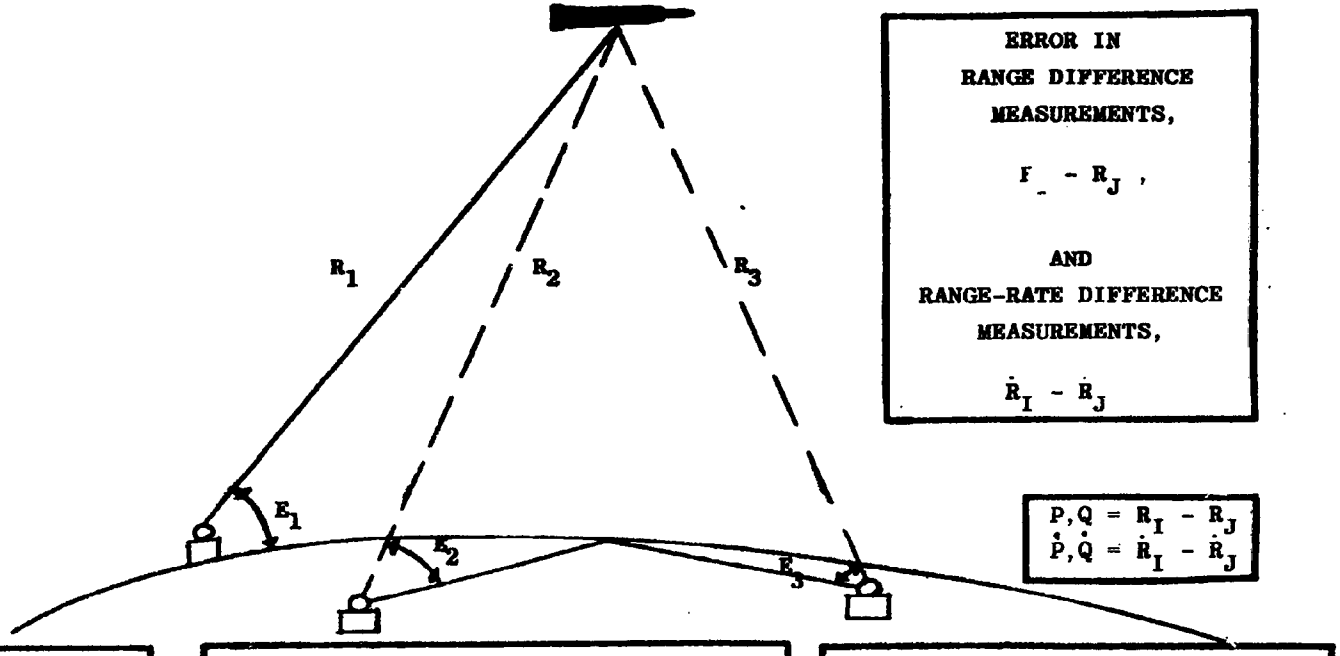

ERROR IN RANGE DIFFERENCE MEASUREMENTS,

$R_I - R_J$,

AND RANGE-RATE DIFFERENCE MEASUREMENTS,

$\dot{R}_I - \dot{R}_J$

$P, Q = R_I - R_J$
$\dot{P}, \dot{Q} = \dot{R}_I - \dot{R}_J$

TYPE OF ERROR	RANGE DIFFERENCE	RANGE-RATE DIFFERENCE
TIMING	$C(\Delta T_I - \Delta T_J) + \Delta T_I \dot{R}_I - \Delta T_J \dot{R}_J + \Delta T_B(\dot{R}_I - \dot{R}_J)$	$(K_B + K_I)\ \dot{E}_1 F(E_1) - (K_B + K_J)\ \dot{E}_2 F(E_2)$
PROPAGATION	$(K_B + K_I)\ F(E_I) - (K_B + K_J)\ F(E_J)$	$\frac{\Delta C}{C}(\dot{R}_I - \dot{R}_J)$
SPEED OF LIGHT	$\frac{\Delta C}{C}\ (R_I - R_J)$	$-\frac{\Delta F_I}{F_I}\ (\dot{R}_I - \dot{R}_J)$
FREQUENCY	$-\frac{\Delta F}{F}\ (R_I - R_J)$	F_I
ZERO SET	ΔS_I	

$$\dot{R}_I(\Delta T_I + \Delta T_B) + (K_B + K_I)\ F(E_1) + \frac{\Delta C}{C} - \frac{\Delta F_I}{F_I}\ R_I + \frac{\Delta S_I}{2}$$

Figure 18

Δ R, Δ P, Δ Q are the differences between the MISTRAM measurements in R, P, and Q and the corresponding measurements of a comparison standard.

$\tilde{R}_o$, E_o is the range refraction correction and elevation angle measured from the central receiver.

$\tilde{R}_T$, E_T is the range refraction correction and elevation angle measured from the central transmitter.

$\tilde{R}_1$, E_1 is the range refraction correction and elevation angle measured from the antennae at the end of the North-South baseline.

$\tilde{R}_2$, E_2 is the range refraction correction and elevation angle measured from the antennae at the end of the East-West baseline.

t is the time of measurement.

Each regression equation contains one or more terms representing each of these main effects and in addition, some other terms to test for possible statistical significance. If the stability of the coefficients can be demonstrated over several tests, the equations can be used to correct flight data, or at least yield an insight into the behavior of the Mistram system.

3. Treatment of the Data

A brief description of the data treatment is presented

in Figure 19. The data from both MISTRAM and ballistic camera systems were reduced by normal procedures, but the large number of ambiguities in the MISTRAM data necessitated special consideration.

A special search program was quickly prepared to detect the existence of ambiguities and discontinuities in the MISTRAM data. Once they were located by time points, a team of analysts and engineers made an on-sight inspection of the analog records to try to identify physical causes system transfer, ambiguity and equipment misbehavior. With this information corrections were made to each point. Mean differences were corrected by hand calculation and regression analyses attempted. The results of these analyses are not nearly complete at the time of writing. They will be presented if they are available by the time of the meeting.

4. Results

At the time of writing the only results available are bias estimates of the MISTRAM system with respect to the ballistic camera system. They are shown in Table 9.

The only two which are statistically significant at the 95% confidence level are those in range and P_1.

D. OUTLINE OF MULTIPLE-SYSTEM COMPARISON

1. Methodology

Multiple system comparisons have been made primarily

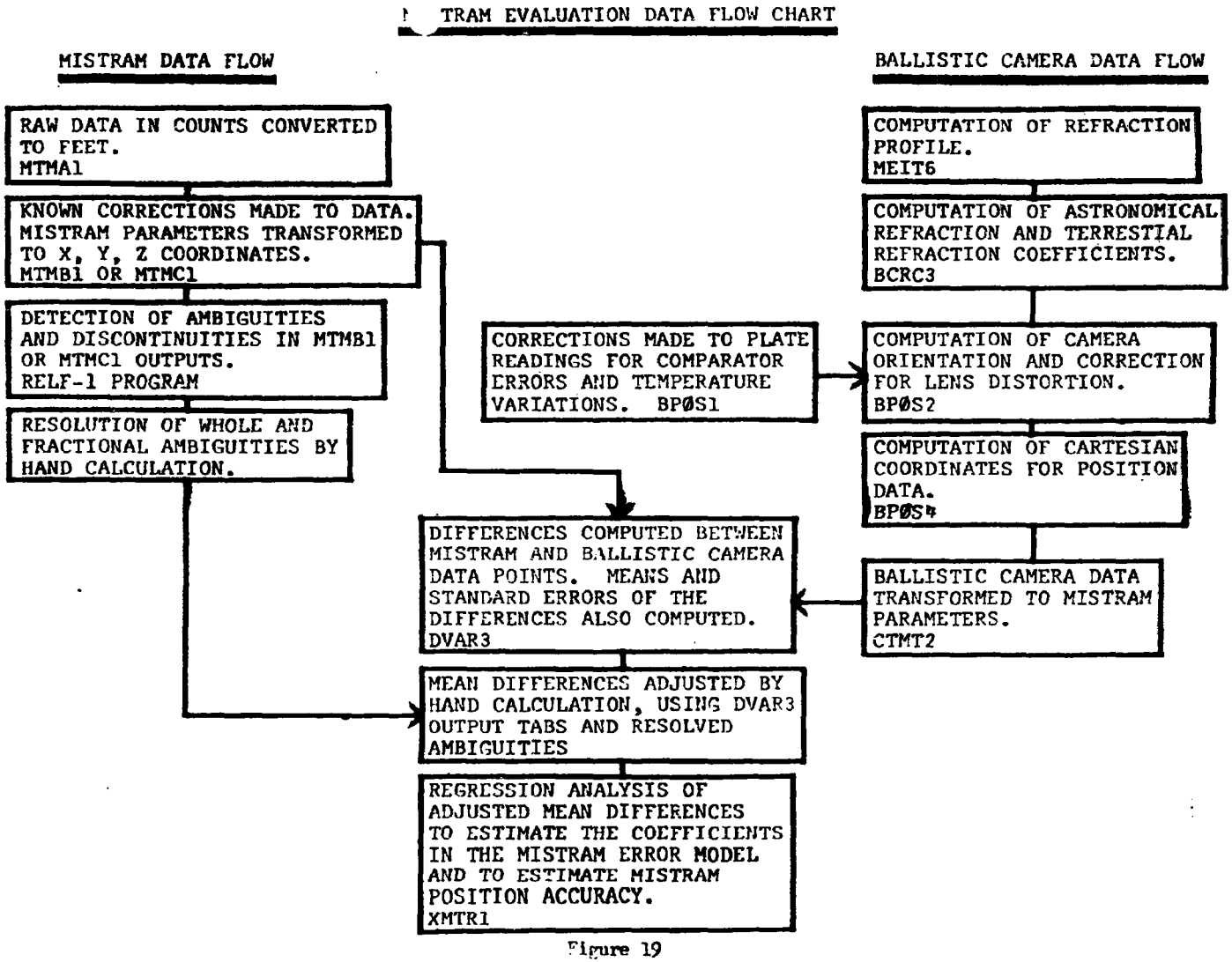
TRAM EVALUATION DATA FLOW CHART
MISTRAM DATA FLOW
BALLISTIC CAMERA DATA FLOW
RAW DATA IN COUNTS CONVERTED TO FEET. MTMA1
KNOWN CORRECTIONS MADE TO DATA. MISTRAM PARAMETERS TRANSFORMED TO X, Y, Z COORDINATES. MTMB1 OR MTMC1
DETECTION OF AMBIGUITIES AND DISCONTINUITIES IN MTMB1 OR MTMC1 OUTPUTS. RELF-1 PROGRAM
RESOLUTION OF WHOLE AND FRACTIONAL AMBIGUITIES BY HAND CALCULATION.
COMPUTATION OF REFRACTION PROFILE. MEIT6
COMPUTATION OF ASTRONOMICAL REFRACTION AND TERRESTIAL REFRACTION COEFFICIENTS. BCRC3
CORRECTIONS MADE TO PLATE READINGS FOR COMPARATOR ERRORS AND TEMPERATURE VARIATIONS. BPØS1
COMPUTATION OF CAMERA ORIENTATION AND CORRECTION FOR LENS DISTORTION. BPØS2
COMPUTATION OF CARTESIAN COORDINATES FOR POSITION DATA. BPØS4
DIFFERENCES COMPUTED BETWEEN MISTRAM AND BALLISTIC CAMERA DATA POINTS. MEANS AND STANDARD ERRORS OF THE DIFFERENCES ALSO COMPUTED. DVAR3
BALLISTIC CAMERA DATA TRANSFORMED TO MISTRAM PARAMETERS. CTMT2
MEAN DIFFERENCES ADJUSTED BY HAND CALCULATION, USING DVAR3 OUTPUT TABS AND RESOLVED AMBIGUITIES
REGRESSION ANALYSIS OF ADJUSTED MEAN DIFFERENCES TO ESTIMATE THE COEFFICIENTS IN THE MISTRAM ERROR MODEL AND TO ESTIMATE MISTRAM POSITION ACCURACY. XMTR1

Figure 19

ESTIMATED BIAS ERRORS OF MISTRAM

WITH RESPECT TO THE BALLISTIC CAMERA SYSTEM

(BASED UPON AIRCRAFT TESTS)

R, Range	-2.1 ± 1.45 feet*
P_1, W 10K leg	+0.131 ± 0.05 foot*
Q_1, S 10K leg	+0.095 ± 0.16 foot
P_2, W 100K leg	+0.108 ± 0.59 foot
Q_2, S 100K leg	+0.179 ± 0.59 foot

*Significant at the 95% level.

Table 9

with data from live missile tests. The procedure is shown in Figure 20.

Data from several systems are acquired and subjected to geodetic transformations appropriate to the system being evaluated. Differences between systems can be computed and subjected to a Simon-Grubb's analysis which, under certain assumptions, permits estimates of errors for each individual system. Other types of analyses can be performed according to the purposes of the investigation. If free fall data are available, residuals can be computed between the system data and a theoretical trajectory fitted to the data. A very powerful analytical tool for estimating rate biases is that of fitting a theoretical trajectory through two measured end points (one, up range; one, down range) using the time-of-flight as a constraint. (This method was brought to the authors' attention by the Staff of Space Technology Laboratories.) Residuals derived by computing differences between the system under investigation and this trajectory yield such information.

Most of the noise error estimates presented in this paper have been derived from applying the Simon-Grubbs analysis to multisystem differences.

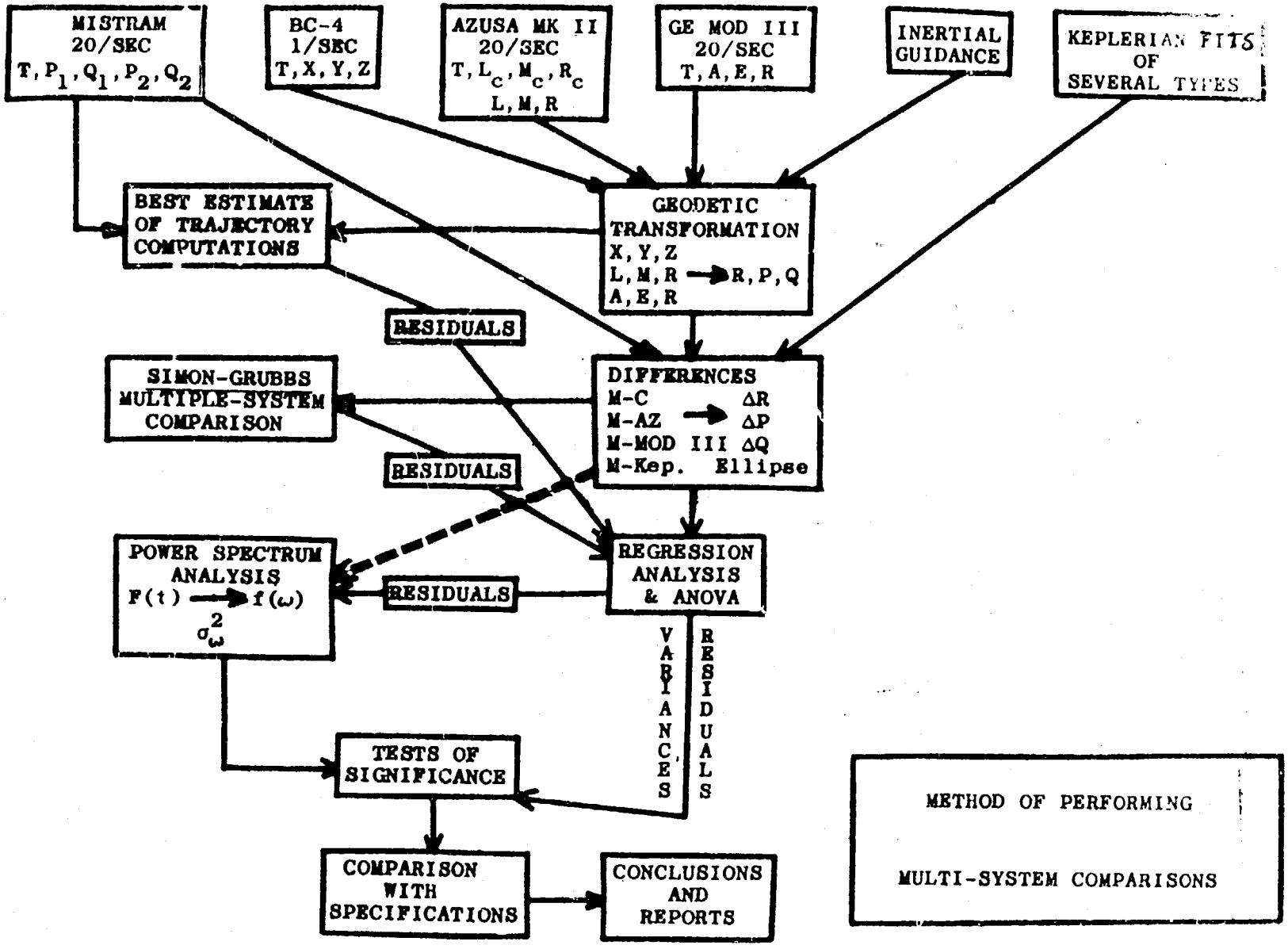
MISTRAM
20/SEC
T, P1, Q1, P2, Q2
BC-4
1/SEC
T, X, Y, Z
AZUSA MK II
20/SEC
T, Lc, Mc, Rc
L, M, R
GE MOD III
20/SEC
T, A, E, R
INERTIAL GUIDANCE
KEPLERIAN FITS OF SEVERAL TYPES
BEST ESTIMATE OF TRAJECTORY COMPUTATIONS
GEODETIC TRANSFORMATION
X, Y, Z
L, M, R → R, P, Q
A, E, R
RESIDUALS
SIMON-GRUBBS MULTIPLE-SYSTEM COMPARISON
DIFFERENCES
M-C → ΔR
M-AZ → ΔP
M-MOD III ΔQ
M-Kep. Ellipse
RESIDUALS
POWER SPECTRUM ANALYSIS
F(t) → f(ω)
σ²ω
RESIDUALS
REGRESSION ANALYSIS & ANOVA
VARIANCES
RESIDUALS
TESTS OF SIGNIFICANCE
COMPARISON WITH SPECIFICATIONS
CONCLUSIONS AND REPORTS
METHOD OF PERFORMING
MULTI-SYSTEM COMPARISONS

Figure 20

SUMMARY

Five missile tests and twenty-one aircraft flights over 36 camera complexes have been analyzed thus far. Our analyses would suggest that the system is approaching its "specification" values, especially in the range-difference and velocity parameters. No determination has been made yet of the existence (or non-existence) of rate-drifts, though there seems to be some indication that they exist.

The MISTRAM system has at least two serious problems at the time of writing: (1) drift of the zero-set, and (2) ambiguities. If these problems can be overcome, the system would seem to be potentially capable of producing data of excellent quality.

709-D

THE GLOTRAC SYSTEM

BY
J. W. Stephenson Jr., R. K. Weller
RCA Missile Test Project
Patrick AFB, Florida

Presented at:
Fourth Joint AFMTC Range User Data Conference
Orlando AFB, Florida
26-28 February 1963

THE GLOTRAC SYSTEM

Abstract

809(D)

The GLOTRAC System is described together with its geographical configuration. The types of electronic equipment involved are given in detail.

The system is described mathematically, its measurements are defined and the anticipated significant error sources are discussed. A detailed description of mathematical formulation to be used in processing the GLOTRAC data is presented.

The application of the method of maximum likelihood adjustment to the processing is briefly examined.

AUTHOR

INTRODUCTION

The Global Tracking Network was designed and developed for AFMTC by General Dynamics/Astronautics.

GLOTRAC measures doppler range rates, unambiguous range, and direction cosines referenced to a land surveyed baseline using continuous wave techniques. By measuring range and range rate from three or more stations, the position and velocity components for a flight vehicle can be determined. To obtain this information, Azusa instrumentation, pulse radars and a doppler type system are used.

The development of a program to make optimum practical use of least squares procedure in the reduction of the tracking data was part of GDA's contractual commitment for GLOTRAC. Since GLOTRAC was system-engineered about the assumption that this program or another like it would be used to reduce GLOTRAC data, any evaluation of GLOTRAC capability made by means of an error analysis should correspond to both the hardware components of GLOTRAC and to its data processing program. Thus an error analysis was performed by GDA on the GLOTRAC system which incorporated the optimum processing of data. The inclusion of an error analysis of the system was also a contractual commitment for the GLOTRAC system.

The GLOTRAC System is often described as one containing both pulse radar equipment and continuous wave radio equipment. Although the data from the pulse radars is used in the processing of the GLOTRAC data, there is no electrical connection between the two systems except for acquisition and pointing purposes.

The continuous wave equipment of the GLOTRAC System operates at a nominal transmission frequency of 5052 mc per second. All of the equipment operates in conjunction with an airborne transponder which maintains phase coherence between its input and its output signals. More precisely, for each 97 cycles received by the transponder, 96 cycles are re-transmitted. The ground equipment in the GLOTRAC System has been divided into five groups. This grouping is based on the area of coverage of the system for certain particular trajectory types.

GLOTRAC SYSTEM INSTRUMENTATION

Segment I. There are seven different geographic locations associated with Segment I. The first of these is Cape Canaveral. The existing AZUSA tracking equipment at Cape Canaveral forms part of the GLOTRAC equipment. This equipment contains a CW transmitter plus ground equipment capable of measuring range differences, often called cosines, and an unambiguous range to the transponder, as well as an ambiguous range formed by integrating the CW range rate

measurement. The multiple modulation ranging system provides the non-ambiguous ranging system. In the first portion of the flight the transponder will always be excited by transmissions from the Cape Canaveral system. On the island of Bermuda the GLOTRAC equipment consists of a transmitter, a non-ambiguous ranging system and an ambiguous ranging system. The San Salvador system contains the same type of equipment as the Bermuda Station. At Cherry Point, North Carolina, at Grand Turk, at Antigua, and possibly at Puerto Rico the GLOTRAC equipment will consist only of ambiguous ranging equipment. All GLOTRAC equipment operates with frequency standards of the atomicron type. Clearly, Segment I is for use in the launch phase and must provide the most accurate data possible.

Cape Canaveral (Main Station)	Modified Azusa Mark II
Cherry Point, North Carolina	Range Rate Station
San Salvador, BWI	Range Rate Station (with transmitter); AN/FPS-16 Radar
Antigua, BWI	Range Rate Station; AN/FPQ-6 Radar with 28-foot dish
Bermuda	Range Rate Station AN/FPS-16 Radar

ERRORS ESTIMATED BY GDA FOR INSTRUMENTATION

An error analysis for the GLOTRAC system to be used on a typical CENTAUR trajectory has been based on certain error estimates in instrumentation.

Errors estimated for the Azusa, Radar and CW Doppler systems are as follows:

Azusa
- Bias in range measurement = 2.8 ft.
- Bias in direction cosine measurement = 8.0 ppm.
- Noise in range measurement = 3.0 ft.
- Noise in direction cosine measurement = 3.2 ppm.
- Noise in direction cosine rate measurements = 0.657 ppm per sec.

Pulse Radar
- A, E, Bias = 0.1 mil
- A, E, Random = 0.1 mil
- R, Bias = 10 ft.
- Random = 10 ft.

CW (Rate Stations)
- Error in $\dot{R}$ = 0.1 ft/sec (Transmitter with Receiver)
- Error in $\dot{R}$ = 0.144 ft/sec (Radar with Receiver)
- Error in $\dot{R}$ = 0.51 ft/sec (Receiver alone)

CW Range
- Error in R = 10 ft + $(5 \times 10^{-6})R$

Survey
- Error in short distance survey = (2.5×10^{-6}) Measurement
- Error in Hiran Survey = (10×10^{-6}) Measurement
- Error in long distance = 1000 ft

Timing Error
- Error $\pm$ 10 ms

REQUIRED TRACKING ACCURACY DATA FOR GLOTRAC

A mathematical error analysis is required to satisfy the contractual obligations of the contractor that these following accuracy requirements are met. The accuracy required of the GLOTRAC system for trajectory data is as follows:

	Time (Seconds of flight)	Accuracy (1 Sigma Values) Position X, Y, Z	Velocity X, Y, Z
1	225 - 500	100 feet	0.5 ft/sec

In the error analysis, the optimum practical use least squares procedures in the reduction of tracking data was employed. Since GLOTRAC was system-engineered about the assumption that this program or another very much like it would be used to reduce GLOTRAC data, any error analysis of the system must include both the hardware components of GLOTRAC and its data processing program.

MATHEMATICAL DESCRIPTION OF THE SYSTEM AND IT MEASUREMENTS

Clearly, all of the CW GLOTRAC equipment actually makes measurements of phase differences between pairs of signals. The geometrical meaning of this measurement, of course, depends upon the origin of the signals whose phase is being continuously compared. While the phase comparison is actually a time difference measurement, it is much more convenient, due to the near constancy of the velocity of propagation of the radio signals involved, to think of the phase measurements as actually being distance measurements of some type. In particular, if we disregard the fact that there is actually a frequency shift within the transponder and again at the receiving point, we can describe the various phase measurements as follows: comparing the phase of a transmitter with the phase of the signal returning from the transponder provides us with what may be called a range sum measurement. That is, we have a quantity which is related to the total time required for passage of a signal from the transmitter to the transponder and back to the receiving point. If we compare the phase of signals received on the ground at two different points we are making a time difference or range difference measurement. That is, we have formed a quantity which is proportional to the difference in distance from each of the receiving antennas to the transponder.

AZUSA. When the AZUSA System is acting as a transmitter, the signal leaving the AZUSA site consists of the continuous wave carrier as well as a modulation signal which is on the carrier. The AZUSA System operates so as to control the exact frequency of the continuous wave signal being transmitted, so that the received signal at the AZUSA site does not deviate from 5000 mc per second. This is, of course, known as an automatic frequency control. The frequency of the modulation transmitted from AZUSA is held constant. If we continuously measure the phase difference between the modulation returning from the transponder and that being transmitted, we have a measurement of the range from transmitter to transponder to receiver. This is the range sum measurement. By the use of lower frequency modulations we can actually resolve the ambiguities in this measurement. That is, we can determine the precise number of cycles in this transmission path. If we also measure the phase difference between the transmitted carrier and the received carrier, we are also making a range sum measurement. Since this particular measurement is not initialized and is not resolved, our measurement is actually an

integration of rate information with the constant of integration missing. In order to initialize or zero set this ambiguous range information, we must provide this constant of integration from some other source. The range difference measurements made by AZUSA are often called cosines. This is true because the quotient of the range difference and the baseline length is very nearly equal to the direction cosine to the transponder. Although, strictly speaking, this is only a range difference measurement. This measurement is, of course, made by comparing the phase of the signal from the transponder being received simultaneously at two different points on the ground. The AZUSA System contains actually three sets of baselines - a 5 meter set, a 50 meter set, and a 500 meter set. Pointing information from a tracking antenna is used to resolve or find the proper cycle in the 5 meter range difference measurement. Once this is found, it can be used to find the proper cycle in the 50 meter measurement. The 500 meter measurement is not initialized nor resolved; hence, it is an ambiguous range difference measurement. It must be initialized, as the ambiguous range, from some outside information.

Range Sum Stations with Transmitters In describing the range sum measurement, it was shown that a comparison of the phase of the transmitted signal and the signal returning from the transponder provides a range sum measurement. That is, the total distance from transmitter to transponder to receiver. In order to make this measurement it is, of course, necessary that the phase of the transmitted signal be available at the receiver in order to provide sufficient electronic information for comparison purposes. If the transmitter and receiver are at the same geographic location, this type measurement is, of course, possible.

Range Sum Stations Without Transmitters Clearly, if the transmitter is not at the same geographic location as the receiver, it is impossible to directly compare the transmitted signal's phase with that of the received signal. We can approximate this measurement though if we can synthesize the actual phase of the signal being transmitted. We can approximate this condition if we use an ultra-stable, very accurate oscillator as a substitute for the transmitted signal. If this oscillator is at the same frequency as that of the transmitter, we simply measure its phase minus that of the received signal. This provides us also a range sum measurement provided the actual transmitter is operating at a frequency equal to that of the accurate oscillator being used at the receiver.

Associated Pulse Radar Measurements The data measured by pulse radars is range information derived from the two-way transit time of the radar pulse. Also angular information; that is, azimuth and elevation angles are derived by a monopulse tracking system which causes the antenna to automatically track the line of sight to the target. The angular measurements are taken by measuring the position of the antenna mount.

DESCRIPTION OF ERROR SOURCES

Biases Almost all trajectory measuring equipment is subject to bias errors of some sort and from some origin. Oftentimes, bias errors are due to imperfect or inaccurate zero setting, initialization, or calibration procedures. Errors of this type are present in the GLOTRAC data. These initialization errors can obviously be very large in cases of uninitialized measurements. As an example, we might examine the measurement made by the ambiguous ranging equipment at Cherry Point, N. C. Since this measurement is simply a phase difference between a local oscillator and the signal coming from the transponder, and no electronic method is available to measure the actual number of cycles in this transmission path, the measurement is com-

pletely uninitialized. These very large error sources must be removed in the processing of the data.

Ambiguities Another type of error which is not infrequent in continuous wave tracking systems is that known as ambiguities. This is simply a loss of count of the number of cycles in the range sum or range difference measurement. This type error appears often as a step function in the data. Since an ambiguity can have only a fixed size, that is, the length of one cycle, it may be detected and removed by simple editing methods.

Time Dependent Errors In systems making measurements using a local oscillator instead of the actual transmitter there will be some, hopefully small, difference between the frequency of the transmitter and the local oscillator. This frequency difference will lead to what might be described as a time dependent error. This description is meaningful in that if the transponder were stationary, the data would appear to be moving as a linear function of time. The rate of this motion is related to the amount of the frequency error. Since this error is not insignificant, it also must be accounted for and removed in the processing of the GLOTRAC data.

Timing Errors It is hoped that the transmission of timing signals through the transponder to the other GLOTRAC receivers will eliminate all significant timing errors.

Survey Error Due to the remoteness of many GLOTRAC locations and also due to the fairly stringent accuracy requirements placed on the system, the survey measurement errors present a problem. Since there is redundant information available, particularly in Segment I of the GLOTRAC System, it is reasonable to think that some of the survey errors may actually be decreased with the use of the GLOTRAC data. For example, if we continuously track a target from a point with an accuracy of approximately ten feet, we can determine, if we know the position of the target, the location of the tracking station also to approximately ten feet. Hence, it is likely that for the stations having large survey errors we may actually be able to reposition these stations in the processing of the GLOTRAC data.

Geodetic Errors Another error source which appears in the GLOTRAC data processing is related to the earth model being used as well as to the accuracy of our gravitational force equations. This should not be a significant error, although some improvement in our knowledge of these constants may result from processing of long spans of GLOTRAC data acquired from orbiting transponders.

These errors and observations are described mathematically as follows:

$$m(t) = \sum_{i=1}^{4} a_i |X - S_i| + a_5 A(X, S_5) + a\, E(X, S_6)$$

$$+ a_7 + a_8 \dot{m}(t) + a_9 t + \epsilon$$

m = measurement at t
a_i = arbitrary coefficients needed to describe measurements
t = time
A = azimuth of X from S
E = elevation of X from S
ϵ = random error
X = missile position vector
S = station location vector

Here the a's and S's may be adjusted and the X is to be estimated.

BASIC MATHEMATICAL FORMULATION

In order to convert the raw GLOTRAC data into a form which is useable by the missile contractors, certain mathematical operations are obviously necessary. The de-coding of the raw data format transmitted from the GLOTRAC sites to the Cape is the first basic operation which is required. The data must also be combined into a single group on magnetic tape, which is more easily processed and manipulated by the electronic computers involved.

The principle underlying processing of the GLOTRAC System data is that of maximum of likelihood adjustment. This method is very much akin to least squares adjustment. Here we have a set of observations from which we would like to estimate the true position and velocity of the transponder as a function of time. We will make this estimate subject to the constraint that the weighted sum of squares of the differences between our estimate and the measurement be minimized. In this mathematical formulation if we have redundant information, that is, more than the minimum necessary number of measurements required to derive the basic position and velocity measurements, we extract from this additional information regarding systematic errors. In particular, we may seek to improve the surveys of the stations involved and to estimate the previously mentioned frequency and timing errors.

Measurements, Random Error and Smoothing Our basic measurements, as previously described, are range sum measurements, range difference measurements, azimuth angle measurements, and elevation angle measurements. These measurements are accompanied by random error. There are other errors in the measurements also, which we will describe shortly. Sometimes the noise or random error on a measurement is large enough to make it necessary to smooth this measurement before further processing. Since smoothing actually removes some information from the data, this is avoided when possible. In the system which I have described, all measurements are actually position measurements. Since we are interested in velocity and often acceleration, as well as position, it is necessary to produce derivatives of the basic measurements. These derivatives in general are provided by numerical differentiation of the basic position measurements. We will refer to these derivatives of the position measurements as measurements themselves. In order to make the maximum likelihood adjustment, it is necessary that we have estimates of the random error content of these measurements. Various methods will be used to produce these estimates, such as numerical filter techniques and variate difference schemes.

Error Model Certain systematic errors have been described as being present in the measurements. In particular, we must describe this systematic error with some mathematical formulation. The three systematic error sources mentioned before, that is, biases, frequency errors, and timing errors, can all be described rather simply, mathematically. That is, biases become unknown additive constants, frequency errors become first degree time functions, and timing errors may be well described by velocity functions, that is, an error proportional to the first derivative of the measurement which is in error. Any other systematic errors which may be detected as present in the GLOTRAC data, which are describable, mathematically, may also be included in future error models.

Constraints In addition to our knowledge of the nature of the basic measurements and the error sources, we may have additional information about the trajectory itself. A very simple and frequently encountered trajectory constraint is that of free-fall. That is, the motion of the vehicle when it is not in powered flight. We may use our information about the trajectory in order to reduce significantly the number of unknowns which must be estimated

in the data processing; since only six initial conditions are needed to fully describe free-fall, assuming we have knowledge of the gravity and drag forces, we may literally have thousands of observations from which to determine only six parameters. These parameters are often taken as the initial position and velocity of the free-fall or orbital motion. Statistically speaking, we have greatly increased the number of degrees of freedom possessed by the formulation. We cannot apply these constraints during periods of powered flight, although the extension of the data from powered flight into free-fall and the increase of the amount of freedom of the formulation in this period will actually lead to better determination of systematic error which applies to powered flight as well as free-fall; thus the use of the free-fall constraint can improve powered flight data. There is also additional information which we are not presently using in the processing. This is information which would describe the motion in powered flight as a series of connected points. We are presently working toward a manageable mathematical formulation which will make use of this additional physical constraint.

Assumptions and Weaknesses In a complex mathematical formulation of a physical problem it is generally necessary to make certain assumptions. The validity of these assumptions strongly influences the validity of the solution. Basic assumptions which allow the maximum likelihood adjustment to be done in a reasonable amount of computing time involve the assumption of no serial correlation among the errors on the basic measurements. Also we must assume that the non-random part of the error is adequately described by the error model used in the formulation. In order to make this first assumption more nearly valid we simply use only points in the processing which are separated by one, two or more seconds for determination of the systematic error model coefficients. We must examine each solution in order to attempt to determine the validity of the assumption of the adequacy of our error model. We intend to test the validity of these assumptions and we also intend to determine the effect of the violation of these assumptions on the data reduction method for GLOTRAC. This test will be made by simulating errors of the serially correlated variety as well as undescribed systematic error sources; thus we may determine the response of our processing techniques to these assumption violations.

CONCLUSIONS

Expectation Since I have been describing a system which is not yet functional, essentially all I have said could be described as expectation. If we examine the philosophy used in the design of the GLOTRAC System, we see that the system lends itself well to mathematical processing schemes of the maximum likelihood variety. It possesses two basic essentials for a formulation of this sort; the first of which is redundancy; the second is geometry. In this first respect, redundancy, the processing is very similar to that known as the Best Estimate of Trajectory and the mathematical methods are very similar. In the second respect, geometry, we have gone beyond the systems which have in the past been used in the Best Estimate of Trajectory project. We have very precise tracking systems down range. We have been studying the formulation of the GLOTRAC data processing mathematics for some time, and we can say that we are encouraged by the results to date. We believe that the major error sources are adequately described by our error models and that the assumption of minimal serial correlation will indeed prove valid. The primary error source for which we have no real feeling at the moment, as far as its behavior and its effect on our solution, is what is best called the residual refraction correction error. Since the GLOTRAC System is so widely separated geographically, many of the stations are operating at elevation angles which

are below 10°. Those familiar with tropospheric refraction effects know that this leads to range errors of about 300 feet or more. Our ability to remove this systematic error from the available atmospheric information along the ray paths involved may present a problem. This problem is also under investigation at this time. The final answer will not be available until actual GLOTRAC data is available. The adequacy of the presently known refraction correction methods will be clearly indicated by an examination of the residuals from our adjustment.

Planning Schedule Present plans call for testing of this system's (Segment I) equipment to be conducted in late spring and early summer of 1963; Segment I is to be operational by late summer 1963.

The preliminary test program calls for four GLOTRAC vans to be installed and tested at temporary locations from time of arrival at Patrick AFB until permanent sites are available. Vans will be installed and operated at MK II Azusa site, the Technical Laboratory site, Jupiter site and MK I Azusa at Grand Bahama Island site. Test directives will be written for aircraft and missile tracking tests and these tests will be conducted to obtain the necessary data for GLOTRAC network preliminary evaluation. These tests will include chassis tests, sub-system tests and complete van tests preceding qualitative aircraft tracking tests with three and/or four vans operating simultaneously.

When the GLOTRAC equipment is installed at permanent sites, all tests up to and including the complete van tests will be conducted again. Missile tests will be conducted at the permanent sites and an evaluation of the performance characteristics and accuracy of the system will be made. Results of the evaluation will be used to commit the GLOTRAC network on an operational basis.

Future Applications If our hopes for the GLOTRAC System indeed materialize and the adjustment possesses the power which it appears to have at present, we may actually use the GLOTRAC data to improve positions of many of our down range tracking sites. Also, the use of the GLOTRAC System with an orbiting vehicle could possibly provide us improved geodetic information. Since the GLOTRAC equipment is easily transportable, it is not unlikely that this equipment or some similar to it may be placed on board ocean-going vessels to provide this extremely accurate coverage in geographical areas now inaccessible.

In closing, I will say that the redundancy of the GLOTRAC System, when combined with the other existing range instrumentation, can lead to the improvement of all precise range data. Undoubtedly, at some future date combinations of the GLOTRAC methods with the Best Estimate of Trajectory methods will lead to extremely good quality trajectory information.

ADVANCED RANGE INSTRUMENTATION SHIPS

by:

Nils L. Hanson
and
A. B. Ward

RCA-Missile Test Project

PAFB, Florida

Presented at:

FOURTH JOINT AFMTC-RANGE USER DATA CONFERENCE

Orlando Air Force Base, Florida

26-28 February 1963

ADVANCED RANGE INSTRUMENTATION SHIPS

ABSTRACT

E24(e)

A brief description of the past and current use of instrumented ships on Atlantic Missile Range (AMR) will be given. As new requirements were placed on the Range, it became necessary to provide more advanced ship capabilities which led to the development of ARIS 1 and 2.

The ARIS 1 equipment configuration and operating concepts are briefly described as is the proposed method of picking up data from the ship at sea.

The reduction of data at AMR from a typical ARIS mission is developed and finally a description of AMR Plans for the ships evaluation is presented.

AUTHOR

PAST AND PRESENT UTILIZATION OF SHIPS ON AMR

The use of instrumented ships on AMR started with simple telemetry ships operating in the 200-megacycle band. (Fig. 1)

The Twin Falls, a converted Victory ship came on the Range in 1961 primarily to support the Pershing program. It was designed to acquire accurate radar trajectory data which could be transformed to a known point in a land-based coordinate system. (Fig. 2) This required a high precision radar and stable reference system as well as an accurate means of locating the ship. (Fig. 3) Experience in the use of this system has shown that the radar itself will perform with essentially the same precision on a ship as on land. Additional errors are in the neighborhood of 100 feet in survey while the ship is in LORAC areas, and a peak of 1 1/2-milliradians radar error caused by ships motion induced lag errors. Post-flight corrections to lag errors are about 85% effective. When the Twin Falls is operated out of the LORAC area of coverage, survey errors up to three miles may be expected. Fig. 4 shows the accuracy experienced with Twin Falls data during 1961.

The DAMP ship equipped with a "C" band and UHF radars was designed primarily to produce cross-section data and has had very limited AMR usage.

NEW SHIP REQUIREMENTS ON AMR

More advanced programs coming to the AMR have dictated new requirements for instrumented ships. Among these are:

1. Accurate trajectory information on small targets at long ranges.

2. Accurate cross-section data at several frequencies.

3. Simultaneous data on more than one target.

4. More advanced telemetry.

5. Accurate survey information in broad-ocean areas.

MISSION OF ARIS 1 AND 2

In 1961, a contract was let to the Sperry Gyroscope Company to instrument two advanced range instrumented ships. The primary mission of these ships is to gather terminal data on ballistic missiles in areas where land-based instruments will not provide coverage. This will provide data for evaluation of overall missile system performance as well as penetration aids studies. Secondary benefits will be nose-cone recovery and terminal area weather data. These ships will have extended cruising ranges and the ability to remain on station for long periods of time.

Fig. 5 shows a possible deployment of ARIS 1 and 2. One ship is about 10 NM from the intended impact point while the other is about 100 NM uprange and offset 50 NM from the plane of the trajectory. This deployment provides side-aspect angle and nose-on tracking coverage. If another tracking ship is available, it could be used to obtain mid-course metric data.

ARIS 1 and 2 are converted C-4 ships, 520-feet long and with a beam of 72 feet and a draft of 25 feet. Maximum sustained speed is 17 knots and the cruising range is in excess of 5000 miles. The ships are equipped with large tracking antennas and a navigation system which will be used to measure accurately the trajectories of ballistic missiles. The reflection characteristics of various types of bodies reentering the atmosphere will be determined at frequencies in the C, L and X bands. They will also receive and track telemetry signals. All functions which are necessary for the gathering and recording of signature and trajectory data are provided.

Instrumentation Equipment and Operation

The ARIS ships can be easily identified by their radar and telemetry antennae as seen in Fig. 6. The primary tracking device is a C-band radar set utilizing a parabolic reflecting antenna 30-feet in diameter. A dual frequency L and X-band antenna 40-feet in diameter gathers signature information while slaved to the C-band antenna position. The 30-foot telemetry dish tracks passively in angle and if it starts tracking before the C-band radar acquires the missile, it will provide master designation angles. Other distinguishing features above decks include the navigational star tracker and the meteorological

balloon tracker. Not visible from outside, but suspended from the supporting base of the star tracker, is the ship's Inertial Navigational System (SINS). The radar electronics, communications equipment, operations control center and data handling equipment are located below decks. The data handling equipment consists of a UNIVAC 1206 Computer and the Central Data Conversion Equipment (CDCE).

The C-band radar will provide trajectory data on a primary and two secondary targets simultaneously. The X and L radars provide signature data on the primary and two secondary targets simultaneously.

The stabilization/navigation sub-system provides inertial navigation information updated from star fixes and sonar beacon fixes as well as data stabilization against ships motion and accurate heading and vertical references.

The telemetry sub-system is an acquisition aid. It receives and records telemetered data from the test vehicle and retransmits recorded data to near-by aircraft for transportation to the data reduction facility.

The flexure monitor sub-system measures ships flexure between:

1. Star tracker/SINS and C-band barbette
2. C-band barbette and LX-band barbette.

This data is used for both real-time and post-flight data correction. The sub-system includes a two-axis monitor for pitch and yaw and a twist autocollimator for roll.

The data handling sub-system consists of the Data Processing Equipment (DPE) and Central Data Conversion Equipment (CDCE). The functions of the DPE are to provide:

1. Shipboard calculations of designate and navigation information.
2. Real-time displays and position/velocity solution for transmission.
3. Computer aided tracking information.
4. Data formatting.

The CDCE functions are to

1. Provide communications control between the computer and all other equipment.
2. Make necessary data conversions for this communication.

3. Record primary data, such as cross-section and trajectory.

The timing sub-system is designed with a basic accuracy of five parts in 10^{10}/day in real time and will remain correlated with Cape Canaveral timing to better than 10 milliseconds.

The communications sub-system provides the following capabilities:

High Frequency	-	Ship-to-Ship
		Ship-to-Aircraft
		Ship-to-Shore
Very High Frequency	-	Ship-to-Aircraft
		Ship-to-Recovery Vehicle
Ultra High Frequency	-	Ship-to-Aircraft
Very Low Frequency	-	Shore-to-Ship

Plus intercom and PA systems

The meteorological sub-system provides the standard weather observations and includes an Arcus rocket launch facility.

The Operations Control Center (OCC) provides centralized control and consists of the following:

1. Trajectory plotter
2. Designate control console
3. Master control console for the Ships Operations Manager and the Ships Instrumentation Manager.

Some of the OCC functions are:

1. Select master sensor
2. Monitor system status
3. Control ships course and position
4. Coordinate all activities with AMR.

Instrumentation System Operational Procedures

The general operational procedure of the ARIS ships is as follows:

1. The ships sail prescribed courses in the vicinity of the expected impact point, measuring position accurately with reference to surveyed sonar beacons.

2. The communications sub-system receives post-burnout orbital parameters from Cape Canaveral via teletype.

3. The computer integrates the equations of motion of the missile faster than real time to determine an acquisition point prior to the missile's arrival. Using measured values of latitude and longitude from SINS, the result is a continually corrected stable acquisition point relative to the ship.

4. SINS supplies heading, pitch and roll through CDCE which the computer combines with the acquisition point to produce designation orders in deck coordinates at a rate of ten samples per second.

5. CDCE converts digital designation orders to synchro voltages for positioning the antennae.

6. The tracking antenna which first acquires the missile signals the Designate Controller who designates that antenna as master.

7. The other antennae are slaved to the master through CDCE with corrections for ship's flexures.

8. When the C-band radar acquires the missile, CDCE converts trajectory and signal strength data to digital form and records on magnetic tape.

9. The computer smooths trajectory data by providing a least squares fit of 31 points to a cubic curve.

10. Based on the predicted missile trajectory, up-to-date position orders are maintained at ten samples per second in case the radar loses track. To assist in tracking through reentry, a computed angular velocity term allowing for air density and ballistics is supplied to the tracking servos.

11. The missile path is plotted from acquisition to impact.

ARIS Operating Modes

Routine operating procedures aboard ship specify periodic celestial or SONAR fixes and instrumentation checkout. Most of the time the data handling system will be in the navigation mode. During this mode, the CDCE converts latitude, longitude, heading, pitch and roll synchro data from SINS to digital form and enters them into the computer. Time from the ship's time mode generator is buffered in also. Using these data and star coordinates manually selected from a stored table, the computer generates star tracker designation angles. CDCE converts the star designation data to synchro form to position the star tracker. After acquisition, CDCE reads digital star tracker angles into the computer for processing position fixes. SINS reset orders are supplied by CDCE as voltage levels whose duration is determined by the computer. The procedure is similar for SONAR fixes except that SONAR readings are entered into the computer manually.

Periodically, but always prior to a shoot, the instrumentation equipment is placed in a checkout mode. For the most part, the sub-systems perform their checkouts independently, but final checks are run with the computer, CDCE and the other sub-systems tied together. Pre- and post-shoot radar calibration runs are made recording data on CDCE tapes. After a mission, the computer and CDCE receivers are used to translate recorded data into a format suitable for transmission or transportation to the data reduction center.

During a mission, the computer program is in the Designation-Acquisition-Track mode while CDCE is converting SINS synchro angles, AC flexures and DC signal strengths to digital form, entering them into the computer, and/or recording them. The sample rate, sequence, and synchronization are controlled by CDCE. AC analog outputs are provided for flexure corrections and regenerative tracking terms, and DC for plotting. Various interconnections are effected by CDCE on command of the Designate Controller in the Operations Control Center. The controller determines whether the computer, C-band radar, or telemetry should be master by evaluating sub-system status indicators, intercom information and the trajectory plot.

In summary, the shipboard data processing for navigation, checkout, formatting, designation, acquisition and tracking are accomplished by the Computer. All communications between the computer and the other instrumentation sub-systems (with the exception of teletype) and data recording are controlled by the Central Data Conversion Equipment.

DATA PICK-UP

The introduction of data pick-up by aircraft on the AMR, particularly from ARIS 1 and 2, follows the successful evaluation of this system by SSD in cooperation with PMR. Fig. 7 shows a

JC-130A aircraft picking up a data package from an ARIS operating 4000 to 5000 NM downrange.

Data preparation aboard ship for aircraft pick-up will take about six hours. Aircraft data delivery mission time will take four hours, with one hour of low altitude flying time for the actual pick-up. Thus, the JC-130A pick-up range will be 1150 NM. Once delivered to a range station, the return to Patrick AFB depends on the data processing schedule urgency. Normally, the data will be returned by a MATS scheduled airliner which makes three weekly trips. Earlier delivery may be made by non-scheduled flights. Or, if priority permits, special aircraft may be used, since the average flying time is 17 hours from Ascension to Patrick AFB.

After splash or loss of target by the ship, all recorded trajectory and nontrajectory radar data, telemetry and pre-flight calibration data can be picked up within one hour. Under these conditions, on-station telemetry aircraft can make the pick-up without scheduling a separate mission. In the case of extensive post-flight data, or if there is no need for telemetry aircraft, a flight will be initiated after splash; this will depend on the ship's preparation time.

For a typical test mission, weight of the data tapes will be small compared to that of the water-tight pick-up container. This results in a weight of about 85 pounds. The master tapes will be kept aboard ship for tape reproduction as needed.

Pick-up is achieved by launching a balloon kite to an altitude of about 200 feet and attaching it to the package to be retrieved. The balloon has a loop which is caught by the arresting gear aboard the aircraft. The aircraft's friction brake winch and the nylon line characteristics reduce package acceleration and the balloon station increases vertical lift from the deck of the ship. The reverse transfer may be made with the aid of a parachute, allowing the package to be hauled to the ship's deck. This allows a transfer in which the package is always in physical contact with the aircraft or ship.

OPERATIONAL DATA PROCESSING

Data Processing for ARIS will consist almost entirely of techniques already familiar to AFMTC Data Processing people. The computer routine for ARIS can quite properly be described as massive; it will be unique in size but not in technique. The proposed processing scheme will be virtually automatic as regards a standard output of trajectory data, impact location, and radar cross-section (magnetic tape and tabular output). (See Fig. 8)

The following pre-processing programs will be used:

Input - (raw data on one-half inch magnetic tape from ship)

1. Missile trajectory data, signal strengths and error signals.
2. Pre- and post-calibration navigation data.
3. Pre- and post-calibration radar data.
4. Missile signature data.

Other inputs will be:

1. AMR processed weather data.
2. Station constants.
3. Digitized boresight film data.

The first job of the program will be to edit and summarize the data by determining such items as:

1. Amount of data.
2. Time history of switch conditions.
3. Rough estimate of variance and the number of bad points replaced.

Editing can be performed on all of the trajectory parameters by obtaining output of the number of points edited, and making a rough estimate of variance to indicate quality of data. Pre- and post-calibration SINS data will be treated by comparison with SONAR. Program option allows printout of any parameter with first and second differences. The output of the pre-processing program will be magnetic tape containing the necessary constants and edited data.

The flow of data through the Reduction Program may be described as follows for trajectory data:

1. Magnetic tape input containing all trajectory parameters and necessary supplemental information such as filtering parameters and weather data.
2. C-band radar will be combined with error signal data to produce A, E, R data of each object being tracked. The error signal data is also saved for signature processing.
3. Correction of all parameters (removal of known errors).

4. Transformation of radar data to required coordinate system, utilizing navigation and flexure data.

5. Computation of impact point and error ellipse.

Signature data processing consists of determining the effective radar cross-section area of the target for the C, L and X-band frequencies, relative to that of a calibration balloon. Antenna beam pattern attenuation, atmospheric attenuation and slant range data are utilized in the calculations.

An average mission will produce two to three 7200-foot reels of magnetic tape, plus four to six rolls of strip-chart recordings. Boresight film is 35-mm movie film; the quantity will be small.

DETAILED EVALUATION PLAN

General

An overall program has been planned to encompass the testing of the ship's instrumentation system. The acceptance test program, which includes both functional and quantitative tests, began as the individual sub-systems were in their final stages of manufacture. These factory tests included complete acceptance tests on some components and limited tests on others. All sub-system testing will be completed after the individual sub-systems are installed on the ship. At the completion of the individual tests, dockside system integration tests will be performed.

The evaluation program will commence as each ship sails from the shipyard enroute to the AMR. At this time, all acceptance tests will have been performed. The evaluation program will perform a metric evaluation of the capabilities of the ship's instrumentation system based on a working and integrated system. The evaluation effort, has been planned to encompass a period of nine weeks for each ship. This is known to be a "tight" schedule, and will require an efficient and coordinated program [illegible] as some degree of range priority to have a reasonable chance of completion on schedule.

There are basically three objectives in the evaluation program. These are:

1. To demonstrate the capability of the system to operate within the specified accuracies.

2. To provide data which will serve as a basis for the system calibration.

3. To provide a basis for developing a long-term analysis and evaluation program after commitment of ships to range support.

The calibration of the system and the check on the accuracy are interdependent objectives which result from the manner in which the accuracies are specified in the Air Force Technical Exhibit. This exhibit states that accuracy values refer to reduced and corrected data. Therefore, the evaluation program will first determine the systematic errors by means of statistically selected data runs. These errors will be removed by proper corrections to the operational data reduction program, thus calibrating the system. The data will then be reprocessed, using the corrected calibration of the system. By this means, the evaluation program objectives of calibration and accuracy determination will be met.

The planning effort for the evaluation period was divided into two phases: the experiment design and the evaluation plan.

Evaluation Plan

The initial phase of the planning program consisted mainly of mathematical work designed to determine the basis for the preparation of the evaluation experiments. The mathematical work included consideration of the three-step data handling process: operational data reduction, data differencing, and regression to determine the error model coefficients. These three steps will provide a closed-loop handling of the data from the evaluation experiments. The experiments, in turn, have been designed to produce data of the type and quantity required for the application of this three-step data handling process.

The operational data reduction will correct and adjust the raw experimental data. This effort will provide inputs to both the data differencing and regression steps. In the data differencing, the reduced data will be compared with data from a suitable standard instrument. The difference data, when statistically analyzed, will provide the logic necessary to demonstrate compliance with the specified system requirements.

The regression will effectively close the loop by determining the error model adjustments to be made on the raw data during the operational reduction effort. The adjustment procedures have been designed to correct the raw data for systematic errors in the instrumentation. By requiring that the difference data be a minimum in the least square sense, suitable values of the error model coefficients will be obtained. Proper determination of these coefficients will result in reduced data which, in a sense, will have been corrected for calibration type deviations and which will more realistically portray the accuracy capability of the system.

To implement the data handling steps outlined above, an error model has been generated to fulfill the requirements set forth in the regression procedure. In addition, every effort has been

made to insure that the data received from the experiments will be of a type which will allow the subsequent calibration or adjustment of the error model coefficients. The variation of data parameters is of essential importance in this consideration. The statistical basis for the evaluation program has been investigated to determine the sampling parameters such as length of data runs, number of times a test must be run and similar considerations which will result in a relatively high confidence level.

Experiment Design

The experiment design phase of the planning effort has been closely coordinated with the evaluation planning program. This insures that the data produced, as a result of these experiments, meets the needs of the mathematical and statistical procedures developed for the data processing. The experiments which are planned for system evaluation are based on the use of aircraft, balloons, satellites and missiles of opportunity. The evaluation program as planned does not necessarily demonstrate all of the quantitative and qualitative requirements of the Technical Exhibit. The program is , however, designed to cover those portions which are not covered by the Dockside System Acceptance or System Integration Tests. Through a combination of these dockside tests and the evaluation program, a demonstration has been made of compliance with all of the Technical Exhibit requirements whenever feasible.

Due to the limitation imposed by time and cost considerations, it was not possible to design a program which would provide test data in every combination of geometry, rates and accelerations, or other parameters as defined by the Technical Exhibit. In order to complete the evaluation over the Range of the technical exhibit requirements, it is necessary to extrapolate the data into values not covered by the particular experiments. The amount and appropriateness of extrapolation into particular areas varies between experiments. For instance, it is possible to track an aircraft over the full range of azimuth angles and nearly the full range of elevation angles prescribed by the technical exhibit. But it is not possible to provide experimental conditions which will give tracking at the maximum angular rates or accelerations required. On the other hand, it is possible to set up an experiment which will determine the capability of measuring the secondary target position with respect to the first, at both extremes of target separation. Satellite and missile tests will be used to extend the range of variables as much as possible.

Description of Experiments

In order to demonstrate the capability of the ARIS System to acquire, track and determine the trajectory of a primary target (e.g., nose cone) with respect to the ship to a high degree of

accuracy, our experiment utilizes a single target aircraft, equipped with appropriate instrumentation, which is tracked simultaneously by range instrumentation and the ship's instrumentation. The position of the ship during the experiment is verified by tracking it with accurate optical instruments located on shore, or by having the ship at dockside. Data are then reduced to compare the deviation between the target position as determined by the ARIS System and by range instrumentation, which in this case is the standard of measurement. This positional data will, in addition, be used for velocity computation.

The ability of the system to observe secondary targets and record their positions with respect to the primary target will also be evaluated in this experiment. This will be done by flying two aircraft, spaced so that they will both be in the radar beam for a portion of the flight path. Both aircraft will be tracked by range instrumentation to determine their spacing while the ships instrumentation system simultaneously tracks the targets to determine the position of the second target with respect to the first. This tracking data will also be used to determine the ability of the system to compute the velocity of a secondary target.

The ships system is required to measure the radar cross-section of a target at L, X and C-band frequencies. This measurement must be made to within ±3 db (reduced data) for primary targets, decoys and fragments. The standard deviation shall not exceed 3 db for observable secondary targets which are within 0.4 of the one-way half-power beam width from beam center.

Metallized six-foot balloons of known radar reflection characteristics will be used to perform the experiment. Balloons will be released from the ship, acquired and tracked by the Star Tracker telescope to a point outside of the minimum range of the radars and then skin tracked until they reach an altitude of approximately 60,000 feet. The balloon rise will be limited to a pressure corresponding to approximately 60,000-foot altitude automatically. Tracking will continue until a slant range of over 100-nautical miles is reached. This test will also be run using a six-inch sphere attached to a balloon.

During these runs, data will be gathered at specified range intervals, by three radars, in two polarization modes. additional data will be gathered in a similar manner except that the radar beams will be offset to simulate the observation of a secondary target. This will appear to place the target near the half-power beam width point.

Another experiment is designed to evaluate the accuracy of the shipboard instrumentation in determining ship position in geodetic coordinates. By conducting an actual SONAR beacon sowing and benchmarking operation and by navigating by means of the beacons, the Stabilization-Navigation Sub-system will

determine ship position in astronomical coordinates and obtain the geodetic position by applying the known gravity anomaly for the test area.

The placement of the beacons will be in water depths ranging from 1000 to 3000 fathoms. The ship will locate the beacons by measuring the slant ranges to them, at the same time determining its own position by celestial fixes. From a knowledge of the water depth and slant ranges at various ship's positions, the position of the beacons will be determined. The ship will then navigate by means of the SONAR beacons, and its position will be compared to the ships position as determined by Lorac B to evaluate the system. The technical exhibit requires that the system be capable of planting and locating a SONAR beacon to a vector error of 1340 feet. In addition, the ship must be able to locate itself with respect to the SONAR beacon to a vector error of 300 feet rms.

The ability of the system to perform this function will be evaluated by actually carring out an operation in placement, location and navigation from these beacons. For the purpose of the experiment, the beacons will be placed in the vicinity of Great Abaco Island in the Little Bahama bank. This area has water of sufficient depth and is within the range of the Lorac B net, which can determine the ship's location to sufficient accuracy to be used as a standard of measurement.

Throughout the nine week evaluation period, as scheduling permits it is planned that the ship will track satellites and missiles of opportunity on a non-support basis. These tests will determine the ships ability to acquire and track live targets under realistic operating conditions. They will be scheduled as often as possible in order to supplement data gathered in the previously described tests.

Acquisition by telemetry, star tracker, real-time orbital elements and classical orbital elements in the case of satellites will be attempted. Lists of useable satellites and available missiles will be prepared for the period of the evaluation. Some of these tests which might require operation downrange beyond the Bahamas will have to be conducted after the nine weeks because of the excessive steaming time involved.

These tests will be primarily operational in nature and will assist in developing operator confidence and techniques as well as serving to round out the data gathered in the evaluation.

PRESENT USE OF INSTRUMENTED SHIPS C" AMR

	NO.	Primary Purpose	Remarks
Various Telemetry Ships	8	200 mc TELEMETRY	DEPLOYED WORLD WIDE
Twin Falls Victory	1	ACQUIRE ACCURATE TRAJECTORY INFORMATION	DEPENDS on LORAC for ACCURATE POSITIONING
American Mariner (DAMP)	1	GATHER SIGNATURE DATA	HAS HAD LIMITED USE ON AMR

Figure 1

PRECISION RADAR TRACKING

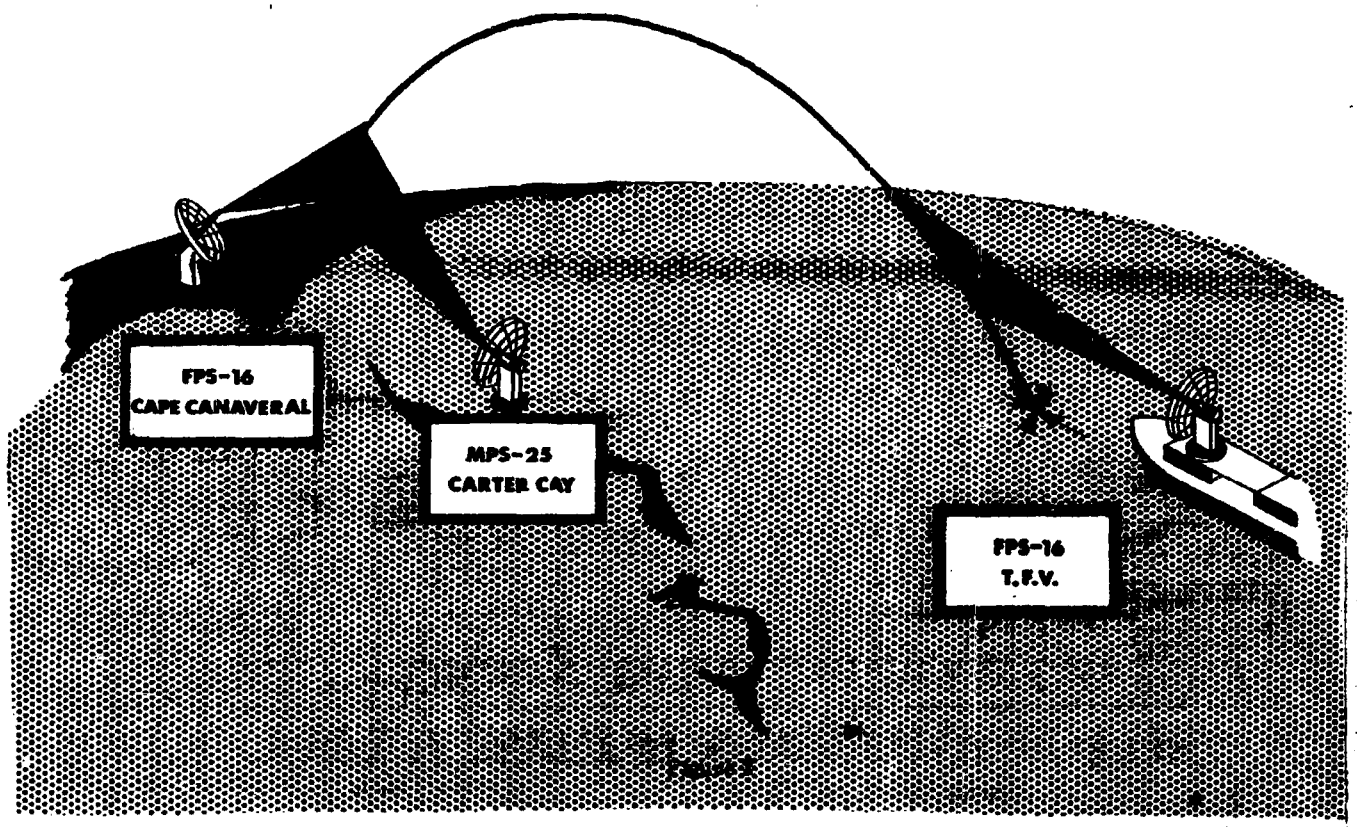

TWIN FALLS VICTORY SHIP

Primary Instrumentation

1. Tracking AN/FPS-16 'C' Band Radar
2. Navigation LORAC 'B' Hyperbolic System
3. Attitude N7G Inertial Navigator
4. Attitude MK 19 Inertial Navigator (Backup)
5. Impact Location AN/SPN-8 'S' Band Radar

Figure 3

TWIN FALLS VICTORY SHIP

1961 ACCURACY STUDY

		1961- - - - - 9 Tests
Systematic Errors	$\overline{\Delta x}$	50.6
	$\overline{\Delta y}$	23.6
	$\overline{\Delta z}$	25.8
Random and Cyclic Errors	σx	16.6
	σy	14.0
	σz	28.9

Notes:

1. All distances are in meters.
2. All computations made at approx. 140,000 feet, Slant range (80,000 ft. alt.) from ship.

Figure 4

Typical ARIS Mission

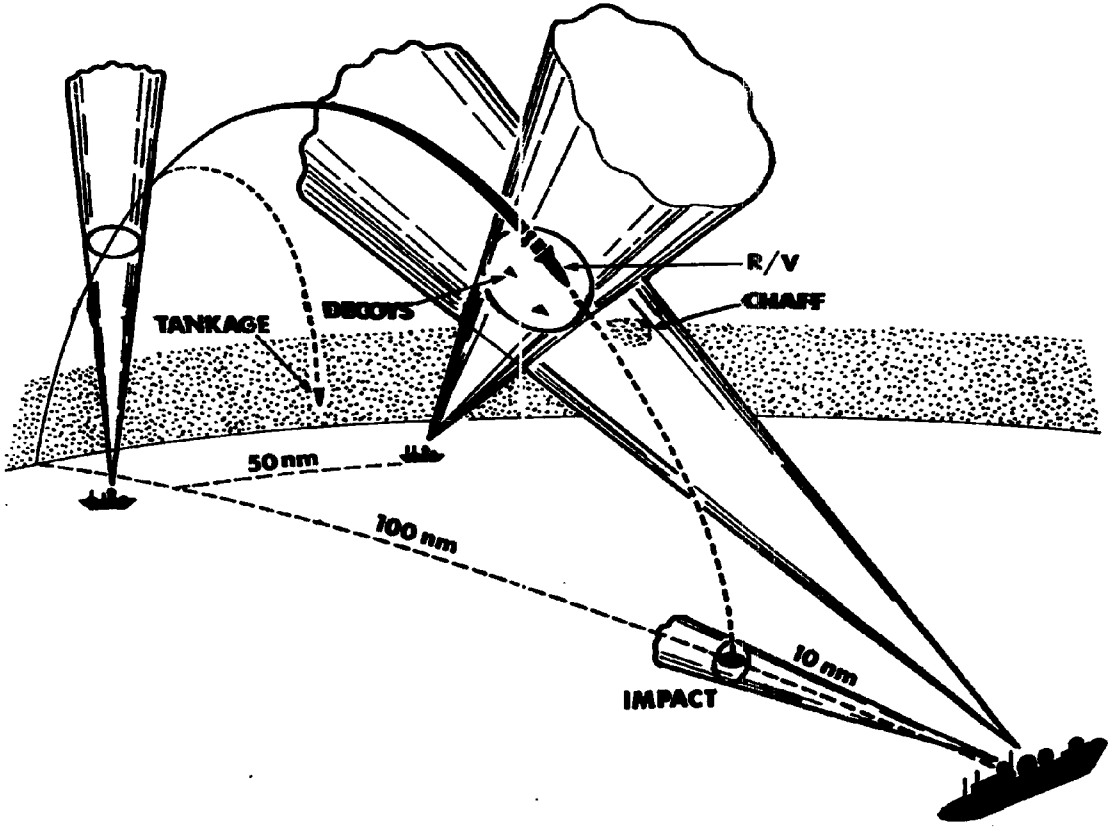

Figure 5

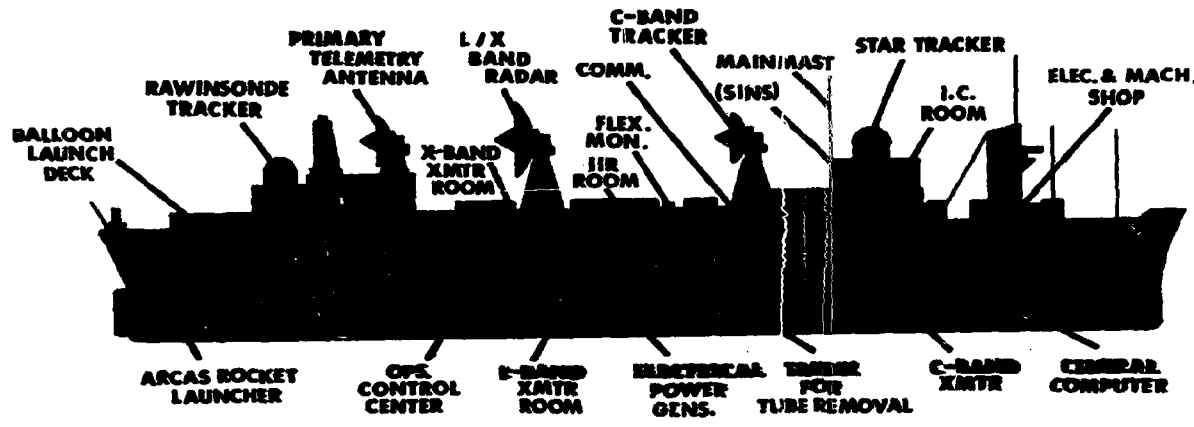

ARIS SHIP

Figure 6

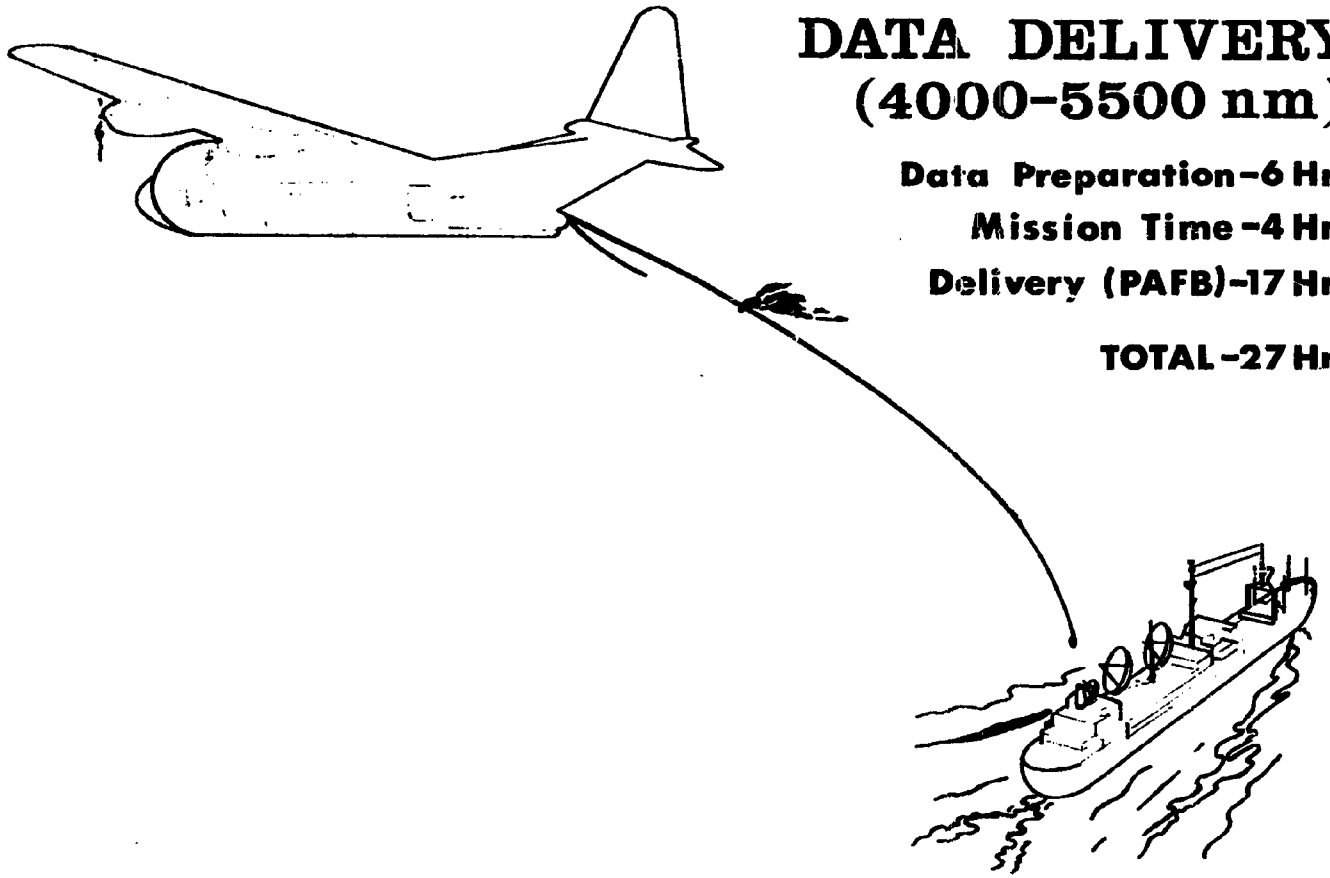
DATA DELIVERY
(4000-5500 nm)
Data Preparation-6 Hrs
Mission Time-4 Hrs
Delivery (PAFB)-17 Hrs
TOTAL-27 Hrs

Figure 7

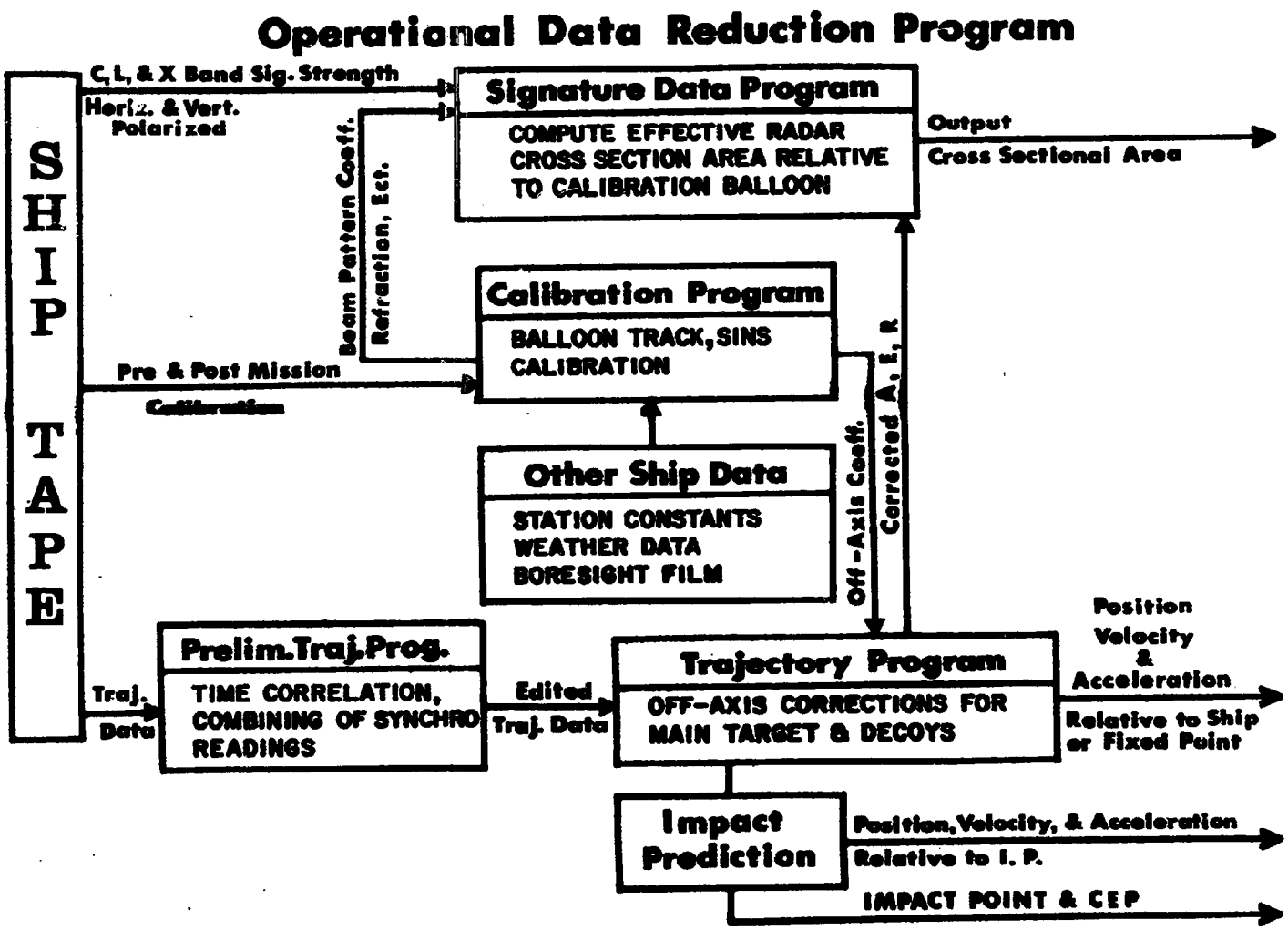
Operational Data Reduction Program
SHIP TAPE
C, L, & X Band Sig. Strength
Horiz. & Vert. Polarized
Beam Pattern Coeff.
Refraction, Ect.
Signature Data Program
COMPUTE EFFECTIVE RADAR CROSS SECTION AREA RELATIVE TO CALIBRATION BALLOON
Output
Cross Sectional Area
Calibration Program
BALLOON TRACK, SINS CALIBRATION
Pre & Post Mission
Calibration
Other Ship Data
STATION CONSTANTS
WEATHER DATA
BORESIGHT FILM
Off-Axis Coeff.
Corrected A, E, R
Prelim. Traj. Prog.
TIME CORRELATION, COMBINING OF SYNCHRO READINGS
Traj. Data
Edited Traj. Data
Trajectory Program
OFF-AXIS CORRECTIONS FOR MAIN TARGET & DECOYS
Position Velocity & Acceleration
Relative to Ship or Fixed Point
Impact Prediction
Position, Velocity, & Acceleration
Relative to I. P.
IMPACT POINT & CEP

Figure 8

N
809-B

THE ERRORS OF INERTIAL GUIDANCE SYSTEMS

by:

Dr. Martin G. Jaenke

Holloman Air Force Base, New Mexico

Presented at:

FOURTH JOINT AFMTC-RANGE USER DATA CONFERENCE

Orlando Air Force Base, Florida

26-28 February 1963

THE ERRORS OF INERTIAL GUIDANCE SYSTEMS

A survey of the activities of the Central Inertial Guidance Test Facility at Holloman Air Force Base, New Mexico. Compiled by Dr. Martin G. Jaenke, Technical Advisor to the Deputy of Guidance Test.

I. INTRODUCTION

The Central Inertial Guidance Test Facility (CIGTF) of the Air Force Missile Development Center (AFMDC) at Holloman AFB, New Mexico, serves as an inter-agency facility for the development testing of guidance systems. Among the many points of view which are relevant in guidance testing, e.g. the problems of reliability, repeatability and environmental sensitivity, the determination of their accuracy, their calibration or the evaluation of their errors, is thought to be of most direct interest to this audience. Therefore, besides giving rudimentary background information to the uninitiated in guidance techniques, this paper endeavors to outline a basic analysis of the errors encountered in the evaluation of the errors of guidance systems. Due to the high quality of present day and future guidance systems, the provision of sufficiently accurate calibration standards, i.e range instrumentation or reference systems, is problematic and thus this point of view will be emphasized.

The mathematics to be used are schematic and simplified and thus are sufficient only to indicate trends. One must be aware, however, that the complete mathematics of this area are extremely complex and mostly not amenable to closed form solutions. Thus, extensive computer simulation studies are needed to perform a fine grain error analysis, an effort which is a continuing important part of the activities of the CIGTF.

The list of references shows a relative abundance of unpublished notes, internal memoranda and office correspondence, an indication of the fact that the art of guidance testing is still under active development. It shows further important contributions by Space Technology Laboratories (STL) who, under contract with the Air Force, evaluate the guidance systems of the Minuteman and Titan II missiles. The exchange of information and ideas with STL was extremely fruitful and it is hoped that this paper will open the way for such discussions on a wider basis.

II. DEFINITION OF THE ERRORS OF INERTIAL GUIDANCE SYSTEMS

The basic principle (1) of inertial guidance is the measurement of acceleration, a function which is performed by inertial accelerometers. To allocate a defined direction to the measured acceleration, the platform carrying such accelerometers must be of known and controllable orientation. This function is performed by gyroscopes, which maintain the platform in a given reference orientation in space, and, by application of proper torques to the gyro gimbals, allow this orientation to be changed in a prescribed manner. Due to the integrating action of the gyros, the angular turning rates of the gimbals are proportional to the respective torques and thus a measurements of these torques provides information on the turning rates of the vehicle carrying the platform in inertial space. These two measured quantities, linear acceleration and angular turning rates are not sufficient to perform the desired guidance function. It is rather necessary to know velocity, in particular "velocity to be gained" if the vehicle is going to be injected into ballistic or orbital flight and to develop discrete commands for termination of thrust and correction commands for the attitude control of the vehicle. All these quantities are computed from the original measurements in the guidance computer, in most cases a digital computer. Thus, an inertial guidance system consists of the "Inertial Measurement Unit" (IMU), the stabilized platform carrying the triad of accelerometers and the gyroscopes and the guidance computer as shown in Figure 1. For purposes of evaluation of the system, the quantities of interest are telemetered to ground, the outputs of the computer through PCM, the outputs of the IMU either through FM/FM or PCM channels.

Inertial Guidance Systems are technical systems and as such limited in their accuracy. Their errors are partially systematic, i.e., they can be described by functional relations, and partially random, i.e., they can be described in statistical terms only. The systematic errors can be compensated for and thus eliminated, at least theoretically, if sufficient information about them is available. It is therefore the primary goal of guidance testing to obtain the necessary information about these systematic errors to a sufficient degree of accuracy. The most important systematic errors and the ensuing error models, where definable, are listed in the figures, in Fig 2 and Fig 3 the ones of the basic systems components and in Fig 4 the ones which are not directly attributable to the components but are characteristic for the whole system. Assuming that it is possible to formulate a comprehensive error model in a specific case either from theoretical considerations or from a careful analysis of test results, it is then necessary to determine the error coefficients accurately enough to achieve desired goals. One of such goals was already indicated, namely, to obtain sufficient information for the compensation of the errors during a mission of the vehicle of which the guidance system is a part. In order to define the necessary accuracy of error coefficient determination, an "Error Budget" has to be established which is based on the specific mission requirements. Selecting as a representative example an ICBM mission, the following considerations can be made:

The measure of accuracy in such a mission is the CEP obtained at the prescribed range. It depends on the conditions which prevail at the moment of injection into ballistic flight, in particular on velocity and flight path angle, both conditions which are under control of the guidance system. The dependency on velocity is shown in Fig 5. For the present demonstration

purposes and to keep this paper unclassified, this description is derived under simplifying assumptions, namely, classical elliptical trajectory in a central, unperturbed force field, non-rotating earth and identity of injection and launch point. (3) Furthermore, the assumption is made that the flight path angle at injection is optimum, i.e., leading to a minimum injection velocity requirement. In this case, the derivative of range with respect to injection angle vanishes and thus it is justified to concentrate in this presentation on the primarily important velocity errors. However, other errors than those caused by the guidance system enter in the uncertainty of the impact point. Examples are uncertainties with respect to the form of the perturbed gravity field, the geographic location of the desired impact point and the survey of the launch point. Since they are not under discussion in this paper, their effect is considered in a round-about way by allocating half of the allowable squared impact errors to such non-guidance sources. (4) Having defined the allowable injection velocity uncertainty it must be translated into an allowable uncertainty in the determination of the error coefficients of the guidance system. This uncertainty is quantitatively described by the covariance matrix, Λ_k, of the coefficients and is a characteristic of the test from which the error coefficients were evaluated, as will be explained later. Fig 6 shows the relation between this matrix and the admissible injection velocity error or the CEP of the mission, respectively. Again it must be kept in mind that sources other than the uncertainties of the error coefficients contribute to the injection velocity error. Examples are approximations in computing processess, in particular the mechanization of compensation terms, and other hardware errors. Their effect is considered in a roundabout way by the factor 2 in equation (5), i.e. by allocating about 75 percent of the squared injection velocity error as resulting from other sources.

Another important goal of error coefficient evaluation is a thorough analysis of the guidance system during its development. Thus it is necessary to separate its various error sources, the terms of the error model. To achieve this, the guidance test must be conducted in such a way, that the off-diagonal terms of the resulting coefficient covariance matrix are as small as possible. Assuming that it were possible to obtain a covariance matrix consisting of diagonal terms only, it still remains to define the admissible amount of these variances of the individual coefficients. Again the flight conditions of the operational missile at injection are used to weight these uncertainties properly, leading to an error budget which is identical to equations (5) and (6) except that the sums containing the off-diagonal terms of the covariance matrix are omitted (equation (6a)). Since the separation of errors is the primary goal of guidance testng at the CIGTF, this latter error budget is used to design the tests. It specifies two basic testing requirements, namely, to select test conditions such that the off-diagonal terms of the resulting coefficients covariance matrix became as small as possible and to make testing errors sufficiently small in order to keep the terms on the main diagonal of this matrix within specified limits.

III. DETERMINATION OF THE ERRORS OF INERTIAL GUIDANCE SYSTEMS

Testing of Inertial Guidance Systems for determination of their errors can be done in various ways. One fundamentally important approach is laboratory testing. (5) These tests are designed to find specified individual error coefficients of a theoretical error model by using special purpose test equipment under carefully controlled test conditions. But a preconceived error model may not be realistic, there may be additional error terms under the conditions of actual missile flight. It is therefore necessary to conduct tests which exercise simultaneously and strongly all the error

sources which come into play during an actual missile flight and provide sufficient accuracy and flexibility of arranging test conditions in such a way that a separation of the error sources is possible. This type of testing will be called "operational" testing, but it must be understood that its conditions are only tentatively identical to those of an actual operational flight of the missile for which the guidance system under test is developed. The operational test methods which will be discussed are: Sled testing, Flight testing of the completed missile under actual flight conditions and GEM (Guidance Evaluation Missile) testing. In all cases of operational testing the velocity of the vehicle carrying the guidance system must be measured by a "reference" system with sufficient accuracy to meet the requirements of the error budget which was established above. Fig 7 describes the basic mechanism of estimating the desired error coefficients and in particular spells out the propagation of the errors in the observation of the guidance systems error function into the errors of the coefficient estimates, or, the coefficient covariance matrix. To clarify concepts, Fig 8 shows a chart of the complete error flow from its sources in the test reference system to its final effects on the mission accuracy of the missile of which the guidance system under test is a part. The present discussion will be restricted to define the admissible effective velocity error of the reference system as represented by $\dot{R}_{adm}$ and no attempt will be made to perform the complicated error analysis of the reference system itself. It is now of interest to compare the effective velocity error which is admissible for the various types of operational tests in order to achieve a specified testing goal. In doing this, it is assumed that this error is serially uncorreleated and stationary, an assumption the justification of which will be discussed later. Fig 9 gives the resulting accuracy requirements for a representative example. The other important requirement, separability of error sources, is discussed in Fig 10.

In order to obtain one figure to describe this separability quantitatively, it is suggested to use an overall correlation factor derived from the ratio of the sums of off-diagonal and diagonal terms of the Λ_k matrix, weighted by the respective coordinate functions at burn-out of the operational missile. However, other descriptions are possible and the feasibility of this γ - factor has not yet been proven in practical use. Inspection of Fig 9 and 10 shows clearly the superiority of GEM testing under the given points of view. In interpreting the quanititative accuracy requirements one must keep in mind that they were derived primarily for comparing the various test methods under equal and simplified assumptions. A thorough error analysis leads to higher requirements in all cases. One must further keep in mind that the correlation factor becomes critical only for values greater than 0.9. A comprehensive operational guidance test program which yields the desired results in the fastest and most economical way must use all three test methods and their respective merits: Sled testing as an economical means for shake-down testing in a severe environment and preliminary error evaluation, GEM testing for fine-grain error evaluation and flight testing for final CEP verification. (6), (7).

The error analysis above was simplified and it is of importance to obtain an understanding of the impact of these simplifications. One of the assumptions made was stationarity of the errors. Presently, there are no conclusive results available about the consequences of this assumption in an error analysis. Thus, this aspect will not be pursued in this presentation. The other assumption was that the errors are uncorrelated. Again, a systematic investigation was not yet performed and thus it is possible only to demonstrate with representative examples how much a serial correlation in the effective velocity error of the reference system, which was assumed to be uncorrelated, will affect the results of the error analysis obtained above.

The correlation structure used in these examples is derived from a special filtering process (8) for the output of which the inverted covariance matrix can be described analytically. (See Fig 11) The consequences of assuming uncorrelated errors in such an analysis while the error actually is correlated are shown in Fig 12. (9) Depending on whether the correlation leads to peaking of the error power spectrum at low or high frequencies, the accuracy requirements for the reference system can be significantly higher or lower than those calculated for the uncorrelated case. If no prior information about the expected character of the error spectrum is available for the error analysis, the estimate based on the assumption of uncorrelated errors thus leads to feasible results.

To describe the practical problems connected with the evaluation of operational guidance tests, the example of sled test evaluation will be used, for which considerable experience has been accumulated at AFMDC. Fig 13 shows first a typical vehicle which is used for this purpose and Fig 14 a typical sled trajectory in terms of its acceleration and velocity profiles. An important characteristic of sled motion is an extremely high vehicle vibration. (12), (13) Fig 15 shows a plot of total vibrational power in the longitudinal direction, demonstrating the non-stationary character of these vibrations and Fig 16 their spectral composition. The "Space-Time" system (10) serves as reference system. It produces electrical pulses when the vehicle passes precisely spaced markers ($13 \pm 1.3 + 10^{-4}$ ft) along the track. (11) These pulses are transmitted thru telemetry to a ground station and are precisely timed ($\pm 1\,\mu$ s), yielding the basic reference information: time as a function of distance. This information is available on a digital data tape for further computer processing. The signal outputs of the guidance system under test are transmitted primarily thru

FM/FM telemetry and after first demodulation are available as a composite signal on magnetic tape. Before computer processing, these signals have to be decommutated and digitized. A special digitizing process is required for the outputs of the accelerometers which produce discrete signals at the times at which certain velocity increments are accrued. The accurate determination of these times and their presentation on digital data tape is performed by the "Event Time Reader", a custom-built device which is incorporated in the "General Input Converter". (19) Fig 17 shows a flow chart of the digital computer programs required for the evaluation of sled tests. There are about 35 of them and they are designed in such a way as to permit any desired intermediate outputs of data tapes, tabular and graphical information and to adapt to special situations caused by inferior data quality. Fig 18 describes the main operations in this chart in a schematic form. Of special interest are the following areas:

Editing Processes

Their basic purpose is to improve obviously wrong data points by removing such points which are due to noise alone, inserting improved estimates for highly deviating points and filling in estimates for missing points. This is done by extrapolating an expected point from an edited stretch of data, by defining a region of acceptability and finally making a decision about the actually observed point. Extreme care must be taken not to bias the data in this process. Such editing programs must be closely tailored to the specific type of data, employing a thorough knowledge of the physics and the logic of the instrument which produces the data, the properties of the data tranmission channels and of the data conversion processes. The systems analyst who evaluates the computer results in many cases can allocate error trends to erroneous editing decisions and a re-run of the computer programs is frequently necessary.

Linear Operations

This heading includes two fundamental operations which are necessary to obtain the desired results, namely, differentiation of Space-Time data and integration of accelerometer data to obtain velocity. Both operations are non-ideal, i.e. they are accompanied by a band-limiting (smoothing) low-pass filter action. One has to keep in mind that the same smoothing process has to be applied to the Space time and accelerometer data and to the coordinate functions to maintain the validity of the error model equation which will be solved for the error coefficients. If this is done properly, then the accuracy of the coefficient evaluation is independent of the smoothing process. Two practical approaches for data smoothing were investigated: moving polynomial arc smoothing and velocity averaging. (14) The first is applied to the space time data which are functions of distance and thus necessitates inversion of the results to obtain velocity on a function of the independent variable, time. It leads to time-variable, velocity dependent filters which are difficult to duplicate for application to the accelerometer data and coordinate functions. (15, 16, 17) The smoothing process which leads to velocity averaging is particularly easy to mechanize on the digital computer in all three applications, Space Time data, accelerometer data and coordinate functions. It is therefore presently used for guidance test evaluation.

The third area of interest is the least squares fitting to obtain the error coefficients. The process presently employed is non-optimum, leading to non-maximum likelihood coefficient estimates because the error in Δ_i is handled as uncorrelated and stationary, represented by a covariance matrix which has only constant diagonal terms. The reason for this simplification is the fact that the actual structure of the covariance matrix is not known and even if it were, its inversion would constitute a formidable task.

But fortunately simulation and analytical studies have shown that the process is relatively insensitive to these simplifications. Fig 19 gives a representative example. However, one must be aware that this is an area of possible improvement. One promising approach which avoids the computational complexities of inverting large matrices would be to remove the correlation of the errors, or to "pre-whiten" the noise, by applying a suitable equalizing filter to the Space-Time and accelerometer data and to the coordinate functions. To design such a filter, the actual structure of the error must be known. Thus, one can define a linear operator to be applied to the observed data and the coordinate functions of a maximum-likelihood estimation process which is "optimum" in the sense that it minimizes the computational complexities of the process. This approach was brought to our attention by Dr. A. J. Mallinckrodt of Communications Research Laboratories in discussions at the Inertial Guidance Test Symposium at Holloman AFB in October 1962; it will be further investigated.

Another important area of interest in the discussion of sled testing is the accuracy of its reference system, the Space-Time system. Its basic accuracy is high due to the virtual absence of systematic errors and its insensitivity to electromagnetic propagation properties. With the given errors in spacing of the markers and in timing of the marker pulses an estimate of the resulting velocity error yields a value of about 0.01 ft/sec and thus the system would essentially meet the requirements developed earlier. However, there is one major source leading to errors in Δ_{v_0} which is independent of the accuracy of the Space-Time system. It is due to the fact that the reference system measures vehicle motion on another point of the vehicle than the guidance system, a fact which may very well play a role

in the other types of operational testing also. (18) Thus, the vibratory motions sensed by the guidance system are different from the ones measured by the reference system and this difference is a major component of the error in Δv. The analysis of the structure of this error, which is of the 0.1 ft/sec order of magnitude, is still under way. There are indications that the spectrum of this error is of the type which peaks at high frequencies and has relatively little power in the critical low frequency area. This is confirmed by the consideration that a substantial very low frequency differential motion can not exist without endangering the structural integrity of the vehicle. Thus this error may not contribute significantly to the uncertainty of the coefficient estimates.

IV. GUIDANCE SYSTEMS AS CALIBRATORS FOR RANGE INSTRUMENTATION SYSTEMS

In view of the difficulty to provide reference systems of sufficient accuracy to calibrate inertial guidance systems, it is challenging to discuss the possibilities of using modern high quality guidance systems for the improvement or calibration of existing reference systems. One has to be fully aware of the logical dangers of such "boot-strap" methods, but in certain cases this philosophy has been used successfully. If the errors of the reference system are clearly separable from the ones of the guidance system, then they can be determined by inspection of the Δv function. This was done successfully to find misplaced markers of the Space-Time systems in sled testing. In case of finite correlation between these two groups, certain error coefficients of the reference system model can be considered as additional unknowns and can be estimated together with the ones of the guidance system error model. Though resulting initially in a deterioration

of the covariance matrix of the guidance systems coefficients, an iterative procedure in which the estimates of the respective reference systems errors are removed from the Δ_{ρ}-function may lead to a final improvement of the test results. Studies are under way to investigate the applicability of such a procedure to GEM testing but results are not yet available. A related approach is described in Fig 20 in which the output of the guidance system under test contributes to the redundancy of the reference measurement. The listed equation for the resulting Λ k matrix holds for the assumption that the errors of the guidance system and those of the reference system are uncorrelated and the measurements from each group are at least sufficient to determine the unknowns. The effects of deviations from the first assumption and thus the feasibility of the approach have to be investigated by a suitable simulation process. (See also (20) Finally, Fig 20 describes the possibility to calibrate the reference system of a given test range with a guidance system which was pretested at another range. In this case, the guidance system serves as a vehicle to transfer accuracy from one test range to another. It shows the error flow from its source R , the error covariance matrix of the original reference system, to Λ_{β}, the covariance matrix of the error coefficients B of the reference system to be calibrated. The efficiency of the process is under control thru proper selection of the flight profiles in both tests as indicated by the various coordinate functions matrices: Ψ , the derivatives matrix of the velocity errors with respect to the error coefficients of the guidance system in the original test, Φ , the same derivatives in the calibration test and M , the derivatives of velocity error with respect to the error coefficients of the reference system in the calibration test. No quantitative evaluation of this approach is available yet, but it will be kept in mind as a possible tool of improvement of the GEM reference system in the preparation of these tests.

V. CONCLUSION

If, in addition to providing a basic familiarisation with the problems of guidance testing, this paper will initiate discussions and exchange of experience with other users of test ranges, it will have served its purpose. To improve existing and develop new test methods using all information which can be made available is one of the most important objectives of the Central Inertial Guidance Test Facility at Holloman AFB.

SCHEMATIC OF INERTIAL GUIDANCE SYSTEM

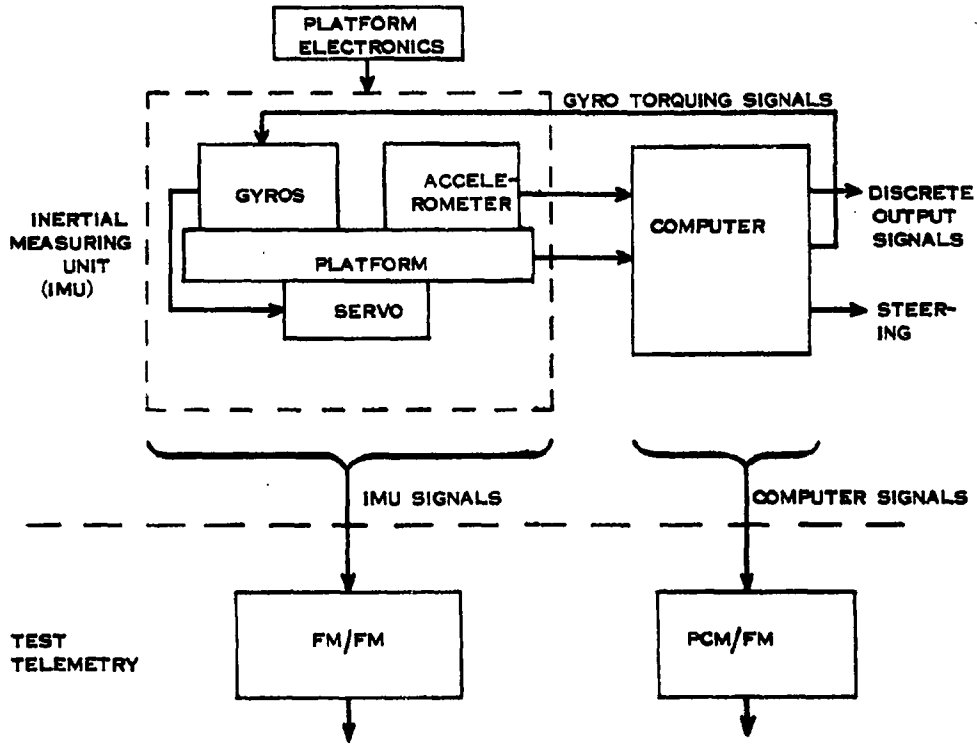

FIG 1

ACCELEROMETER ERRORS

$a(t)$: ACCELERATION ALONG SENSITIVE AXIS

$a_T(t)$: ACCELERATION ALONG TRANSVERSE AXIS

ERROR COEFFICIENT	COORDINATE FUNCTION	DESCRIPTION
K_0	1	BIAS ERROR
K_1	$a(t)$	SCALE FACTOR ERROR
K_2	$a^2(t)$	NON-LINEAR ERRORS
K_3	$a^3(t)$	
K_4	$a(t)\,a_T(t)$	CROSS-COUPLING ERROR
K_5	$\dot{a}(t)$	DYNAMIC ERROR

VELOCITY ERROR MODEL

$$\text{(1)}\quad \Delta v(t) = K_{00} + K_0 t + K_1 v(t) + K_2 \int_0^t a^2(t)\,dt + K_3 \int_0^t a^3(t)\,dt + K_4 \int_0^t a(t)\,a_T(t)\,dt + K_5\, a(t)$$

FIG. 2

GYRO ERRORS

INDICES: i ALONG INPUT AXIS

S ALONG SPIN AXIS

ERROR COEFFICIENTS	COORDINATE FUNCTION	DESCRIPTION
C_o	1	CONSTANT DRIFT RATE
C_1	$a_i(t)$	DRIFT RATE DUE TO MASS UNBALANCE ALONG SPIN AXIS
C_2	$a_S(t)$	DRIFT RATE DUE TO MASS UNBALANCE ALONG INPUT AXIS
C_3	$a_i(t)\, a_S(t)$	DRIFT RATE DUE TO GIMBAL COMPLIANCE

ERROR MODEL FOR DRIFTS AROUND INPUT (STABILIZATION) AXIS:

$$(2)\quad \phi(t) = C_{oo} + C_o t + C_1 v_i(t) + C_2 v_S(t) + C_3 \int_0^t a_i(t)\, a_S(t)\, dt$$

FIG. 3

SYSTEM ERRORS

DEVIATIONS FROM ORTHOGONALITY IN COMPONENT MOUNTING

ALIGNMENT ERRORS

DYNAMIC ERRORS OF PLATFORM STABILIZATION LOOP

EFFECTS OF APPROXIMATIONS IN COMPUTING PROCESSES

ENVIRONMENTAL INFLUENCES

ADMISSIBLE INJECTION VELOCITY ERROR (σ_{v_0})

IN ICBM MISSION

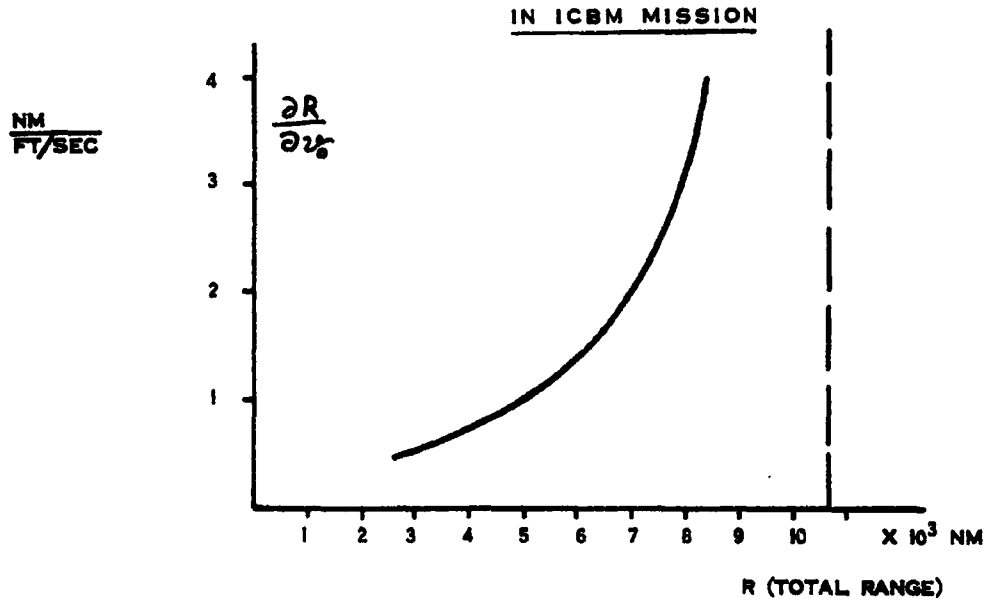

(3) $\sigma_{v_0} \leq \sigma_R \left(\frac{1}{\frac{\partial R}{\partial v_0}}\right) \leq \text{CEP} \frac{1}{1.18} \left(\frac{1}{\frac{\partial R}{\partial v_0}}\right)$

UNDER CONSIDERATION OF OTHER ERROR SOURCES:

(4) $\sigma_{v_0} \left[\frac{\text{FT}}{\text{SEC}}\right] \leq \text{CEP} \left[\text{NM}\right] \left(\frac{0.6}{\frac{\partial R}{\partial v_0}}\right)$

FIG. 5

ADMISSIBLE ERRORS IN DETERMINATION OF ERROR COEFFICIENTS

Λ_K: COEFFICIENT COVARIANCE MATRIX (N X N FOR N-TERM ERROR MODEL)

$\lambda_{i,j}$: ELEMENTS OF Λ_K - MATRIX

$\varphi_{i,j}$: INSTANTANEOUS VALUES OF COORDINATE FUNCTIONS AT INJECTION

$$(5)\quad \sigma_{\varphi_R} = 2\left[\sum^{i} \lambda_{ii}\ \varphi_i^2 + 2\sum^{ij} \lambda_{ij}\ \varphi_i\ \varphi_j\right]^{1/2}$$

ERROR BUDGETS:

FOR ERROR COMPENSATION:

$$(6)\quad CEP = \left(\frac{\partial R}{\partial \varphi_R}\right) \frac{1}{0.3}\left[\sum^{i} \lambda_{ii}\ \varphi_i^2 + 2\sum^{ij} \lambda_{ij}\ \varphi_i\ \varphi_j\right]^{\frac{1}{2}}$$

FOR SYSTEM EVALUATION:

$$(6_a)\quad CEP = \left(\frac{\partial R}{\partial \varphi_R}\right) \frac{1}{0.3}\left[\sum^{i} \lambda_{ii}\ \varphi_i^2\right]^{1/2}$$

FIG. 6

ERROR COEFFICIENT DETERMINATION

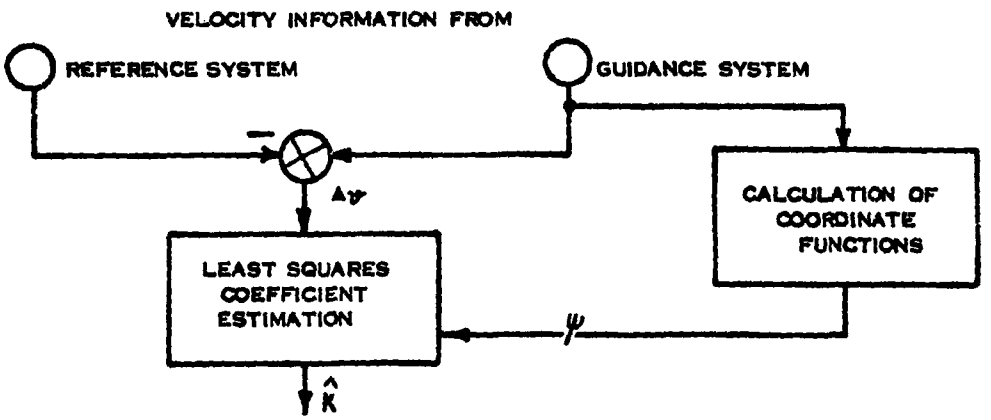

$$(7)\quad \hat{K} = \left[\psi^T R_{\Delta v}^{-1} \psi\right]^{-1} \psi^T R_{\Delta v}^{-1} \Delta v$$

$$(8)\quad \Lambda_K = \left[\psi^T R_{\Delta v}^{-1} \psi\right]^{-1}$$

DEFINITIONS FOR N-TERM ERROR MODEL AND M OBSERVATIONS

Δv: M X 1 MATRIX OF VELOCITY ERROR OBSERVATIONS

$R_{\Delta v}$: M X M COVARIANCE MATRIX OF OBSERVATIONAL ERROR

ψ : M X N MATRIX OF COORDINATE FUNCTIONS

$\hat{K}$: N X 1 MATRIX OF COEFFICIENT ESTIMATES

Λ_K : N X N COVARIANCE MATRIX OF COEFFICIENT ESTIMATES

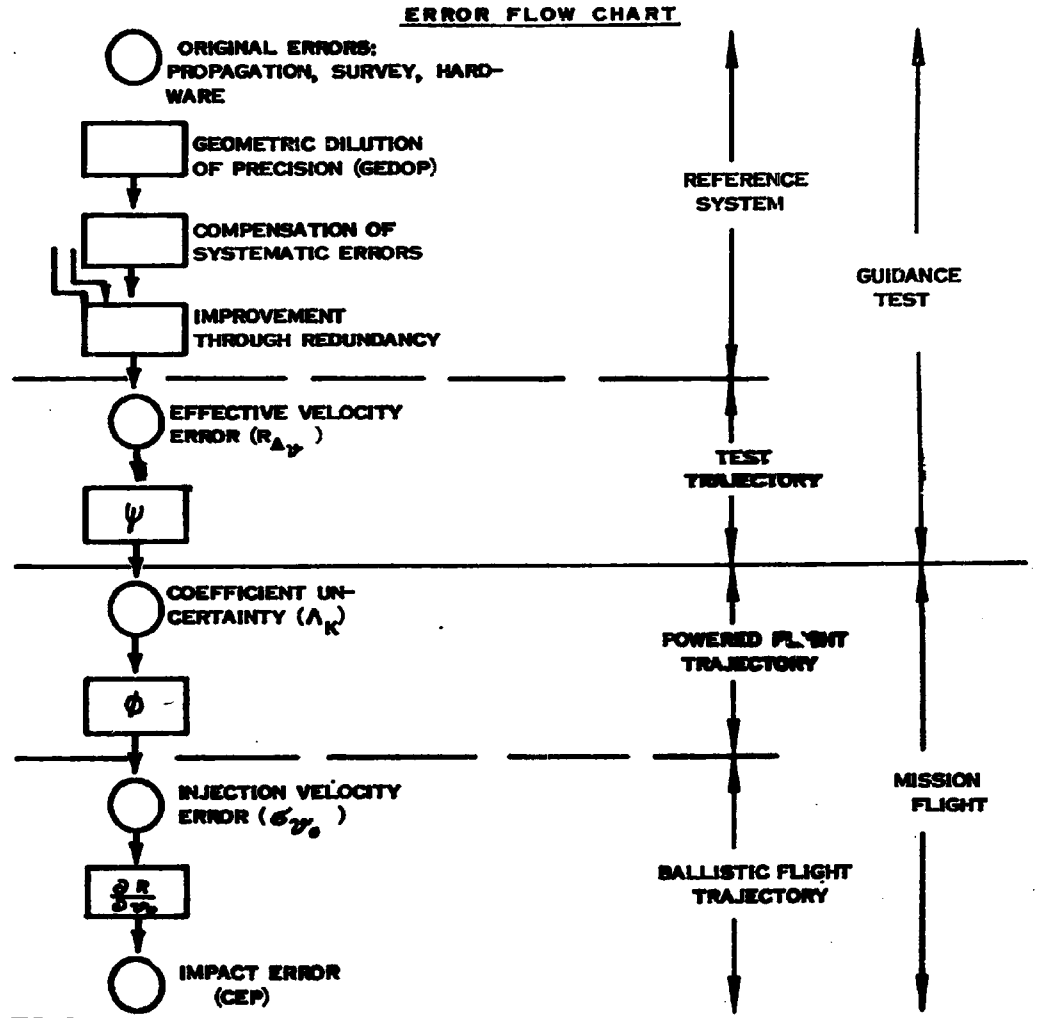
ERROR FLOW CHART
ORIGINAL ERRORS: PROPAGATION, SURVEY, HARD-WARE
GEOMETRIC DILUTION OF PRECISION (GEDOP)
COMPENSATION OF SYSTEMATIC ERRORS
IMPROVEMENT THROUGH REDUNDANCY
EFFECTIVE VELOCITY ERROR (R_{Δ_V})
ψ
COEFFICIENT UN-CERTAINTY (Λ_K)
ϕ
INJECTION VELOCITY ERROR (σ_{V_0})
$\frac{\partial R}{\partial V_0}$
IMPACT ERROR (CEP)
REFERENCE SYSTEM
TEST TRAJECTORY
POWERED FLIGHT TRAJECTORY
BALLISTIC FLIGHT TRAJECTORY
GUIDANCE TEST
MISSION FLIGHT

FIG. 8

ADMISSIBLE EFFECTIVE VELOCITY ERROR

ASSUME UNCORRELATED ERROR

$$(8_a)\ \Lambda_K = \tau^2_{\Delta v} \left[\psi^T \psi\right]^{-1}$$

THEN:

$$(9)\quad \tau_{\Delta v} \leq \text{CEP} \left(\frac{0.3}{\frac{\partial R}{\partial v_0}}\right) \left[\sqrt{\sum^{i} \lambda_{ii}\, \psi_i^2}\right]^{-1}$$

COMPARATIVE EVALUATION OF TEST METHODS

ASSUMPTIONS:

A. ERROR MODEL: $\Delta v = K_0 t + K_1 v + K_2 \int a^2 dt + K_3 \int a^3 dt$

B. MISSION REQUIREMENTS: R = 5500 NM; $\frac{\partial R}{\partial v_0} = 1.20$

	SLED	FLIGHT	GEM(A)
C. TEST TRAJECTORY CHARACTERISTICS			
MAXIMUM VELOCITY $\left[\frac{FT}{SEC}\right]$	1620	21500	14000
TOTAL TEST TIME [SEC]	32.4	340	250
DATA SAMPLING RATE $\left[\frac{1}{SEC}\right]$	50	10	10
ADMISSIBLE VELOCITY ERROR $\tau_{\Delta v}$/CEP $\left[\frac{FT/SEC}{NM}\right]$	0.020	0.048	0.36

FIG. 9

SEPARABILITY OF ERROR SOURCES

WEIGHTED CORRELATION FACTOR γ :

(10) $$\gamma = \frac{2\sum_{i,j} \lambda_{ij}\, \varphi_i \varphi_j}{\sum_{i} \lambda_{ii}\, \varphi_i^2}$$

$\gamma = 0$: IDEAL SEPARABILITY

$\gamma = 1$: IMPOSSIBILITY TO SEPARATE

COMPARATIVE EVALUATION OF TEST METHODS

ASSUMPTIONS: AS IN FIG. 9

	SLED	FLIGHT	GEM (A)
γ	0.021	0.97	0.58

FIG. 10

BROWN FILTER

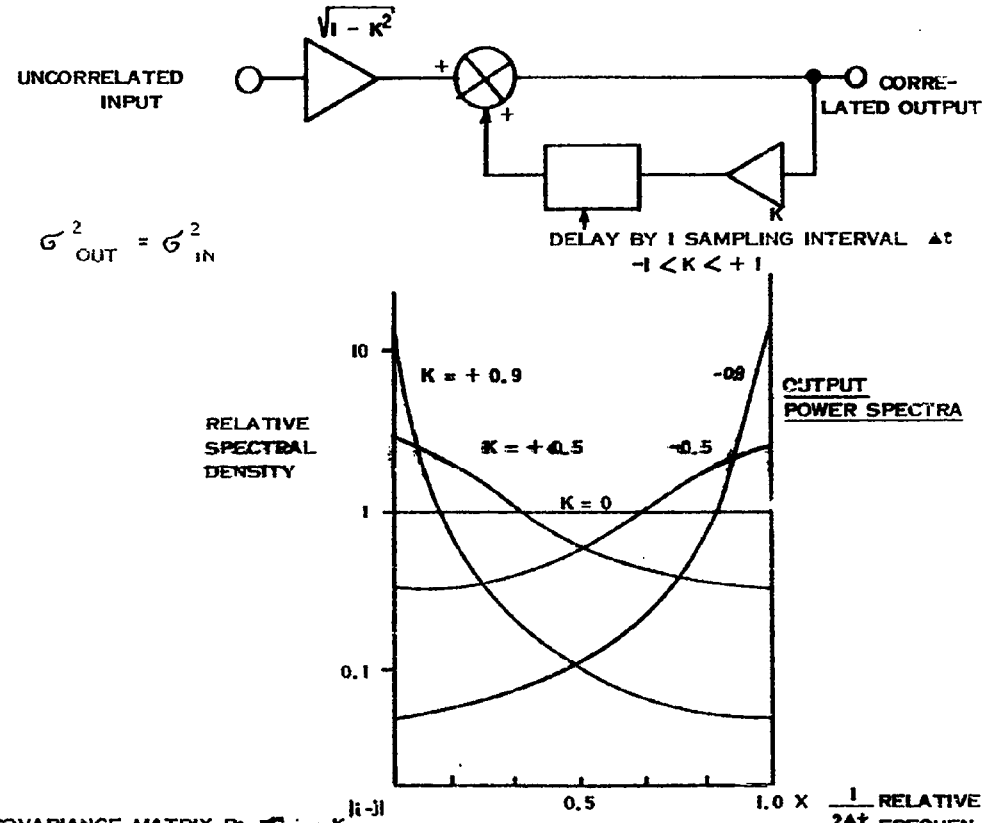

COVARIANCE MATRIX R: $r_{ij} = K^{|i-j|}$

INVERTED COVARIANCE MATRIX R^{-1}:

$$\beta_{ij} = \frac{1+K^2}{1-K^2} \qquad i=j$$

$$= \frac{1}{1-K^2} \qquad ij = 1 \text{ OR } = M$$

$$= \frac{-K}{1-K2} \qquad |i-j|=1$$

$$= 0 \qquad |i-j|>1$$

FIG II

EFFECTS OF ERROR CORRELATION

DESCRIBED BY: $\alpha = \left(\frac{r_{\Delta v} / CEP}{r_{\Delta v} / CEP}\right)_c \Big/ \left(\frac{r_{\Delta v} / CEP}{r_{\Delta v} / CEP}\right)_o$

INDICES: $_c$ FOR CORRELATED ERROR
$_o$ FOR UNCORRELATED ERROR

EXAMPLE: SLED RUN PROFILE

ERROR MODEL:
$$\Delta v = K_0 t + K_2 \int a^2 dt + K_3 \int a^3 dt$$

MISSION REQUIREMENT: R = 5500 NM

ERROR CORRELATION: FROM BROWN FILTER,
DESCRIBED BY K.

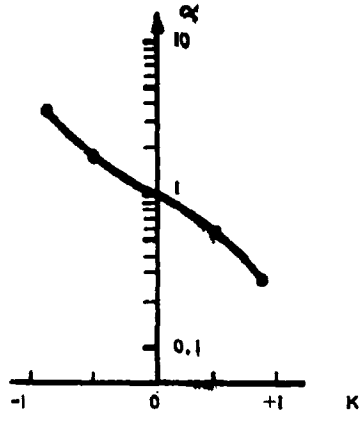

FIG. 12


U.S. AIR FORCE

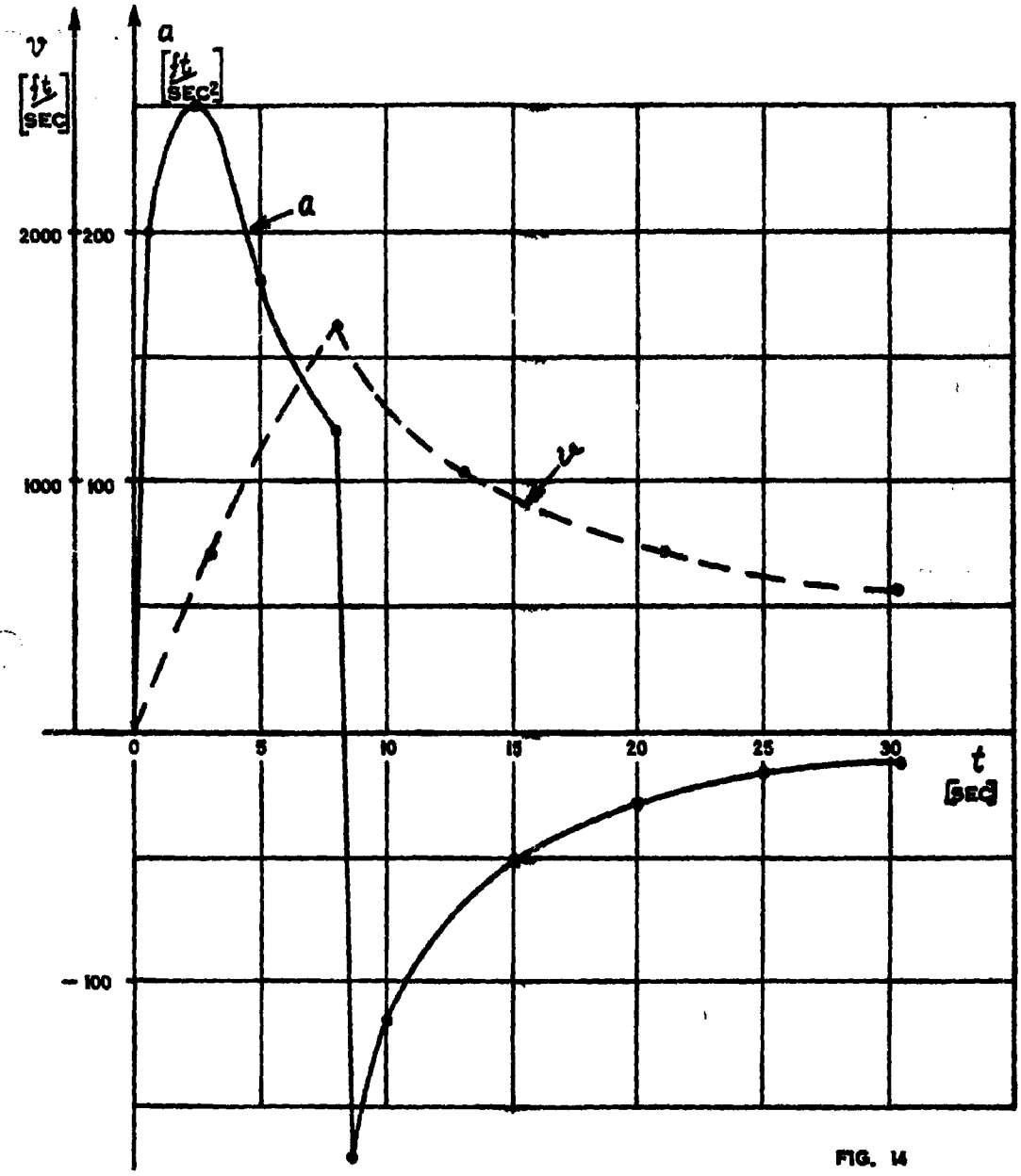

FIG. 14

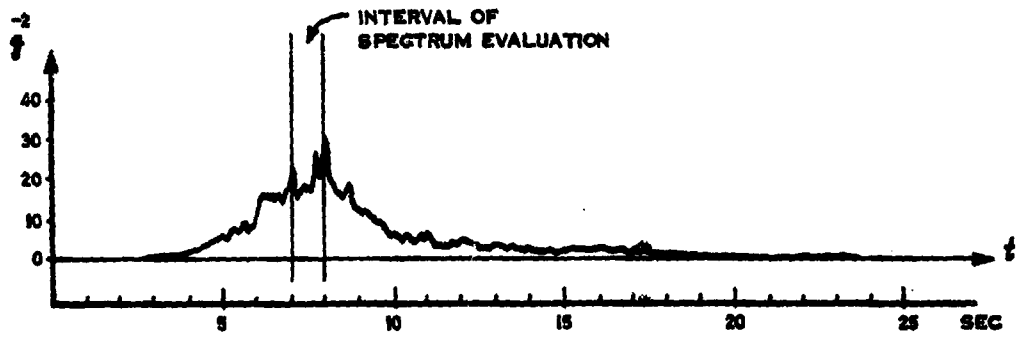

MEAN POWER OF LONGITUDINAL SLED VIBRATION

FIG. 15

POWER SPECTRUM OF LONGITUDINAL SLED VIBRATION

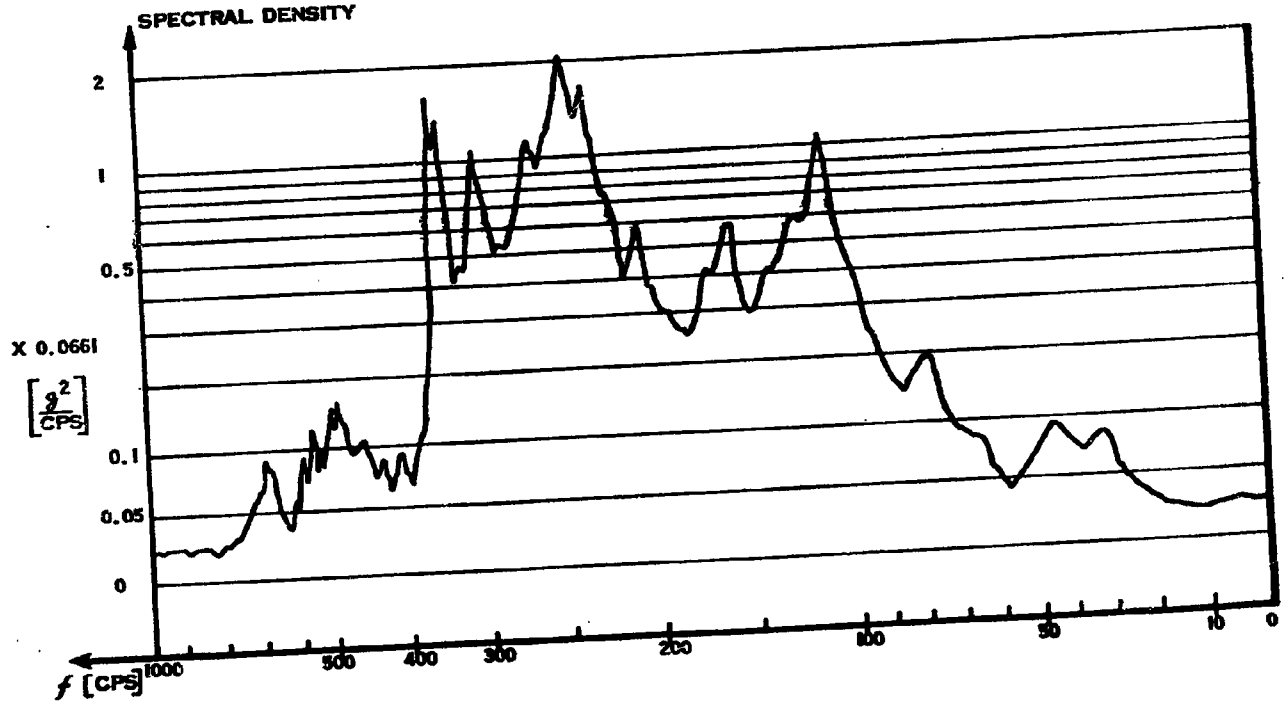

FIG 16

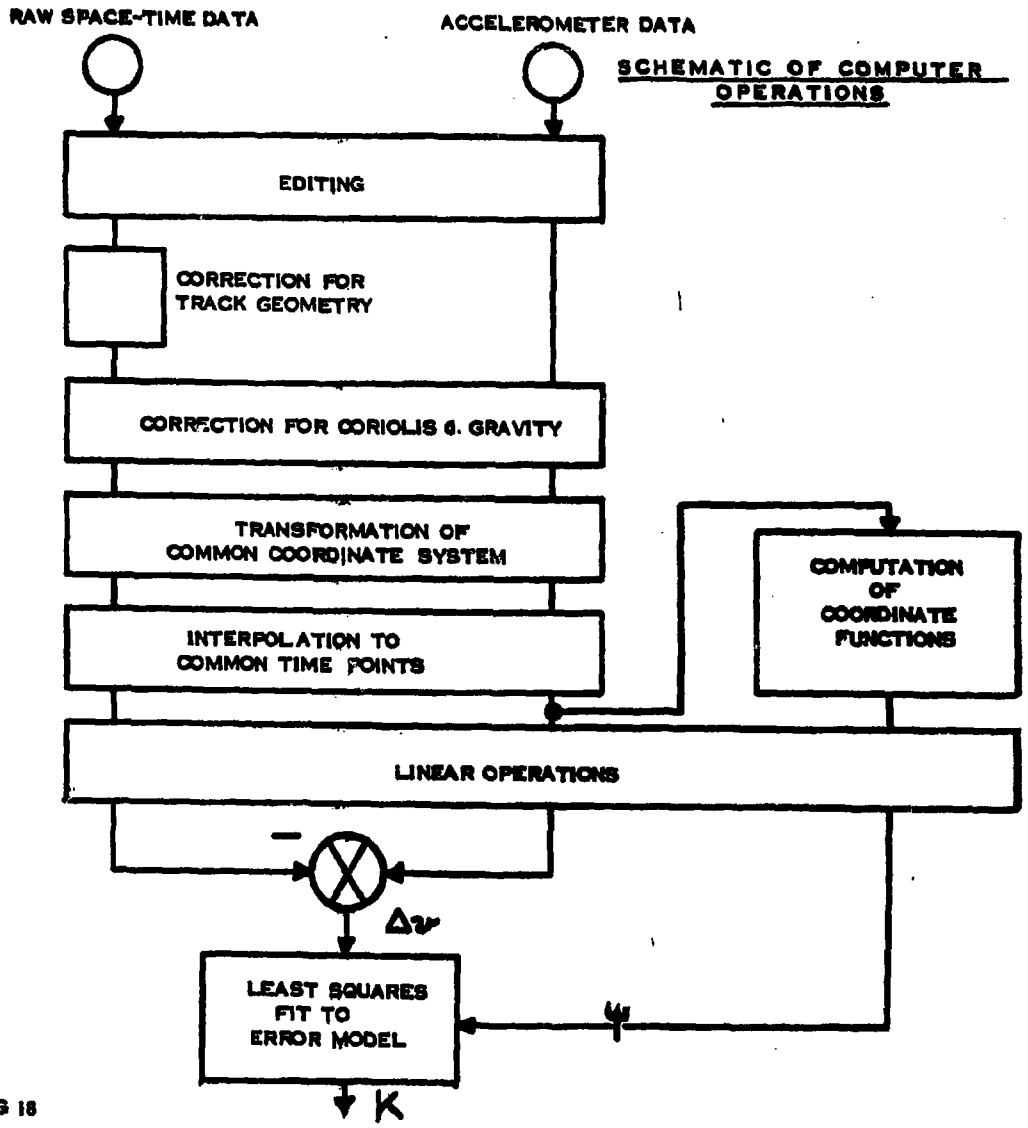
RAW SPACE-TIME DATA
ACCELEROMETER DATA
SCHEMATIC OF COMPUTER OPERATIONS
EDITING
CORRECTION FOR TRACK GEOMETRY
CORRECTION FOR CORIOLIS & GRAVITY
TRANSFORMATION OF COMMON COORDINATE SYSTEM
INTERPOLATION TO COMMON TIME POINTS
COMPUTATION OF COORDINATE FUNCTIONS
LINEAR OPERATIONS
−
Δv
LEAST SQUARES FIT TO ERROR MODEL
K

FIG 18

EFFECTS OF NON-OPTIMUM COEFFICIENT ESTIMATION*

Λ_K IN OPTIMUM CASE: $\Lambda_K = \left[\psi^T R^{-1}_{\Delta v} \psi\right]^{-1}$

Λ^X_K IN NON-OPTIMUM CASE
(ERROR IS CORRELATED BUT IS
TREATED AS UNCORRELATED): $\Lambda^X_K = \left[\psi^T \psi\right]^{-1} \psi^T R_{\Delta v} \psi \left[\psi^T \psi\right]^{-1}$

EXAMPLE: SLED RUN PROFILE

ERROR MODEL: $\Delta_v = K_0 t + K_2 \int a^2 dt + K_3 \int a^3 dt$

ERROR CORRELATION FROM BROWN FILTER

WITH K = + 0.5 AND + 0.9

		K = 0	+0.5	+0.9
WEIGHTED EFFECT $\left(\frac{CEP}{\sigma_{\Delta v}}\right)$	OPTIMUM	11.8	20.24	42.0
	NON-OPTIMUM	11.8	20.38	44.8

FIG 19

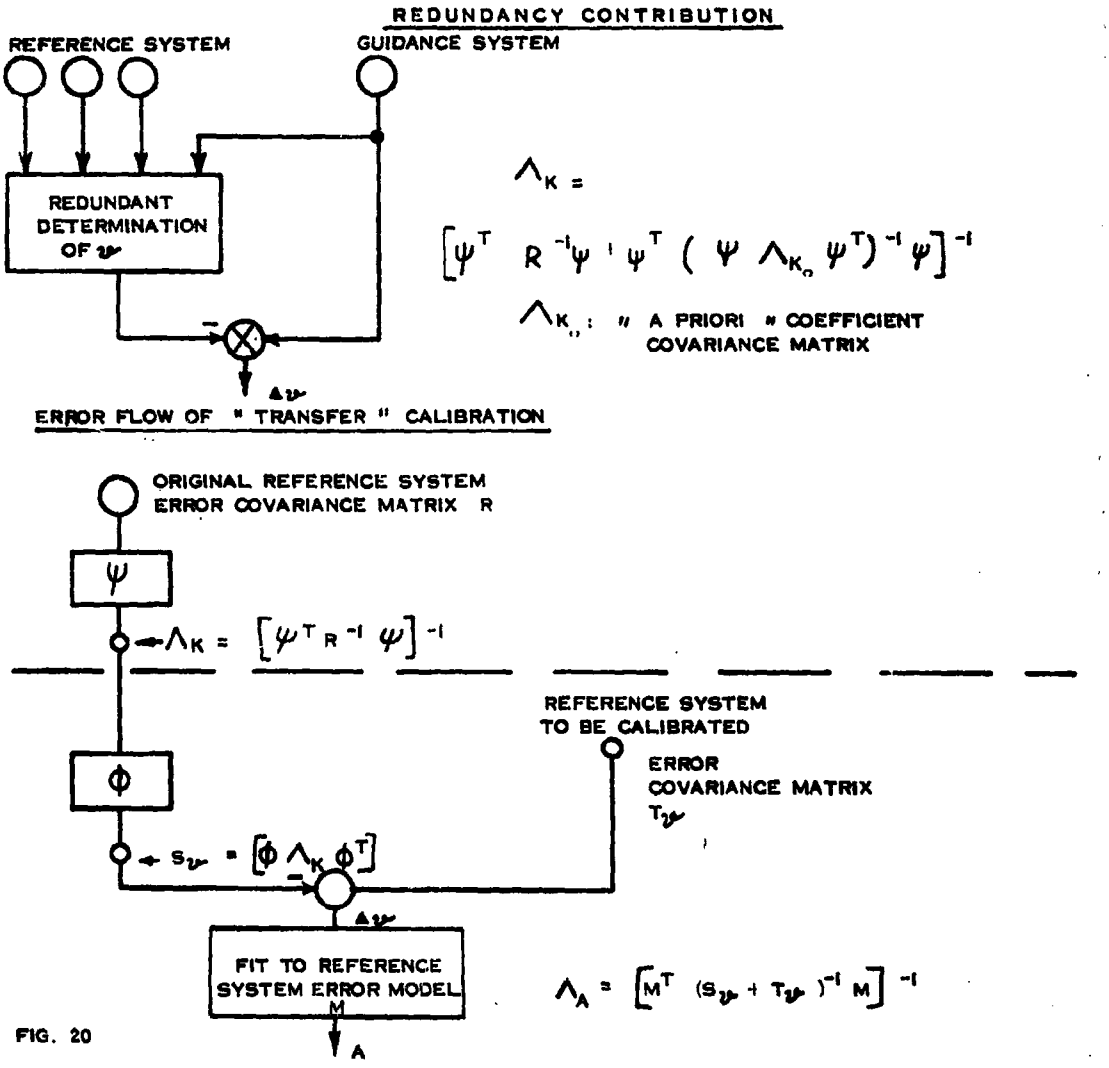
REDUNDANCY CONTRIBUTION
REFERENCE SYSTEM
GUIDANCE SYSTEM
REDUNDANT DETERMINATION OF ψ
$\Lambda_K =$
$\left[\psi^T R^{-1}\psi + \psi^T (\Psi \Lambda_{K_o} \psi^T)^{-1}\psi\right]^{-1}$
Λ_{K_o} : " A PRIORI " COEFFICIENT COVARIANCE MATRIX
$\Delta\psi$
ERROR FLOW OF " TRANSFER " CALIBRATION
ORIGINAL REFERENCE SYSTEM ERROR COVARIANCE MATRIX R
ψ
$\Lambda_K = \left[\psi^T R^{-1} \psi\right]^{-1}$
REFERENCE SYSTEM TO BE CALIBRATED
ERROR COVARIANCE MATRIX T_ψ
Φ
$S_\psi = \left[\Phi \Lambda_K \Phi^T\right]$
$\Delta\psi$
FIT TO REFERENCE SYSTEM ERROR MODEL
M
A
$\Lambda_A = \left[M^T (S_\psi + T_\psi)^{-1} M\right]^{-1}$

FIG. 20

F

809-7

DATA SMOOTHING

by:

J. R. Garrett, D. B. Gennery

RCA-Missile Test Project

PAFB, Florida

Presented at:

FOURTH JOINT AFMTC-RANGE USER DATA CONFERENCE

Orlando Air Force Base, Florida

26-28 February 1963

DATA SMOOTHING

Historically the problem of smoothing or filtering data as we know it today may be said to have originated about 20 years ago. The appearance of radar during World War II brought with it the problem of smoothing and differentiating time series data. A satisfactory solution to this problem was needed so that electromechanical devices could be provided which would enable the radar to determine and predict position and velocity of moving objects in the presence of signal noise arising from countermeasures, equipment, malfunction, or natural causes.

In 1942 Norbert Wiener solved this problem. His assumptions were that the observing system's characteristics were invariant in time, that the system operated on all past data, that the input signal and noise were statistically stationary, and that the optimum system was characterized by the minimum output mean square criterion. In 1944 Phillips and Weiss analyzed the problem of smoothing position data for gunnery prediction under assumptions similar to Wiener's. Zadeh and Ragazzini published a paper in the Journal of Applied Physics (1950) in which Wiener's results were extended to permit the input signal to contain a non-random polynomial component and the observation time to be finite.

Solutions to this problem have taken the form of an integral equation which must be solved for the system weighting function. Lees, Johnson, Ormsby, Pavley, Arabadjis, and a host of others have considered various aspects of deriving the filter that is optimum in some sense. The concept of a quantity which has been optimized is a very appealing one, but one which can be misleading. The implication is that the circumstances surrounding a problem are perfectly understood if the solution has been "optimized." Since a perfect understanding is not always possible, certain simplifying assumptions must be made relative to the physical or mathematical facts, and then accompany these by some definition of optimization in terms of some criterion. Thus, if the probability distributions are Gaussian then the minimum mean squared error criterion leads to optimization. If this assumption is not realistic then other standards are needed, and the output of the filter will depend in some way on the underlying assumptions. Accordingly, the design of the filter will, therefore, depend upon the use which is anticipated for it.

The digital data obtained from a missile trajectory measuring system consists of a desired signal, i.e., the actual position of the missile as a function of time, and unwanted "noise," which represents errors due to atmospheric effects, thermal noise in the electronic circuitry, servo jitter in the

tracking system, and so forth. In order to reduce the effect of the noise, some type of digital smoothing technique can often be employed. One technique which is often used is the moving-arc linear midpoint filter. This class of filters can be represented as follows:

$$\bar{x}_i = \sum_{k=-n}^{+n} h_k \, x_{i+k} \qquad (1)$$

where x represents the unsmoothed data, $\bar{x}$ represents the smoothed data, h represents the filter weights or data multipliers, and the subscripts denote successive data points in the time domain. The frequency response H(f) of such a filter can be obtained by taking the Fourier transform of h_k as a function of k.

In missile trajectory work the usual assumption is that the desired signal consists mainly of low-frequency components, whereas the noise is more or less evenly distributed throughout the spectrum with perhaps local concentrations at certain frequencies. The filter therefore should generally be some type of low-pass filter. That is, it should have an amplitude response of approximately 1 at low frequencies and approximately 0 at high frequencies, with a gradual cutoff at some frequency chosen by considering the nature of the signal and noise. For purposes of comparison, I shall define the cutoff frequency of a low-pass filter to be that frequency at which the amplitude response of the filter is 0.707 of its response at zero frequency.

Since the signals occurring in missile trajectory work normally have a very large zero frequency component, the response of the filter at zero frequency should be exactly 1. This condition can be met by establishing the following constraint on the position data multipliers:

$$\sum h_k = 1 \qquad (2)$$

In addition to a constant component, the signal may contain a significant trend in the form of fairly large low-order derivatives with respect to time. To insure that the r^{th} derivative does not bias the smoothed position data, the following constraint is necessary:

$$\sum h_k k^r = 0 \qquad (3)$$

In terms of the frequency domain, this is equivalent to:

$$\left.\frac{d^r H(f)}{df^r}\right|_{f=0} = 0, \qquad (4)$$

provided that

$\frac{d^{r-1} H(f)}{df^{r-1}}$ is everywhere continuous.

If the condition of equation (2) holds and the condition of equation (3) holds for all values of r from 1 to p, the filter can be said to be constrained to pass a p^{th} order polynomial, since if a pure p^{th} order polynomial with no noise is fed into the filter, the output will reproduce the polynomial exactly with no error.

Last year at this conference Pavley described two types of moving-arc linear midpoint filters. These were the least-squares polynomial filter, and a filter first described by Ormsby, designed to approximate a linear rolloff in its frequency response.

The least squares polynomial filter was designed by establishing constraints given by equations (2) and (3) for values of n up to and including the desired degree of polynomial, and by establishing the additional constraint that for a given span (2n + 1) in the time domain the sum Σh_k^2 must be minimum. The cutoff frequency of this type of filter is determined by the span and the degree of polynomial chosen. The frequency response of the 31 point 2^{nd} degree version is shown in Figure 1. It can be seen that an undesirable property of this type of filter is that it has a significant response to high frequencies which we usually assume to contain mostly noise. An advantage of this type of filter, however, is the fact that, to achieve a given cutoff frequency, the time span of input points which influence a given smoothed point is minimum.

The Ormsby filter which was described last year was designed to have an ideal frequency response as follows:

$$H(f) = 1 \qquad (0 \leq f \leq f_1)$$

$$H(f) = \frac{f_2 - f}{f_2 - f_1} \qquad (f_1 \leq f \leq f_2)$$

$$H(f) = 0 \qquad (f > f_2)$$

The above frequency response cannot be achieved exactly unless an infinite time span were used. Taking the Fourier transform of the above function and truncating it to produce a set of data multiplier with a finite time span produces a filter with a somewhat altered frequency response. Pavley then showed how this filter could be constrained to pass a polynomial of desired degree by adding additional terms to the above derived data multipliers so as to satisfy constraints (2) and (3). The frequency response of such a filter is also shown in Figure 1. The example shown was chosen to have the same cutoff frequency and the same degree of constraint as the least squares filter also shown in Figure 1, so that they can be directly compared. Note that with the Ormsby filter an improved frequency response is obtained at the expense of a somewhat longer span.

I will now describe a type of filter in which the frequency response can be improved even more without further increase in the span.

The reason for the response remaining at the higher frequencies in the Ormsby type filter shown in Figure 1 is that when the filter was truncated in the time domain, data multipliers of significant amplitude were discarded, thus introducing discontinuities in the time response of the filter. These discontinuities in the time domain result in the oscillations in the frequency domain at the higher frequencies. In order to reduce this effect a function must be chosen which decays more rapidly in the time domain, so that truncation at a reasonable span length will discard data multipliers of much smaller magnitude. Slowness of decay in the time domain is caused by discontinuities in the derivatives, particularly the zeroth and other low order derivatives, in the frequency domain. Therefore, it was decided to use a function in which all of the derivatives are continuous.

The function decided upon is of the following form in the time domain:

$$h_k = ce^{-\frac{1}{2}(2\pi ak)^2} \frac{\sin(2\pi bk)}{2\pi bk} \qquad (5)$$

where the constants a and b are chosen as will be described shortly and c is adjusted to satisfy constraint (2). The frequency response of this filter is a pair of superimposed error functions (integral of the normal curve) of appropriate amplitude arranged symmetrically around zero frequency, as shown in Figure 2.

It can be seen that this ideal frequency response and all of its derivatives are everywhere continuous, that its first derivative at zero frequency is equal to 0, and that the function rapidly approaches 0 as the frequency increases. For fairly small values of a the response for positive frequencies is closely approximated by a single error function. In this case the frequency at which the response is ½ is approximately equal to the constant b, although the cutoff frequency as defined earlier is somewhat less than this, and the rapidity of cutoff (or rolloff) is determined by the constant a, since the response drops from approximately .68 to .32 in a frequency interval of 2a. For larger values of a the two error function curves merge together more, and the cutoff frequency becomes dependent chiefly upon a. In the limiting case where b = 0, the frequency response curve becomes the gaussian function, or normal curve, with the response at a frequency of a equal to .607. This fact can be obtained by taking the limit of the sums of the two error functions as b approaches zero, but is more easily derived from the fact that equation (5) reduces to the gaussian function when b = 0, and the Fourier transform of this is another gaussian function, as follows:

$$H(f) = e^{-\frac{1}{2}\left(\frac{f}{a}\right)^2} \qquad (b = 0) \qquad (6)$$

For reasonable values of the constant a, equation (5) decays to zero very rapidly as k increases. Therefore, reasonable span lengths can be used without discarding values of h_k that are appreciably different from zero. This fact enables the ideal frequency response described above to be approached very closely, thus insuring nearly complete rejection of high frequencies.

When values for a and b are chosen in order to produce the cutoff and rolloff desired, a suitable value of the semi-span n must then be chosen. A good rule of thumb for most purposes is:

$$n > \frac{1}{2a}$$

although best results are obtained if an integral multiple of 1/2b is chosen when b is not close to zero compared to a.

Next the value of c is chosen so that:

$$\sum h_k = 1$$

The filter is therefore automatically constrained to have a response of one at zero frequency.

Since the filter is symmetrical in time, the conditions of equations (3) and (4) are met automatically for all odd values of r. For even values of r it can be seen that these conditions are never met exactly for the ideal filter (infinite span). However, as the constant a decreases and the rolloff becomes steeper, it is obvious that the response at zero frequency becomes flatter. This means that the low order derivatives are becoming smaller. Therefore, condition (4) can be approached as closely as desired for a given value of r by making a sufficiently small. For example, in order to pass a second degree polynomial with no appreciable change, the sum $\Sigma h_k k^2$ must be close to zero. This can be achieved sufficiently well for most purposes if $a/b < 1/3$. For higher order terms the ratio a/b must of course become even smaller.

For certain combinations of a, b, and n, the above condition for any one order can be met exactly due to the effect of the truncation in the time domain. A case of particular interest is where the following relationships hold:

$$a = .342\ b$$

$$n = \frac{1}{b} \qquad (7)$$

In this case, $\Sigma h_k k^2$ is for all practical purposes equal to zero for any value of b. Thus, without any additional terms for constraining purposes, the filter automatically will pass a second degree polynomial.

Figure 3 shows the actual frequency responses of the filter described in this paper with three different rolloff rates but with the same cutoff frequency for purposes of comparison. The curve in the middle represents the case constained to pass a second degree polynomial (and therefore a third degree also) by satisfying equation (7). It thus can be compared directly to the two types of filters previously described and shown in Figure 1, since these also are shown for the same cutoff frequency. Note that its rejection of higher frequencies is superior to either of the other types. In addition, its span length is slightly less than that of the Ormsby filter shown, although it is of course greater than that of the least-squares polynomial filter. The filter in the right of Figure 3 will pass a first degree polynomial exactly, and the one in the left of the figure will pass a fifth degree polynomial almost exactly.

In order to obtain different cutoff frequencies, a, b and 1/n are adjusted proportionally to the cutoff frequency. When the same ratios are kept among these quantities, the shape of the frequency response curve is the same except that it is "stretched" proportionally to the cutoff frequency.

Figure 4 shows a portion of a hypothetical signal which might be considered to contain both a desired signal and unwanted noise. The 17 point and 47 point filters show the result of smoothing this signal with the species of filter defined by equation (7) and illustrated by the middle curve on Figure 3 but with different cutoff frequencies in the two figures. The last curve on Figure 4 shows the result of smoothing the same data with a 2nd degree least-squares polynomial filter with the same cutoff frequency as the 47 point filter shown in the same figure. In comparing 47 point filters and the least squares filter, some of the high frequency components can be seen in the data smoothed by the least-squares polynomial filter, whereas they are absent in the 47 point filter. This illustrates the effect of the improved frequency response.

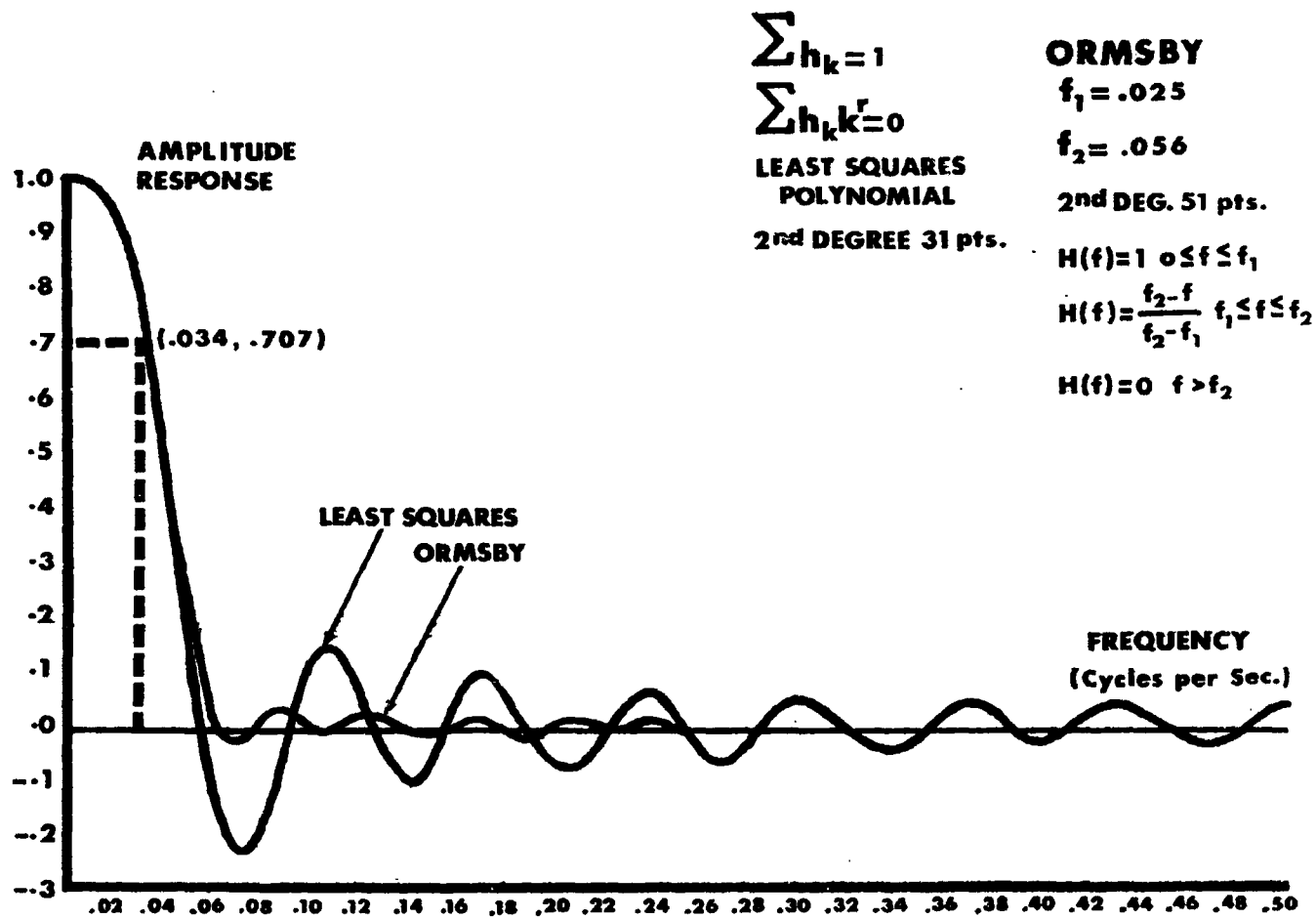
$\sum h_k = 1$
$\sum h_k k^r = 0$
LEAST SQUARES POLYNOMIAL
2nd DEGREE 31 pts.
ORMSBY
$f_1 = .025$
$f_2 = .056$
2nd DEG. 51 pts.
$H(f) = 1 \quad 0 \le f \le f_1$
$H(f) = \frac{f_2 - f}{f_2 - f_1} \quad f_1 \le f \le f_2$
$H(f) = 0 \quad f > f_2$
AMPLITUDE RESPONSE
1.0
.9
.8
.7
.6
.5
.4
.3
.2
.1
.0
-.1
-.2
-.3
(.034, .707)
LEAST SQUARES
ORMSBY
FREQUENCY
(Cycles per Sec.)
.02 .04 .06 .08 .10 .12 .14 .16 .18 .20 .22 .24 .26 .28 .30 .32 .34 .36 .38 .40 .42 .44 .46 .48 .50

FIG. 1

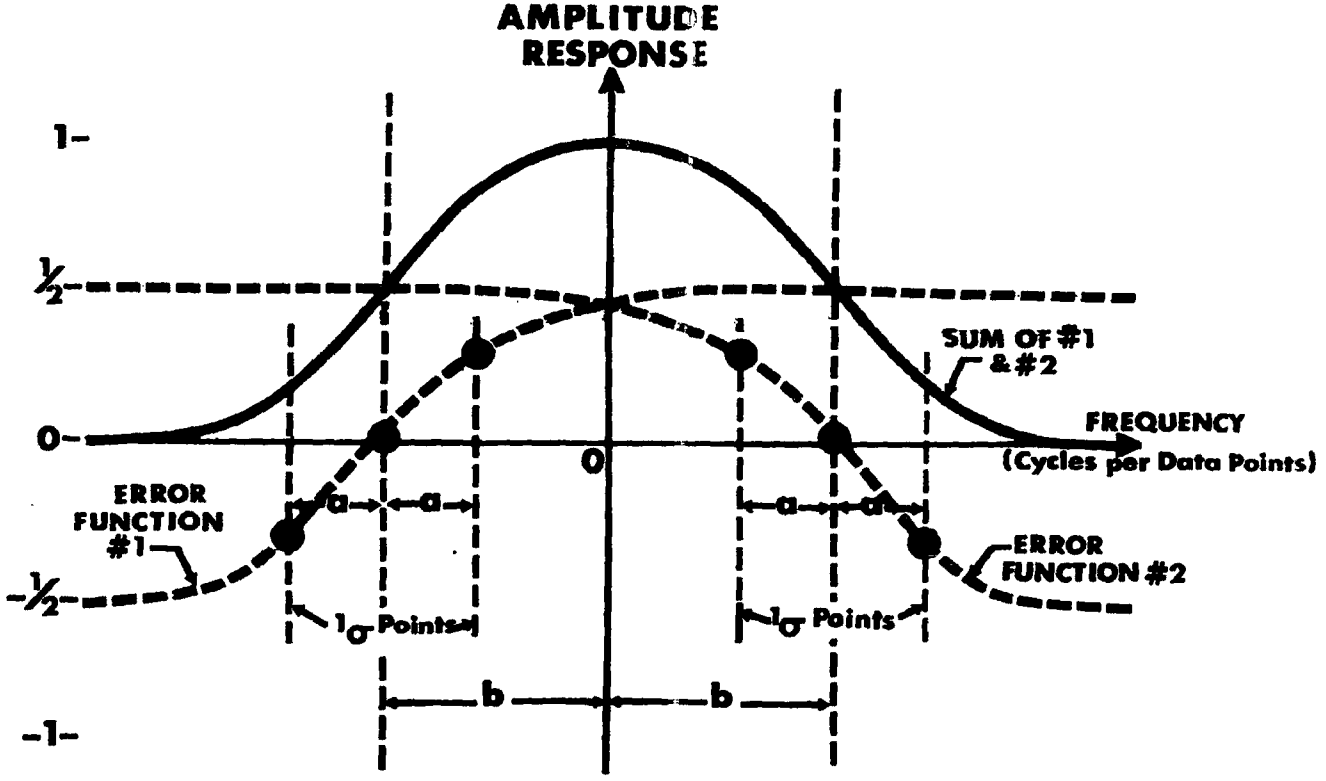
AMPLITUDE RESPONSE
1–
½–
0–
–½–
–1–
SUM OF #1 & #2
FREQUENCY (Cycles per Data Points)
0
ERROR FUNCTION #1
ERROR FUNCTION #2
a
a
a
a
1σ Points
1σ Points
b
b

FIG. 2

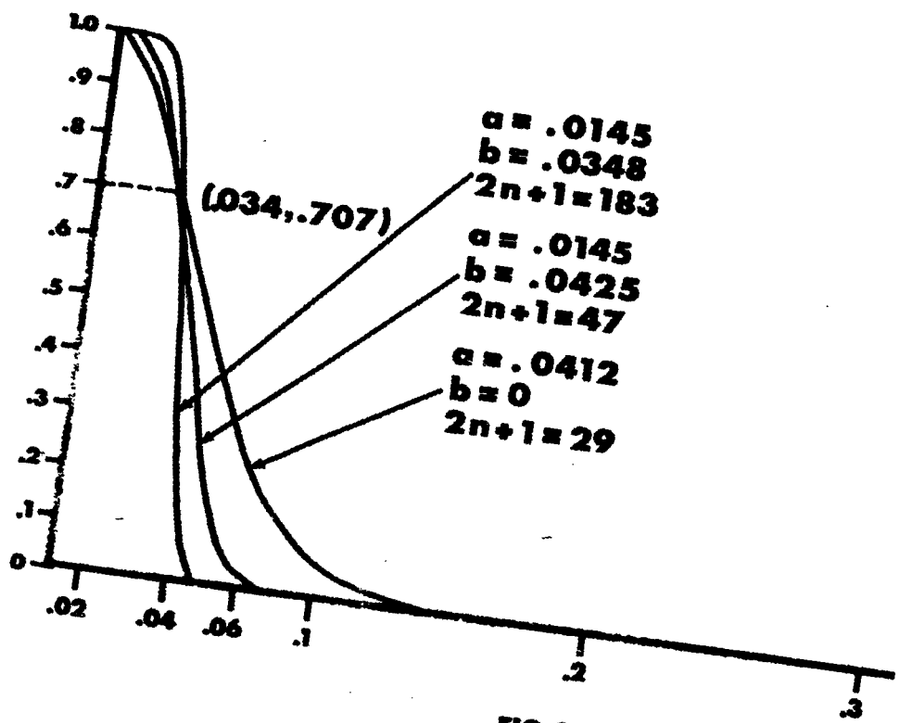
1.0
.9
.8
.7
.6
.5
.4
.3
.2
.1
0
.02
.04
.06
.1
.2
.3
(.034,.707)
a = .0145
b = .0348
2n+1=183
a = .0145
b = .0425
2n+1=47
a = .0412
b = 0
2n+1=29

FIG. 3

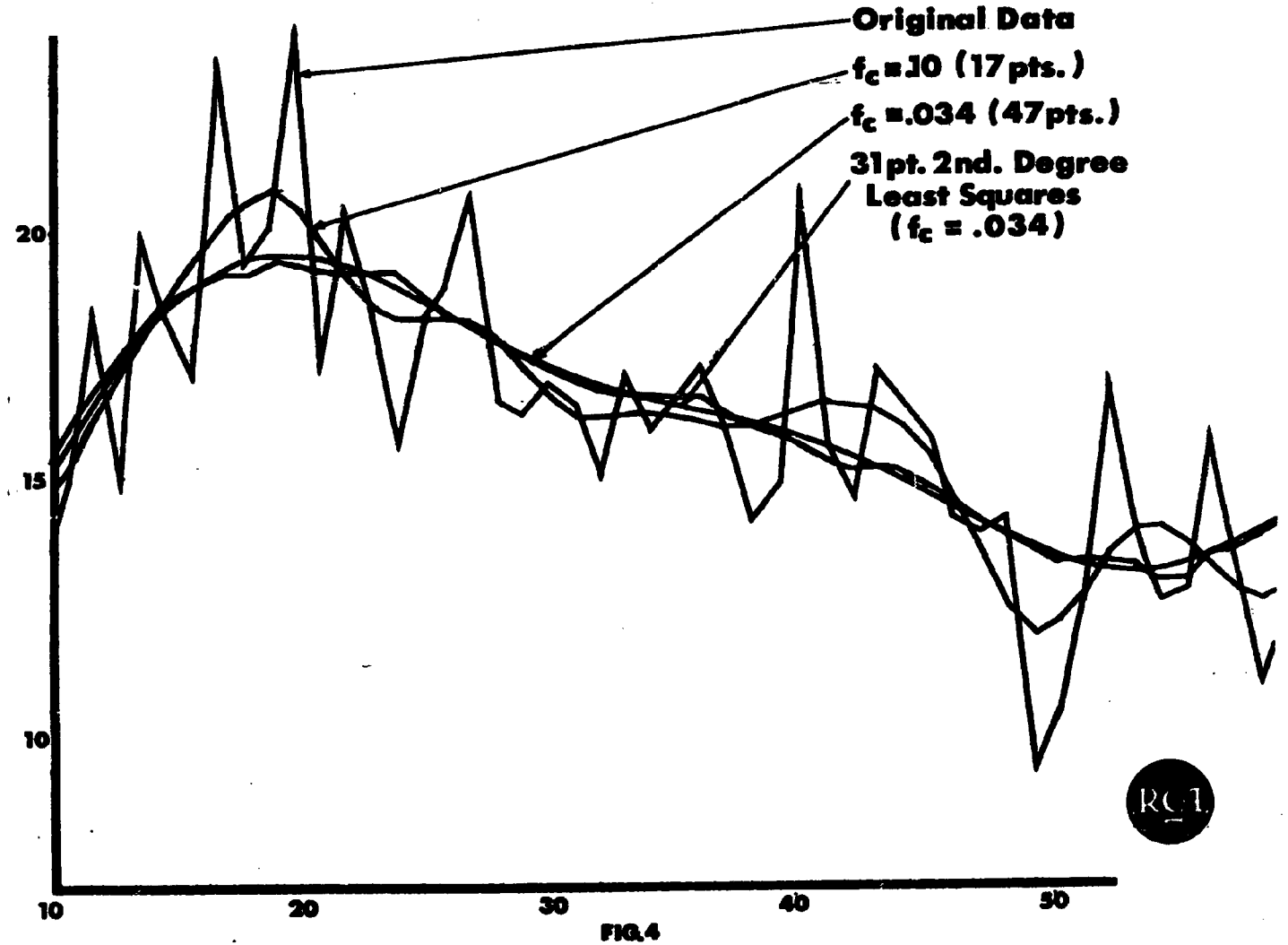
Original Data
f_c = .10 (17 pts.)
f_c = .034 (47 pts.)
31 pt. 2nd. Degree
Least Squares
(f_c = .034)
20
15
10
10
20
30
40
50

FIG. 4

FOURTH JOINT AFMTC/RANGE USER DATA CONFERENCE

ORLANDO, FLORIDA

FEBRUARY 27,1963

809-G

APPLICATIONS OF DIGITAL FILTERING TECHNIQUES TO DATA PROCESSING

by

MARCEL A. MARTIN

MISSILE & SPACE DIVISION

GENERAL ELECTRIC COMPANY

PHILADELPHIA 1, PENNA.

ABSTRACT

809(9)

Interpretation of digital filters as linear transducers characterized by their transfer functions leads to practical methods for specifying filters and evaluating their performance. Applications of the theory to filters used in smoothing, differentiation, interpolation and power spectrum analysis of sampled data are discussed. During the last six years, these filtering techniques have been used extensively in the Missile and Space Division of General Electric Company. Classical methods, as polynomial least square fit, Lagrange interpolation formula, are evaluated as particular cases of filtering techniques. Quality of the information provided by filters designed from frequency domain considerations and precautions to take in the use of these filters are pointed out.

AUTHOR

For the last six (6) years, filtering techniques have been extensively used in data processing operations at what is now called the Missile and Space Division of G. E. I would like to discuss some essential characteristics of the filtering techniques, the power and limitations of those techniques and the precautions which have to be taken in the applications.

It is well known that a set of sampled data, that is data taken at constant sampling rate or sampling frequency, define a continuous function only if the two following simultaneous conditions are met: First, the data must cover times which go from $-\infty$ to $+\infty$; secondly, the data must not contain any component of frequency higher than half the sampling frequency. If these two conditions are satisfied, the defined function can be considered as a sum, finite or infinite, of components having each its own frequency.

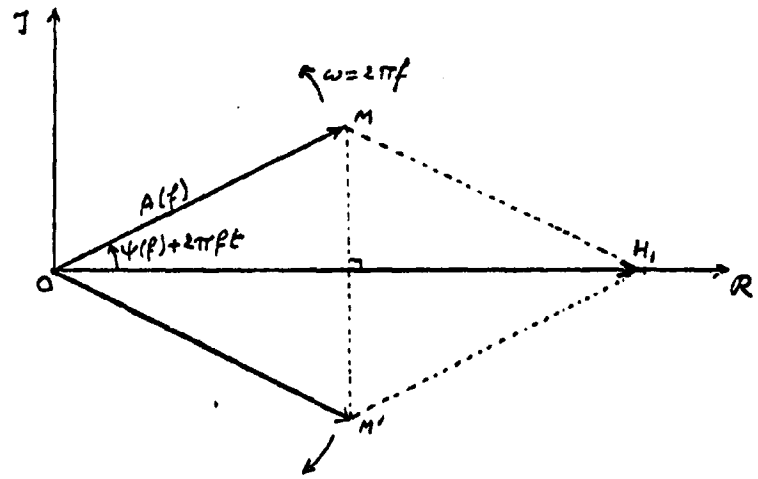

FIGURE 1

Each component can be defined by its frequency f, its amplitude A(f) and its phase angle $\psi(f)$ at time zero. The value of the contribution of the component at a time t is a complex number which can be represented by a vector $\overrightarrow{OM}$ (Figure 1) of length A(f) rotating at angular rate $\omega = 2\pi f$ and which makes at time $t = 0$ an angle ψ with the real axis. Since to each component of frequency f can be associated a component of frequency -f represented by a vector $\overrightarrow{OM'}$ which, at all times, is symmetric of $\overrightarrow{OM}$, the sum of the contributions of these two frequencies can be represented by a vector $\overrightarrow{OM_1}$, which is twice the projection of the vector $\overrightarrow{OM}$ on the real axis. Consequently, when we consider a range of frequencies from $-\frac{f_s}{2}$ to $\frac{f_s}{2}$, the contribution of each frequency component is the complex number

$$A(f)\ e^{j[\psi(f) + 2\pi ft]} =$$

$$A(f)\left\{\cos[\psi(f) + 2\pi ft] + j \sin[\psi(f) + 2\pi ft]\right\}$$

When we consider a range of frequencies from 0 to $\frac{f_s}{2}$, the contribution of each frequency component is the real number $2A(f) \cos[\psi(f) + 2\pi ft]$.

A <u>numerical filter</u>, or <u>digital filter</u>, we will say simply a <u>filter</u>, is a set of weights B_k (k varying from an integer N_1 to an integer N_2) which can be applied to the successive sampled values $g_i(k\tau)$ at times $t = k\tau$, where τ is the <u>sampling interval</u>, so that a weighted average $g_o(m\tau)$ is obtained and assigned to the time $t = m\tau$, where m is any specified number (Figure 2).

That is:

$$g_o(m\tau) = \sum_{k=N_1}^{N_2} B_k \, g_i(k\tau) \qquad (1)$$

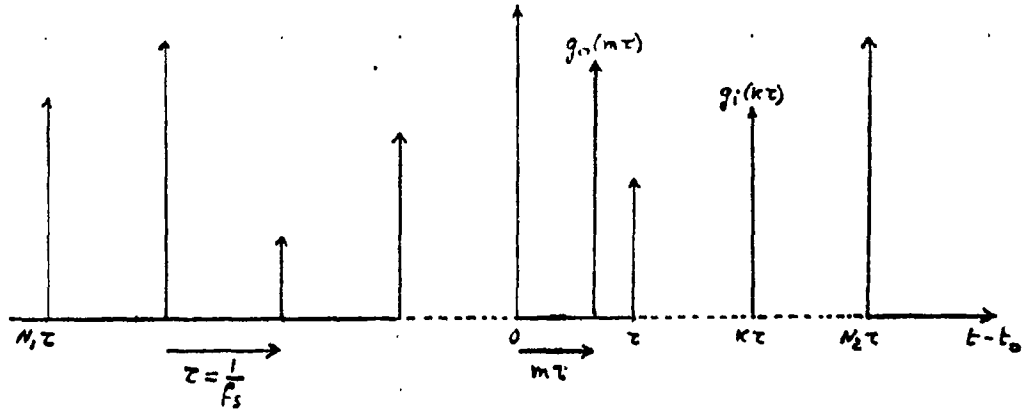

FIGURE 2

Filtering a set of sampled data consists in performing this weighted average on the first $N_2 - N_1 + 1$ data points, then moving the filter over the data displaced by one sampling interval, and so on until all the data have been processed.

When a sum of functions is filtered, the output is the sum of the outputs obtained by filtering each individual function. Since the input function $g_i(t)$ can be considered as sum of frequency components, the effect of filtering a function $g_i(t)$ can be analyzed by evaluating the effect of filtering each of the frequency components.

It is convenient to normalize the frequency f by considering the frequency ratio, ratio of f to the sampling frequency f_s

$$r = \frac{f}{f_s} \tag{2}$$

If the origin of times is at time of application of the weight B_o, that is at the sampling time corresponding to $k = 0$, and if the frequency component of frequency $f = r\, f_s$ has unit amplitude $A(r\, f_s) = 1$, and zero phase $\psi(r\, f_s) = 0$ at time zero, the output of the filtering process, assigned at time $t = m\tau$, is called the transfer function $Y_1(m, r)$ of the filter for the time ratio m and the frequency ratio r, that is (Figure 3a)

$$Y_1(m, r) = \sum_{k=N_1}^{N_2} B_k\, e^{j\, 2\pi kr} \tag{3}$$

This can be written as

$$Y_1(m, r) = G_1(m,r)\, e^{j\, \phi_1(m,r)} \tag{4}$$

which shows the gain $G_1(m, r)$ and the phase shift $\phi_1(m, r)$.

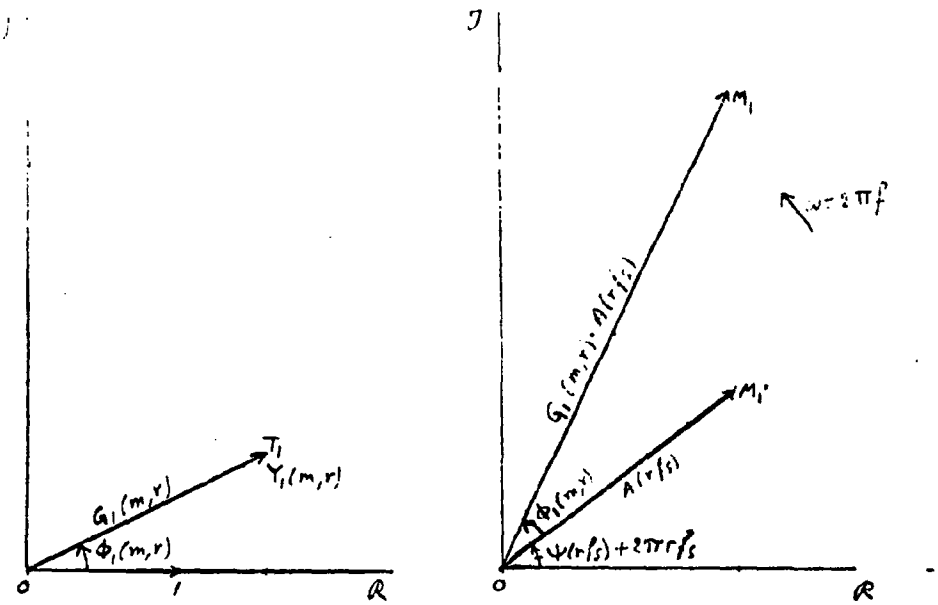

a) b)

FIGURE 3

From (3), it can be seen readily that if r is changed to -r, the transfer function $Y_1(m, r)$ is changed to its conjugate. The representative vectors are symmetric with respect to the real axis; consequently, we will often consider only positive values of r.

If the filter is applied to a frequency component of amplitude $A(r f_s)$ and phase $\psi(r f_s)$ at time zero (time at which the weight B_o is applied), the effect of filtering is to multiply the amplitude $A(r f_s)$ by $G_1(m, r)$ and to introduce a phase shift $\phi_1(m, r)$. If the filter is moved along the

sampled points of the input frequency component represented by the rotating vector $\overrightarrow{OM_1}$ (Figure 3b) the output of the filter is represented by the vector $\overrightarrow{OM_1}$ rotating at the same rate. The filter acts as a linear transducer characterized by its gain and phase shift for each frequency.

The design of a filter consists in selecting the limits N_1 and N_2 and in determining the weights B_k (k from N_1 to N_2) so that the actual transfer function $Y_1(m,r)$ of the filter approximates a transfer function $Y(m, r)$ desired for a fixed value of m and a selected range of values of r.

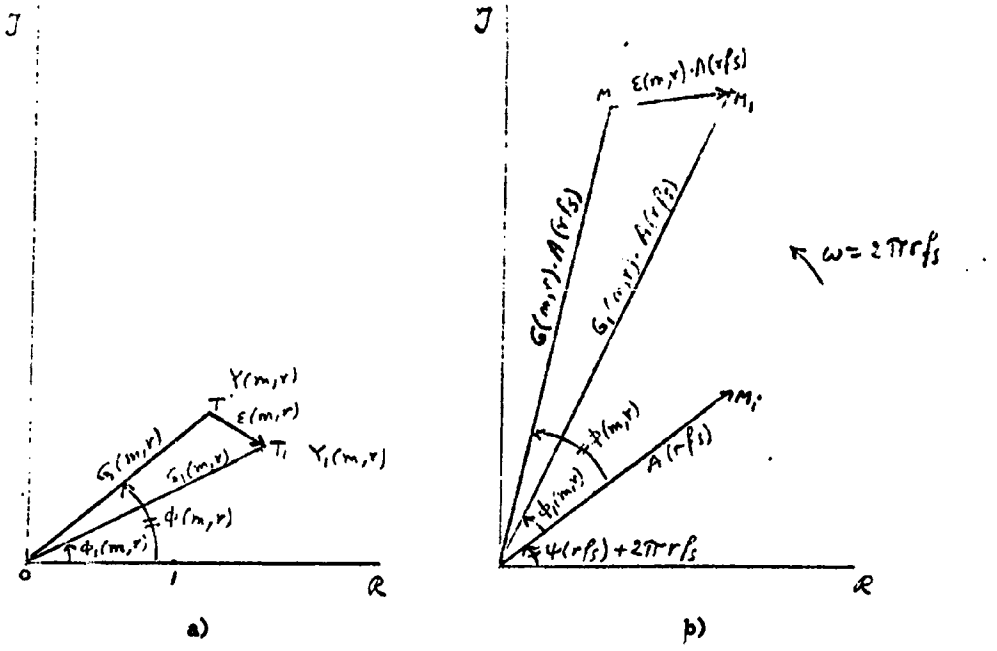

FIGURE 4

Figure 4 is a generalization of Figure 3 which shows the desired and actual transfer function and the desired and actual effects on a frequency component of amplitude $A(r\ f_s)$ and phase $\psi(r\ f_s)$ at time of application of the weight B_o. It can be seen that if $\mathcal{E}(m, r)$ is the complex error in transfer function

$$\mathcal{E}(m, r) = Y_1(m, r) - Y(m, r) \tag{5}$$

the error on the contribution of the frequency component is $A(r\ f_s)\cdot\mathcal{E}(m,r)$.

If the magnitude of $Y(m, r)$ is different from 1, it is usually more convenient to consider the relative error

$$\eta(m, r) = \frac{\mathcal{E}(m,r)}{|Y(m,r)|} \tag{6}$$

If we associate the components of frequencies f and -f, the contribution of the pair of components is as explained previously, double the projection of $\overrightarrow{OM_1}$ on the real axis. Since the transfer function of the filter exhibits the same property of symmetry with respect to the real axis, the desired output of the filter for that pair of components is twice the projection of $\overrightarrow{OM}$ on the real axis, the actual output of the filter is twice the projection of $\overrightarrow{OM_1}$ on the real axis and the error in the output is twice the projection of $\overrightarrow{MM_1}$ on the real axis. Since all the vectors $\overrightarrow{OM_1}$, $\overrightarrow{OM}$ and $\overrightarrow{OM_1}$ rotate with the same angular ratio ω, the maximum output occurs when $\overrightarrow{OM_1}$ is parallel to the real axis, and the maximum error in the output occurs when $\overrightarrow{MM_1}$ is parallel to the real axis.

The maximum error in the output is equal to the magnitude of $\mathcal{E}(m, r)$ multiplied by twice the maximum amplitude $A(r\ f_s)$ of the input complex frequency component.

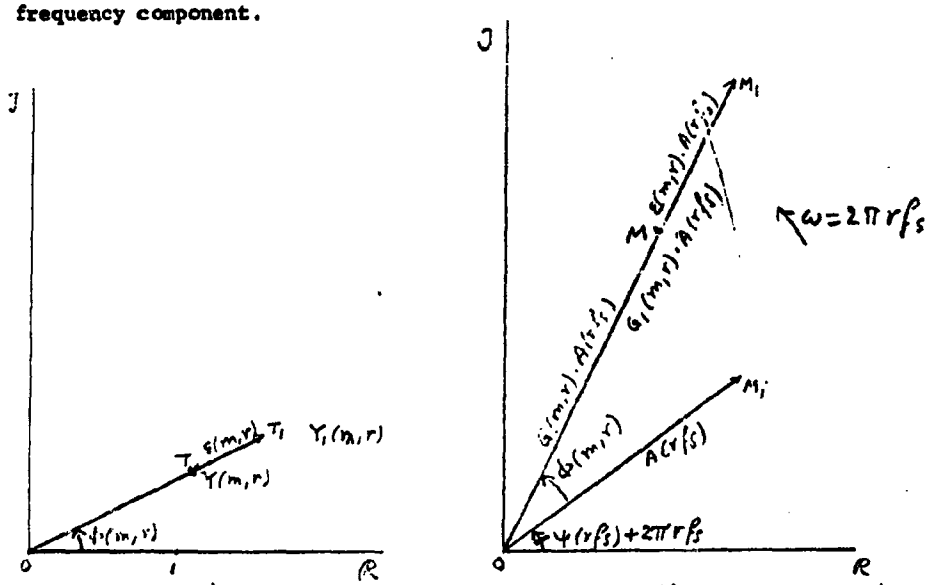

FIGURE 5

The maximum error occurs at the time of the maximum output only if the vectors $\overrightarrow{OM}$ and $\overrightarrow{OM_1}$ are colinear (Figure 5), that is when the desired and actual phase shifts are equal or differ by 180°. In order to avoid this ambiguity, it is convenient, when $\overrightarrow{OM}$ and $\overrightarrow{OM_1}$ are colinear, to consider phase shifts always equal, and <u>algebraic gains</u>: if the vector $\overrightarrow{OT_1}$

representing $Y_1(m, r)$ makes the angle $\phi(m, r)$ with the real axis, the gain is positive; if $\overrightarrow{OT_1}$ makes an angle $\phi(m, r) + 180^\circ$ with the real axis, the gain is negative.

There are usually constraints (relations between the weights of the filter) which have to be satisfied. When these constraints are taken into account, the problem of designing a filter consists in determining the coefficients a_i of a linear combination of known functions $\Psi_i(r)$ to approximate a desired function $H(r)$, that is

$$\sum_{i=n_1}^{n_2} a_i \Psi_i(r) \cong H(r) \qquad (7)$$

The coefficients a_i represent some of the weights of the filter; the other weights are subsequently determined by the imposed constraints. When the permissible error $\varepsilon(m, r)$ on $Y_1(m, r)$ is known, the permissible error on $H(r)$ is known. At the Missile and Space Division of General Electric, we have developed a method (the min-max technique) which minimizes the absolute error on $H(r)$. This method requires selection of discrete values of r. It is basically an iterative process of weighted least squares, the first iteration being a regular least squares fit (all weights equal to one); the weights for an iteration are proportional to the residuals, that is the errors on $H(r)$, obtained in the preceding iteration. The method applies to complex functions $\Psi_i(r)$ and $H(r)$ as well as to real functions. In the case of real functions, some systematic procedure permits usually to speed up the convergence of the process.

So far I have talked about general methods of evaluating the performance of filters and of designing the filters. Now I would like to discuss briefly a few specific types of filters we have found useful in our data processing investigations.

The first category of filters I want to talk about is what I call the cosine type filters. They are symmetric filters in which

$$N_1 = -N \qquad N_2 = N \qquad B_{-k} = B_k \tag{8}$$

and the output is assigned to the time of application of the weight B_o.

The actual transfer function of such filters is a real function, in other words the phase shift is zero, and the transfer function is equal to the algebraic gain, that is

$$\phi_1(0, r) = 0$$

$$Y_1(0, r) = G_1(0, r) = B_o + 2 \sum_{K=1}^{N} B_k \cos 2\pi kr \tag{9}$$

Such filters do not change the phase, but alter the amplitude of the frequency components of the sampled input. Filters of that category we are going to discuss are the low low-pass filters for very strong smoothing determination of mean and trend analysis, the cosine type sampling filters for frequency analysis and the low-pass filters for smoothing.

The low low-pass filter, ideally passes the DC component without alteration , passes the very low frequencies with an attenuation which increases with the frequency ratio, and does not pass any frequency beyond a frequency ratio r_d.

For the design, we specify the constraint $G_1(0,0) = 1$: this condition is necessary so that a constant input is unchanged by the filter. As a consequence of the symmetry of the filter, any straight line is preserved by the filter. Also for a certain number of values of r from r_d to .5, the desired gain is zero (Figure 6a). No specification is necessary for the <u>downcurve</u> (for r between 0 and r_d), but it is hoped (and this is effectively the case) that the actual gain of the designed filter will drop monotonically from 1 to about zero in the downcurve. In the min-max method of design, for a specified number N (the filter has $2N+1$ weights), the value r_d is selected by trial and error so that for r between r_d and .5, the error $\mathcal{E}(0, r)$ on the gain does not exceed .01 in absolute value. That is, such a filter does not pass more than 1% of the maximum amplitude of any frequency of frequency ratio higher than r_d (Figure 6b). It has been found that for N between 5 and 50, the product Nr_d is approximately equal to the constant value .85.

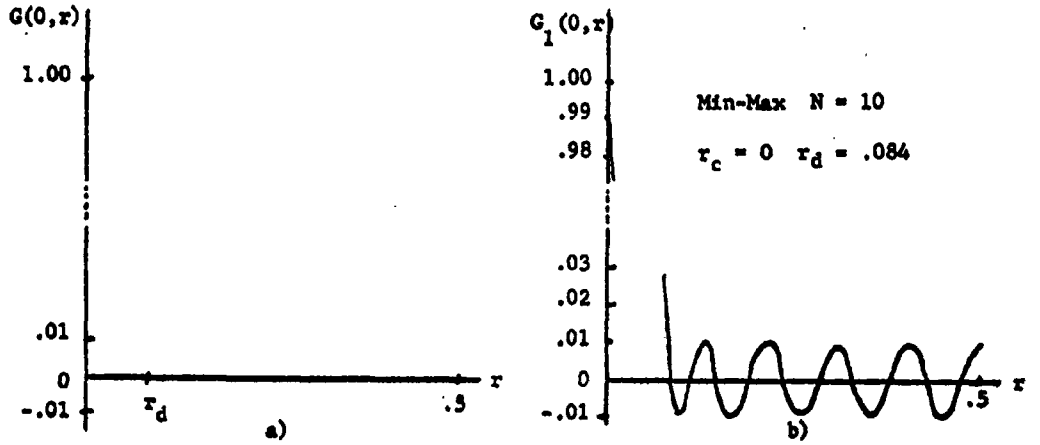

FIGURE 6

Consequently, the larger the number of weights in the filter, the lower the maximum frequency which can be passed by the low low-pass filter, hence the closer to the mean the output of the filter remains. At one extreme, if we have P sampled data, if we could design a low low-pass filter having P weights ($N = \frac{P-1}{2}$), we would have only one possible output: the mean. In order to determine a trend, several output points are required. The smaller N, the larger the number of output points available, but also the more wiggling the trend curve can have, because the low low-pass filter passes higher and higher frequencies. At the other extreme, a filter with N=0 ($B_o = 1$, and all other weights zero) passes all the frequencies, does not do any smoothing at all and gives the maximum number P of points to determine the trend, but with the maximum wiggling. Hence, one must be very careful about what is desired to determine the trend.

Very well known low low-pass filter is the filter giving the commonly called mean or average. All the weights are equal to $\frac{1}{2N+1}$. That filter is also the filter equivalent to least square polynomial fit of degree zero.

The filter which gives the DC Component in Fourier analysis is a low low-pass filter having all its weights equal to $\frac{1}{2N}$ except the weights B_{-N} and B_N which are equal to $\frac{1}{4N}$. For large values of N, the gain of that filter is practically the same as the gain of the filter for determining the mean.

Figure 7 shows the algebraic gains of two low low-pass filters with N=50: one designed by min-max, the other the Fourier low low-pass filter. It can be seen that the Fourier filter drops to zero gain more rapidly than the min-max filter, but exhibits a strong phase reversal (gain down to -.22) and has oscillations which do not exceed .01 only when r becomes larger than .20 .

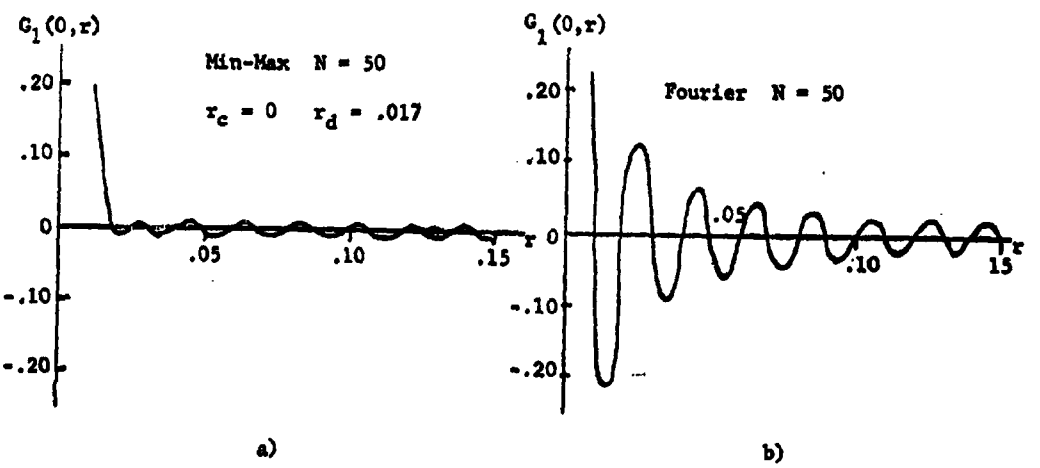

FIGURE 7

If we multiply the weights $B_k^{(LL)}$ of a low low-pass filter by $2 \cos 2\pi k r_s$, r_s being a selected value of r, the algebraic gain of the obtained filter is the sum of the algebraic gain curves of the low low-pass filter centered at frequency ratios r_s and $-r_s$.

Since for frequency ratios departing from zero by more than r_d the oscillations of the low low-pass filter are negligible, the resulting filter has a gain which is practically the gain of the generating low low-pass filter centered at frequency ratio r_s(and $-r_s$, since all the cosine type filters have algebraic gains which are even functions of r). The resulting filter is then a narrow band-pass filter centered at frequency ratio r_s. It is called the cosine type sampling filter. Usually slight corrections to the weights are needed to satisfy the constraints $G_1(0,0) = 0$ and $G_1(0,r_s) = 1$. In case of the Fourier filters, these constraints are satisfied automatically when r_s is one of the multiples of $\frac{1}{2N}$, which are the values always used in Fourier analysis.

The sampling filter can help us in understanding something I consider fundamental in the interpretation of the filtering techniques: this is the frequency content of a finite set of sampled data. When I started this exposé, I assumed that the set of sampled data was infinite, hence the various frequency components were defined and the effect of a filter on the input function represented by this infinite set of sampled data could be predicted by analyzing the effect of the filter on each individual frequency component. But the filter has only P weights (or if we want all the weights for k outside the range -N to N are zero), hence the output of the filter depends only upon the sampled values to which these weights

can be applied. On the contrary, the function defined by the infinite series of sampled data depends mostly upon the sampled values not used by the filter. Consequently, it can be said that there are intrinsic frequencies in the finite set of sampled data which are filtered, and properties of these frequencies can be shown by moving sampling filtering along the data. A few examples will illustrate this point. If the sampled data have all the same value, the sampling filter with $r_s = 0$ (this is the low low-pass filter) will produce a constant output equal to the input value; sampling filter with any other value of r_s will produce an output identically zero. If a pure sine function is sampled, the output of a sampling filter is a sine function of same frequency and of amplitude equal to the amplitude of the input sine function multiplied by the gain of the sampling filter for that frequency ratio. A third example: after sampled data have been passed through for instance a low-pass filter or a band-pass filter, some frequencies have been eliminated; any sampling filter centered on any of the eliminated frequencies produces an output which is practically zero. Consequently, we can say that in a finite set of sampled data, there are frequencies, but we cannot separate them, because the available tools (sampling filters) have a finite bandwidth. The larger the number of weights of the sampling filter, the narrower the bandwidth can be: if the number N becomes infinite, the bandwidth becomes zero and each frequency can be isolated; such a filter is the Fourier filter with N infinite.

But now, we come to the critical problem in frequency analysis. If we move the sampling filter along a set of data, we can notice that the amplitudes of the approximate sine functions obtained as output vary. The spectrum is not constant. Hence compromise must be made between frequency analysis over a small number of data with relatively crude tools, but sufficiently accurate to detect the spectrum variations of interest, and frequency analysis over a large number of data points which provides a fine, but possibly useless, average spectrum.

It is the beauty and power of the filtering techniques that, through an algorithm as simple as a weighted average with a moving strip, it is possible to operate with great precision on a very complicated combination of frequencies.

I would like, now, to talk about the low-pass filter. This is a filter which, ideally, passes without alteration, all frequencies for frequency ratio from 0 to r_c (the cut-off frequency ratio), and does not pass any frequency beyond a frequency ratio $r_c + r_d$. In the downcurve, for frequency ratio r between r_c and $r_c + r_d$, the gain should decrease monotonically from 1 to 0.

As for the low low-pass filter, the constraint, $G_1(0,0) = 1$ is imposed, and, in the min-max method of design, r_d is selected by trial and error to limit $|\varepsilon(0,r)|$ to .01. It has been found that for N between 5 and 50, the product $N r_d$ is approximately equal to unity.

Theoretically, the larger the number of weights in the filter, the steeper it is possible to make the downcurve. This is advantageous in smoothing, because no frequency for frequency ratio smaller than r_c is altered, all frequencies beyond frequency ratio $r_c + r_d$ are eliminated, but the frequencies in the downcurve are only attenuated. When smoothing is performed, it is assumed that all the information of interest is contained within frequencies lower than r_c f_s, and that the downcurve contains a negligible amount of information. Although a low low-pass filter can be considered as a low-pass filter with $r_c = 0$, it differs fundamentally from the low-pass filter in the fact that all the information of interest is contained in the downcurve.

The cut-off frequency ratio r_c should be selected large enough so that no information of interest is lost, but as small as possible to reduce the noise to a minimum. This selection may be very difficult and only the engineer or physicist who is user of the data is usually in position to make the decision. The data processing man can approximately what frequencies are present in the data, for instance by counting the number of data points in a period (either in the principal harmonic or in some of the ripples): the corresponding frequency ratio is the reciprocal of that number of points. But, without knowledge of the phenomenon under study, the data processing man cannot state which frequencies belong to the phenomenon, and which are noise. Incidently, in some cases, the engineer or physicist cannot either and processing with various values of r_c may be useful.

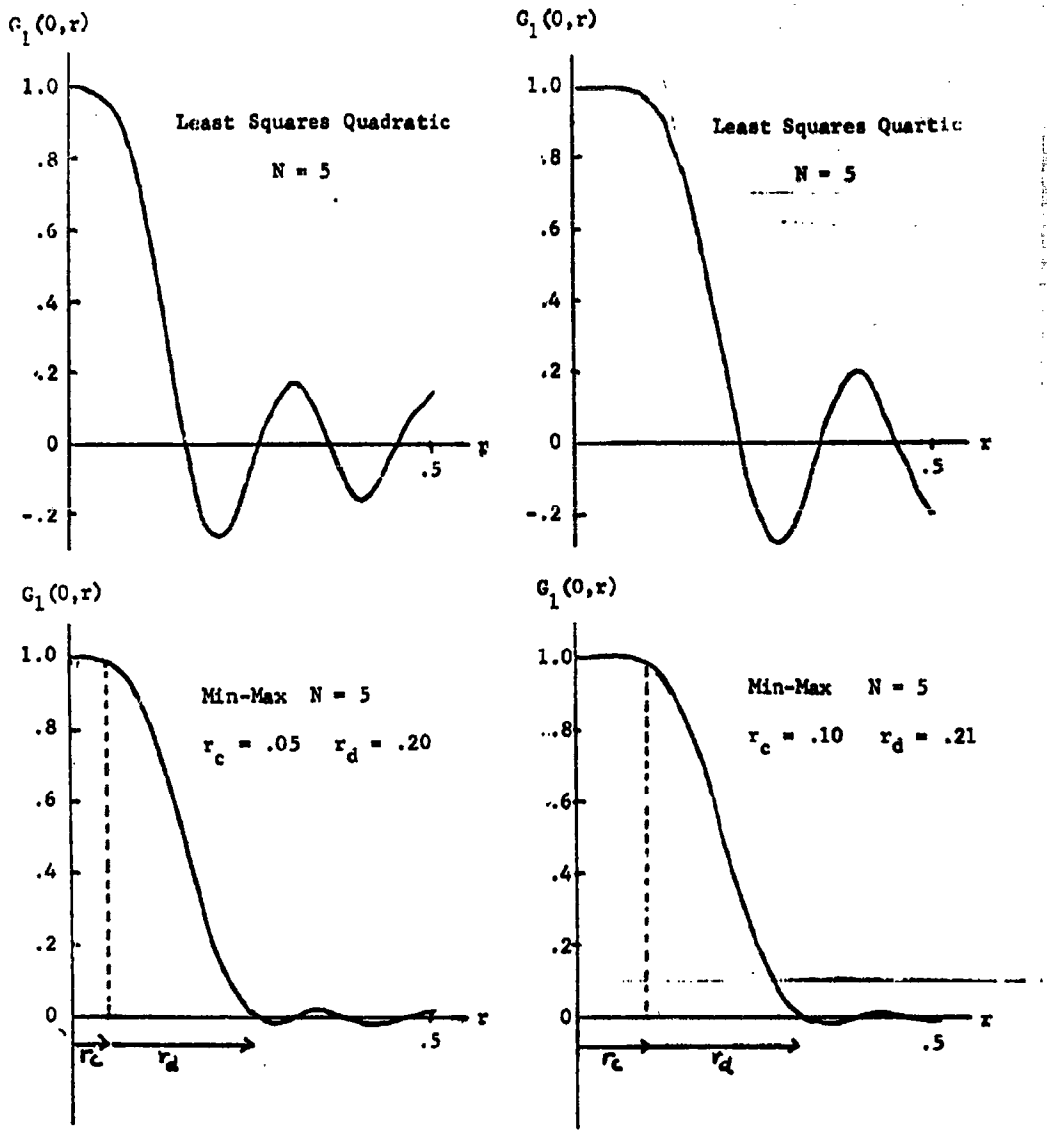
$G_1(0,r)$
1.0
.8
.6
.4
.2
0
-.2
.5
r
Least Squares Quadratic
N = 5
$G_1(0,r)$
Least Squares Quartic
N = 5
$G_1(0,r)$
Min-Max N = 5
r_c = .05 r_d = .20
r_c
r_d
$G_1(0,r)$
Min-Max N = 5
r_c = .10 r_d = .21

FIGURE 8

The least square polynomial fit of sampled data is equivalent to a low-pass filter whose weights and algebraic gain can be determined. For instance, Figure 8 shows the algebraic gains of filters equivalent to least square polynomial fits of degrees 2 and 4 over 11 points (N=5) and two low pass filters designed by min-max with the same number of weights. It can be seen that beyond the first zero crossing, the least square polynomial filters exhibit strong oscillations. For instance, the least square quadratic filter still passes 10% of the amplitude of frequency components of frequency ratio .30. The least square polynomial fit of sampled data is just a particular case of filtering techniques. Consequently, there is no sense in talking of least square polynomial fit versus filtering techniques. The question is: Do we want a filter with a gain curve like the one corresponding to a least square polynomial fit? Personally, I do not think this is a very good choice as the Figure 8 shows for instance. The degree and number of points of the least square polynomial fit determine the gain curve. On the contrary, the great advantage of the general filtering techniques is that the same gain curve can be specified for any number N: the larger N, the closer it is possible to approximate the specified gain curve, that is all. In our data processing of flight test data, we commonly use low-pass filters with N=50 (101 weights) and a large variety of cut-off frequency ratios.

I would like to say a few words about another category of filters, the sine type filters. They are skew symmetric filters, in which

$$N_1 = -N \quad N_2 = N \quad B_{-k} = -B_k \quad B_o = 0 \tag{10}$$

and the output is assigned to the time of application of the weight B_o.

The actual transfer function of such filters is a pure imaginary function; in other words, the phase shift is $+90^o$, and the transfer function is equal to the product of j by the algebraic gain, that is

$$\phi_1(0, r) = 90^o$$

$$Y_1(0, r) = j \; G_1(0,r) \tag{11}$$

with $$G_1(0,r) = 2 \sum_{k=1}^{N} B_k \sin 2\pi kr$$

We will discuss two examples of sine type filters: the differentiator and the sine type sampling filters.

A differentiator is a filter used to determine the derivative at the central point of a set of $2N+1$ sampled data. The gain of an ideal differentiator is

$$G(0,r) = 2\pi f = 2\pi r \, f_s \quad (-.5 \leq r \leq .5) \tag{12}$$

For $r = .5$ and $-.5$, the respective values of the ideal gain are πf_s and $-\pi f_s$. But for $r = \pm .5$, the value of the gain of an actual differentiator is 0, hence an actual differentiator can approximate an ideal differentiator only for a limited range, $-r_2$ to r_2, of values of r.

Since, when r varies from 0 to r_2, the ideal gain varies from 0 to $2\pi r_2 f_s$, the performance of the actual differentiator can be best evaluated by the relative error

$$\eta(0,r) = \frac{\mathcal{E}(0,r)}{G(0,r)} \tag{13}$$

In order for the relative error to remain small in the neighborhood of $r = 0$, the derivative of the absolute error $\mathcal{E}(0,r)$ for $r = 0$ must be zero. This provides a constraint between the weights of the differentiator. When this constraint is satisfied, the actual differentiator yields a constant value for the derivative of a sampled linear function.

When differentiators are designed by min-max technique, it is found that only a few weights are needed. For instance N=2 (5 weights) gives a relative error not exceeding .1% for r up to .10, and 1% for r up to .18.

When differentiation follows smoothing by a low-pass filter, it is assumed that the frequency components in the downcurve of the low-pass filter gain are negligible per comparison with the components of frequency ratio smaller than the cut-off frequency ratio. If this is not the case, the results may be grossly in error, because the gain of a differentiator is proportional to the frequency ratio. As a consequence, since all the information passed by a low low-pass filter is contained in its downcurve, results of differentiation after smoothing by a low low-pass filter depend very strongly upon the selection of the low low-pass filter.

Incidently, a simple algorithm permits to compute the weights of a single filter producing the same result as the application of two filters in succession (for instance, low-pass filter followed by differentiator) but this does not have much practical interest.

If we multiply the weights $B_k^{(LL)}$ of a low low-pass filter by $2 \sin 2\pi k r_s$, the obtained filter is of the sine type, and its algebraic gain is the difference of the algebraic gain curves of the low low-pass filter centered at frequency ratios r_s and $-r_s$. The resulting sine type sampling filter is a very narrow band-pass filter which behaves like the cosine type sampling filter that we have discussed previously, except that it introduces a phase shift of 90° instead of 0° on all frequency components. The comments we made on the cosine type sampling filters can be applied to the sine type sampling filters.

The last category of filters I want to talk about is the generalized filters, which have no symmetry, hence have complex transfer functions. I will discuss only one type: the interpolation filter. This is a filter which ideally, for all frequency components of frequency ratio not exceeding a selected maximum value r_2, has unit gain and phase shift equal to $m.360^\circ$, where m is the fraction of the sampling interval corresponding to the time at which the interpolated value is desired. Each value of m requires a separate filter. Usually two constraints are added so that a linear function is not altered after being passed through the interpolation filter.

Interpolation filters have been designed by min-max technique. It has been found that for $r_2 = .20$, filters designed with $N_1 = -3$, $N_2 = 3$ and various values of m from $-.5$ to $.5$, have transfer functions for which the magnitude of $\mathcal{E}(m, r)$ does not exceed .0004 for values of r not exceeding .20.

For any value of m, there is a generalized filter equivalent to the Lagrange Interpolation Formula using sampled data points for k from N_1 to N_2. Hence it is possible to evaluate the Lagrange interpolation formula by determining the transfer function of its equivalent generalized filter. It can be shown that when N_1 and N_2 go respectively to $-\infty$ and $+\infty$, the Lagrange interpolation filter becomes a perfect interpolation filter, that is $\mathcal{E}(m, r) \equiv 0$ for all values of r from 0 to .5. It is good practice to take $N_1 = -N_2 = -N$ and have m between $-.5$ and .5. For given m and selected permissible maximum value of the absolute error $|\mathcal{E}(m,r)|$, r_2 increases monotonically as N increases. For instance, for $N = 50$, and m not exceeding .5, $|\mathcal{E}(m,r)|$ does not exceed 10^{-7} for any value of r not larger than .30.

It must be remembered that, for a finite set of sampled data, there is no such thing as the value of the function at any time other than at the sampling times: a function is defined only if k goes from $-\infty$ to $+\infty$. But it is possible to consider the sequence of approximations of that unknown value obtained by Lagrange interpolation formula with increasing values of N. Beyond a certain value of N, the successive approximations are equal for all practical purposes. Care must be taken to limit the round off errors:

for large values of N, each weight must be defined with enough significant digits, hence double precision may be necessary for computing the interpolation value.

It is often said that "wiggling" increases when the degree of the Lagrange interpolation polynomial increases. If the wiggling is not produced by the skewness of the filter (N_1 not close to $-N_2$), and by m being larger than .5, the wiggling really exists in the data, and is shown when N is sufficiently large. Eliminating this wiggling is a smoothing operation, which can be best performed by first smoothing the sampled data points by a low-pass filter as discussed above, then interpolating with a Lagrange interpolator. Frequencies contained in the data have been eliminated.

I would like finally to say a few words about various methods of frequency analysis.

We have discussed the Fourier method, which is computer time consuming when applied to a large number of data points, and is of poor accuracy when applied to a small number of data points. From the result of the cosine type and sine type Fourier sampling filters, estimates of the power spectral density $A^2(r_s f_s)$ can be computed by the square root of the sum of the squares of the output of the sampling filters for $r = r_s$. Estimate of the phase $\psi(r_s f_s)$ can be obtained also.

The power spectral density can also be determined by averaging the squares of the outputs of one sampling filter (cosine type or sine type). This is the digital equivalent of a classical analog filter technique. The digital operations are quite time consuming and the result depends upon the compromise between the bandwidth of the sampling filter and the number of outputs available for squaring and averaging.

In brief, frequency analysis by filtering techniques is not very efficient. On the contrary frequency analysis by Fourier transform of autocovariance (average lagged products) is very fast. The accuracy is limited by two facts: with a finite set of sampled data, only estimates of autocovariance can be obtained, and only a finite number of terms of the Fourier series are available. The result is a noisy spectrum which has to be smoothed. Tukey uses a very weak low low-pass filter having N = 1. We have obtained results which appear more satisfactory by using a low low-pass filter having N=5. However, one always wonders how the information is altered by smoothing. In addition, as explained previously, any frequency analysis involves a compromise between a rough but varying spectrum defined by a small number of data points and a fine average spectrum defined by a large number of data points.

Filtering techniques can be used advantageously in power spectral analysis of very low frequencies contained in extremely large sets of sampled data. The data are passed through a low-pass filter so that the sampled frequency of the filtered data can be reduced considerably; in that manner, the number of calculations necessary in the determination of autocovariances is not prohibitively large.

In this exposé, I have attempted to stress the importance of the notion of frequency content of a finite set of sampled data, to show how this can be used to develop filtering techniques and apply them intelligently and with caution. I have limited to a minimum the number of equations. Mathematical developments in the theory and design of the filters, and numerical results, for instance the weights and performance of specific filters, some of them which have not been discussed here, can be found in a report (*) which is available upon request.

(*) M. A. Martin -- Digital Filters for Data Processing, TIS NO. 62SD484, General Electric Company, Missile and Space Division, P. O. Box 8555, Philadelphia 1, Pennsylvania, October 1962.

809-4

RADAR ANALYSIS PROGRESS

BY
A. E. Hoffman-Heyden
RCA Missile Test Project
Patrick AFB, Florida

Presented at:
Fourth Joint AFMTC/Range User Data Conference
Orlando AFB, Florida
26-28 February 1963

RADAR ANALYSIS PROGRESS
PRESENTATION TO DATA USER'S CONFERENCE 1963

ABSTRACT

1. Introduction

The presentation on radar topics given to the 1962 Data User's Conference familiarized the audience with the philosophy of RCA/MTP radar accuracy evaluations and characterized several associated projects. In continuing the program outlined at that time, the radar systems evaluation activities during the past year covered studies of the operational accuracy of several AN/FPS-16 radars which not only permitted consolidation of the present accuracy capabilities but also revealed areas of errors and tracking problems which require continued efforts towards adequate solution.

In supporting the ANR radar activities, a variety of problems in the categories of Systems Application, Data Utilization and Operational Techniques were dealt with. To illustrate these efforts in improving the ANR radar utility, highlights are presented on the subjects of reflectivity measurments as the "4th data coordinate", refinements in terminal trajectory coverage, and experience from MERCURY radar operations.

2. Accuracy Evaluation

To gain a realistic survey of the accuracy of the uprange AN/FPS-16 radars during live missile operations, the radars at Cape Canaveral, Grand Bahama, Carter Cay and San Salvador were examined in great detail, and numerical investigations were extended to the radars at Patrick A.F.B., East Island (F.R.)

and Ascension. For the uprange radars, the AZUSA MK II system's position data served as reference, and typical ballistic missile tests were selected to obtain overlapping data coverages well in excess of 100 sec. duration.

The common objectives of the evaluations consisted of determining the dispersion and bias values in the radar data under the conditions characteristical for the investigated tests. Furthermore, efforts were devoted to the identification of errors of unexpected nature and magnitude which were detected frequently and stressed the importance of the station-by-station analyses. In selecting missile tracks for radar accuracy evaluation purposes, a long data time span is of primary importance and, secondly, it is desirable to cover favorable as well as problematic tracking conditions in order to display the resulting variations in data quality. It should be noted that only few vehicles are equipped with beacon antenna systems which provide continuously good signal propagation for the uprange and midcourse radars and, therefore, almost every missile type reveals tracking peculiaritities which exert some degrading effects upon the quality of radar track.

The random errors in the radar data which are customarily evaluated by the ariate difference method over short (2 sec) time spans, have not revealed new information and again confirmed good correlation between their magnitude and the predictable receiver noise effects. For this reason, checks on consistency between predicted and observed random noise are a valuable tool for detecting departures from nominal performance as they may occur due to imperfect systems alignment (radar-dependent causes) or due to target glint, beacon pattern effects, or signal scintillations (target-dependent causes). As examples for this type of checks, Figs. 1 and 2 display estimates of

random errors in radar angle data vs time-coincident reciever S/N ratio, and the straight reference lines $\sigma_{th}(S/N)$ represent the nominal relationship between random errors and signal-to-noise ratio predicted on the basis of the technical radar operating parameters. Whereas Fig. 1 testifies remarkably good agreement of the experimental data and a somewhat better than expected radar performance, Fig. 2 portrays the situation when the radar was in basically good alignment but encountered severe disturbances from beacon pattern irregularities and associated shifts of the radar balance point.

In general, the AMR experiences with AN/FPS-16 radars show that the random noise can be held close to the thermal noise predictions, and the guide values σ_R = 10 ft and $\sigma_A, \sigma_E \leq 0.1$° are considered as a conservative standard for track under fairly stable signal conditions. There are conditions where the random noise renders lower than predicted values. These departures usually coincide with tracking conditions which approach the static case, i.e., when the dynamic servo requirements are small or negligible. Necessarily, any stiction effects produce the net result of no noise during the time the antenna is held stationary, and conversely, the appearance of zero noise during track at low angular rates is a good indicator for the existence of stiction.

The combined <u>random-and-cyclic errors</u>, which are evaluated from the radar/reference differences and expressed in terms of standard deviations about a constant mean, displayed values larger than the random errors. This is as expected since the AZUSA/Radar differences reflect the error spectrum down to virtual zero frequency components (constant bias) and, consequently, reveal the radar's low frequency errors which are excluded by the variate difference evaluation.

When ignoring those tracking portions where multipath interference or verified target-dependent disturbances produced excessive tracking jitter, the grand average of the dispersions obtained from a total of several thousand seconds tracking time yielded the guide values $\sigma_{\Delta R}$ = 20 ft and $\sigma_{\Delta A}$ $\sigma_{\Delta E}$ = 0.2°. These estimates necessarily include the noise contributions by the AZUSA reference data and a slight inflation due to the fact that the parallax between AZUSA and Radar tracking reference on the vehicle was not reconciled. The errors originating from this cause are most pronounced in the radar range data and even permit to reconstruct the magnitude of the apparent parallax. It is worth noting and testifies for the general performance status of the radars that there are no drastic differences between the average data quality of different radar stations. Test-to-test variations are certainly noticeable and largely related to target type, tracking geometry, and signal quality.

In the class of radar bias errors, the accuracy evaluations failed yet to display consistently small magnitudes of the elevation and range bias although the field radar orientations and any corrections are carried out most diligently. The problems in this area are more deep-rooted, and continued investigations are necessary to assess the stability of the orientation targets, consistency of radar alignment, effects of propagation between radar and tracked vehicle, and the errors which may be hidden even in the reference data and their transformation. To illustrate the bias problem, it was found that the AZUSA MK II/Radar data comparisons yielded average negative range bias in the radar data from all stations, and that the test-to-test dispersions were smallest for radar 1.16. Whereas the general tendency cannot be explained at this time, the display of a particularly small spread in the radar 1.16 range calibrations appears to be the result of zero settings on

an uncluttered range target (located in the Indian River) and of the fact that this radar can usually measure the range to the missile already prior to its launch and align the range tracker's beacon delay correction according to the surveyed radar/pad distance. At several downrange stations, the range calibration targets are less favorably located. Since the beacon delay adjustments need to be made on the basis of reported uprange measurements, zero-set bias introduced by the local reference target remains in the data. Aside of the examination of the radar accuracy under field operating conditions, the station-by-station studies proved quite beneficial with regard to the detection of tracking problems peculiar to the physical and tracking environment of individual radars. A few of these unforeseen problems and the actions taken to their solution are presented:

a. The radar 3.16 displayed unusually large Azimuth errors when track was acquired on ballistic missile launches at low elevation angles, and larger than typical overwater multipath noise persisted in the elevation data up to about 2.5°. The compilation of data from a number of similar tests and their normalization with respect to Azimuth-dependent errors $\Delta A_{(A)}$ formed a fairly well behaved pattern which proved that the radar's Azimuth data in the direction of Cape Canaveral contain errors with magnitudes between -1^{-} and -3^{-} as long as $E \leq 1.5^{\circ}$. Figure 3 displays the results from four tests in the form of plots of ΔA vs. A with accompanying curves E(A).

A plausible explanation for these phenomena consists of the radar 3.16 surroundings by high trees some of which are cut off to form an aisle in the direction of the launch area. The tree formations along the aisle are well capable of generating multipath interference, particularly when high humidity raises their reflection coefficient. Since the errors are beyond control and

their test-to-test variations are rather sizeable, no satisfactory error correction can be accomplished and it was found preferable to limit the publication of radar 3.16 flight test data (xyz) to the condition where $E \leq 2.5^{o}$.

b. During tracks on particular missile types, the radar 0.16 and 3.16 AZUSA data comparisons evidenced temporary systematic Azimuth and Elevation errors which occur time coincident with the passage of strong cross-polarization between beacon and radar antenna. The errors represent a special version of target-dependent angular scintillation noise such as commonly known as glint and also encountered in conjunction with the passage of beacon pattern minima. In these particular cases, the angular aberrations reached magnitudes of up to approximately 2° at Radar 3.16 and of up to more than 1° at Radar 0.16. The significance of this kind of disturbances which were observed occasionally also at other stations, lies in the difficulty of their identification and in the great problem of their correction. Of particular interest is the situation at Radar 3.16 (Fig. 4) where the shift progresses quite slowly and gives no other indication than a barely noticeable decay and recovery of the signal strength. By comparison, the error development takes place far more rapidly at Radar 0.16 and, consequently, manifests itself by servo errors proportional to the dynamic torque requirements. Regardless of this indication, only a knowledgeable observer is able to properly interpret these recordings in real time (Fig. 5). To avoid that this type of errors inadvertently enters the flight test data publications, several approaches are taken:

a. On the basis of AZUSA/Radar data comparisons, the radar tracking quality is examined and spans containing position differences in excess of 200 ft. are not published.

b. The data spans missing from a certain station on account of editing (a. above) are replenished if data from another radar are available.

c. In the case of polarization - dependent errors, it is attempted to obtain undegraded data from a radar circumventing the problem by using circular antenna polarization.

d. As a long-term solution, improved vehicle/radar antenna compatibility is pursued.

e. If a solution (d) cannot be accomplished and the trajectory/radar geometry permits, skin track can be selected as alternate mode to bridge the time portions during which beacon track is disturbed. Even a moderate degradation of data quality by increased noise is preferable to the uncertainties of disturbed beacon track, particularly in real-time data utilization for present-position and Impact Prediction displays.

In pursuing the instrumental solutions, the operation of the Carter Cay Radar with circular antenna polarization has rendered quite satisfactory results, demonstrated by apparent immunity against balance point shifts which were experienced simultaneously at the Grand Bahama Radar under closely similar tracking geometry. To gain better insight into the parameters governing this particular problem, a cross-polarization/tilted phase front simulator is engineered to permit tests under controlled conditions.

Fig. 6 shows the results of a cross-polarization run which demonstrates the radar's Azimuth and Elevation axis shift at cross-polarization angles above 70°.

3. Radar Cross-Sectional Area Measurements

In the past 1-1/2 years, the AMR received an increasing demand for reflectivity data on various vehicles; e.g., entire missiles, reentry bodies, and space vehicles. To meet these demands with adequate accuracy and

processing efficiency prior to the availability of the AN/FPQ-6, AN/TPQ-18 and AMR radars, several AN/FPS-16 radars were suitably instrumented and processing routines developed. The chart (Fig. 7) shows the extent of present facilities by listing the AMR C-Band radar stations and their equipment for signal strength recordings. Aside of the standard strip chart recording, four radars are equipped with DC/FM converters, five radars with dual channel recording capability, and one radar offers video film recording of the output of a lin-log receiver for multi-target registration.
The dual channel modification is noteworthy for the reason that it permits collection of echo data by means of a separate (non-tracking) receiver channel which is gated at echo arrival time while the radar tracks the vehicle's beacon. In this manner, echo data can be obtained from operational targets without interference between the objectives of high-quality metric data collection and reflectivity measurements.
While the reduction of reflectivity data from analog and film recordings requires tedious hand reading of the individual measurements, at the desired sampling rate, the DC/FM converted AGC voltage measurements are suitable for automated processing of large and densely sampled data quantities and thereby offer higher time resolution and fine-grain amplitude quantization. For these advantages, the necessary computer programs were established and radar calibration methods finalized which deliver high-grade cross-sectional data as a side product of the radar missile tracking operations. The flow diagram (Fig. 8) shows the principal steps of the program which yields C-Band reflectivity data in plotted and tabular form at a data rate of 10/sec (filtered AGC) or 100/sec (unfiltered):
The radar's analog AGC voltage controls a telemetry-type DC/FM converter the frequency of which is recorded on magnetic tape, using a spare

channel of the standard digital data recorder. To provide the required frequency discrimination, a tape speed of 15 ips is employed. The FM recordings are linearized and quantized in the Automatic Telemetry Reduction (TARE) process and yield numerical values S/N (t) at a sampling rate of 100/sec.

Radar cross area data A_e (t) are derived in the "RACO" program which filters the 100/sec S/N measurements, accepts the radar range data R(t) and solves

$$A_{e_i} \text{ (db/m}^2\text{)} = S/N_i \text{ (db)} + 40 \log R_i \text{ (yds)} + C$$

where C is the station constant describing the radar's RF loop gain, derived from track on a target of known radar cross-sectional area (usually the standard 6" diameter aluminum sphere). The computer results A_e (t) are presented in tabular form as exemplified by Fig. 9, consisting of a machine plot with time-coincident tabulation of the numerical reflectivity values. The amplitude resolution of the maching plot is usually selected to display 0.5 db/step, whereas the numericalvalues are rounded off at the 3rd decimal place. To aid the data interpretation by the user, the GEPL display contains in addition to the data A_e (t) a machine plot and tabulation of the values S/N(t) recorded by the radar. These data permit easy recognition of conditions under which the reflectivity data become of questionable value or invalid; e.g., when S/N = 0 or when the S/N ratio exceeds the dynamic range of the DC/FM converter, thus resulting in clipped reflectivity data.

To demonstrate the reproduction of signal strength measurements by the DC/FM conversion process, Fig. 10 shows a brief interval of analog echo AGC recording and the time-corresponding unfiltered "TARE" data. Note that the limited response of the analog recording obscures details of the signal structure, particularly when large amplitude variations alternate in

in rapid sequence.

When reconciling the field measurements, radar AGC calibration, sphere track, and computer processing required for producing reflectivity data, the question may be raised why the data manipulation does not resort to the somewhat simpler method of comparing test vehicle measurements directly with sphere track measurements. This method which lends itself to a solution requiring only a relative rather than an absolute S/N calibration of the radar's AGC voltage has been considered but was bypassed for reasons which are peculiar to the AMR radar operations philosophy.

In order to monitor and document the radar RF systems performance, sphere tracks are made at regular intervals, and furthermore, the post-flight performance evaluations require dependable S/N calibrations which permit comparison between predicted and observed signal strength and investigation of phenomena such as flame attenuation and reentry propagation losses. For these purposes, accurate S/N calibrations are a matter of daily routine, and any sphere track is used to re-check the radar's RF performance. With these field procedures being a matter of course and delivering the calibrations S/N vs. AGC and the constant C, it is most expedient to design the reflectivity data processing as initially outlined.

The quality of reflectivity measurements produced by the described program has been analyzed from the viewpoints of absolute accuracy, dispersion, and dependency on signal level. For this, sphere tracks were conducted and the routine processed data compared with the nominal results. The tabulation (Fig. 11) lists the numerical results of such an evaluation in terms of the mean error in a 10 sec. data span, the standard deviation of the data in the same span, and finally, the grand totals for runs performed by three different radars. Each set of measurements belongs to a certain

target distance, and the range difference between successive sets is 2,000 yds. Fig 12 displays the error distributions from the same data sets and stresses the small station-to-station variability as well as the relatively small dispersions and their nearly uniform station-to-station profile. On the basis of these anlyses, it was found safe to state that the measurements collected by any one of the radars would produce reflectivity data with errors of less than 3 db at a 95% confidence level.

A separate factor entering the reflectivity data quality is the influence of the S/N ratio upon dispersion and bias, since at low S/N the effects of receiver thermol noise become pronounced, and small systems instabilities may cause bias errors. To check this problem, sphere tracks were carried out to low S/N values, and Fig 13 illustrates that the bias and dispersion behavior for the range between 50 db and 17 db does not reveal any characteristic changes. These were found, however, as soon as S/N $\leq$ 5 db and displayed a rapid growth of the dispersions and also of larger bias fluctuations. (It is to be noted that the tests conducted for this type of studies necessitate careful control even over the sphere launch. In cases where high humidity results in spurious reflectivity of the carrier balloon, the measurements have shown to become severely contaminated by target-dependent signal fluctuations).

In conclusion of the topic on radar cross-sectional measurements, it may be stated that the efforts in using AN/FPS-16 operational echo signal strength measurements have resulted in a production program which furnishes cross-sectional data with quite satisfactory accuracy and with a resolution well suited for signature, spectral and statistical analyses by the Data User. The calibration techniques developed in support of this program permit checks on the radar's RF loop gain to within $\pm$ 0.5 db, and the radar

threshold calibrations were found to be reproducible to within ± 0.25 db.

4. Terminal Area Radar Track

Radar data from reentry vehicle coverages were analyzed to determine their utility for impact location purposes. If the radar tracks the vehicle to splash, the location is determined by the slant range and azimuth measurements coinciding with the time of the reentry vehicle's signal disappearance, and the geodetic impact location merely requires transformation of the radar measurements. The splash event is to be determined from the radar signal strength recording or from video signal documentation. The analog strip chart record of the receiver AGC voltage was found to render the instant of beacon signal failure to approximately 0.05 sec., whereas pulse-to-pulse video photography produced timing accuracies to approximately 0.003 sec. Fig. 14 illustrates the beacon signal failure at splash as recorded by both of the above methods, and emphasizes that the analog recording may introduce some timing uncertainties due to limited pen response and also as the result of signal trend variations which are not related to the splash event.

Using the final MILS impact locations as reference, several Radar 12.16 impact measurements were evaluated and rendered the scatter display of Fig. 15. It is noteworthy that all radar-measured impacts agree to better than 150 ft. with the MILS data and indicate an apparent radar range bias in the order of +120ft. The radar's angular accuracy in measuring the Azimuth to impact is shown to be better than 0.3 mils and, consequently, well within the dispersion to be expected under these tracking conditions. The accuracy of this rather simple method, the independence from other systems, and the ease of processing the radar data make the procedure attractive for impact outside the MILS net and, furthermore, offer the

possibility for rapid processing; e.g., for quick-look purposes. More experiences need to be gained to assess the limitations of the method and to define the most suitable data handling. Of particular importance is a definition for the ability of the radar in measuring impact range and azimuth at distances near and beyond the radar horizon where multipath and ducting have strong effects upon signal propagation and data noise content.

5. MERCURY Support

The manned orbital missions during 1962 gave the opportunity to examine the radar tracking performance and technical/operational radar problems associated with launch phase, orbital passes, and re-entry. Of special interest were the effects of pattern wobbulation, the usefulness of the automatic range acquisition system, and the C-Band propagation conditions during the capsule descent.

The pattern wobbulation, applied to two sectors of the capsule's C-Band antenna coverage for the purpose of pattern smoothing, was utilized on all manned tests. A detailed evaluation showed that the system provided exactly those coverage and tracking improvements which were predicted on the basis of theory and preceding simulations. Fig 16 illustrates the reduction in signal variations by showing the power level spread which was experienced by Radar 1.16 when looking into the modulated and into the unmodulated pattern portions. The significance of the reduced amplitudes is to be seen in a drastic flattening of pattern nulls which otherwise give rise to increased tracking noise and balance point shifts, and forthermore, in the improved signal detection probability by a radar which shall acquire the capsule while looking into the interference pattern portion. Numerically, the pattern smoothing reduced the level spread (worst conditions) from between 23 and 30 db down to approximately 8 db.

...e to lack of external reference, no analysis was conducted of the total errors experienced during lobe passages. On the basis of the experiences with Radars 3.16 and 3.16, however, it is likely that the radar track, when exposed to the unmodulated pattern portions, contained sizeable temporary errors. The increased data noise shown in Fig 2 is indicative for these events.

The automatic range acquisition system (ARAT), developed for the purpose of expeditious radar acquisition under adverse signal conditions, was incorporated at radar 1.16 and employed during MERCURY orbital passes. Fig. 17 exemplifies the range track position as a function of time for a typical high-speed target acquisition, and Fig 16 compares the acquisition delays of ARAT with those which are typical for manual range tracker control by skilled operators. The main features of this acquisition ...l are to be seen in the well controlled logic and in the almost perfect immunity to remotely triggered beacon replies as they are present in multi-station operations. The latter was achieved through "bilateral coding" which permits the radar to acquire only that target signal which appears with a special locally generated pulse-spacing, and relinquishes the need for the operator to determine which one of the received signals represents the local reply.

Valuable experiences were ...ained during the MERCURY re-entries along the AMR. The signal strength measurements during this flight portion rendered data on the C-Band propagation losses due to re-entry ionization which showed to be in the order of 20 db max, and permitted to sustain continuous radar track during the capsule's descent. The fact that the C-Band beacon loop as the only RF link remained operable, prompted an investigation of its use as an auxiliary communication means. Pulse position

modulation and the characteristic range modulation caused by the pattern wobbulation were considered as carrier for two-way narrow-band communication and telemetry purposes, and checked during ground tests and live capsule track.

In the proposal of this system, special care was taken to ascertain full compatibility between the communications function and the pulse-sequencing required for multi-station radar track, and furthermore, that no degradation of the radar tracking performance could arise with this additional utilization of the radar beacon loop.

Figure 1

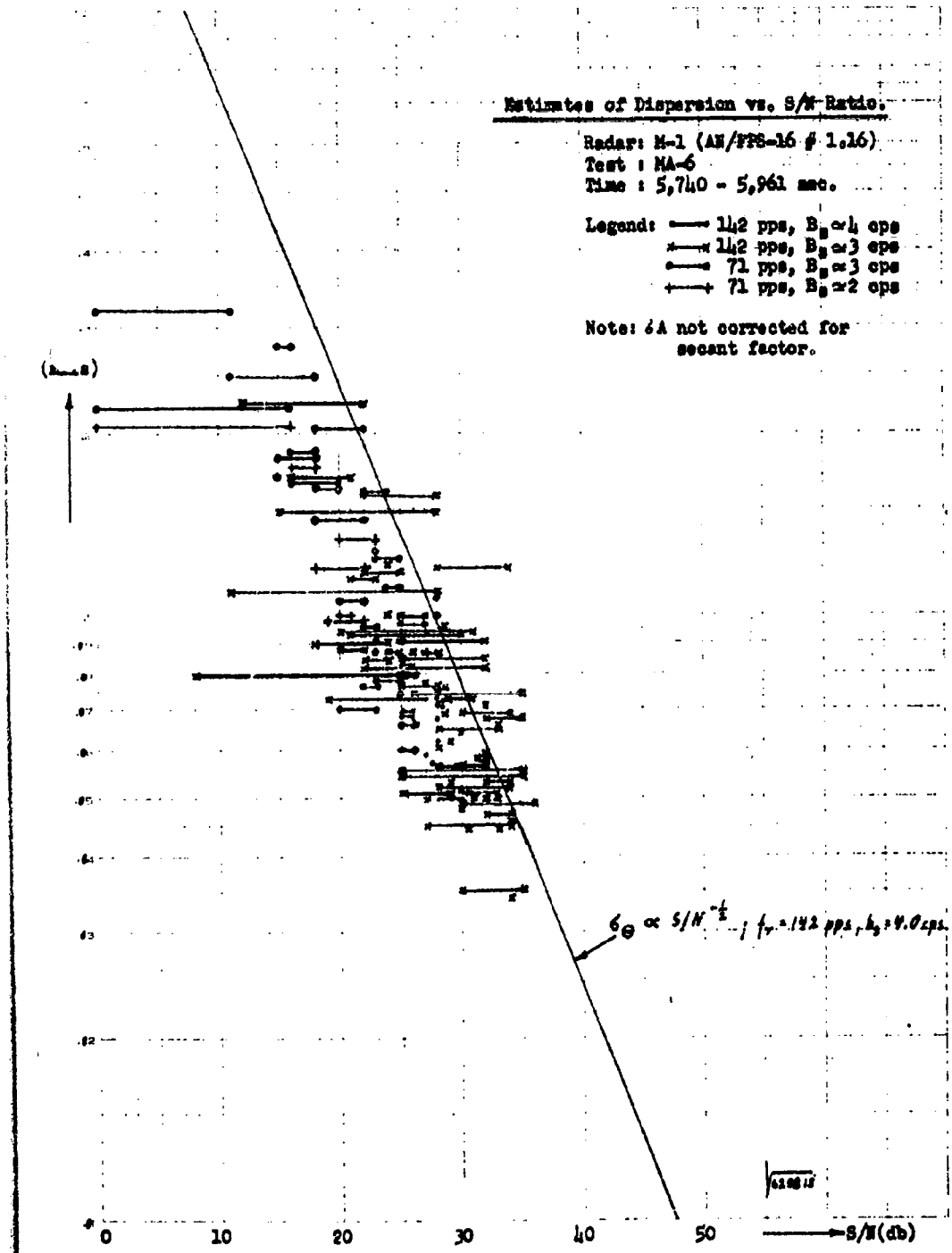
Estimates of Dispersion vs. S/N Ratio.
Radar: M-1 (AN/FPS-16 # 1.16)
Test : MA-6
Time : 5,740 - 5,961 sec.
Legend: 142 pps, $B_g \simeq 4$ cps
142 pps, $B_g \simeq 3$ cps
71 pps, $B_g \simeq 3$ cps
71 pps, $B_g \simeq 2$ cps
Note: δA not corrected for secant factor.
$\delta_\Theta \propto S/N^{-\frac{1}{2}}$; $f_r = 142$ pps, $B_g = 4.0$ cps.
0
10
20
30
40
50
S/N(db)

Figure 2

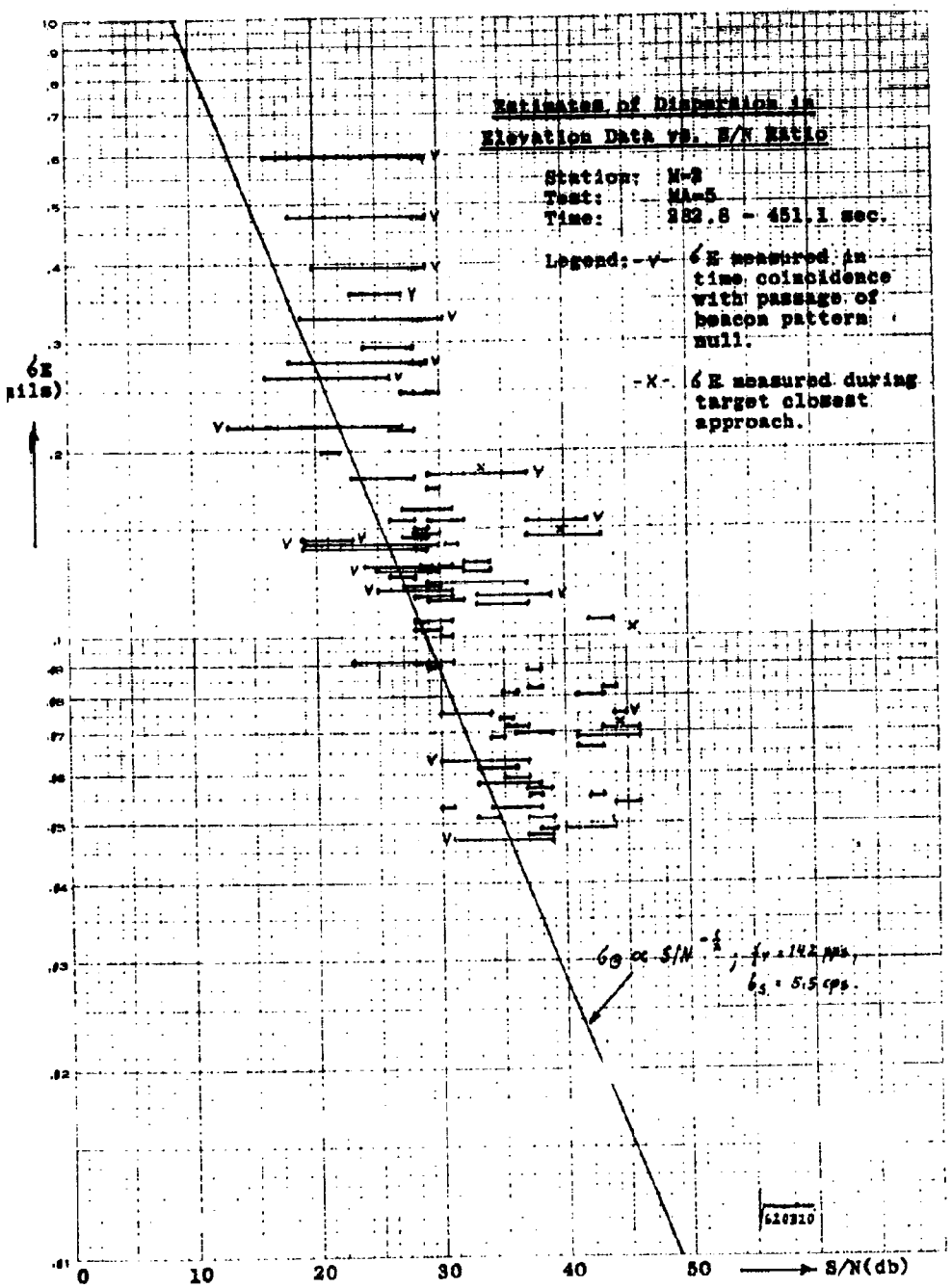
Estimates of Dispersion in Elevation Data vs. S/N Ratio
Station: M-2
Test: MA-5
Time: 382.8 - 451.1 sec.
Legend: -V- δE measured in time coincidence with passage of beacon pattern null.
-X- δE measured during target closest approach.
δE (mils)
S/N(db)
0
10
20
30
40
50
δθ ∝ S/N^-½ ; fv = 142 ppm, fs = 5.5 cps.
620310

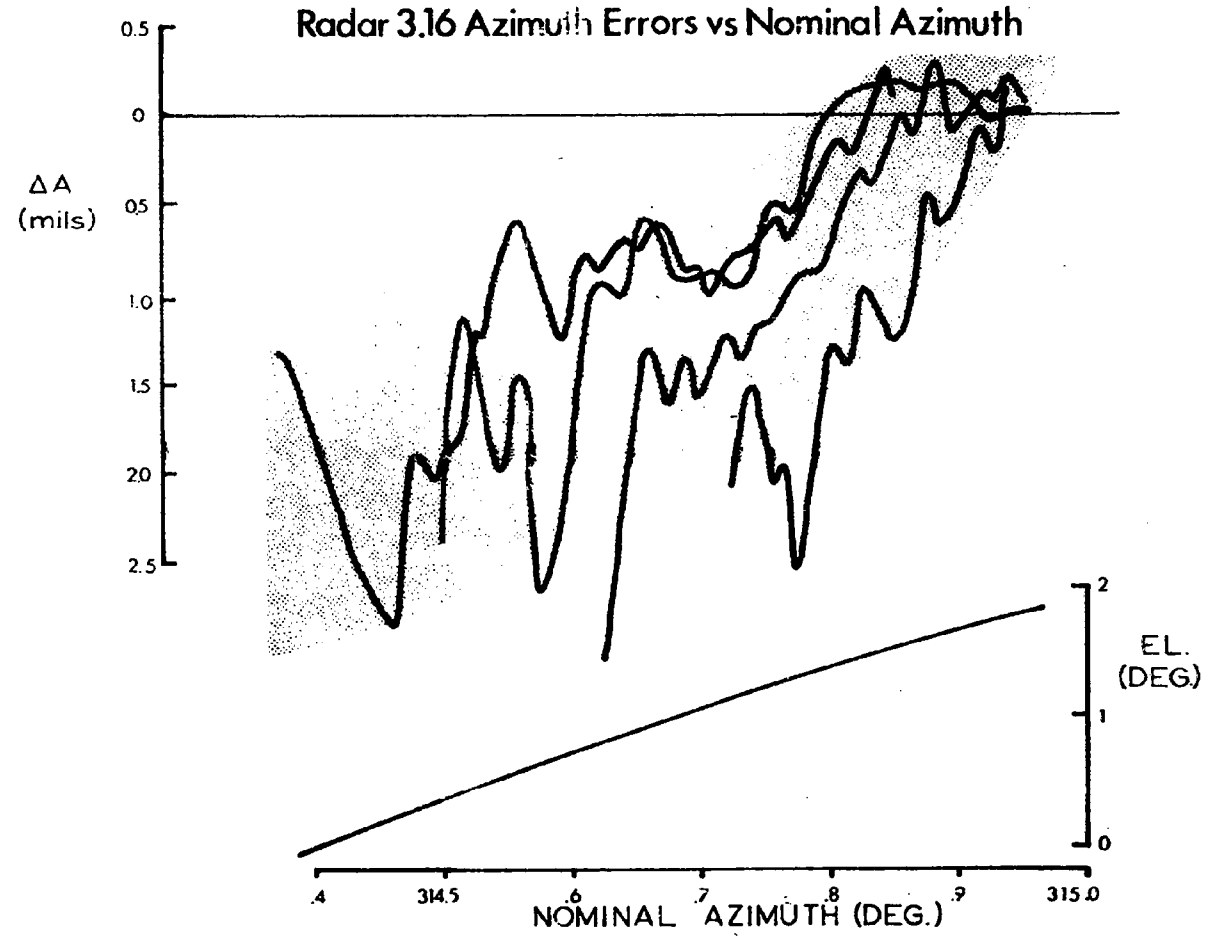
Radar 3.16 Azimuth Errors vs Nominal Azimuth
ΔA
(mils)
0.5
0
0.5
1.0
1.5
2.0
2.5
EL.
(DEG.)
2
1
0
.4
314.5
.6
.7
.8
.9
315.0
NOMINAL AZIMUTH (DEG.)

Figure 3

Figure 4

RADAR 3.16 ERROR SIGNALS AND ANGLE ERRORS

DURING BALANCE POINT SHIFT

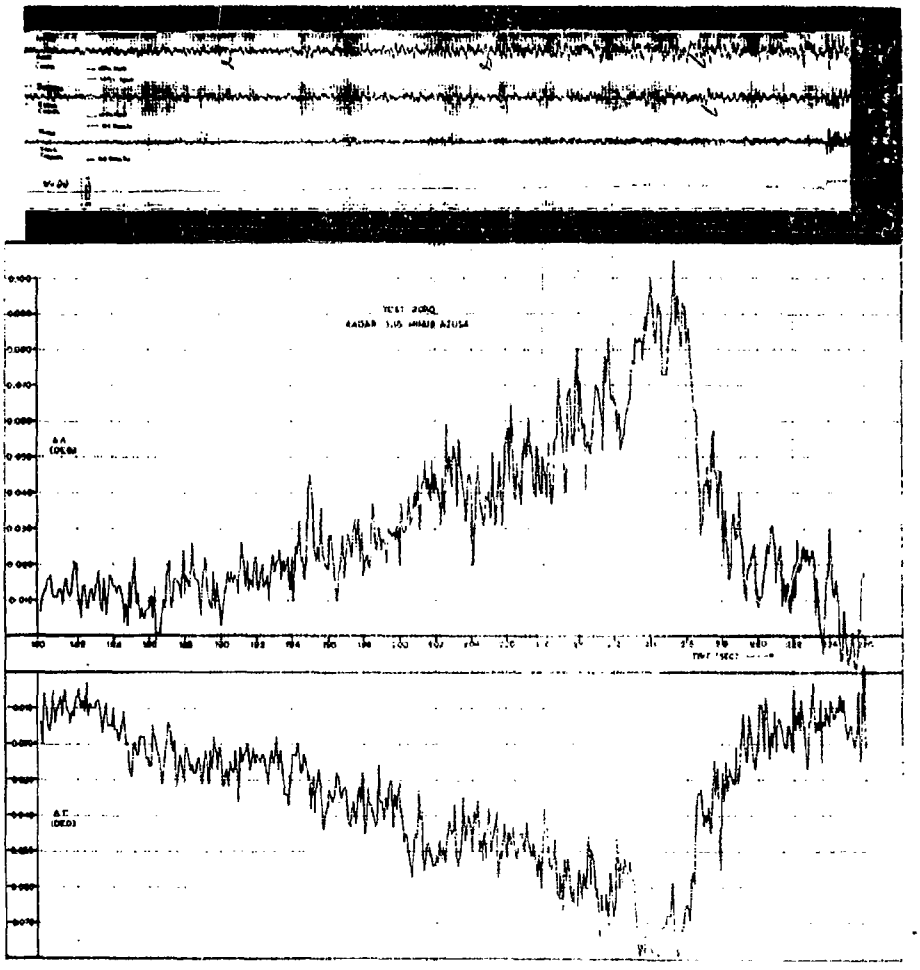

Figure 5

RADAR C.16 ERROR SIGNALS AND ANGLE ERRORS

DURING BALANCE POINT SHIFT

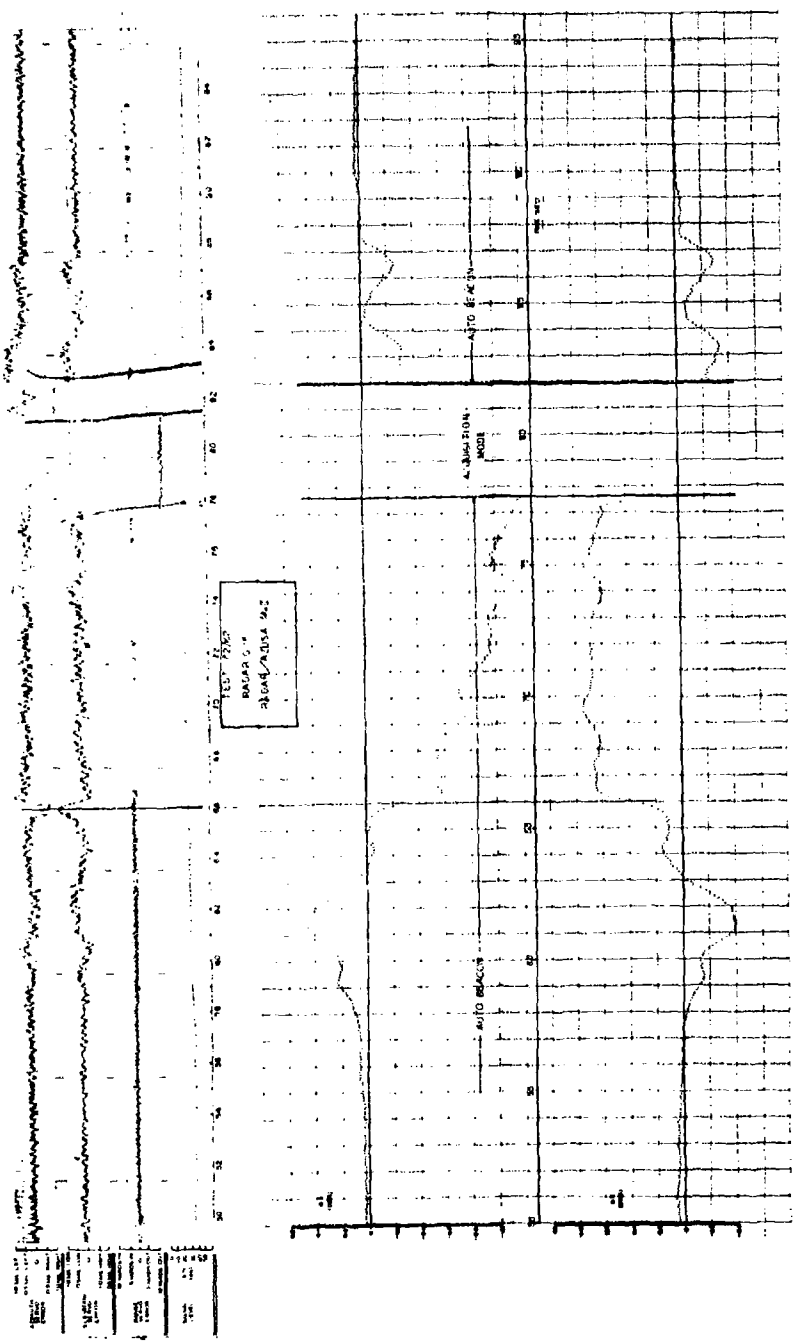

AN/FPS-16 Boresight Shift vs. Crosspolarization Angle

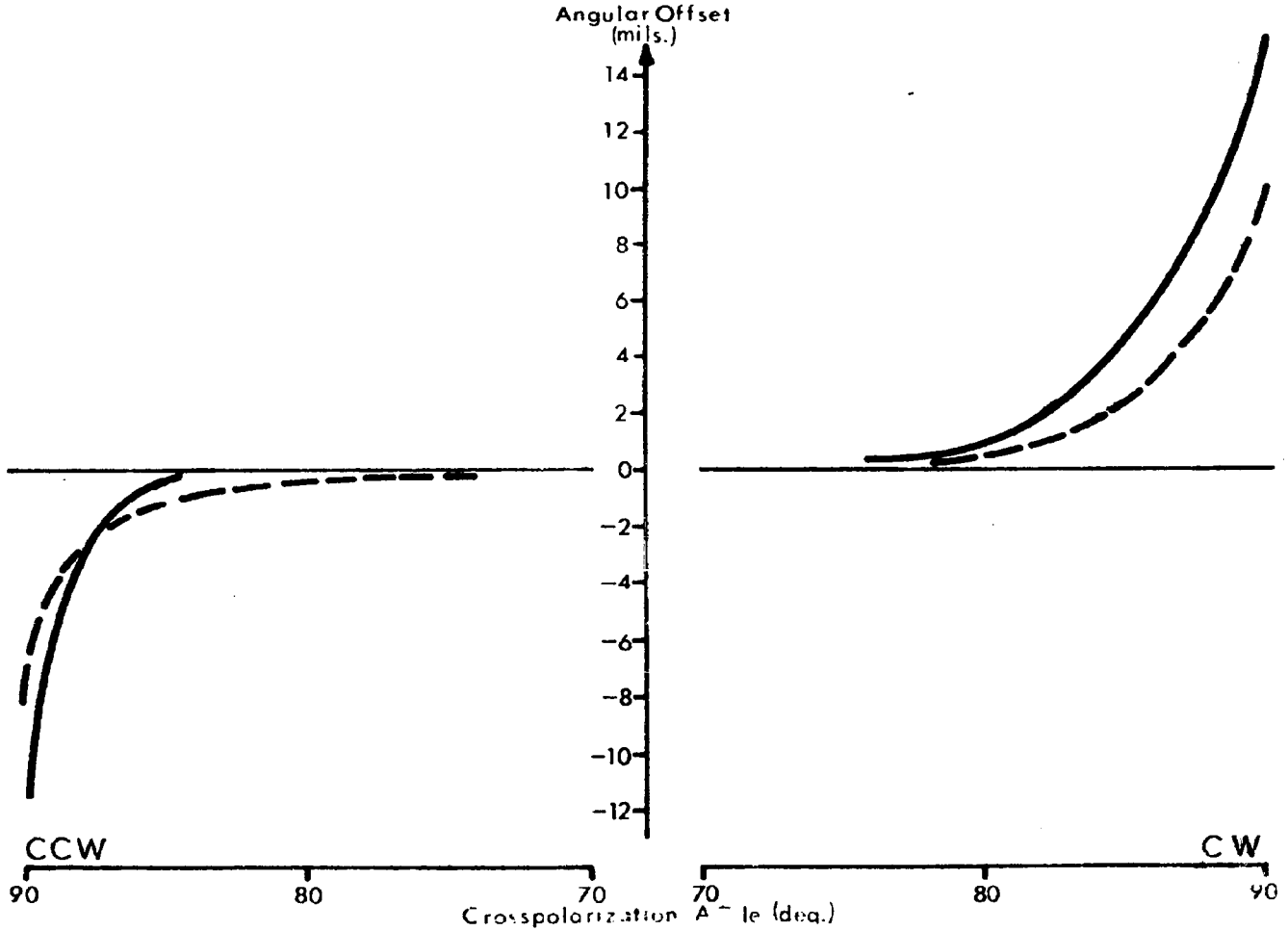

Figure 6

AN/FPS-16 SIGNAL STRENGTH RECORDING EQUIPMENT

RADAR SITES		RECORDING MEANS			
RADAR	LOCATION	Tracking Channel Analog	AGC/F-M Converter	Dual Channel Analog	Ungated Video-A scope Film
1.16	Cape Canaveral	x	x	x (3)	(2)
0.16	Patrick A.F.B.	x			
3.16	Grand Bahama Isld.	x	x	x (3)	
42.16	Carter Cay	x		x	
5.16	San Salvador Isld.	x	x		
92.16	East Island (P.E.)	x			
12.16	Ascension Isld.	x		x	x (1)
13.16	Pretoria, S.A.	x			(2)
86.16	Twin Falls Victory	x	x	x (3)	
Target Resolution		One Gated Target	One Gated Target	One Gated Target Skin and Beacon	Multiple Targets
Sampling		Con-tinuous	100/sec. max. after process-ing	Con-tinuous	P.R.F.

NOTES: (1) Ungated video displayed from lin-log receiver output.

(2) Ungated video recording of non-tracking (manually gain-controlled) receiver output as required.

(3) AGC/FM conversion can be employed with both channels.

FIGURE 7

AN/FPS-16 Radar Cross-Section Measurements

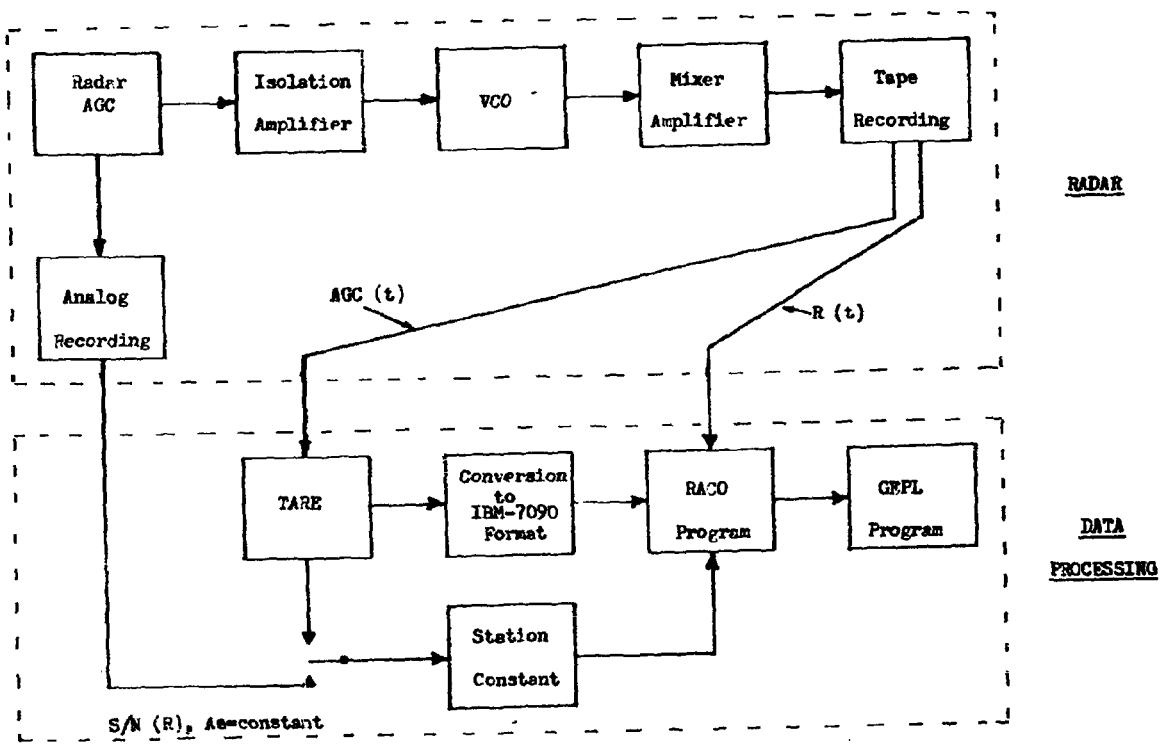

Figure 8

Figure 9: PRESENTATION OF SIGNAL LEVEL AND RADAR CROSS-SECTIONAL AREA DATA

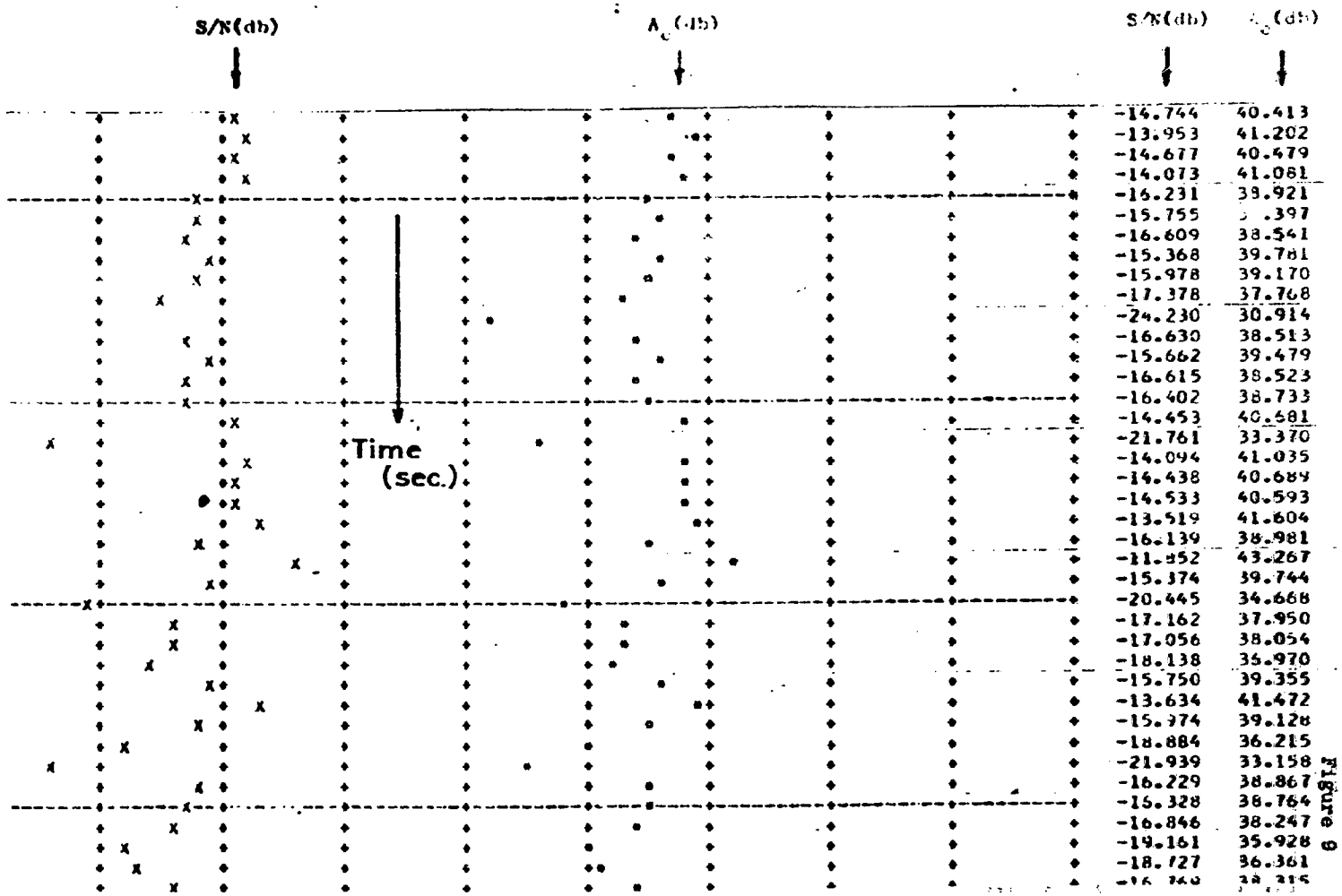

Figure 9

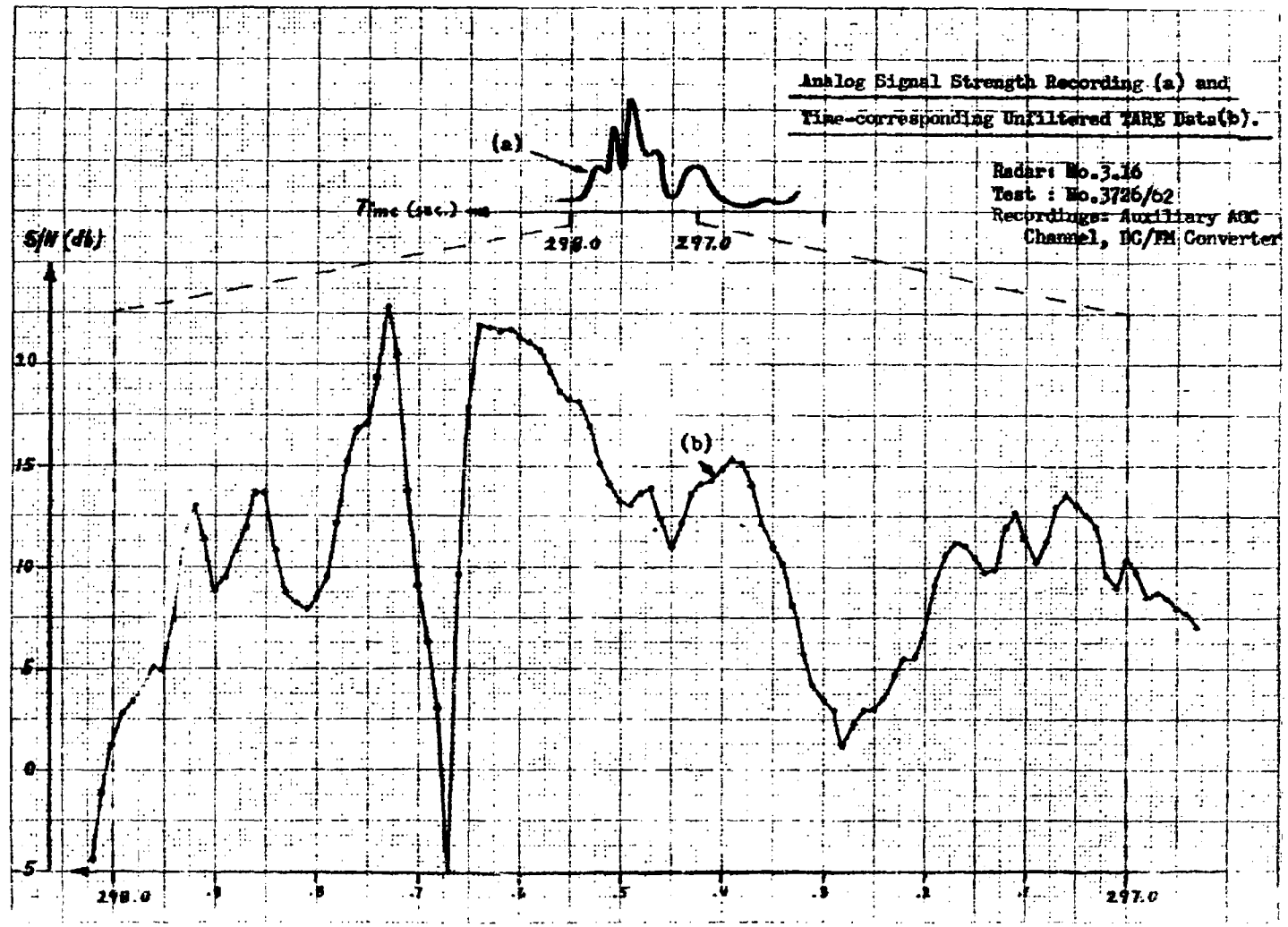

TABLE I

Results of Radar Cross-Sectional Area Measurements on 6" Sphere

Radar 1.16			Radar 3.16			Radar 5.16		
Standard Deviation (db)*	Mean Error (db)**	S/N Ratio (db)	Standard Deviation (db)*	Mean Error (db)**	S/N Ratio (db)	Standard Deviation (db)*	Mean Error (db)**	S/N Ratio (db)
1.81	+1.21	62	1.55	+0.19	49.5	0.89	+0.45	34
1.24	-0.42	50	1.66	-0.01	44.5	0.76	-0.70	31
1.50	-0.89	43	1.79	-0.02	40.6	0.81	+0.27	28.2
0.79	-1.29	34	1.17	-0.25	37.5	0.87	+0.31	26
1.18	-1.04	31	1.35	+0.24	34.8	0.61	-0.35	22
1.03	-0.48	28.2	1.16	+0.01	32.5	0.71	-0.61	19
0.98	-0.53	26	0.90	+0.47	30.3	0.72	+0.20	17.4
0.94	-0.99	24	1.00	+0.66	28.6	0.61	+1.02	16.2
1.02	-0.18	22	1.45	-0.26	27	0.80	-0.34	15
0.99	-0.12	20.4	1.28	-0.20	25.5	0.62	-0.22	13.8
1.00	-0.69	19	1.15	+0.08	24	0.62	-0.38	12.7
1.04	-0.68	16.2	1.36	-0.22	22.6	0.58	-0.12	11.6
1.08	-1.32	15	1.44	+0.24	20.3	0.81	-1.18	10.8
1.27	-1.89	12.9	1.01	+0.14	19.2	0.77	-0.97	10
1.12	-1.69	11.9	1.06	+0.59	18.2	1.11	-1.36	8.2
			2.47	+0.20	17.2	1.10	-1.48	7.5
						1.17	-0.74	6.7
						1.56	-2.19	6
						1.03	-3.66	5.3
Test Summary:			Test Summary:			Test Summary:		
Mean Error:	-0.73 db		Mean Error:	+0.11 db		Mean Error:	-0.77 db	
Standard Deviation:	1.36 db		Standard Deviation:	1.43 db		Standard Deviation:	1.28 db	

* Standard Deviation about mean departure from theoretical value

** Mean departure from theoretical value

Figure 11

Figure 12

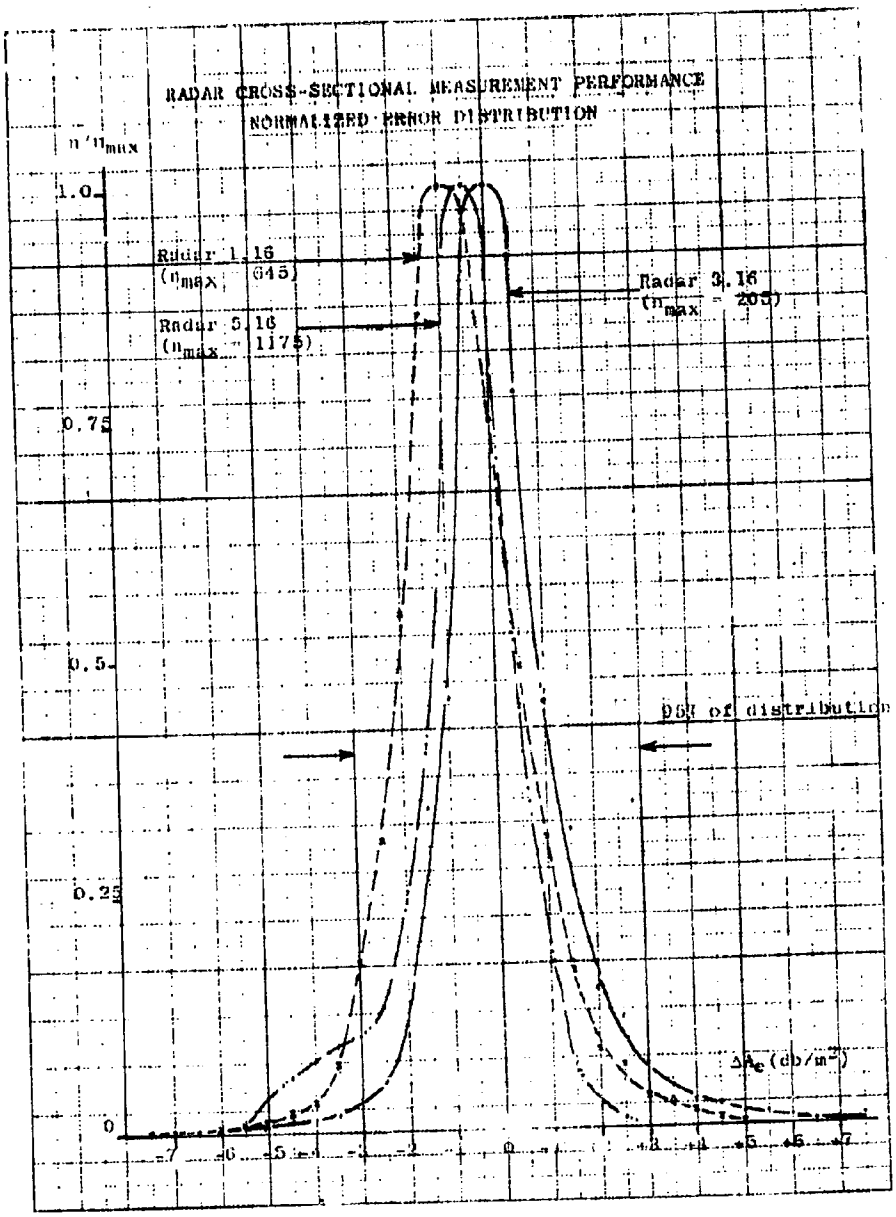
RADAR CROSS-SECTIONAL MEASUREMENT PERFORMANCE
NORMALIZED ERROR DISTRIBUTION
n/n max
1.0
0.75
0.5
0.25
0
Radar 1.16
(n max = 645)
Radar 3.16
(n max = 205)
Radar 5.16
(n max = 1175)
95% of distribution
Δσ (db/m²)
-7
-6
-5
-4
-3
-2
-1
0
+1
+2
+3
+4
+5
+6
+7

Figure 13

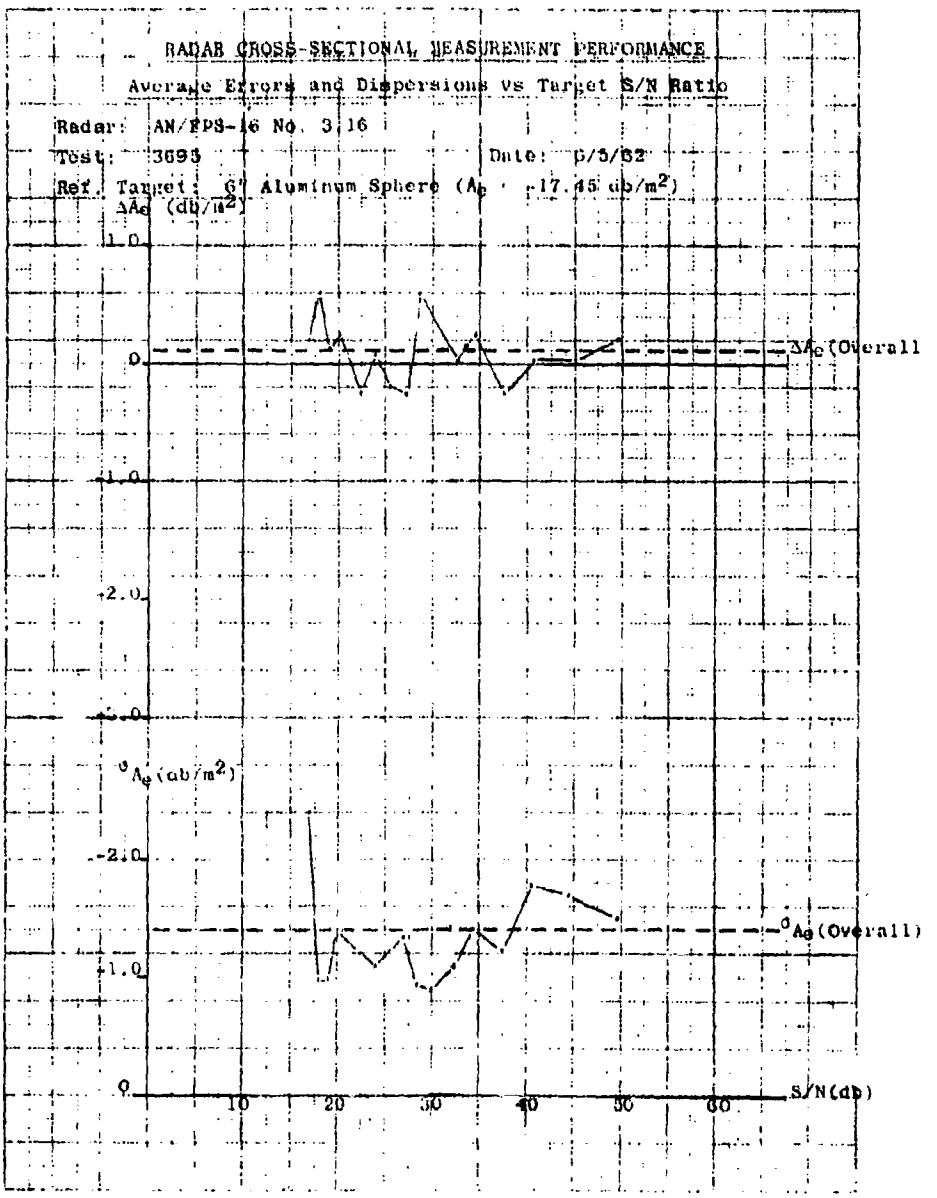
RADAR CROSS-SECTIONAL MEASUREMENT PERFORMANCE
Average Errors and Dispersions vs Target S/N Ratio
Radar: AN/FPS-16 No. 3,16
Test: 3693
Date: 5/5/62
Ref. Target: 6' Aluminum Sphere (A_e = +17.45 db/m²)
ΔA_e (db/m²)
1.0
0
-1.0
-2.0
ΔA_e (Overall
σA_e (db/m²)
-2.0
+1.0
0
σA_e (Overall)
10
20
30
40
50
60
S/N(db)

Figure 14

Analog A/C Recording and Video Film of Splash 2

Radar: No.10.16 Test No.272L/62

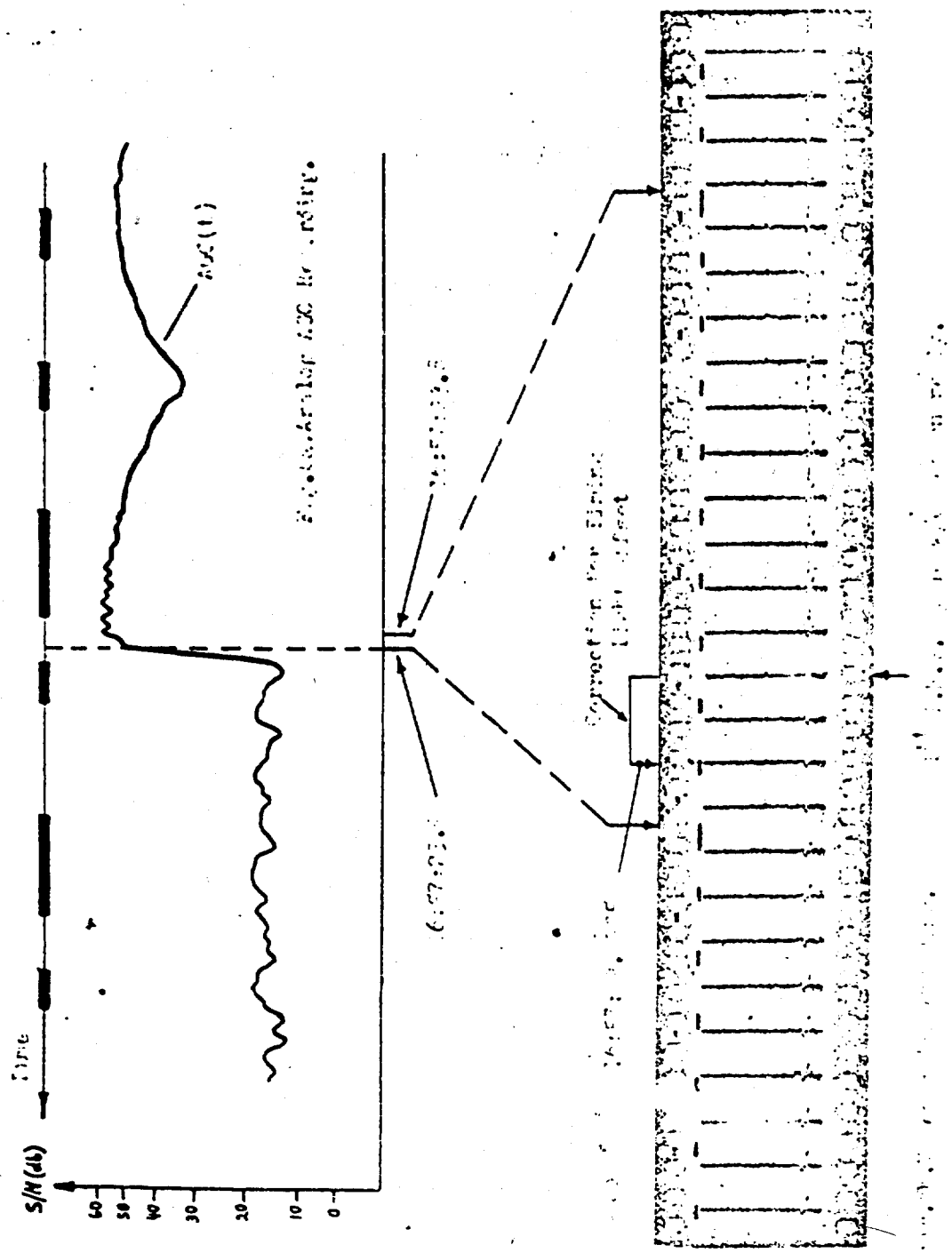

Radar 13.1C TARIF/MILS Impact Location

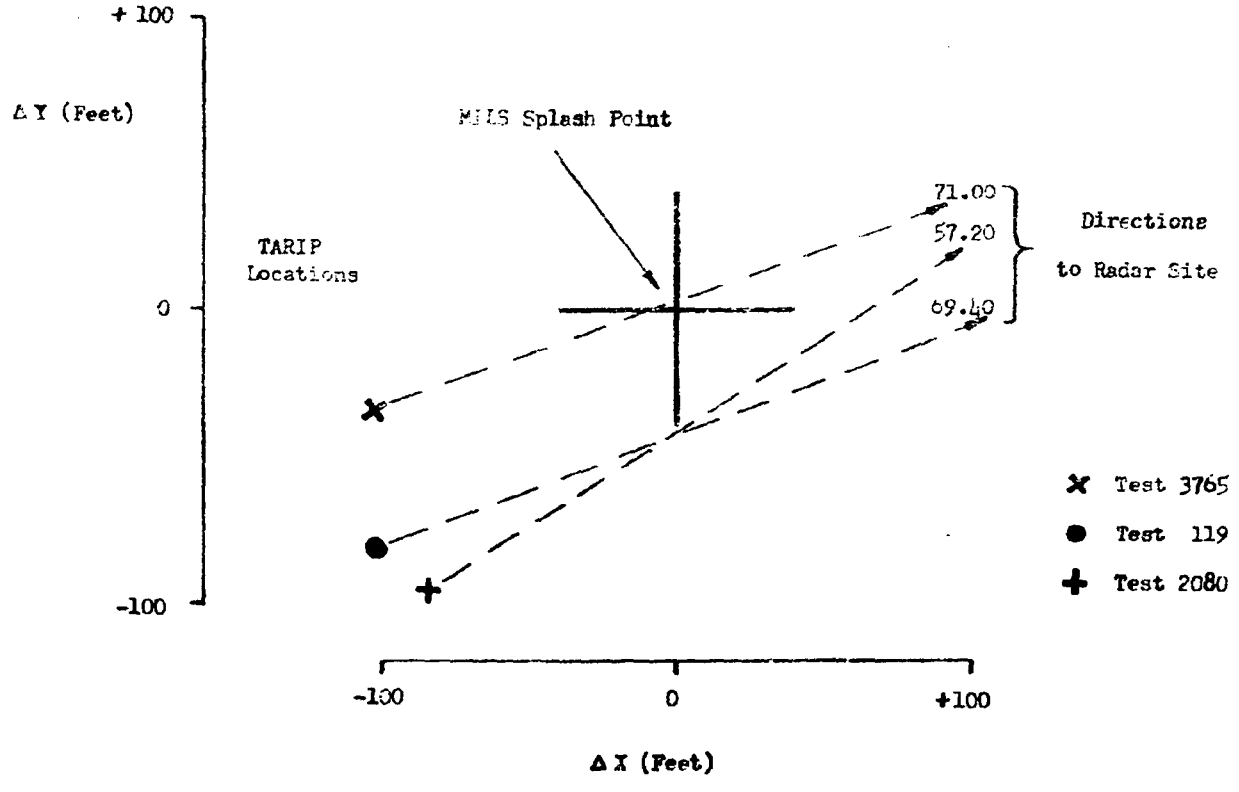

Figure 15

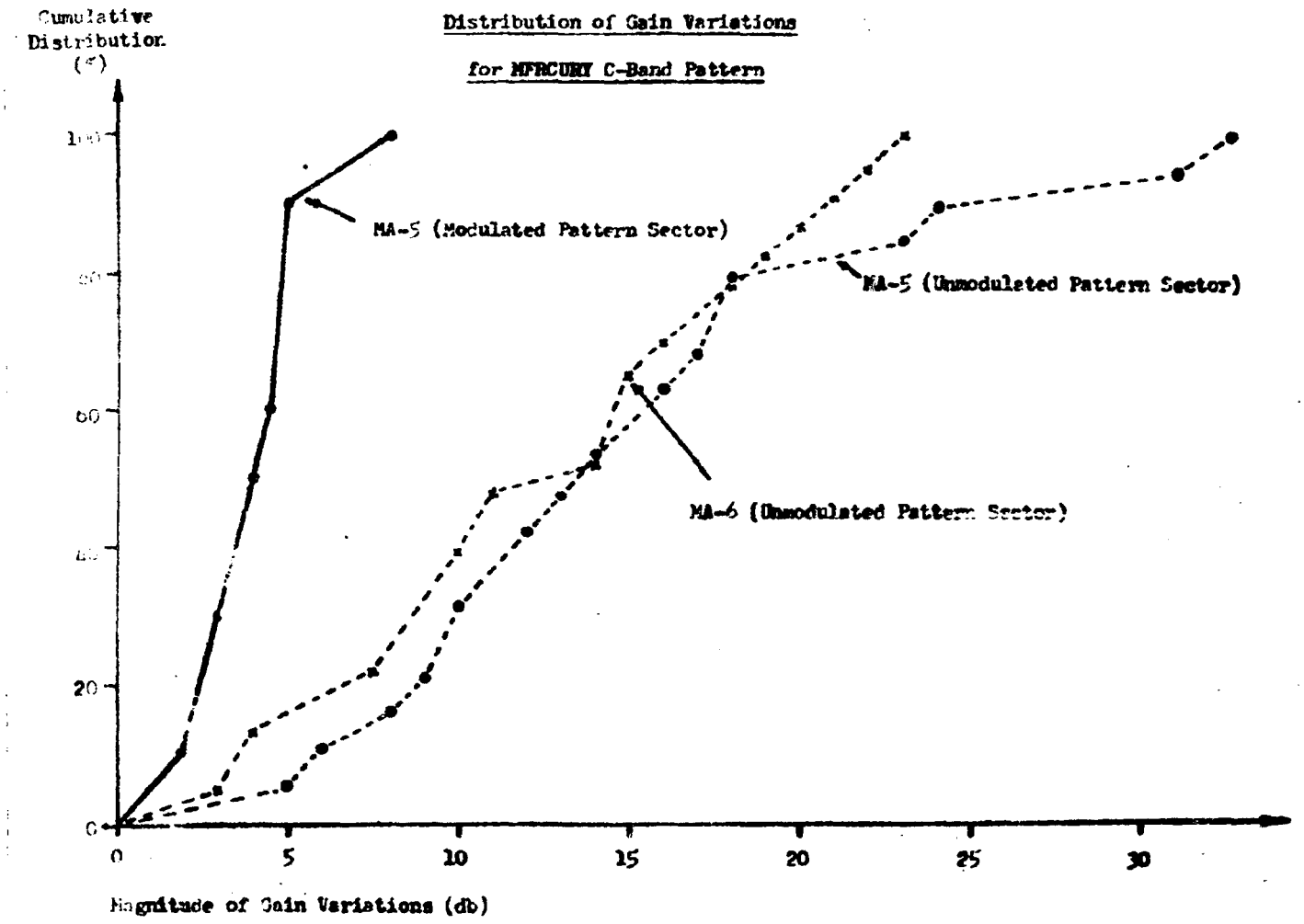
Distribution of Gain Variations
for MERCURY C-Band Pattern
Cumulative Distribution (%)
MA-5 (Modulated Pattern Sector)
MA-5 (Unmodulated Pattern Sector)
MA-6 (Unmodulated Pattern Sector)
60
20
0
0
5
10
15
20
25
30
Magnitude of Gain Variations (db)

Figure 16

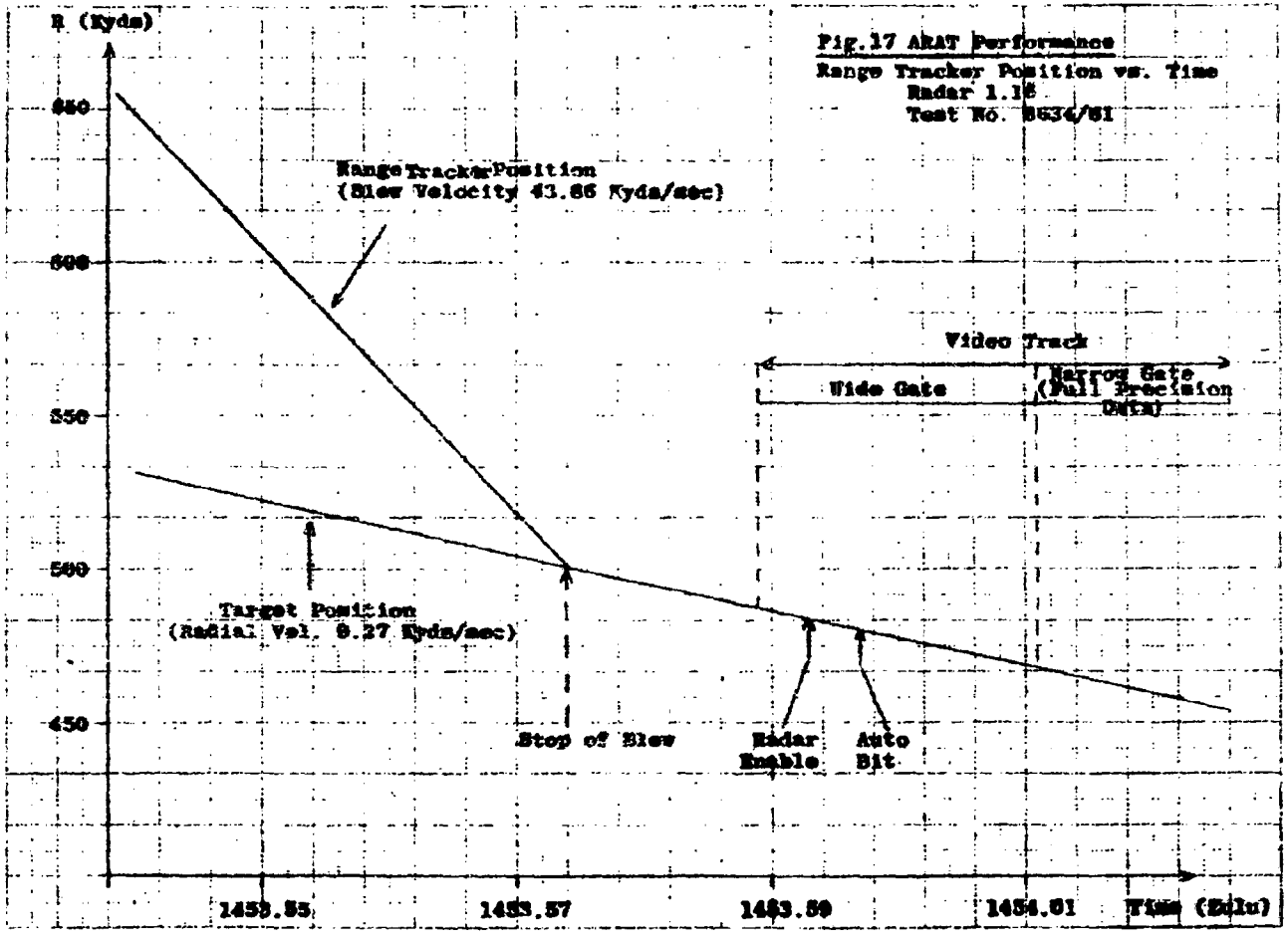

Pig.17 ARAT Performance
Range Tracker Position vs. Time
Radar 1.1E
Test No. 8534/81

Figure 17

Probability of AN/FPS-16 Range Acquisition

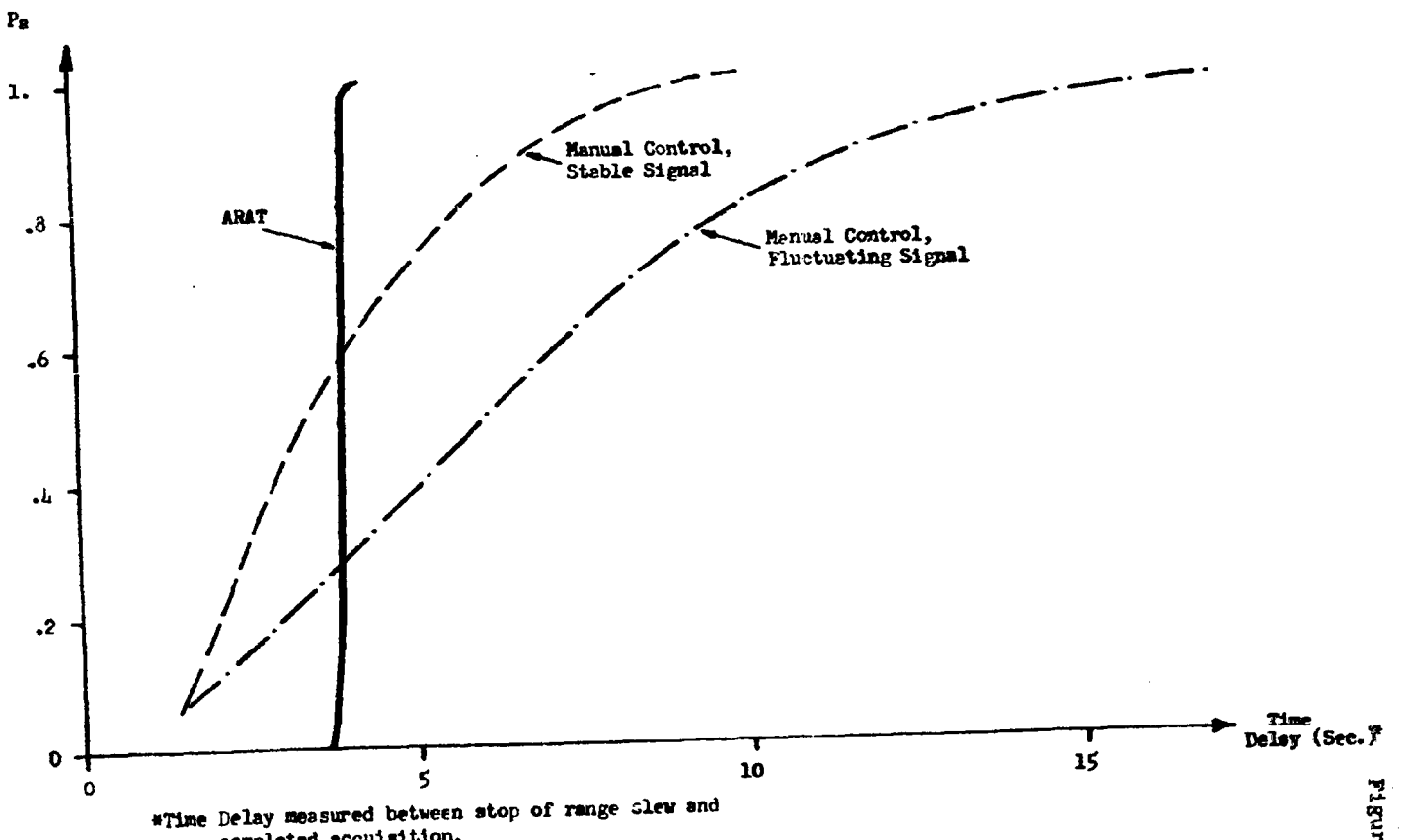

*Time Delay measured between stop of range slew and completed acquisition.

Figure

809 I

THE CYCLIC ERROR AS AN ATMOSPHERIC REFRACTION PHENOMENON

by:
W. A. Dryden and O. J. W. Christ
RCA-Missile Test Project
PAFB, Florida

Presented at:
FOURTH JOINT AFMTC RANGE USER DATA CONFERENCE
Orlando Air Force Base, Florida
26-28 February 1963

THE CYCLIC ERROR AS AN ATMOSPHERIC REFRACTION PHENOMENON

Abstract

Examples of the cyclic error in missile free-fall data collected by AZUSA MK II are discussed. A suggestion that anomalous atmospheric refraction is the source of this error is offered. In support of this suggestion two possible causes are presented: (1) Turbulent mixing of the lower atmosphere can lead to differential refraction effects in a phase comparison tracking system and can lead to temporal changes in the zero-set of the instrument. (2) A wave-like perturbation on the interface between two different-density layers of the atmosphere can lead to apparent cyclic deviations of a missile from a ballistic orbit.

The effects of time variability of the index of refraction on the zero-set of AZUSA MK II is analyzed. It is shown that spurious phase differences are introduced into the data that are linearly proportional to the variability of the index of refraction along the path between the instrument and the target pole. A paucity of evidence of the turbulent nature of the atmosphere, at the particular frequencies of concern, precludes one from making any comparisons between the periods and amplitudes of the turbulence and those of the data.

A much simplified model of a sinusoidal wave on the interface of a two-layer atmosphere is also discussed with regard to its effect on a phase comparison tracking system. It is shown that such a model can lead to quasi-periodic oscillations in the data collected by the instrument. The periods and amplitudes of the noise generated by such a model are in general agreement with what is observed.

1. INTRODUCTION

For practical purposes, after the thrust of a ballistic missile is terminated, the missile will travel in an elliptical orbit which intersects the surface of the earth at some point down range. The routine evaluation of the AZUSA tracking system includes fitting post-burn-out data to an ellipse* and differencing the individual data points and this computed Keplerian ellipse.

---

*Strictly speaking, since there are perturbing effects, the orbit is not exactly an ellipse. A power series solution to the equations of motion is assumed, and the coefficients of the series (which is truncated at the fourth power) are determined by a least-squares fit of the data.

Among the deviations from the ellipse that have been noted is a deviation or noise which appears to be cyclic in nature. Periods of this cyclic noise are on the order of seconds. The periods are obtained by a power spectrum analysis of the Keplerian differences.

The amplitude of the noise is not constant, but rather varies from day to day. It has been noted that on the days when the noise is most pronounced we find several associated facts: In the first place, during the zero-set procedure, while AZUSA is looking at a target pole, the apparent motion of the target pole is not zero. In addition, on the days when the noise level is high the pre-flight calibration, or zero-set, differs considerably from the post-flight zero-set. It has been noted in a very subjective manner that the days on which high noise levels are observed the weather in the vicinity of the launch site is of a particular type; whereas, on days when the noise level is low the weather situation is considerably different.

A great many hypotheses have been advanced to explain the cyclic deviations from the Keplerian ellipse during missile free-fall. For one reason or another, most of the hypotheses have been abandoned. It appears at the present time that the data error has its source in the atmosphere. Today we shall look into this matter from the standpoint of possible atmospheric effects. In particular, we shall consider two possible hypotheses and in a very cursory manner attempt to show that these hypotheses can explain at least a part of the low-frequency or cyclic noise. Until recently, lack of adequate instrumentation has prevented us from attempting a rigorous test of the hypotheses. The necessary instrumentation is now available, and we are in the process of collecting the necessary data.

There are at least two ways in which the atmosphere can affect a tracking system such as AZUSA. Firstly, the level of turbulence, that is the mixing of the air, can distribute water vapor in such a fashion as to create anomalous refraction zones in which the signal arriving at one antenna is affected in a different manner from a signal arriving at another antenna. Secondly, we shall consider the possibility of perturbations on a density interface in the lower atmosphere.

2. EXAMPLES OF THE PROBLEM

Figure 1 is a graph showing the Keplerian differences of the direction cosines ℓ and m and the range R as functions of time for Range Test 101. The procedure used to construct this graph is as follows: The data taken after final burn-out, that is after all engines have shut down, are fitted by least squares to a truncated power series solution to the equations of motion. Once this orbit has been constructed each individual data point is then differenced from the orbit and these differences are plotted in Figure 1. Several features of the graph can be noted, and these will be discussed as time proceeds. The first feature to be noticed is

that the curves shown in this figure are not horizontal, straight lines as would be the case if all the data points fit the orbit perfectly. There is a certain amount of jitter noticeable and in particular we should notice the cyclic oscillation present in the data. It is this phenomenon about which we shall speak today.

Figure 1 also includes a graph of the power spectrum of the direction cosine difference $\Delta\ell$ for Test 101. The abscissa is frequency in cycles per second and the ordinate is the relative power contained at each frequency. It should be noted that, in general, there is a very high DC component of the power, and that there is a gradual decrease as frequency increases. It should also be noted, however, that there are several slope discontinuities present in the spectrum. In particular, one should notice the slope discontinuity located at a frequency of about 10^{-1} cycles per second - a frequency corresponding to a period of ten seconds. This is a result of the contributions of the cyclic oscillation which we noticed in the Keplerian differences.

Figure 2 shows the Keplerian differences plotted as functions of time for Test 101. We notice in this figure the same general features which were noticed in the previous figure. The power spectrum shows a very high DC component with a gradual drop-off with increasing frequency. Again we notice certain anomalies present in the power spectrum of the data, in particular, in the vicinity of 10^{-1} cycles per second. Our problem now is to try to explain this phenomenon. What are these oscillations present in the data? How can we get rid of them?

3. TURBULENT TIME VARIABILITY OF THE INDEX OF REFRACTION

Phase comparison tracking systems such as AZUSA are based on the fact that there will be a discrete time difference between the receipt of the signal at one point and the receipt of the same signal at some other point. Owing to the large propagation speed of electromagnetic energy, it is more convenient to measure phase differences from which the time differences can be obtained. In any event, the distance between the points can be determined from the time differences, provided the speed of propagation is known.

The speed of propagation of the electromagnetic energy is a function of the index of refraction along the ray path. In a phase comparison tracking system the energy effectively travels along different paths from the transponder in the target to the individual receiving antennas on the ground. As long as there are no horizontal inhomogeneities in the refractive index, the propagation speed along each ray path will be the same, level for level. The result will be a time-varying bending effect that can be compensated for reasonably well by ray-path reduction.

If, on the other hand, the refractive index is not homogeneous in the horizontal, the propagation speeds will be different

that the curves shown in this figure are not horizontal, straight lines as would be the case if all the data points fit the orbit perfectly. There is a certain amount of jitter noticeable and in particular we should notice the cyclic oscillation present in the data. It is this phenomenon about which we shall speak today.

Figure 1 also includes a graph of the power spectrum of the direction cosine difference $\Delta\ell$ for Test 101. The abscissa is frequency in cycles per second and the ordinate is the relative power contained at each frequency. It should be noted that, in general, there is a very high DC component of the power, and that there is a gradual decrease as frequency increases. It should also be noted, however, that there are several slope discontinuities present in the spectrum. In particular, one should notice the slope discontinuity located at a frequency of about 10^{-1} cycles per second - a frequency corresponding to a period of ten seconds. This is a result of the contributions of the cyclic oscillation which we noticed in the Keplerian differences.

Figure 2 shows the Keplerian differences plotted as functions of time for Test 1[illegible]. We notice in this figure the same general features which were noticed in the previous figure. The power spectrum shows a very high DC component with a gradual drop-off with increasing frequency. Again we notice certain anomalies present in the power spectrum of the data, in particular, in the vicinity of 10^{-1} cycles per second. Our problem now is to try to explain this phenomenon. Why are these oscillations present in the data? How can we get rid of them?

3. TURBULENT TIME VARIABILITY OF THE INDEX OF REFRACTION

Phase comparison tracking systems such as AZUSA are based on the fact that there will be a discrete time difference between the receipt of the signal at one point and the receipt of the same signal at a more distant point. Owing to the large propagation speed of electromagnetic energy, it is more convenient to measure phase differences from which the time differences can be obtained. In any event, the distance between two points can be determined from the time difference, provided the speed of propagation is known.

The speed of propagation of the electromagnetic energy is a function of the index of refraction along the ray path. In a phase comparison tracking system the energy effectively travels along different paths from the transponder in the target to the individual receiving antennas on the ground. As long as there are no horizontal inhomogeneities in the refractive index, the propagation speed along each ray path will be the same, level for level. The result will be a bias-creating bending effect that can be compensated for reasonably well in the data reduction.

If, on the other hand, the refractive index is not homogeneous in the horizontal, the propagation speeds will be different

for each ray path. One signal will, for example, be retarded more than the other signal. This anomalous refractive effect will appear as a spurious phase difference in the tracking equipment and will lead to an erroneous position determination. Moreover, if the differential refraction of the two signals changes with time, any target velocity measurements or calculations, will be deleteriously affected.

It is a matter of common knowledge that the atmosphere is not horizontally stratified with regard to index of refraction so that anomalous propagation effects are to be expected. The turbulent mixing and movements of high refractive index air in the tracking environment should and do introduce noise into missile trajectory data.

Unfortunately, it is a physical impossibility to be able to monitor the time changes of index of refraction throughout the entire region of space to be traversed by the radio signals. We can, however, measure the index of refraction and its time variability at a point or a series of points on the ground. If we then make some assumptions about the spatial variation of the index, it becomes possible to say a little bit about the effects of the turbulent mixing of the atmosphere on the tracking system data.

At the present time the AZUSA zero-set is corrected by using an index of refraction obtained by conventional metecrological means. Since the zero-set is corrected only at the beginning of a test, any changes in local index during the test will result in errors in data recorded during the test.

Recently a recording refractometer has been installed at the AZUSA site, making it possible to check the variations in index of refraction during tests. Of the recordings made during several recent tests it was noted qualitatively that the differences between pre- and post-calibrations of the direction cosines ℓ and m and the range R on the various target poles were correlated with the variability of the refractometer recordings. Figure 3 shows two examples: In Test 82, the refractometer recording is relatively smooth and the differences between pre- and post-calibrations are small. In Test 2883 the refractometer recording is quite variable and the differences between pre- and post-calibration are, in general, large.

The principle on which AZUSA is based is shown schematically in Figure 4. The phase angle between two signals is given by

$$\phi = \frac{2\pi n}{\lambda} D \quad , \qquad (1)$$

where n is the average index of refraction along the ray path, λ is the wave length of the signal in a vacuum, and D is the geometric path length difference.

The phase angle between the reference signal from the oscillator and the received signal from the target transponder is contained in the signal out of each of the mixers. We may thus express the phase angle out of each mixer respectively as

$$\Phi_1 = \frac{2\pi n_1 s_1}{\lambda} \tag{2}$$

and

$$\Phi_2 = \frac{2\pi n_2 s_2}{\lambda}, \tag{3}$$

where s_1 and s_2 are the distances between the target and each antenna. Let $2\pi/\lambda = K$, then

$$\Phi_1 = Kn_1 s_1 \tag{4}$$

$$\Phi_2 = Kn_2 s_2. \tag{5}$$

If we assume that the signal from the reference oscillator introduces no additional phase difference, then the difference between Φ_1 and Φ_2 out of the phase detector expresses the phase difference between the signal traveling path s_1 and that traveling path s_2; thus differencing (4) and (5) yields

$$\Phi_1 - \Phi_2 = \delta\Phi = K(n_1 s_1 - n_2 s_2). \tag{6}$$

Let us consider two cases: Case I where $n_1 = n_2$ and Case II where $n_1 \neq n_2$.

Case I: $n_1 = n_2 = n$.

Equation (6) may now be written as

$$\delta\Phi = Kn\,(s_1 - s_2) = KnD. \tag{7}$$

Since K and D are invariant, the error in $\delta\Phi$ is a function of the error in n:

$$\delta\Phi + \Delta\Phi = KnD + KD\Delta n \tag{8}$$

$$\Delta\Phi = KD\Delta n. \tag{9}$$

Equation (9) shows the relationship between the error in the phase difference (consequently the direction cosine) and the error in determining the index of refraction.

It is immediately apparent that $\Delta\Phi$ decreases if D is decreased. In fact, if D is made equal to zero, no error in the phase difference will occur regardless of the error in index of refraction.

Case II: $n_1 \neq n_2$.

Let $n_2 = n_1 + \delta n$. Equation (6) may now be written as

$$\delta\Phi = K\left[n_1 s_1 - s_2(n_1 + \delta n)\right]. \tag{10}$$

Simplification yields

$$\delta\Phi = K(n_1 D - s_2 \delta n). \tag{11}$$

Since, in the reduction of the AZUSA data, δn is assumed to be zero, the difference between equations (7) and (11) represents an error of $-Ks_2\delta n$. If we now consider an error in the determination of n_1, (11) can be expressed as

$$\delta\Phi + \Delta\Phi = Kn_1 D + K\Delta n_1 D - Ks_2\delta n; \tag{12}$$

whence,

$$\Delta\Phi = K(\Delta n_1 D - s_2\delta n), \tag{13}$$

where Δn_1 is the error in determining the mean index of refraction, and δn is the difference between the true indices of refraction along the two ray paths.

The first error term in (13) can be reduced by letting D approach 0. For a stationary target the second error term will average to zero over a reasonable time period if δn behaves in a random fashion.

Consider the time changes in the index as being caused by a spatial distribution of index passing across the observation point. It can be seen that, in all probability, the δn in (13) does not behave in a random fashion. As a matter of fact, evidence gathered by the National Bureau of Standards and others tends to indicate that it does not. Power spectra of turbulent wind data and turbulent index of refraction data show marked peaks at various frequencies in the spectrum. Unfortunately, little if any data are available in the region of interest to us; that is, in the region of about 10^{-1} cycles per second. The National Bureau of Standards is undertaking a contract to study this problem along with the

problem of variable baseline length and will concentrate their efforts in the region of about 10^{-1} cycles per second.

4. PERTURBATION HYPOTHESIS

For many years vertical soundings of the atmosphere over the AMR, both by rawinsondes and by airborne refractometers, have revealed the persistent existence of a virtual discontinuity in the vertical distribution of index of refraction. Through the lowest layers of the atmosphere the index decreases moderately with increasing altitude as is to be expected. At an altitude of about 3000 to 5000 feet, however, there appears a sharp decrease in index of some 30 to 50 parts per million through a relatively shallow layer of perhaps 100 to 300 feet. Above this point the index again exhibits a moderate decrease with altitude. A typical profile of refractive index for Cape Canaveral is shown in Figure 5. The ordinate is altitude in thousands of feet and the abscissa is the refractivity N which is related to the index of refraction n by

$$N = 10^6 (n-1) = \frac{A}{T}\left(p + \frac{Be}{T}\right), \qquad (14)$$

where T is the absolute temperature in degrees Kelvin, p is the atmospheric pressure in millibars, e is the vapor pressure in millibars, and A = 77.6 deg per millibar and B = 4810 deg are empirically determined constants.

The AMR, along with other sub-tropical regions, lies in an area which is characterized by a large scale subsidence of air aloft. As this upper air descends it is warmed dry adiabatically giving a layer of quite warm and quite dry air somewhere around 3000 feet. Since the refractivity is inversely proportional to temperature, and directly proportional to moisture content, this subsidence inversion results in the observed refractivity profile. The marked plateau in the vertical distribution of N observable in Figure 5, between the altitudes of 3000 and 3500 feet, is a manifestation of this subsidence inversion.

If one considers three dimensions, he finds that this inversion exists over a large portion of the sub-tropics. In reality then, one can consider the lower tropical troposphere as being composed of two layers of air: the lower one is characterized by relatively cool, moist (hence high refractive index) air surmounted by warm, dry (hence low refractive index) air extending upward. The interface separating these two layers is quite sharp, approaching a zero order discontinuity in density (or index of refraction).

Students of hydrodynamics will attest to the fact that such a situation will result in undulations on this interface very much like the undulations which are felt on the interface between the atmosphere and the ocean. In other words, it is not surprising that one finds wave motions on the atmospheric duct.

If one considers a phase comparison tracking system looking through such an atmosphere and slewing downward as the ballistic target travels down range he should anticipate that the pairs of ray paths will be differentially affected by the atmospheric wave phenomenon. As one ray is passing through a wave crest the other ray may be passing through a trough. At that time the former ray will travel through more of the high-index air. At a later time the reverse will be true. The question which is raised is: "Can such a physical model explain the quantitative properties of the observed data noise; i.e., period and amplitude?"

In a preliminary attempt to answer this question let us suppose the following:

Suppose the target remains in the vertical plane containing one of the baselines of the tracking system. Such an assumption does not compromise the analysis, it merely offers simplicity. Let the baseline length be b, and the angle $E = \cos^{-1}\ell$, where ℓ is the direction cosine relative to the baseline under consideration. In this simple, co-planar model E is also the elevation angle. The radio ranges to the target are being determined simultaneously from antennas A and B (Figure 6.) Assume the rays to be parallel. Also, for the purposes of the present discussion, neglect the bending which would normally take place at the interface.

Within the atmosphere, postulate the existence of a surface of discontinuity in refractive index. Further postulate that the shape of the surface can be simply described as an infinitely long, stationary, sinusoidal wave. In particular, let the altitude of the surface above its equilibrium altitude be given by

$$\zeta(x) = a \cos \frac{2\pi}{L} (x + \epsilon), \tag{15}$$

where a is the amplitude, L is the wave length and ϵ is a displacement between the first uprange crest of the wave and the antenna.

The total radio ranges to the target from each of the antennas can be written

$$R_A = \int_0^{R_1} n_I ds + \int_{R_1}^{R_2} n_{II} ds + \int_{R_2}^{R^*} n_{II} ds + \int_{R^*}^{R^* + \Delta R} n_{II} ds \tag{16}$$

and

$$R_B = \int_0^{R_1} n_I ds + \int_{R_1}^{R_2} n_I ds + \int_{R_2}^{R^*} n_{II} ds, \tag{17}$$

where n_I and n_{II} are the indices of refraction below and above the discontinuity, respectively, ds is an increment of length along the ray path; R_1 R_2 and R^* are explained in Figure 6; and ΔR is the true range difference. (Normally ΔR is taken at the bottom of the atmosphere; but for simplicity it is taken here in the vicinity of the target.)

If the assumption is made that the atmosphere is horizontally homogeneous within each layer separately, the radio range difference from the two antennas is

$$R_A - R_B = \int_{R_1}^{R_2} (n_{II} - n_I)ds + \int_{R^*}^{R^* + \Delta R} n_{II}ds, \tag{18}$$

in which the second integral represents the desired or noise-free range difference. The first integral in (18) is the term which introduces noise into the data, and it might be called the anomalous refraction error and denoted by δR.

Assuming

$$n_{II}(s) - n_I(s) = \Delta n = \text{constant}, \tag{19}$$

one finds that

$$\delta R = \Delta n(R_2 - R_1). \tag{20}$$

For the purposes of the present analysis one does not make a significant error if he makes a flat earth assumption:

$$R = z \csc E, \tag{21}$$

where z is the altitude of the wave surface above the horizontal plane containing the base line. In (21) we have neglected the bending at the interface. If the equilibrium altitude of the wave above the base line plane is denoted by Z, one obtains

$$R = \left[Z + a \cos \frac{2\pi}{L} (x + \epsilon)\right] \csc E \tag{22}$$

for each intersection; whence,

$$R_2 - R_1 = a \csc E \left[\cos \frac{2\pi}{L}(x_2 + \epsilon_2) - \cos \frac{2\pi}{L}(x_1 + \epsilon_1)\right] \tag{23}$$

Consider the trigonometric identity

$$\cos u - \cos v \equiv -2 \sin \tfrac{1}{2}(u + v) \sin \tfrac{1}{2}(u - v). \qquad (24)$$

Applying this identity to the brackets of (22), one gets

$$\cos \frac{2\pi}{L} (x_2 + \epsilon_2) - \cos \frac{2\pi}{L}(x_1 + \epsilon_1) =$$

$$-2 \sin \frac{\pi}{L} (x_2 + x_1 + \epsilon_2 + \epsilon_1) \cdot \sin \frac{\pi}{L} (x_2 - x_1 + \epsilon_2 - \epsilon_1). \qquad (25)$$

Let $x_2 + x_1 = 2\bar{x}$, and $\epsilon_2 + \epsilon_1 = 2\bar{\epsilon}$, where the bar denotes an arithemetic average. From Figure 6 one can see that $\epsilon_2 - \epsilon_1 = b$. Now $x_2 - x_1$ will be variable between the limits

$$b/2 \leq x_2 - x_1 \leq b. \qquad (26)$$

with an average value of $3b/4$. As a result

$$x_2 - x_1 + \epsilon_2 - \epsilon_1 = 7b/4 \approx 2b \qquad (27)$$

Furthermore, from Figure 6 one can see that

$$\bar{x} = Z \cot E. \qquad (28)$$

Using (23), (25), (27), and (28), one can write (20) as

$$\delta R = -2a\Delta n \sin(\frac{2\pi b}{L})\csc E \sin \frac{2\pi}{L}(Z\cot E + \bar{\epsilon}), \qquad (29)$$

of, if b is small compared to L,

$$\delta R = - \frac{4\pi a b \Delta n}{L} \csc E \cdot \sin \frac{2\pi}{L}(Z\cot E + \bar{\epsilon}). \qquad (30)$$

Equation (30) describes the anomalous refraction noise as being periodic in E as indicated by the sine term, with an amplitude which is a function of the cosecant of E among other things. If the tracking system is slewing downward such that E is a simple function of time, (30), can be thought of as being a cyclic function of time.

Strictly speaking, (30) is valid only for

$$E \geq \tan^{-1}(\frac{2\pi a}{L}), \qquad (31)$$

since at smaller angles the rays can begin to cut through the tops of the waves. The result of this is a decrease in amplitude of the noise and an additional cyclic term modulating the data.

Since for the AZUSA System, at least, the direction cosine is the range difference divided by the base line, the noise in ℓ is

$$\delta\ell = -\frac{4\pi a\Delta n}{L} \csc E \cdot \sin\frac{2\pi}{L}(Z\cot E + \bar{\epsilon}). \qquad (32)$$

Figure 7 is a graph of (32) in which $\delta\ell$ is plotted as a function of E. For the purposes of the calculations the results of refractometer flights made by an AFCRL aircraft were used. The values of the various parameters are listed in Table I.

TABLE I. Value of Quantities in Equation (31) Used to Plot Figure 7.

Parameter	Numerical Value
a (wave amplitude)	100 ft.
Δn (refractive index difference)	3×10^{-5}
L (wavelength)	6000 ft.
Z (altitude of wave)	3000 ft.
ϵ (phase of wave)	0 ft.

It should be noted from Figure 7 that $\delta\ell$ is very definitely cyclic. Further, it should be noted that the amplitude of $\delta\ell$ increases with decreasing E as a result of the cosecant term, and that the period decreases because of the cotangent term. The root-mean-square amplitude for the span $15 \geq E \geq 6$ degrees was computed to be 26.8 ppm. Of course, owing to the term cosecant E the rms amplitude will depend on the span of data used.

To get a feel for the period as a function of time, elevation angles from a live test were used in an additional computation of (32). Most of the angles were below the angle noted in (31) so that a critical evaluation is not justified; however, since only gross results were being sought, it was not felt that this fact would be of great importance. The small angles would introduce additional periodicities.

Computed values of $\delta\ell$ in ppm are also plotted versus time in Figure 7. The time span chosen was one in which the target was presumably in free-fall. The RMS $\delta\ell$ was calculated to be 32.3 ppm for this time span. In Figure 8 we see the Keplerian data of Test 5460 for which the previous analysis was done. The cyclic noise is evident in the graph of $\Delta\ell$ and the power spectrum.

5. CONCLUDING REMARKS

It is of interest to note that Greene (1962) independently performed a regression analysis of 32 missile tests in an attempt to determine what parameters were important in the Keplerian-difference noise. He found that, of the five quantities studied, the amount of low clouds, the cosecant of the elevation angle, and the span length of free-fall data used in the Keplerian calculations were significant. The two quantities which [illegible] as

insignificant were signal strength and surface index of refraction. In Figure 9 we see the regression equation used by Greene and the coefficients computed from the data used by him. In addition, we see also the variance analysis and the correlation matrix.

The importance of cosecant E and span length have already been mentioned with regard to the present analysis. It should also be mentioned that the wave phenomenon considered here is intimately related with low cloud occurrence in the sub-tropical atmosphere. In addition we should also note, with interest, that the surface index of refraction appeared insignificant. This should not be surprising, since a single observation of the surface index has no relationship to the noise. As was pointed out in Section 3, the time variation of the surface index is what is significant.

Presently the necessary instrumentation to measure the atmospheric parameters in (32) is being installed in aircraft. It is intended in the very near future that simultaneous tracking and atmospheric data be collected and utilized in a more rigorous test of the hypothesis.

Since both of the preceding hypotheses show promise of at least a partial solution to the cyclic noise problem, it is strongly urged that additional analysis and experiment be undertaken. On-range analysis should continue, and off-range experiment and analysis should be strongly supported by AFSC through research and through contractual arrangements.

A step in the right direction has been taken by AFSC, through the Electronic Systems Division, in the support of two parallel approaches to a solution to the problem. The National Bureau of Standards will investigate the turbulence hypothesis discussed earlier, while the Geophysics Research Directorate will study the perturbation hypothesis for both clear-air and cloudy atmospheres.

REFERENCES

Cunningham, R. M., 1962: The effects of horizontal refractive index variations on interferometer missile guidance systems. Paper presented to the Fourth Conference on Applied Meteorology, Hampton, Va., 17 September.

Christ, O. J. W., 1962: An analysis of the effects of index of refraction error and target pole location on the zero-setting of the MARK II AZUSA. RCA Systems Analysis Technical Note No. 14, 16 August.

Dryden, W. A., 1962: A possible explanation for the cyclic error in AZUSA free-fall data. RCA Mathematical Services TM-62-10, August.

Greene, J., 1962: Preliminary results of study to predict the within-in test error (cyclic plus random) from AZUSA MK II. RCA Systems Evaluation memorandum for the record (unpublished).

National Bureau of Standards, 1958: An experimental study of phase variations in line-of-sight microwave transmissions. NBS Report 6CB105, 26 August.

Relf, K. E., 1961: Fifteen day report, AZUSA MK II, Tests 5104 and 5105, 3 March.

Space Technology Laboratories, Inc., 1958: Tropospheric scintillations, STL Report GM-TM-0165-00308.

Strand, J. N., 1962: Lateral-rate noise caused by atmospheric humidity layers (theoretical approach). GE Systems Programming and Evaluation Engineering SE-EM-16, 9 February.

Swanson, S. E., 1962: Effects of rapid variations in local index of refraction on the zero-set accuracy of the AZUSA MK II system. RCA Systems Evaluation memorandum for the record (unpublished), 6 September.

Effects of Refraction on Azusa Calibration

T-82

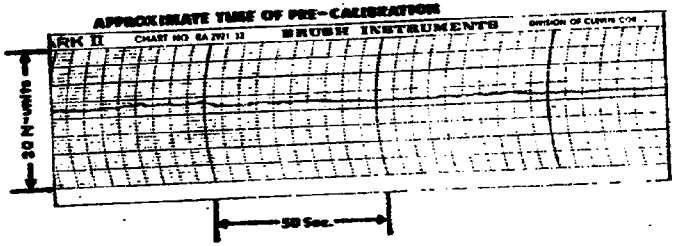

Target	L (ppm)	M(ppm)	R(ft)
CIP-1	0	2	12
CIP-2	0	5	4
CIP-3	2	0	5
KFP	20	2	10
RT	0	2	5
RWG	0	2	5

$\Delta t \approx 1.5$ hr

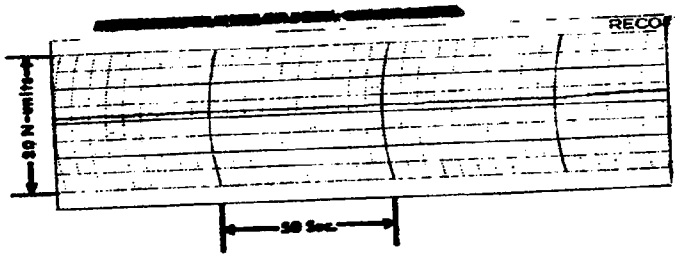

T-2883

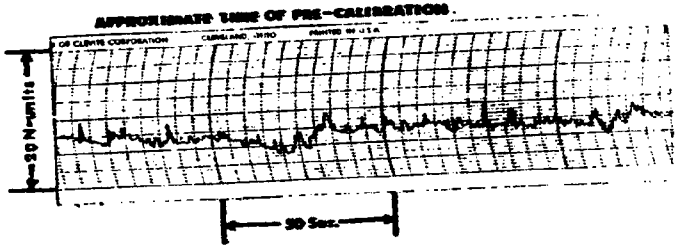

Target	L(ppm)	M(ppm)	R(ft)
CIP-1	22	6	0
CIP-2	32	21	1
CIP-3	40	6	2
KFP	43	5	1
RT	37	2	2
RWG	1	2	1

$\Delta t \approx 2.3$ hr

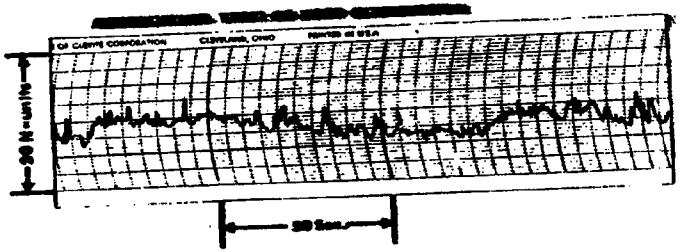

Effects of Refraction on Azusa Calibration

T-82

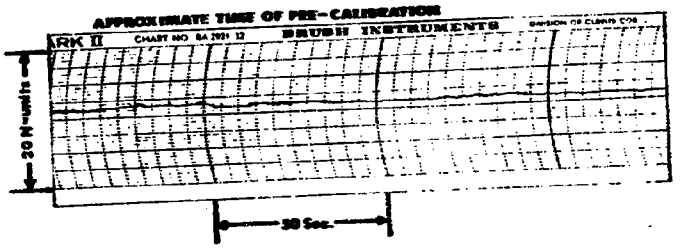

Target	L (ppm)	M(ppm)	R(ft)
CIP-1	0	2	12
CIP-2	0	5	4
CIP-3	2	0	5
KFP	20	2	10
RT	0	2	5
RWG	0	2	5

$\Delta t \approx 1.5$ hr

T-2883

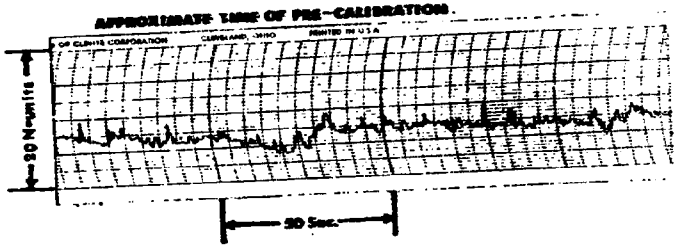

Target	L(ppm)	M(ppm)	R(ft)
CIP-1	22	6	0
CIP-2	52	21	1
CIP-3	40	6	2
KFP	43	5	1
RT	37	2	2
RWG	1	2	1

$\Delta t \approx 2.3$ hr

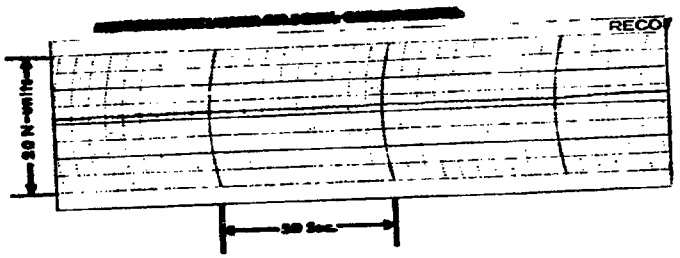

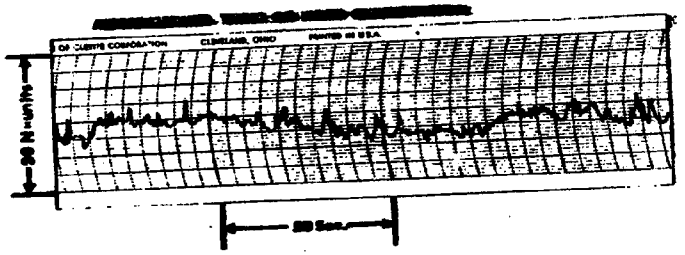

Keplerian Differences

TEST-125

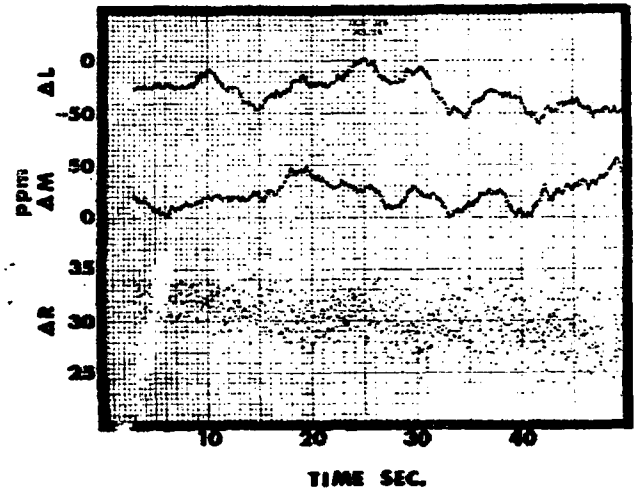

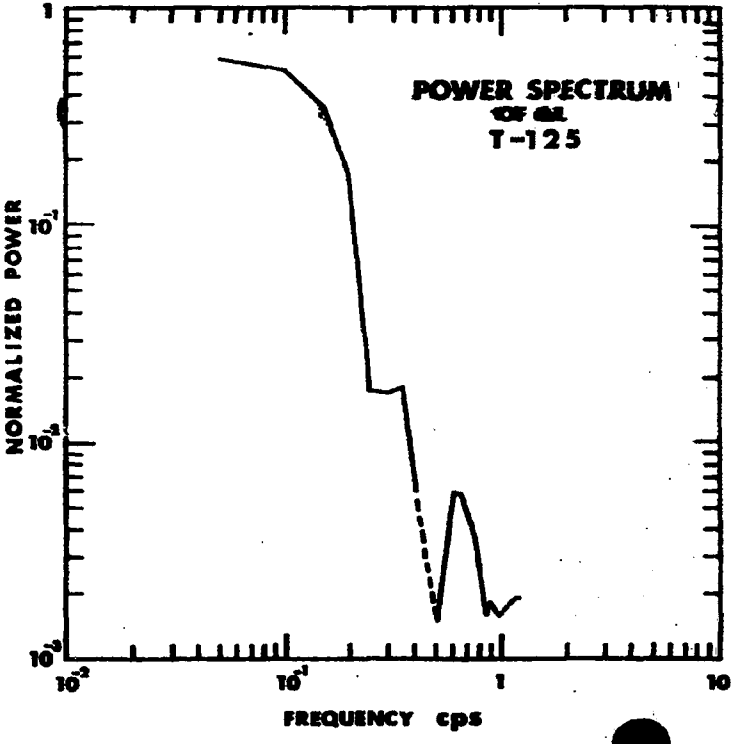

Keplerian Differences

TEST 101

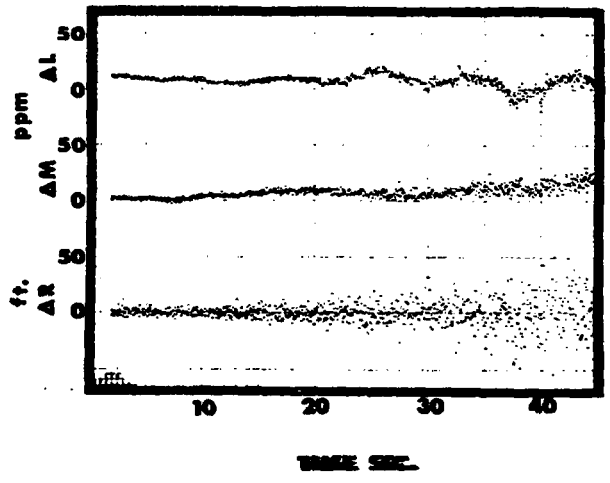

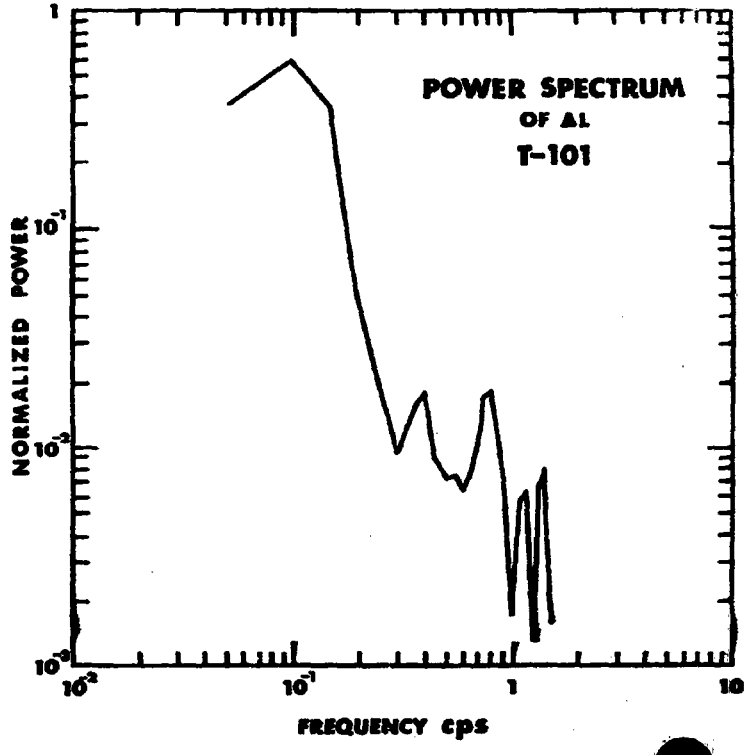

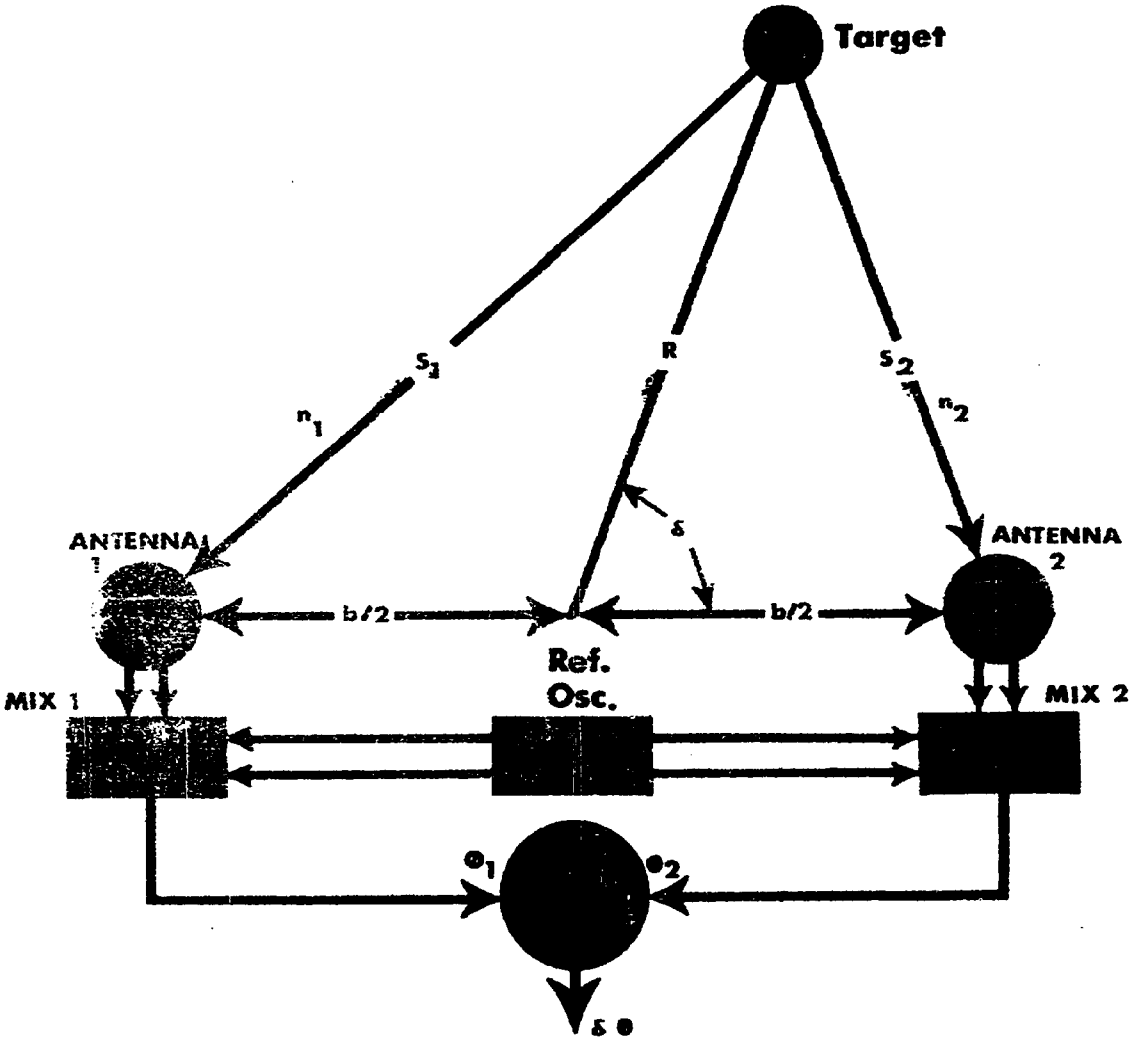
Target
S_1
R
S_2
n_1
n_2
δ
ANTENNA 1
ANTENNA 2
b/2
b/2
Ref. Osc.
MIX 1
MIX 2
ϕ_1
ϕ_2
δ φ

Typical Refractivity Profile for Cape Canaveral

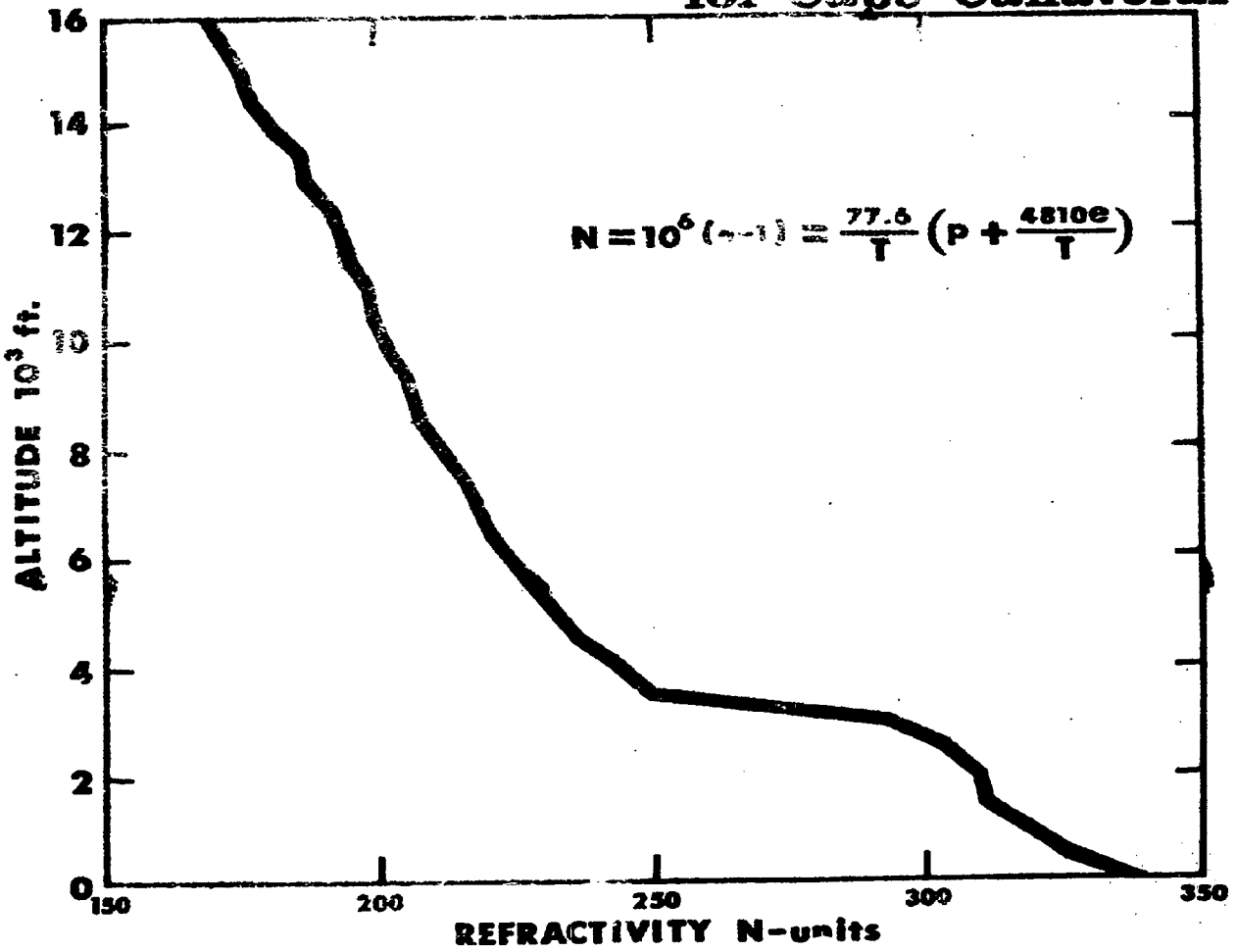

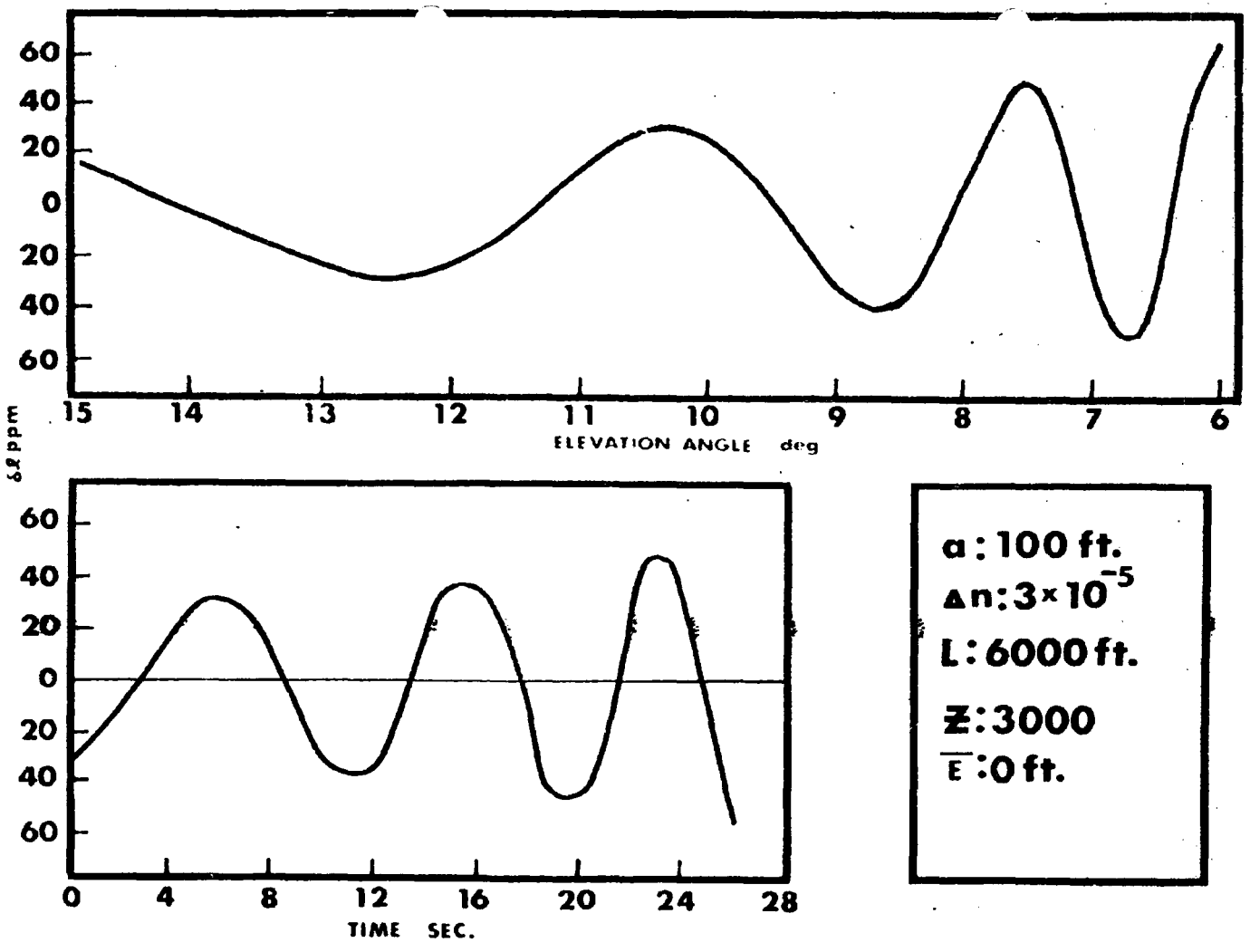
60
40
20
0
20
40
60
15
14
13
12
11
10
9
8
7
6
ELEVATION ANGLE deg
δℓ ppm
60
40
20
0
20
40
60
0
4
8
12
16
20
24
28
TIME SEC.
a : 100 ft.
Δn : 3 × 10⁻⁵
L : 6000 ft.
Z : 3000
E : 0 ft.

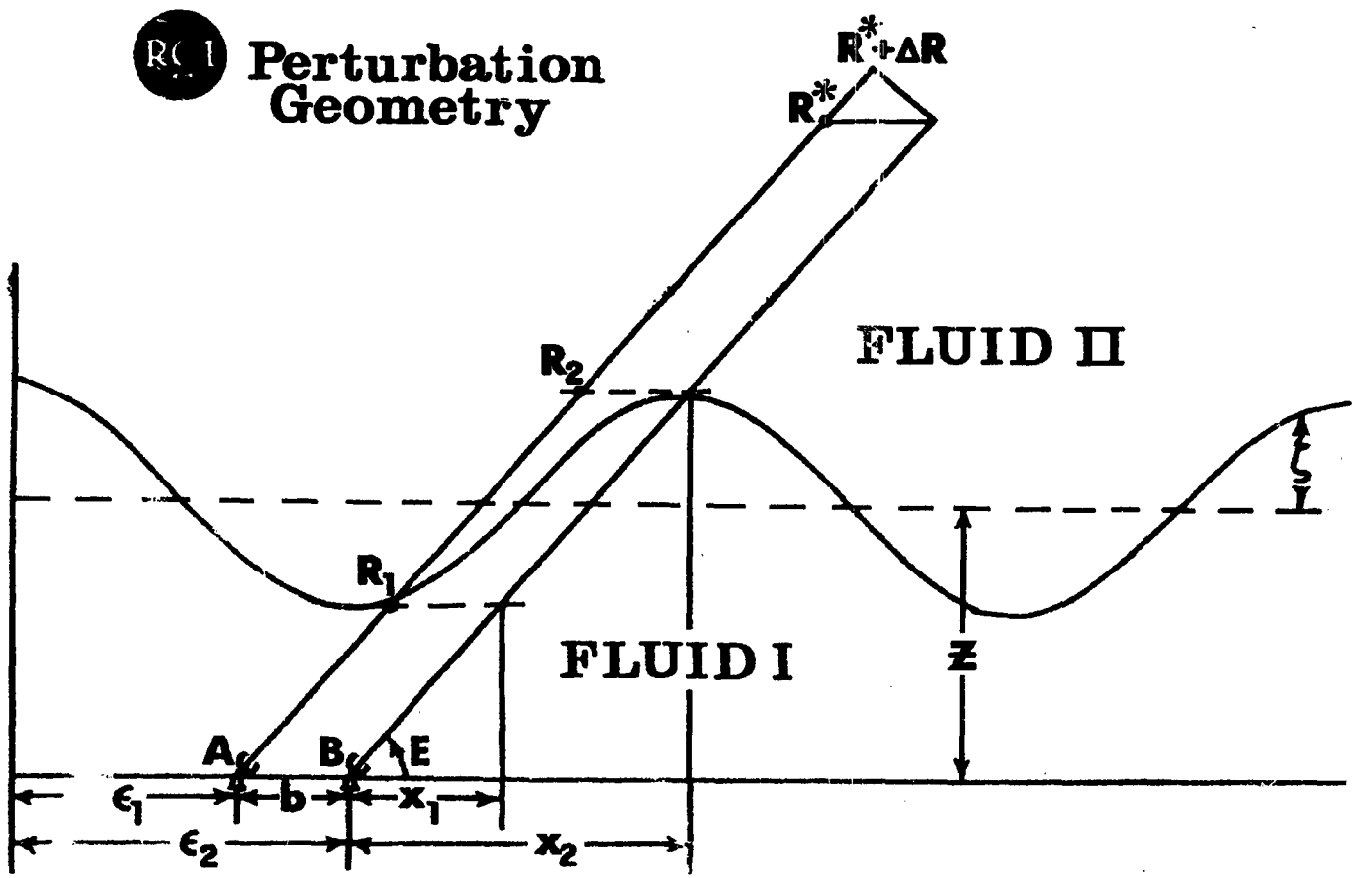
Perturbation Geometry
R* + ΔR
R*
FLUID II
R2
R1
FLUID I
ζ
Z
A
B
E
ε1
b
x1
ε2
x2

$$\frac{A}{\sigma_L} = b_0 + b_1 X_1 + b_2 X_2 + b_3 X_3 + b_4 X_4 + b_5 X_5$$

Where σ_L = Standard error of L, estimated from dispersion about the Keplerian ellipse during free fall.

X_1 = Tenth of low clouds (<10,000 ft.)

X_2 = Cosecant of elevation angle.

X_3 = Signal strength (db).

X_4 = Span length of free-fall data used to calculate σ_L (sec.).

X_5 = Surface refractivity (N-units).

Coefficient	Value	F-ratio	$F_{0.95}$
b_1	1.84	54.89	4.23
b_2	0.94	23.36	4.23
b_3	0.06	0.69	4.23
b_4	0.06	6.02	4.23
b_5	0.005	0.03	4.23

SIMPLE CORRELATION MATRIX

	X_1	X_2	X_3	X_4	X_5	σ_L
X_1	1.00	0.06	-0.11	0.36*	0.06	0.77*
X_2		1.00	-0.06	0.06	-0.12	0.46*
X_3			1.00	0.02	0.22	-0.11
X_4				1.00	-0.49	0.49*
X_5					1.00	-0.02
σ_L						1.00

*Significant at 95% level

Keplerian Differences

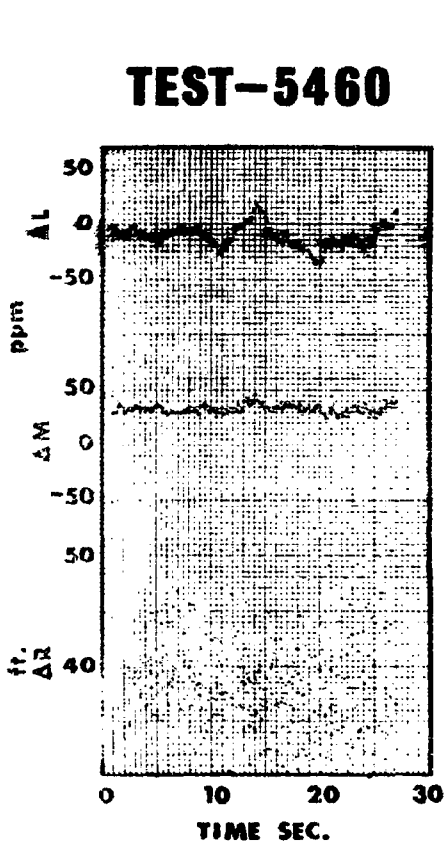

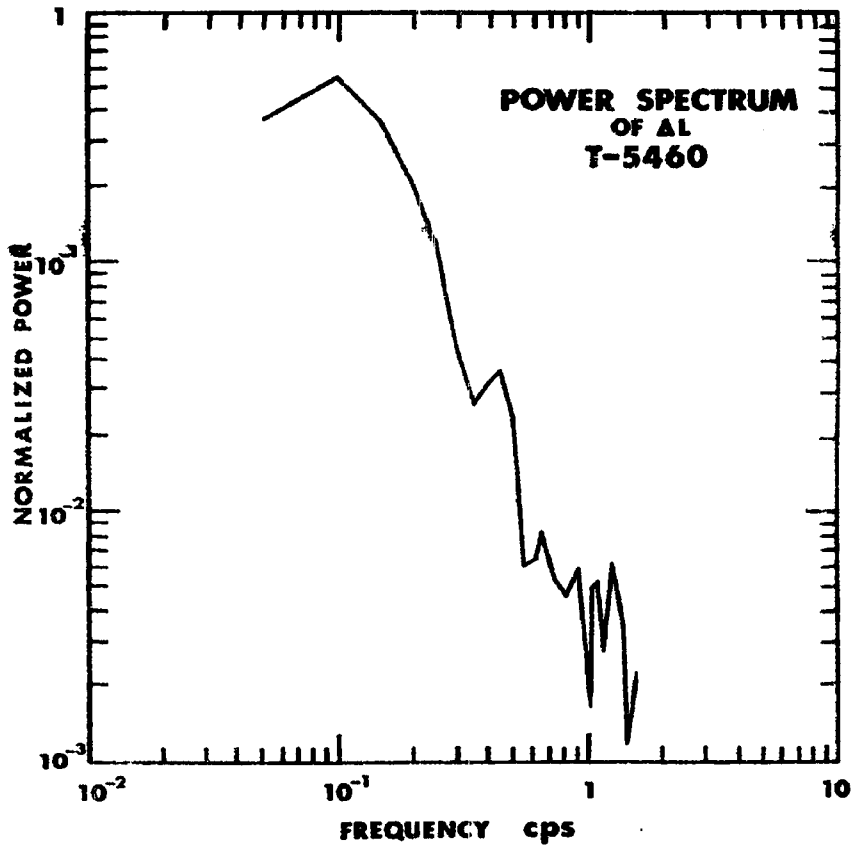

709 - J

INSTRUMENTATION ERRORS DUE TO ATMOSPHERIC REFRACTION

by David K. Barton
Missile and Surface Radar Division
Radio Corporation of America
Moorestown, New Jersey

February 27, 1963

(This paper is a summary of the Report of the Ad Hoc Panel on Electromagnetic Propagation, National Academy of Sciences, to be distributed during March, 1963.)

UNCLASSIFIED

1. INTRODUCTION

The Ad Hoc Panel on Electromagnetic Propagation was convened as part of a continuing effort by the National Academy of Sciences - National Research Council on behalf of the Atlantic Missiles Range as requested by Headquarters, Air Force Systems Command.

The Ad Hoc Panel on Basic Measurements discussed in its Report how well we can measure, at the present time, such fundamental quantities as length, time, and the velocity of light. The Report notes that there are fundamental limitations to tracking accuracy imposed by our inability to measure these basic quantities with more precision, but it points out that the state of the instrumentation art has not yet approached these limitations. There are, however, other fundamental limitations to tracking accuracy which today are beginning to restrict the capability of our instrumenta. One of these major limitations is that imposed by atmospheric refraction. Consequently, the Ad Hoc Panel on Electromagnetic Propagation was formed to consider this problem.

This Panel met on 11 May 196[illegible] in Washington, D. C. and heard discussions as to how tracking accuracy requirements were arrived at for one particular program, of the current tracking capabilities of the AMR, and of various research work which instrumentation and atmospheric physics people are conducting. Due to the quantity and divergence of the material presented, the Panel could not arrive at a consensus regarding a report. Consequently, Mr. David K. Barton was appointed Editor of the Panel's Report by the Chairman. Mr. Barton drafted the Report of the Panel from material contributed by Dr. Robert S. Fraser, Dr. John B. Smyth, Mr. Preston Landry, and himself.

In the Report of the Ad Hoc Panel on Electromagnetic Propagation, the objective was to state the current extent of our knowledge concerning atmospheric refraction and its effect on tracking accuracy, for the benefit of range users as well as range operators. The Panel also made recommendations which, if followed, should lead to increased accuracy both in the near and in the more distant future.

2. Current Status of Report

During January of 1963, the report was reviewed by the entire panel, and a number of suggested changes were incorporated. The final version of the report is scheduled for distribution during March.

The Panel Members who participated in the original discussion and who reviewed the report are identified in the following list:

Mr. David K. Barton	RCA, Moorestown, N. J.
Mr. John Berbert	Goddard Space Flight Center
Mr. Charles F. Chubb	Sperry Gyroscope Company
Dr. Warren A. Dryden	RCA, Patrick Air Force Base
Dr. A. B. Focke, Chairman,	Dept. of Physics, Harvey Mudd College, Claremont, Cal.
Dr. J. J. Freeman	J. J. Freeman Associates, Silver Spring, Maryland
Dr. John B. Garrison	Applied Physics Laboratory, Johns Hopkins University
Mr. Dean Howard	Naval Research Laboratory
Dr. Henry P. Kalmus	Chief Scientist, Diamond Fuse Lab.
Mr. Preston Landry	Chairman, Electromagnetic Propagation Working Ground, IRIG, Eglin Air Force Base
Dr. Robert B. Muchmore	Space Technology Laboratories

Dr. Louis Neelands	General Electric Co., Syracuse
Dr. Henry Plotkin	Goddard Space Flight Center
Mr. C. W. Querfeld	White Sands Missile Range
Mr. Joseph Salerno	MIT Lincoln Laboratory
Dr. John B. Smyth	Smyth Research Associates, San Diego, Cal.
Mr. Robertson Stevens	Jet Propulsion Laboratory
Dr. A. W. Straiton	University of Texas
Dr. Moody C. Thompson	National Bureau of Standards, Boulder, Col.
Mr. E. W. Bullington	Executive Secretary, Advisory Committee to AFSC, National Academy of Sciences

3. Contents of Report

The Report of the Ad Hoc Panel contains discussions of the following subjects:

a. Tropospheric errors
b. Ionospheric errors
c. Tropospheric correction procedures
d. Effects on typical instrumentation systems

Conclusions and recommendations are also included, and these will be presented in full below. First, we will present the tables and figures which summarize the information on atmospheric errors. The various effects were classified as shown in Table 1.

a. Tropospheric errors. Figures 1 and 2 indicate the magnitude of errors in range and elevation angle encountered by systems with tracking antennas. Figure 3 compares the elevation angle errors measured by trackers and by horizontal interferometers. The curve for the short-baseline system

is also indicative of the residual value of error in a tracker after subtraction of the term $N_s \cot\theta_o$ (see right-hand scale on Figure 2). This correction is unnecessary in the interferometer.

Fluctuating errors in angle and angle rate, which affect both tracking antennas and interferometers, are shown in Figures 4 and 5, for the special case of a target which remains fixed in angle relative to the tracking system. These errors are due to variations in the refractive index of the troposphere, which have a spectral distribution shown in Figure 6. Measurements made by the Bureau of Standards have provided data on spatial correlation of errors as well as on temporal correlation, and these measurements suggest that the two effects are closely related. In fact, as shown in Figure 7, the two correlations agree if the troposphere is assumed to consist of a "rigid" pattern of refractivity variations which drift over the surface of the earth at a speed near 10 ft/sec. The relative velocity of the troposphere with respect to the measurement ray will also depend upon the angular rate of the target, and a fast-moving target will lead to more rapid variation in the angular errors measured by the instrument. Figures 8 and 9 show the position and velocity errors caused by refractivity variations which are described by Figure 6. The velocity v_w represents the average crosswind velocity with respect to the measurement rays, and v_b represents the velocity of these rays relative to the troposphere when tracking a moving target. The velocity is averaged over the portion of the troposphere which contributes the refractivity variations, and is approximately that applying to an altitude of 10,000 feet.

b. Ionospheric errors. Figures 10 and 11 show the errors in range and elevation angle introduced by the normal, daytime ionosphere, indicating the dependence upon operating frequency.

An estimate of the fluctuating component of range error is shown in Figure 12, while Figure 13 shows the error in the angle at which the measurement ray passes the target, at an altitude of 300 km. Unlike the tropospheric error, the error due to the ionosphere is largely unpredictable, even when the ionosphere has been measured by radio backscattering. A typical monthly scatter of elevation angle errors at three different sites is indicated in Figure 14. Further measurements carried out on the California coast indicated that the errors could not be predicted on the basis of ionograms any better than by using average monthly forecasts of electron density profiles, and that the residual errors after attempted correction were almost as great as the original error values. The inability to predict the error encountered at a given time indicates that accurate systems must operate at frequencies high enough to reduce the initial value of error to a tolerable level. For the accuracy requirements described to the panel (velocity measurements in the order of one ft/sec or better), this would imply operation at frequencies above 3000 Mc. The only known exception to this applies when two frequencies are used in a system which makes redundant measurements to cancel out the ionospheric error.

c. Tropospheric correction procedures. The correction procedures used at the ranges to compensate for tropospheric error are discussed in the report. These are based on ray-tracing computations carried out in a digital computer, using refractivity profiles calculated from radiosonde or refractometer data. Table 4 gives an estimate of the minimum residual errors, after application of such a process to tracking data. Surface refractivity would have to be measured with the best available instruments to meet these accuracy figures when using a tracker. Residual angle bias in an interferometer system might be somewhat less, since absolute refractivity data would not be needed for correction.

The values listed in Table 2 have been criticized by some as being overly optimistic, and by others as being too pessimistic. It is believed that they represent a fair statement of the performance attainable using accurate readings of surface refractivity in combination with radiosonde profiles for higher altitudes.

d. Effects on typical instrumentation systems. The information on atmospheric errors, including both bias and variable components, was applied to a specific target example: a satellite or missile in horizontal flight at an altitude of 160 miles. This case was chosen because it represents a number of the actual tracking problems which are met by the test ranges, and because it illustrates the procedure for applying the error analysis developed in the report. The results are given in a series of Tables, which describe the errors encountered by three different types of tracking system.

4. Description of Error Analysis Example

Three different equipment configurations were assumed, with two operating frequencies compared. The results are summarized in Tables 3 through 5. In each case, the target was assumed to have the following characteristics:

Target altitude:	$h=160$ n. mi.$=10^6$ ft
Target range:	$R=660$ n.mi.$=4\times10^6$ ft
Tangential velocity:	$V_t=10{,}000$ ft/sec
Angular rate of beam motion:	$\omega = 2.5$ mr/sec
Effective tropospheric velocity relative to beam:	$v_b = 250$ ft/sec
Beam elevation angle:	$\theta_o = 6^o = 105$ mr

The errors are given for "average" weather conditions, corresponding to the median curves of Figures 4 and 5, or to a condition where small amounts of cumulus clouds are present.

The errors for heavy cloud cover would be about twice those listed, while for clear sky they would be about half as great. Similarly, the ionosphere was assumed to follow the daytime model used in Figures 10 and 11, without extreme sunspot or other disturbed characteristics. Where ionospheric errors are important, the variation in their magnitudes may be assumed to range from a factor of three above those listed to about one-third of these values, depending upon time of day and portion of the sunspot cycle.

The velocity errors for the tracker and interferometer systems have been found from Figures 4, 5, 8, and 9, taking into account the measured spectra of tropospheric errors. For the trilateration system, the prediminant error has been calculated from the uncertainty in the ray-bending component, according to Millman's study. Total error has been found as the rms sum of all bias and fluctuating components, and has been expressed in terms of range, angle, target position, and target velocity. In each case, the components due to angular measurement (or equivalent) are seen to govern the accuracy of the system, and of these the elevation component is of greatest importance. The results are not consistent with some of the published figures for interferometer systems, but are believed to represent the most accurate values for this tracking problem. The primary cause of the difference lies in the fact that the satellite may have appreciable tangential velocity, causing the measurement beams to move through the atmosphere at rates which greatly magnify the frequencies in the atmospheric error spectrum. If similar calculations were made for targets which had little or no tangential velocity (as, for instance, missiles traveling directly away from the instrumentation site), the errors would be appreciably lower in magnitude, at least insofar as velocity data is concerned.

5. Conclusions

5.1 Tropospheric bias errors are highly predictable using radiosonde or refractometer profiles; residual errors from 1% to 3% of the initial bias levels are commonly attained using procedires described in the Panel Report. Data to within one-half foot in range and 40 to 70 μradians in angle can be expected at elevation angles above five degrees.

5.2 Tropospheric fluctuation errors are not correctable using any known procedure, and will amount to a few tenths of a foot in range, and 10 to 50 μradians in angle (depending on the baseline or aperture used for measurement), under normal weather conditions.

5.3 The relationship between temporal and spatial correlation of tropospheric fluctuations has been investigated, based on data obtained by the National Bureau of Standards. The effect of short-period fluctuations is described in Figures 4 and 5, and is consistent with a drift of tropospheric anomalies across a fixed measurement path at the speed of the prevailing wind.

5.4 In range instrumentation applications, where the beam is not fixed, the residual "bias" and long-term error components will change as the beam moves, and additional atmospheric rate errors will be generated, as shown in Figure 9. These errors will be proportional to the tangential velocity of the missile, and will typically be five to fifty times the errors measured for a fixed beam.

5.5 The uncertainty in tropospheric paths leads to errors equivalent to motion of the instrument on the ground. The motion of the "virtual source" typically amounts to several feet normal to the path and a few tenths of a foot along the path.

5.6 Ionospheric errors are essentially unpredictable, and will exceed the residual tropospheric errors when operating frequencies below 3000 Mc are used. Even in the 5000-6000 Mc band the ionospheric errors will contribute to overall atmospheric error during daytime operation.

5.7 Redundant measurements performed at two frequencies below 3000 Mc can be used to correct for ionospheric error in both range and angle.

5.8 The lowest atmospheric errors are found in trilateration systems using very long baselines. Total position and velocity errors for a typical satellite track (660 miles range, 160 miles altitude) through average weather, are as follows:

	RMS Position Error (feet)	RMS Velocity Error (ft/sec)
Range-angle tracker at 6000 Mc	310	16
Interferometer at 10,000 Mc (Mistram)	100	2.4
Trilateration system		
at 2000 Mc	19	0.9
at 6000 Mc	2.5	0.15

The above errors may be increased or decreased by a factor of two or three for different weather conditions (and at 2000 Mc for different ionospheric conditions). The trilateration errors shown are dependent upon perfect survey of station location, as well as instrumental errors below one-half foot in range and 0.02 ft/sec in range rate.

6. Recommendations for Achieving Increased Accuracy Today

6.1 Since ionospheric refraction cannot at present be predicted to within better than about 50% of any instantaneous value, the use of microwave bands or of dual-frequency measurements is necessary in precision tracking of targets above 100 miles. Single-frequency systems requiring velocity data better than one foot per second should operate above 3000 Mc to minimize the ionospheric refraction effect.

6.2 A continuing program of data analysis at the various ranges should be instituted to evaluate and improve the atmospheric correction procedures described in the Panel Report. Some of this work is being done at AMR now (and perhaps at other ranges) in connection with other activities. However this work is so important that it should be supported as a separate function; this is the only way it will receive the attention which it deserves. Data is available at all the ranges; it is only necessary that qualified people be assigned to an analysis of it. This work should be fully supported by all the services at their respective ranges. The data analysis conducted at each particular range should be fully coordinated among the ranges and with the NBS measurement program. Other interested agencies, such as NASA, should also be invited to participate. The Inter Range Instrumentation Group has done an excellent job in the past of providing coordination and dissemination of technical information among the ranges on an informal basis and is well qualified to do so in this case. This coordination of effort, especially among the National Ranges, and undoubtedly best accomplished by themselves, should receive the full support of DOD.

6.3 Standard procedures should be adopted for atmospheric correction of tracking data by all of the ranges and range

users, and estimates of residual bias errors agreed upon for each procedure. The methods discussed in the Panel Report are suggested as a basis for such standards and are consistent with efforts now underway by the Electromagnetic Propagation Working Group of the Inter Range Instrumentation Group. The EPWG is currently working on a range instrumentation manual which it hopes will lead to more standardization. The work of the individual members of EPWG on this project should be given the full support of each particular range where they are located and the project as a whole should have the complete support of DOD on an inter-range basis.

7. Recommended Research for Future Increase in Accuracy

7.1 Future tracking systems should be designed to tolerate the unpredictable fluctuations of the measurement ray paths in the atmosphere. When targets of high velocity must be tracked with accurate three-coordinate velocity measurements, the measurement system baselines should be as long as possible and they should be consistent with target altitude. Systems which require that instrumentation sites be located with an accuracy on the order of one foot or better do not appear to be consistent with our ability to predict ray paths in the troposphere.

7.2 A specific procedure for measuring and correcting tropospheric errors on a real-time basis has been proposed to the panel. A brief discussion of this technique appears in Appendix B of the Panel Report. Theoretically this technique appears very promising. It is now a question of determining whether experimental verification can be obtained. This work should receive full support from the Air Force.

7.3 The National Bureau of Standards (Boulder) has outlined a program of atmospheric measurements which it is attempting

or would like to attempt. This program is discussed in Appendix C of the Panel Report. These measurements would provide much needed data on spatial and temporal correlation of tropospheric range (or phase) errors. The panel recommends that this program be pressed as rapidly as possible and fully supported by the Air Force to provide much needed information for both the interferometer systems and the longer-baseline systems using range and range-rate data.

7.4 When tracking at interplanetary distances the errors imposed by the atmosphere become proportionately less. Consequently one limiting factor to tracking accuracy at such distances would appear to be the precision with which we know the velocity of light, currently felt to be about one part per million. (A discussion of our knowledge of the velocity of light is given in the report of the Ad Hoc Panel on Basic Measurements.) The efforts by the National Bureau of Standards to determine this value with more accuracy should be fully supported.

7.5 With our current tracking techniques for interplanetary distances an even more critical need than a better determination of "c" is that of a better frequency standard. For Doppler tracking a target over such distances a frequency standard or clock having a short-time stability of one part in 10^{13} is needed now. (At the present time we can measure time with an accuracy of about one part in 10^{11}. This is discussed in the Report of the Ad Hoc Panel on Basic Measurements.) The continuing efforts of the National Bureau of Standards to develop more stable frequency standards should receive full support.

7.6 Since the accuracy limits of current tracking instruments and propagation correction procedures are on the order of about one foot, there is a definite need for geodetic

systems or procedures capable of locating our tracking instruments or systems to this same accuracy over intercontinental distances. It is recommended that a study group be convened to determine what are the most fruitful areas for investigation which could lead to better determination of locations on a global basis and which might ultimately lead to the accuracy mentioned above.

8. Further Recommendations

8.1 The ranges should make the systems designers and/or range users familiar with the basic limitations on tracking accuracy imposed by the atmosphere as described in the Panel Report. It is futile for range users to request accuracies which cannot be obtained for reasons discussed therein. And the Panel does not anticipate that significant improvement over the potential accuracies discussed here will be attained in the near future, although more consistent use of correction techniques will improve on past performance. However, if the research recommended in the report is undertaken and adequately supported it may disclose means of reducing the basic uncertainties connected with propagation through the atmosphere which could be applied within the next decade.

8.2 In order to make the best use of the available resources for the development of instrumentation systems and techniques for propagation, the responsible agencies should arrive at consolidated requirements for missile and satellite measurement accuracies instead of new and different requirements for each individual program. The consolidated requirements should be stated and published in such a manner as to encourage scientific work on the most fundamental instrumentation programs, and should not be hampered by the security restrictions and need-to-know of any particular weapon or weapon system.

This is a DOD-wide problem and DOD should take the lead in trying to implement this. However, the Air Force could do much along this line with those programs under its cognizance.

Acknowledgements. The foregoing material represents the work of many members of the Ad Hoc Panel, and of others whose names are included in the list of references accompanying the full report of the Panel. In particular, as Editor of the report, I would like to acknowledge the contributions of Dr. Robert S. Fraser of Space Technology Laboratories, Dr. John B. Smyth, and Mr. Preston Landry, who supplied material on different aspects of the propagation problem, and of Dr. A. B. Focke, Chairman of the Panel, Mr. E. W. Bullington, and others on the staff of the National Academy of Sciences who organized the effort and made the report possible.

References

1. National Academy of Sciences, National Research Council, "Report of the Ad Hoc Panel on Electromagnetic Propagation", 1962, supported by the Air Force Systems Command under contract AF 18 (600) - 1895.

2. Bean, B. R., and G. D. Thayer, "CRPL Exponential Reference Atmosphere", NBS Monograph 4, 1959.

3. Space Technology Laboratories, Inc., "Tropospheric Scintillations", STL Report GM-TM-0165-00308, 1958.

4. Thompson, M. C., H. B. Janes, and R. W. Kirkpatrick, "An Analysis of Time Variations in Tropospheric Refractive Index and Apparent Radio Path Length", Journal of Geophysics Research 65, Jan. 1960.

5. Barton, D. K., "Reasons for the Failure of Radio Interferometers to Achieve Their Expected Accuracy", to be published in future Correspondence to the IEEE Proceedings.

6. Pfister, W., and T. J. Keneshea, "Ionospheric Effects on Positioning of Vehicles at High Altitudes", Air Force Surveys in Geophysics, No. 83, March 1956.

7. Barton, D. K., "The Future of Pulse Radar for Missile and Space Range Instrumentation", IRE Trans. MIL-5, No. 4, October 1961.

8. Millman, G. H., "Atmospheric Effects on VHF and UHF Propagation", Proc. IRE, Vol. 46, No. 8, August 1958.

Table 1

Classification of Atmospheric Errors by Type.

There are many ways of describing propagation errors in precision tracking systems. The four classifications shown in Table I are suggested to cover the characteristics of most interest to the developers and users of missile and space range instrumentation:

a.	Source of Error:
	Tropospheric
	Ionospheric
b.	Measured Quantity
	Angle of arrival or phase difference
	Range delay or signal phase
c.	Spatial Correlation of Error:
	Across radar aperture (5 to 100 feet)
	Across short baseline (100 to 1000 feet)
	Across long baseline (1000 to 100,000 feet)
d.	Temporal Correlation of Error:
	Bias (fixed during one track)
	Fluctuation (periods of seconds or minutes)

For each combination of the above characteristics, the error should be known as a function of operating frequency, target altitude, elevation angle (or slant range) and state of the atmosphere. Except in rare instances, the instrumentation system may be assumed to be at sea level.

The present state of the art in correction of range and elevation data, using combined radiosonde and refractometer data to derive accurate surface refractivity and profiles, is estimated to provide the accuracy of correction shown in Table 2.

TABLE 2.

Optimum Accuracy of Range and Angle Corrections

		$\theta_o = 5^o$	$\theta_o = 20^o$
Long-Range Case (R 300 n. mi.)			
Initial range bias ΔR_e	(ft)	75	22
Residual range bias σ_{rb}	(ft)	0.75	0.2
% residual error		1	1
Initial angle bias δ	(μrad)	3500	900
Residual angle bias $\sigma_{\theta b}$	(μrad)	70	20
% residual error		2	2
Short-Range Case (R = 50 n. mi.)			
Initial range bias ΔR_e	(ft)	22	7
Residual range bias σ_{rb}	(ft)	0.5	0.15
% residual error		2	2
Initial angle bias δ	(μrad)	2000	700
Residual angle bias $\sigma_{\theta b}$	(μrad)	60	20
% residual error		3	3

(Values shown should be doubled for disturbed meteorological conditions such as heavy cloud cover, fronts, and inversions; also for lack of reliable and frequent soundings covering the entire tropospheric path used in measurement).

Table 3 Typical Atmospheric Errors

Tracking Radar on Satellite Tracking Mission

A. Tropospheric Components (average weather)

Range bias ΔR_e (Fig. 1):	60 ft
Angle Bias δ (Fig. 2):	2500 μrad
Residual range bias σ_{rb} (Table 2):	0.3 ft
Residual angle bias $\sigma_{\theta b}$ (Table 2):	50 μrad
Range fluctuation σ_{rf}:	0.1 ft
Angle fluctuation $\sigma_{\theta f}$ (Fig. 8):	60 μrad
Range rate bias $\sigma_{\dot{r}b}=v_t\sigma_{\theta b}$:	0.5 ft/sec
Range rate fluctuation $\sigma_{\dot{r}f}=v_t\sigma_{\theta f}$:	0.6 ft/sec
Angle rate fluctuation $\sigma_{\dot{\theta}}$ (Fig. 9):	4 μrad/sec

B. Ionospheric Components (normal ionosphere)

Operating frequency	2000	6000 mcps
Range bias Δr^i (Fig. 10):	10	1.1 ft
Range fluctuation σ_{r_i} (Fig. 12):	0.05	.006 ft
Angle bias δ^i (Fig. 11):	8	0.9 μrad
Ray error $\Delta\alpha_i$ (Fig. 13):	30	3.3 μrad
Range rate error $\sigma_{\dot{r}_i}=v_t\Delta\alpha_i$	0.6	.066 ft/sec

C. Total Error

Operating frequency	2000	6000 mcps
Range error σ_r	10	1.2 ft
Angle error σ_θ	78	78 μrad
RMS target position σ_p	310	310 ft
RMS target velocity σ_v	16	16 ft/sec

Significant error components:

Residual tropospheric range and angle bias
Ionospheric range bias (2000 mcps only)

Table 4 Typical Atmospheric Errors

Interferometer System (Mistram) on Satellite Track

A. Tropospheric Components (average weather)

Range bias ΔR_e (Fig. 1):	60 ft
Angle bias $\Delta\beta'$ (Fig. 3):	180 μrad
Range-difference bias (El. b'=1000 ft)	0.18 ft
Residual range bias σ_{rb} (Table 2):	0.3 ft
Range fluctuation σ_{rf}:	0.1 ft

	Elevation	Azimuth
Effective baseline b' (position data):	1000	10,000 ft
Residual range-difference bias $\sigma_{\Delta rb}$:	.02	.06 ft
Residual angle bias $\sigma_{\theta b}$:	20	6 μrad
Range-difference fluctuation $\sigma_{\Delta rf}$ (Fig. 8):	.014	.06 ft
Angle fluctuation $\sigma_{\theta f}$ (Fig. 8):	14	6 μrad
Effective baseline b' (velocity data):	10,000	100,000 ft
Range-rate difference fluctuation $\sigma_{\Delta \dot{r} f}$:	.006	.0014 ft/sec
Angle rate fluctuation $\sigma_{\dot{\theta} f}$ (Fig. 9):	0.6	0.14 μrad/sec

Table 4 (continued)

	Elevation	Azimuth
B. Ionospheric Components (normal ionosphere, f=10,000 mc)		
Range bias Δr^i (Fig. 10):		0.2 ft
Range fluctuation σ_{ri} (Fig. 14):		.001 ft
Angle bias δ^i (Fig. 11):		0.16 μrad
Ray error $\Delta\alpha_i$ (Fig. 13):		1.0 μrad
Range rate error $\sigma_{\dot{r}i}$:		.01 ft/sec
Ray difference error	0.1	0.3 μrad
Range rate difference error	.001	.003 ft/sec
Angle rate error	0.1	0.03 μrad/sec
C. Total Error		
Range error σ_r		0.35 ft
Angle error σ_θ		25 μrad
RMS target position σ_p		100 ft
RMS target velocity σ_v		2.4 ft/sec

Significant error sources:
Tropospheric range bias
Tropospheric angle bias and fluctuation

Table 5 Typical Atmospheric Errors

Wide-Baseline Trilateration System on Satellite Track

A. Tropospheric Components (average weather)

Range bias ΔR_e (Fig. 1):	60 ft
Residual range bias σ_{rb} (Table 2):	0.3 ft
Range fluctuation σ_{rf}:	0.1 ft
Geometrical dilution factor:	3
Equivalent angle bias $\sigma_{\theta b}$:	0.33 μrad
Equivalent angle fluctuation $\sigma_{\theta f}$:	0.11 μrad
Ray error bias $\sigma_{\alpha b}$:	2.5 μrad
Range rate bias $\sigma_{\dot{r}b}$:	.025 ft/sec
Equivalent angle rate bias $\sigma_{\dot{\theta}b}$:	.027 μrad/sec
Ray error fluctuation $\sigma_{\alpha f}$:	1.4 μrad
Range-rate fluctuation $\sigma_{\dot{r}f}$:	.014 ft/sec
Equivalent angle rate fluctuation $\sigma_{\dot{\theta}f}$:	.015 μrad/sec

B. Ionospheric Components (normal ionosphere)

	2000 mcps	6000 mcps
Range bias Δr^i (Fig. 10):	4.5	0.5 ft
Range fluctuation σ_{ri} (Fig. 12):	.03	.0033 ft
Equivalent angle bias $\sigma_{\theta b}$:	4.8	0.53 μrad
Equivalent angle fluctuation $\sigma_{\theta f}$:	.032	.0035 μrad
Ray error bias $\Delta\alpha_i$ (Fig. 13):	20	2.2 μrad
Range-rate bias $\sigma_{\dot{r}b}$:	0.2	.022 ft/sec
Equivalent angle rate bias $\sigma_{\dot{\theta}b}$:	0.22	.024 μrad/sec

Table 5 (continued)

C. Total Error

Frequency	2000 mcps	6000 mcps
Range error σ_r	4.5	0.6 ft
Equivalent angle error σ_θ	4.8	0.64 μrad
RMS target position σ_p	19	2.5 ft
RMS target velocity σ_v	0.9	0.15 ft/sec

Significant error components:

At 2000 mcps: Ionospheric range bias and ray error
At 6000 mcps: Ionospheric and tropospheric range bias and ray error (tropospheric is slightly greater than ionospheric at this frequency)

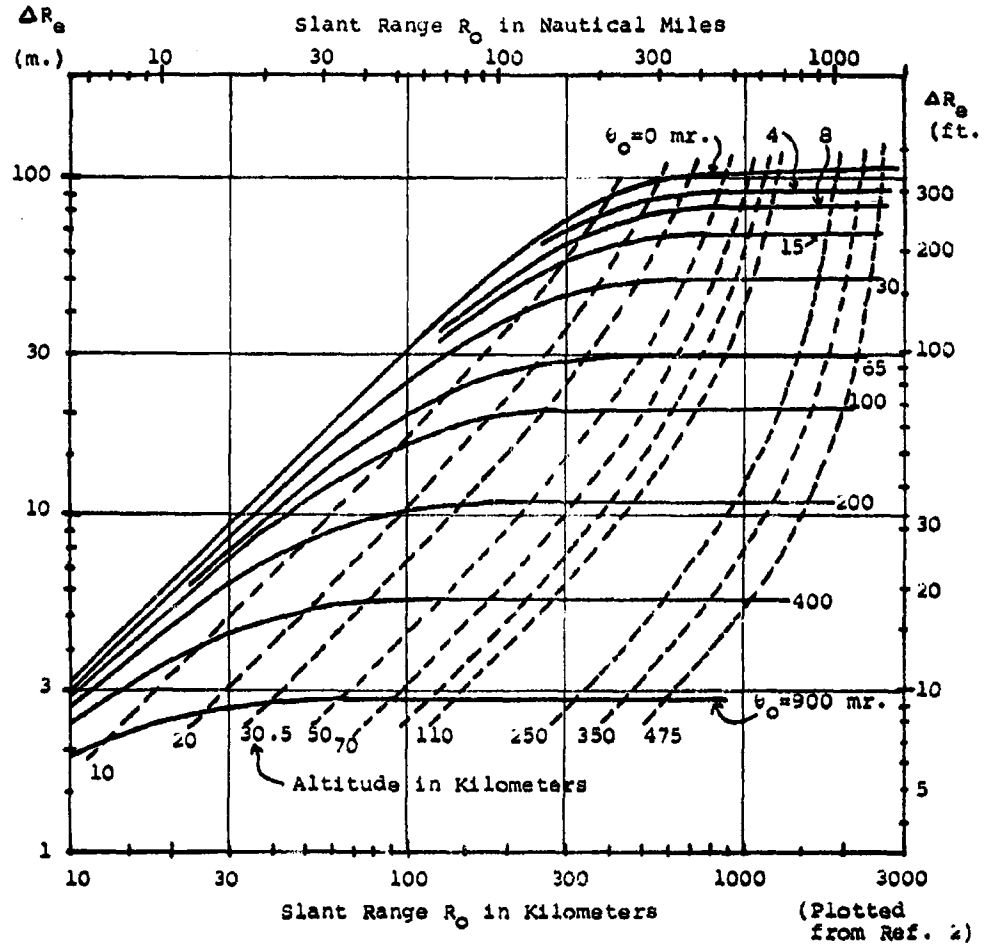

Range Bias vs. Range for CRPL Exponential Reference Atmosphere (N_o = 313)

Figure 1.

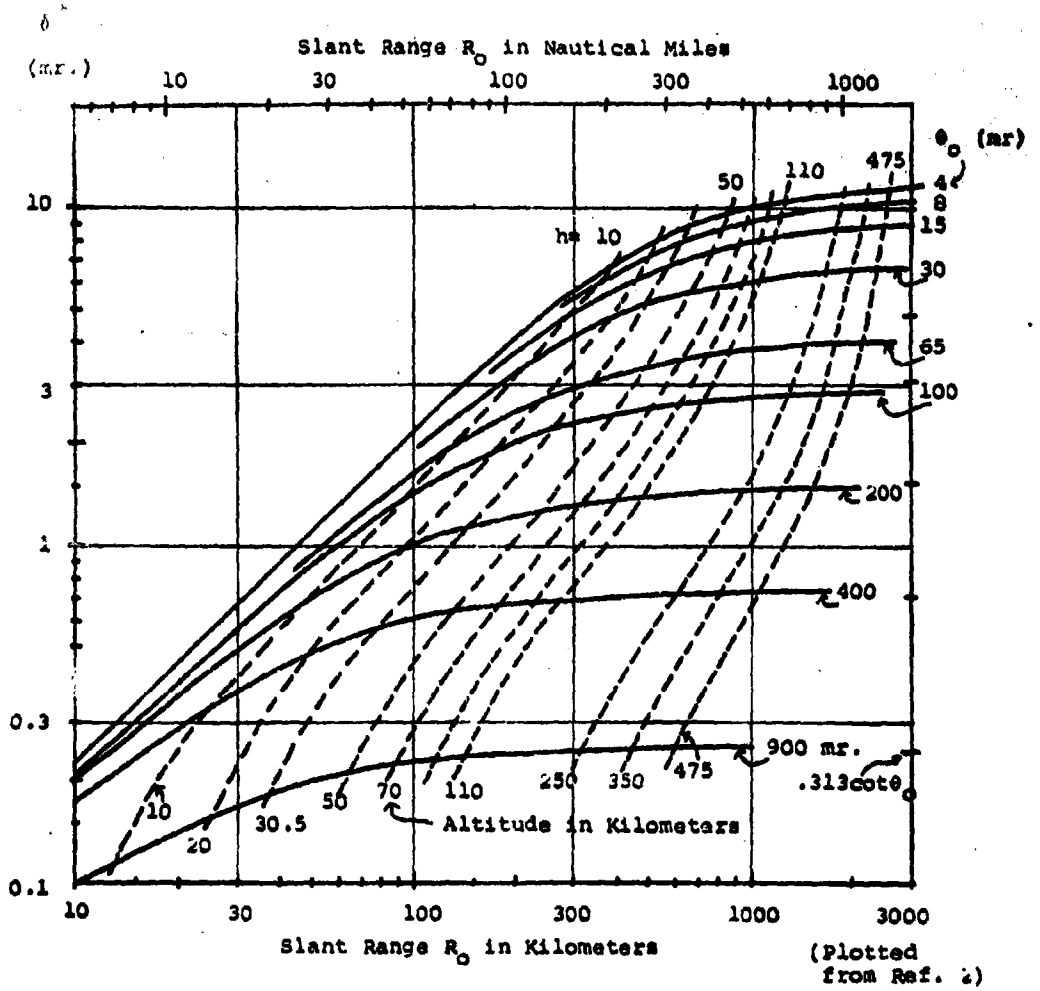

Tracker Elevation Angle Error vs. Range
for CRPL Exponential Reference Atmosphere
(N_o = 313)

Figure 2.

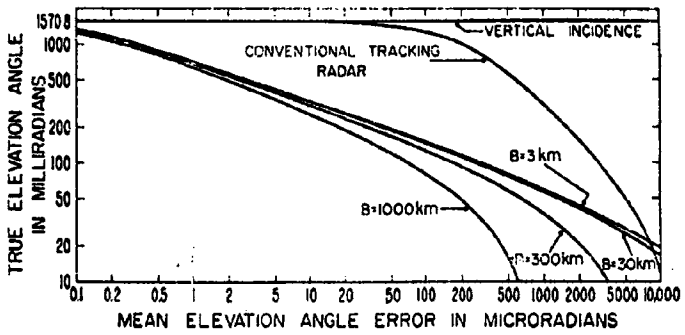

Figure 3. Mean tracker and interferometer refraction errors. The curve for B=3 km also represents the residual tracker error after correction according to $N_s \cot\epsilon_o$.

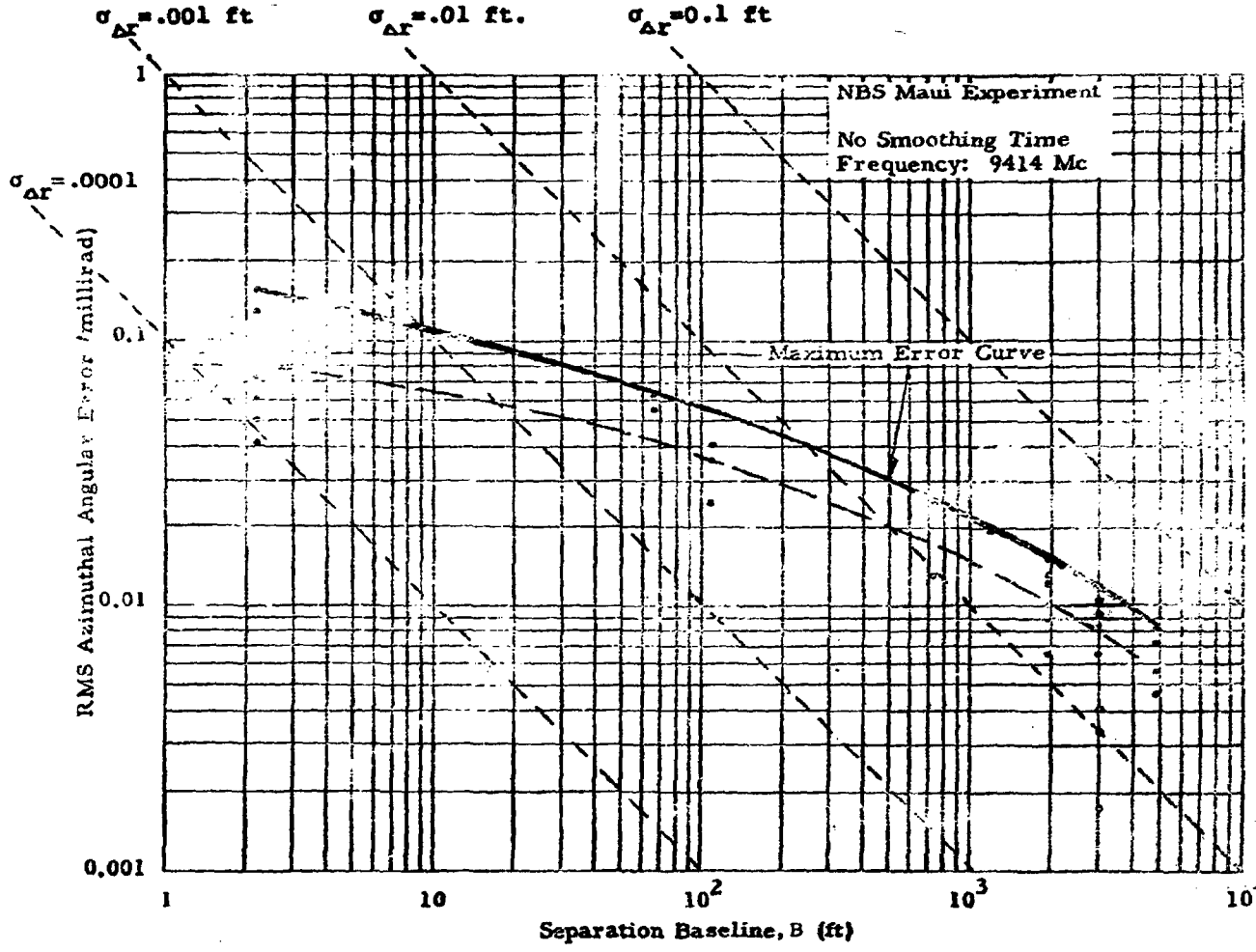

Figure 4. Measured Variation of Azimuthal Angular Position Error as a Function of Interferometer Baseline Length. (From Ref. 3)

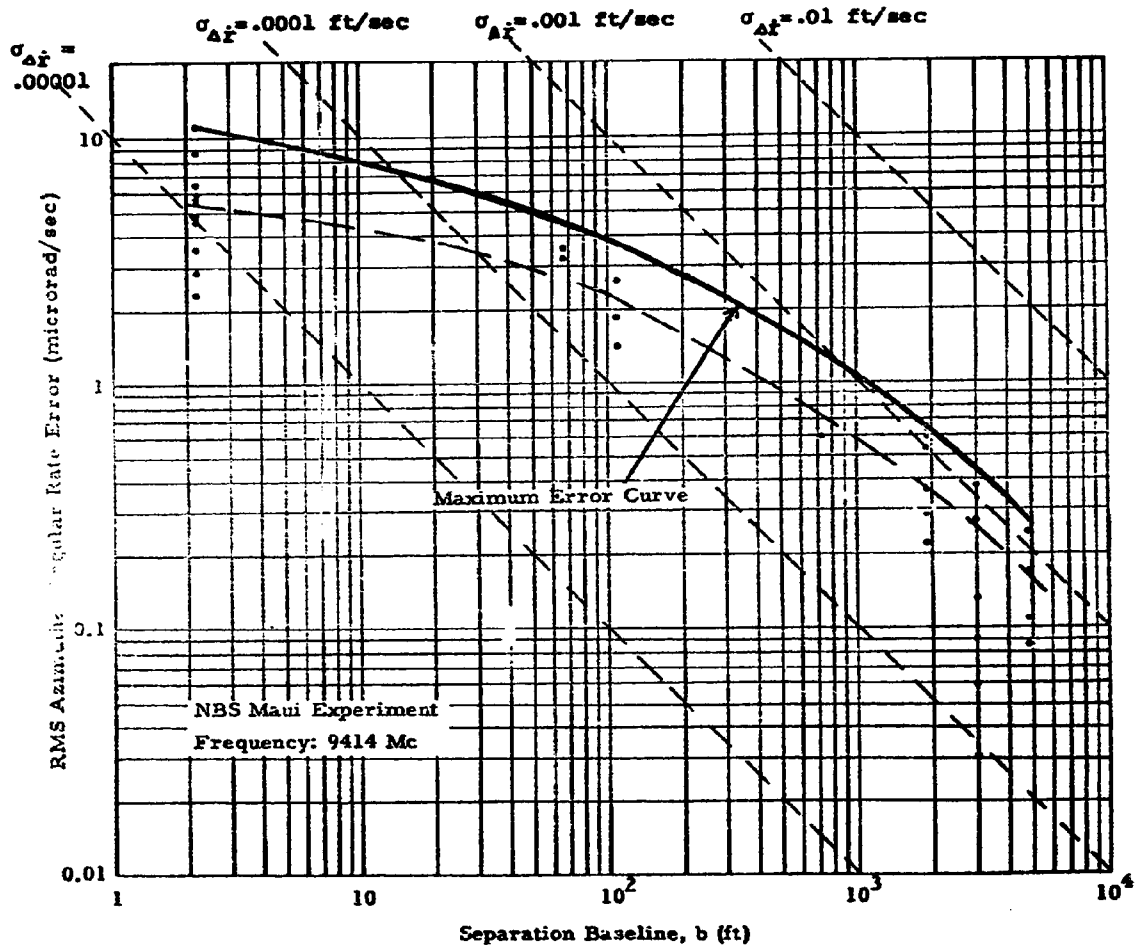

Figure 5. Measured Variation of Azimuthal Angular Rate Error as a Function of Interferometer Baseline Length, 20 Sec Smoothing. (From Ref. 7)

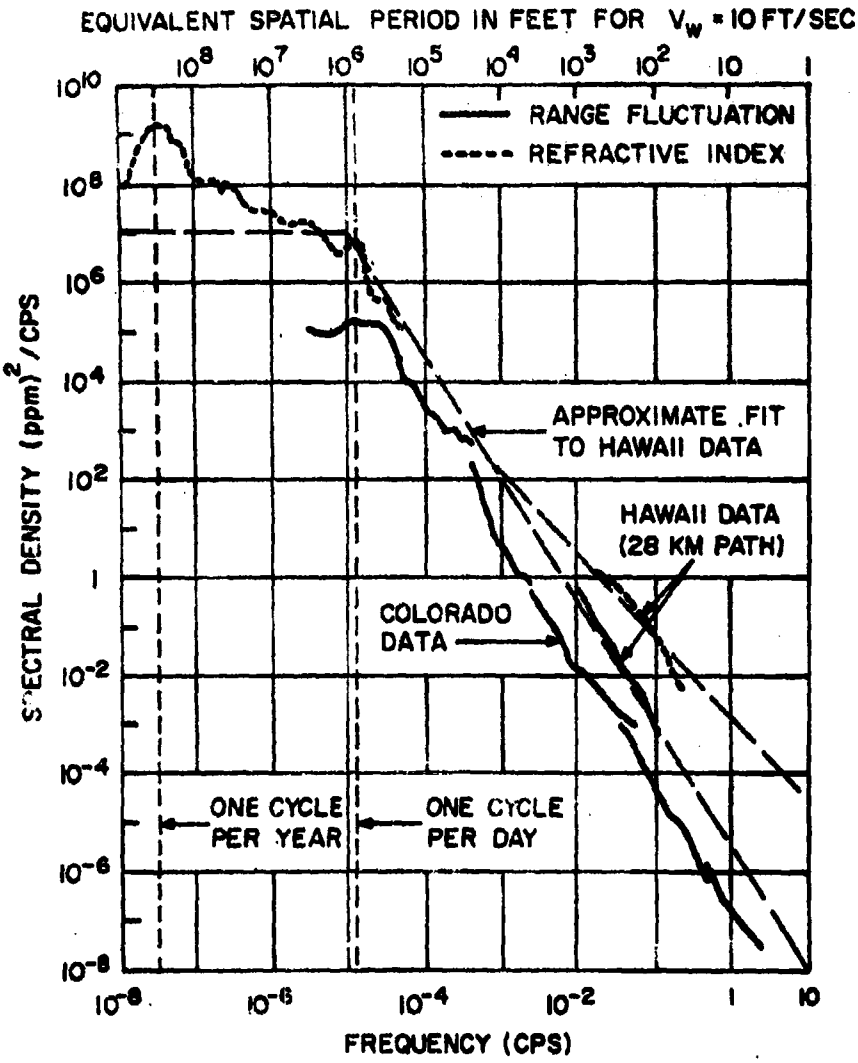

Figure 6. Spectra of Refractivity and Range Fluctuation (after Ref. 4)

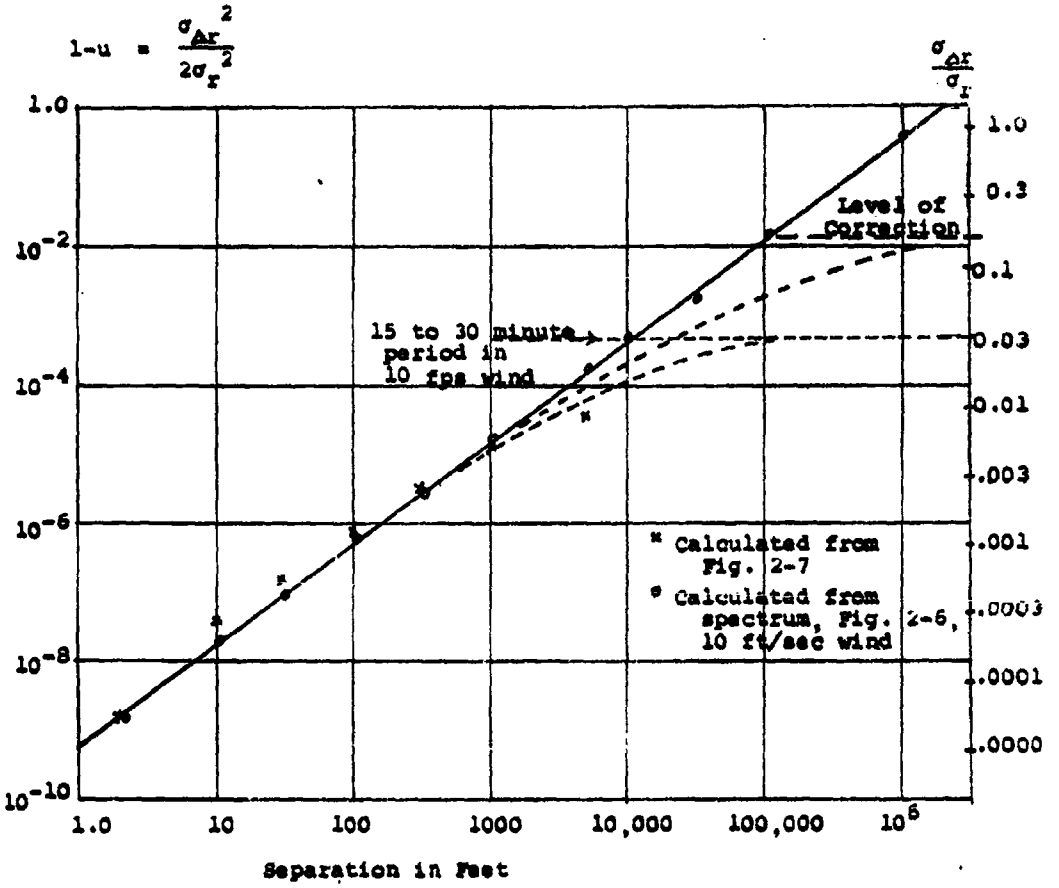

Figure 7. Spatial Correlation calculated from Phase-difference data and from single-path spectra.

Correlation coefficient for two paths $u = \frac{\sigma_{r_1 r_2}}{\sigma_{r_1}\sigma_{r_2}}$

Range-difference error $\sigma_{\Delta r} = \sigma_r\sqrt{2(1-u)}$

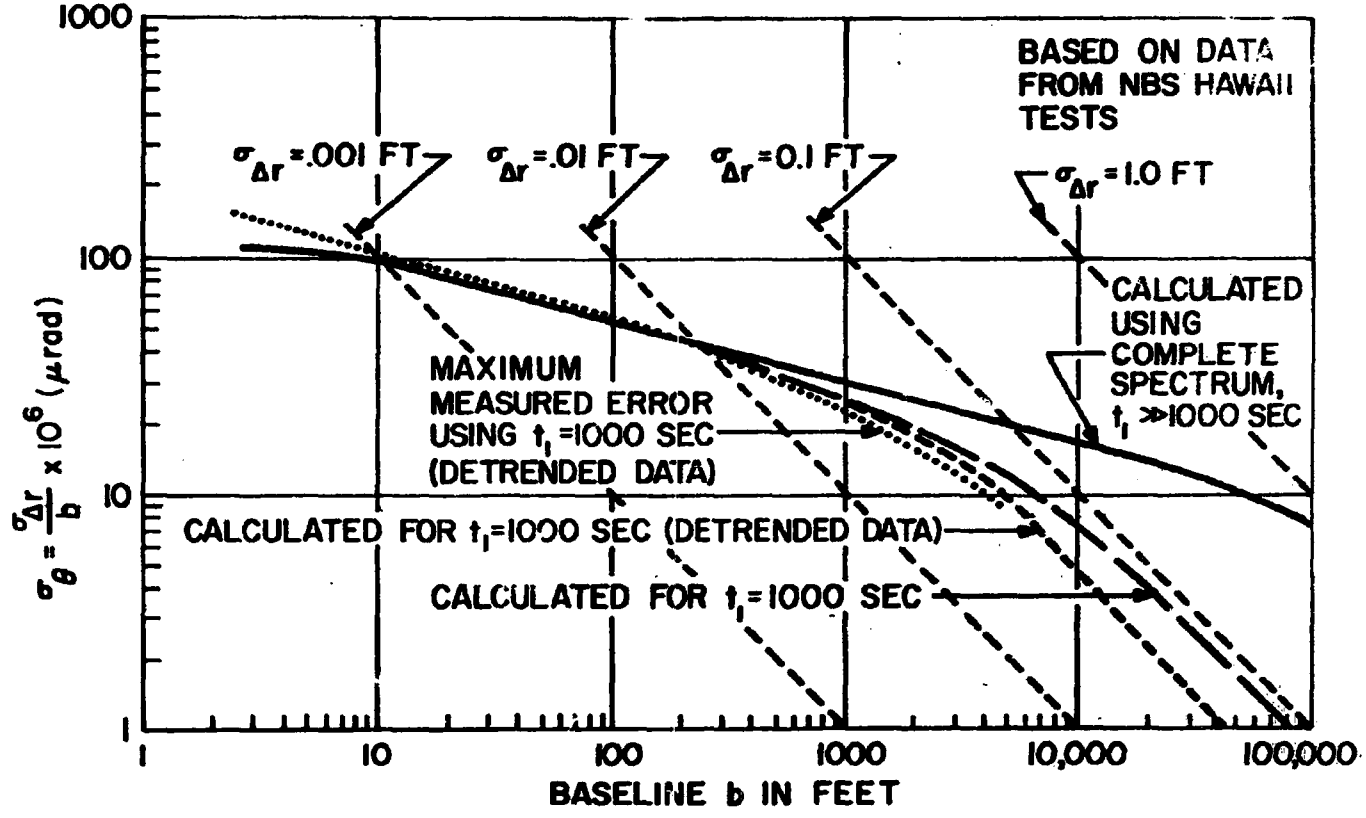

Figure 8. Equivalent Angular Position Error vs. Baseline Length (from Ref. 5)

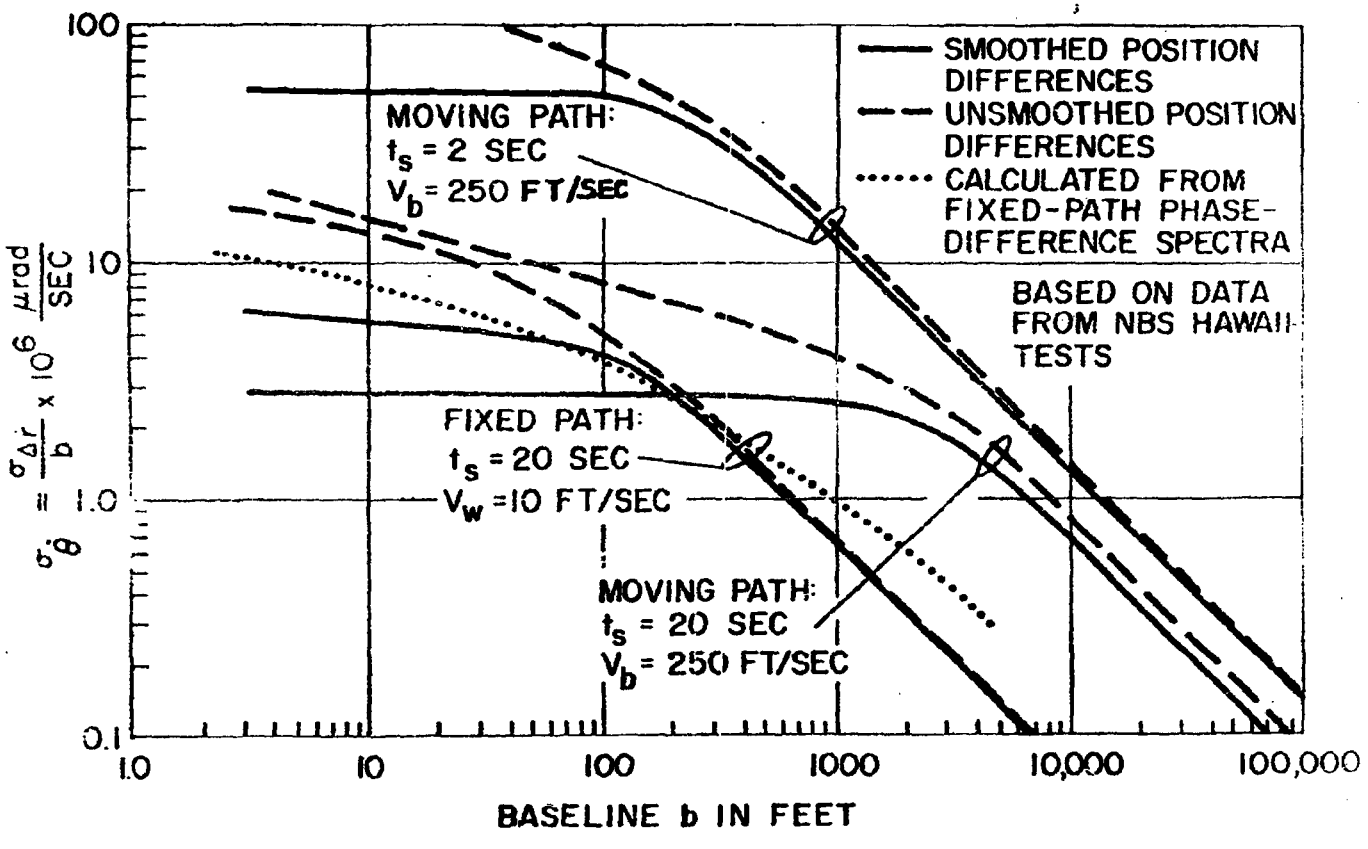

Figure 9. Equivalent Angular Rate Error vs. Baseline Length for Fixed and Moving Paths. (from Ref. 1, 5)

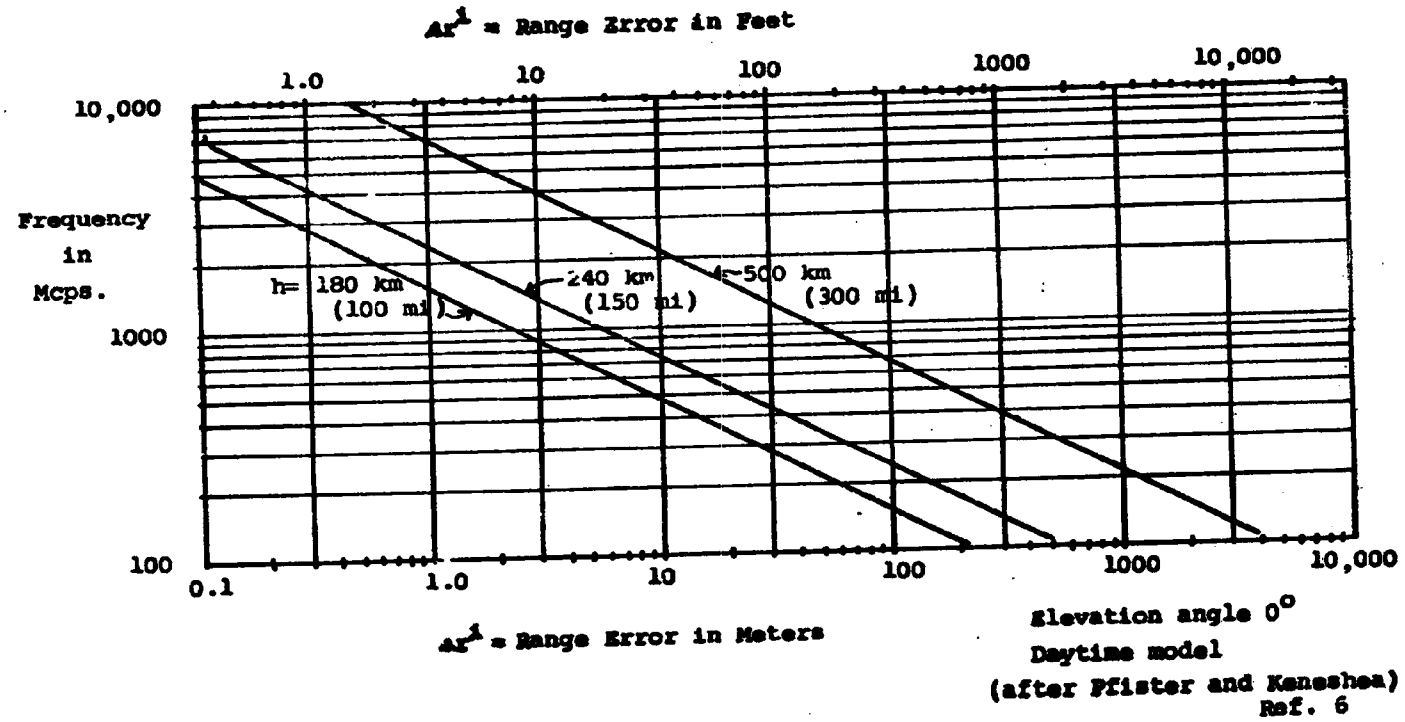

Figure 10. Ionospheric range error vs. Frequency

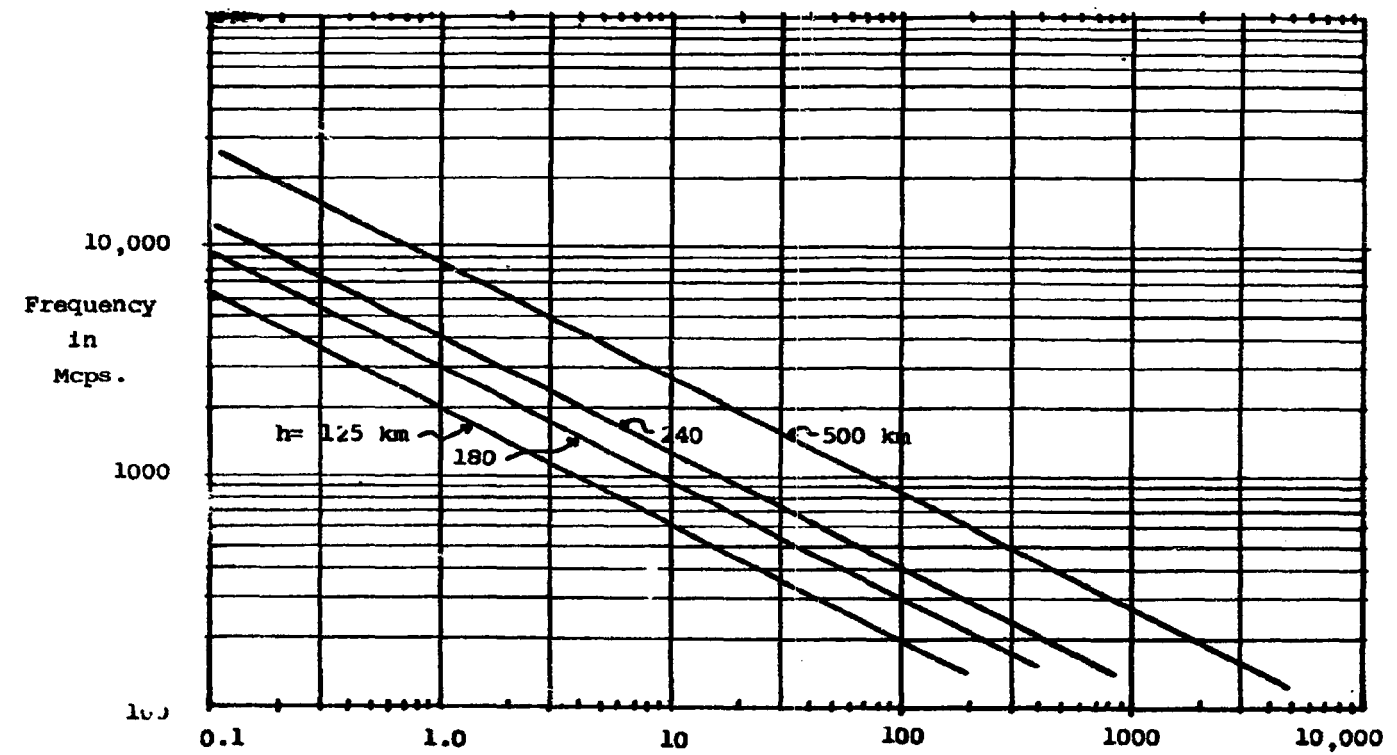

Figure 11. Ionospheric angle error vs. Frequency

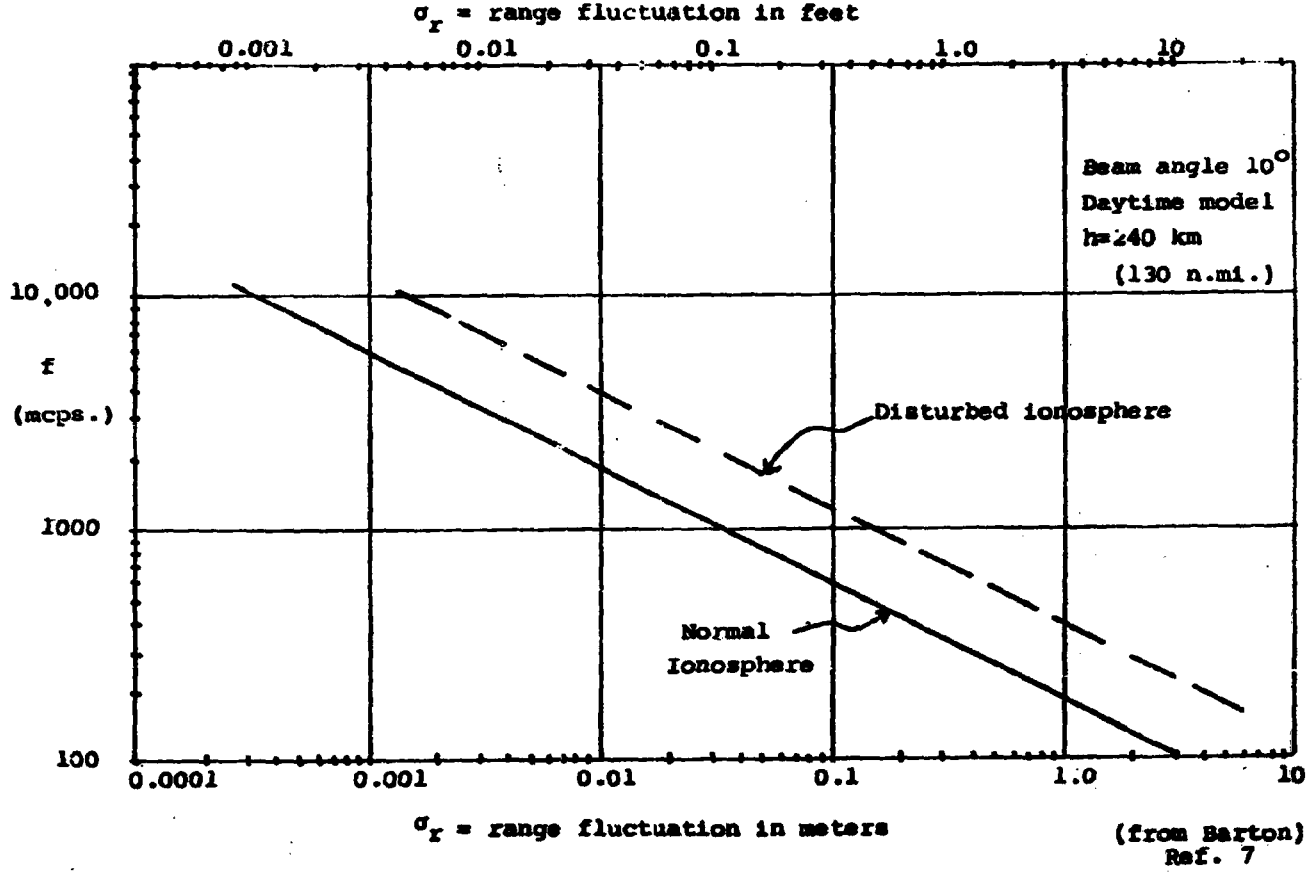

Figure 12. Ionospheric range fluctuation vs. Frequency

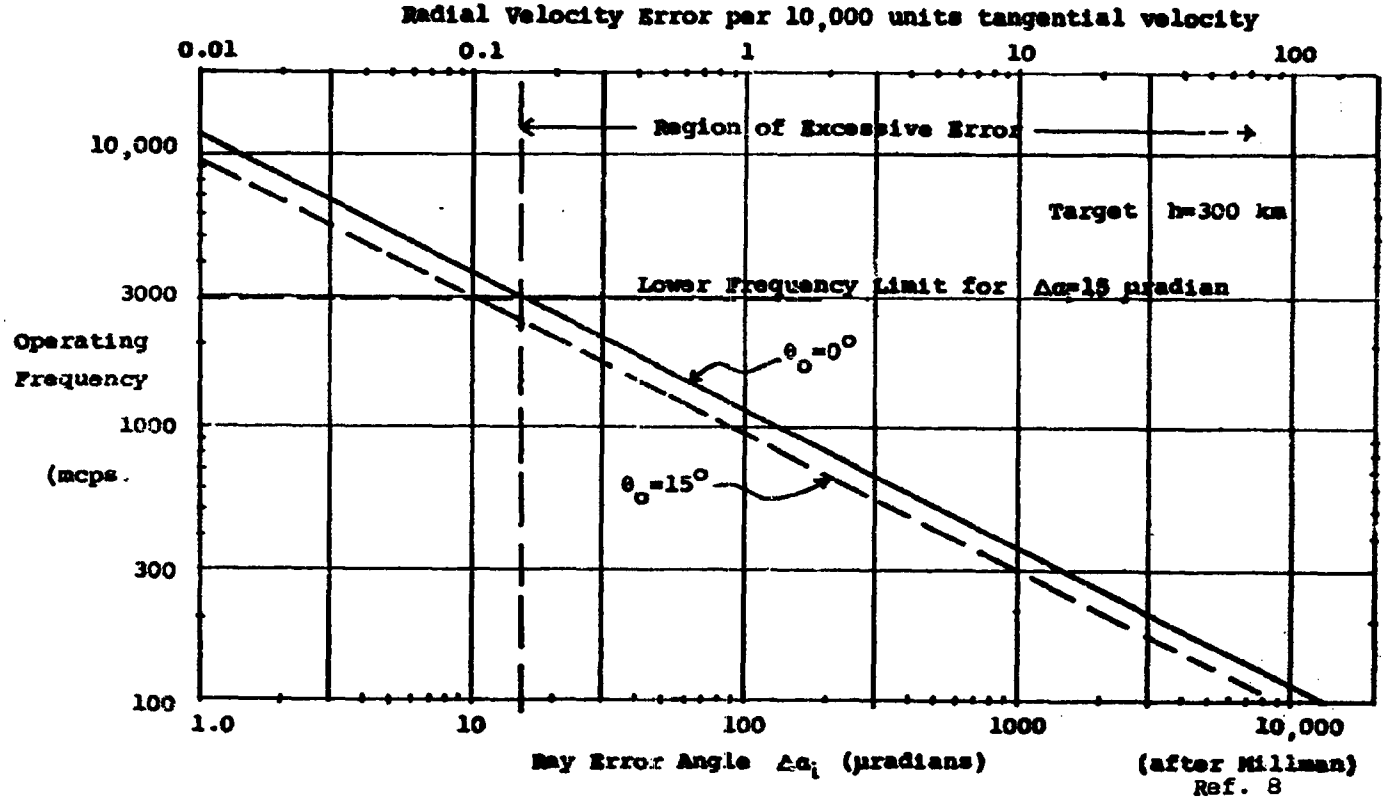

Figure 13. Ray Error Angle vs. Operating Frequency

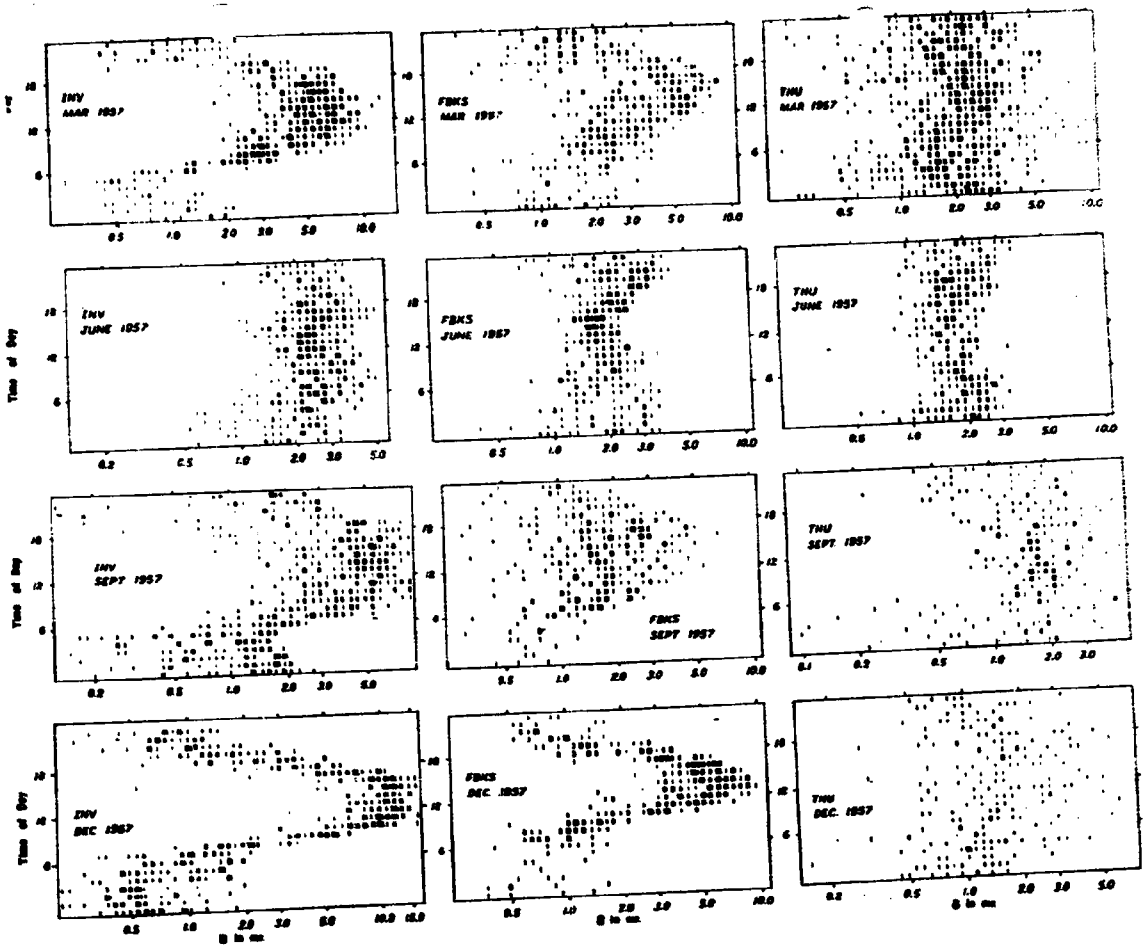

Figure 14. Distribution of ionospheric angle error
(f=100 mcps, θ_o=0, h=1000 n.mi.)
High sunspot activity.

METEOROLOGICAL SUPPORT TO MISSILE TESTS

by:

Lt Col Peter E. Romo

Staff Meteorologist

Presented at

FOURTH JOINT AFMTC-RANGE USER DATA CONFERENCE

Orlando Air Force Base, Florida

26-28 February 1963

323

METEOROLOGICAL SUPPORT TO MISSILE TESTS

Lt Col Peter E. Romo, Staff Met, AFMTC

As background for a discussion of meteorological data on the AMR, I will describe some of the more important relationships between missile testing and weather. I'll do this for the various phases of the missile's testing, from the time it goes up on the pad to the time it impacts downrange.

First of all, a missile may be on the launch pad as much as a year, although in most cases it's only a few weeks. During the time that it's in an upright position, it is highly vulnerable to winds. This includes cross-sectional winds (which might blow it off its pad) and gusts. To explain the latter's effect, it is necessary to understand that the structure of the missile, although apparently imposing and rugged, is really quite light and delicate; this is because, as an example, it would take 60 pounds of fuel to raise into orbit every pound of structure devoted to rigidity or strength. For that reason, the bare minimum of weight is devoted to this purpose. Accordingly, a very thin skin is used and this thin skin can be vibrated by the small-scale variations in the wind-field. If these occur in a certain manner, it's possible that a resonance will be set up in the skin of the vehicle and this could be sufficient to cause severe damage, or even cause destruction of the system.

While in the upright position there is a threat from lightning strikes, which could damage the structure and would certainly damage electronic components. In addition, solid-fuel missiles have a danger from lightning strikes in that the fuel may be ignited.

Low-level humidity and air temperature affect the vehicle while on the pad in that certain of the fuels used can operate only within a limited range of these parameters. Also, certain guidance systems must be kept within a narrow range of temperature, and therefore temperature measurements and forecasts are necessary during the time the missile is on the launch pad.

Once the missile has left its pad in the early stages of its launch, we find that wind is still important, not only for the structural effects as described previously for the stationary position, but also for control and quidance computations. The vehicle's structure is susceptible to the same effects that were present during the portion of the missile's launch-pad testing, due to the usual horizontal-wind gusts and also due to the vertical wind-shear through which the missile will fly. Beside the effect on the structure of the missile, wind variation (shear and speed) can effect the missile's control and guidance systems. To explain these a bit, it's necessary to point out that in its early flight, while it is hovering or just barely beginning to climb, a missile is inherently unstable and one would expect that it would fall over to one side or to the other. This effect is counter-balanced by adjusting the thrust so as to create a force in the opposite direction. However, in all systems, there is only a certain amount of control available. If the wind-shear or wind-speed appear likely to overcome

the capability of the thrust components to correct variations in the angle of attack, then the test must be postponed until a more favorable time.

Density figures into this phase of the vehicle's flight in that it's really a combination of density and wind which will decide the overall effects on the structure and control guidance, as well as on thrust. In particular, there is an area (which varies between 20,000 and 40,000 feet for the various missiles) where the most critical Q-area (dynamic-pressure area) occurs, and density must be measured in order to forecast/analyze the effect of this high-Q area.

In describing the effect of humidity, it's necessary to go back to explain the function of the Range Safety Officer on any missile test. It's his responsibility to decide when the missile is passing beyond safe limits, e.g., when it might endanger populated areas, and he must destroy the vehicle as necessary to allow all debris to fall in safe areas, considering the effect of the wind on the descending debris. To give him the data on which to base these decisions, missile ranges are equipped with high-accuracy tracking systems. These are pulse radar or continuous-wave systems such as the MISTRAM, but in any case, they are highly accurate and very expensive. However, these systems do not become effective until the missile has passed through the first 2000 ft (approximately) of atmosphere. Below that level, blast effects and ground clutter distort the image and the Range Safety Officer cannot rely on the data from these tracking systems. For this lowest level of the flight, he must rely on visual tracking of the missile and this implies a knowledge of clouds and visibility.

Even after the missile has passed through the first 2000 feet, the data can be extremely accurate only if there is some knowledge of the index of refraction for the path between the missile and the tracking systems. As an example of the possible effects of this parameter, the specified accuracy claimed for the MISTRAM (Missile Tracking and Measurement) system is about 3 parts per million for the cosine angles. In contrast to that stated accuracy, the uncertainties in the atmosphere can cause errors of as much as ten parts per million, or three times the tolerances of the basic system.

Finally, the effect of temperature, although secondary in the launch phase, is still of some importance. Temperature figures into computations of thrust and drag and therefore most tests require some knowledge of the temperature field through which the missile passes, at least for the lowest 100,000 feet of the atmosphere.

During the mid-flight phase of the test, tracking data are required and this implies that humidity data are needed to compute the effect of the index of refraction on the measurements. Also, range aircraft fly along this portion of the flight path to gather telemetry data in those areas where neither ships nor land stations are available, so that flying-weather forecasts are necessary. Furthermore, clouds and visibility figure into the operation of ballistic cameras, whose data are used to calibrate the measurements which are gathered by other means.

As the re-entry body nears its impact point, we find that humidity data must be gathered for correcting tracking/impact computations. And now density becomes very important because re-entry heating is partially dependent on density distribution, as is the decay of the orbit in the case of a space shot. Clouds and visibility affect the flight of the telemetry aircraft which fly in this part of the flight path in order to take pictures of the re-entry body as it enters the atmosphere and to gather telemetry data during the last phase of the flight. Also, these and other aircraft figure in the recovery operation of capsule and/or man (or animals) in other tests.

Because of the delay in gathering and processing our data, most meteorological data are usually provided for post-flight computations, where they are of great importance. However, forecasts for the parameters which are used for predicting structural and control-guidance effect are often provided in advance of the test in order to run the data through automatic computers to simulate the effects on the system.

These are the major measurements and services currently provided by meteorologists for the average missile test. It is apparent, though, that we must go beyond this in order to support orbital flights and also to support flights which will re-enter from beyond space, beyond our own atmosphere. Also, more sophisticated systems will need equally-sophisticated meteorological measurements and service.

To gather the necessary data, the AMR relies on both the AF's Air Weather Service (AWS) and on PAA's Meteorological Division. The AWS does all forecasting on the AMR and operates the weather station at Patrick AFB. PAA uses approximately 140 men to take weather observations on the major stations of the AMR and on Ocean Range Vessels. AWS and PAA work closely on items of mutual interest, e.g., planning, supply, and supervision of the meteorological operation.

Weather stations have been established at many points along the AMR, at locations where tracking and telemetry stations exist. These weather stations normally provide weather observational data which, when used with other available observations, form the basis for operational forecasting services required to support missile testing on the AMR.

In addition, these stations provide the environmental measurement of atmospheric parameters to help the range users determine what the environment contributed to the missiles' performance.

Of prime importance are the corrective data, such as index of refraction for electromagnetic and optical wavelengths, that are provided so that radar, cw, and optical tracking systems data can be corrected.

Atlantic Missile Range Weather Stations presently active at the launch point, Cape Canaveral, Grand Bahama (200 miles downrange), Eleuthera (310 miles downrange), San Salvador (430 miles downrange), Grand Turk (660 miles downrange), Antigua (1240 miles downrange) and Ascension Island (at 4400 miles downrange). In addition, 5 Ocean Range Vessels, which operate at various seaward locations as needed, also have active weather stations on board.

The following are the day-by-day observations on the AMR to which are added special observations as needed to satisfy our customers' requirements:

A. Surface Observations

1. Twenty-four hour airways, special and local observations from the Cape.

2. Airways, special and local observations from 0900 to 2400 Zulu from Grand Bahama, San Salvador, Grand Turk and Antigua.

3. Three and six hourly synoptic observations from Grand Bahama, San Salvador, Grand Turk and Antigua.

4. Six hourly synoptic observations from the Ocean Range Vessels when they are at sea.

B. Rawinsonde Observations

1. Four rawinsonde observations daily from Cape Canaveral.

2. Two rawinsondes and two pilot balloon observations daily from Grand Bahama, San Salvador, Grand Turk and Antigua.

3. Two pilot balloon observations daily at 0000Z and 1200Z from Ocean Range Vessels while they are at sea.

C. Meteorological Rocket Observations will be furnished with data to be available on a climatological basis from Antigua, Grand Turk and San Salvador. These rockets are fired in support of missile tests and the Meteorological Rocket Network. Data are available to 200,000 feet.

All range rawinsonde data are reduced in our central facility, which is equipped with an electronic digital computer. 700 - 500 and 200-millibar data are transmitted by this unit for each rawinsonde at 0200 Zulu plus each 6 hours for the Cape and at 0200 Zulu plus each 12 hours for the other range stations through Antigua.

Our meteorological data are processed according to the desires expressed by the range customer, and are distributed to the agencies listed in AMR documents. Handling and distributing these data are becoming increasingly complex as more and more customers ask for data, but the AMR is happy to provide them to all users.

AFMTC STAFF METEOROLOGIST

BRIEFING

AFMTC / RANGE USER
DATA CONFERENCE
FEB 1963

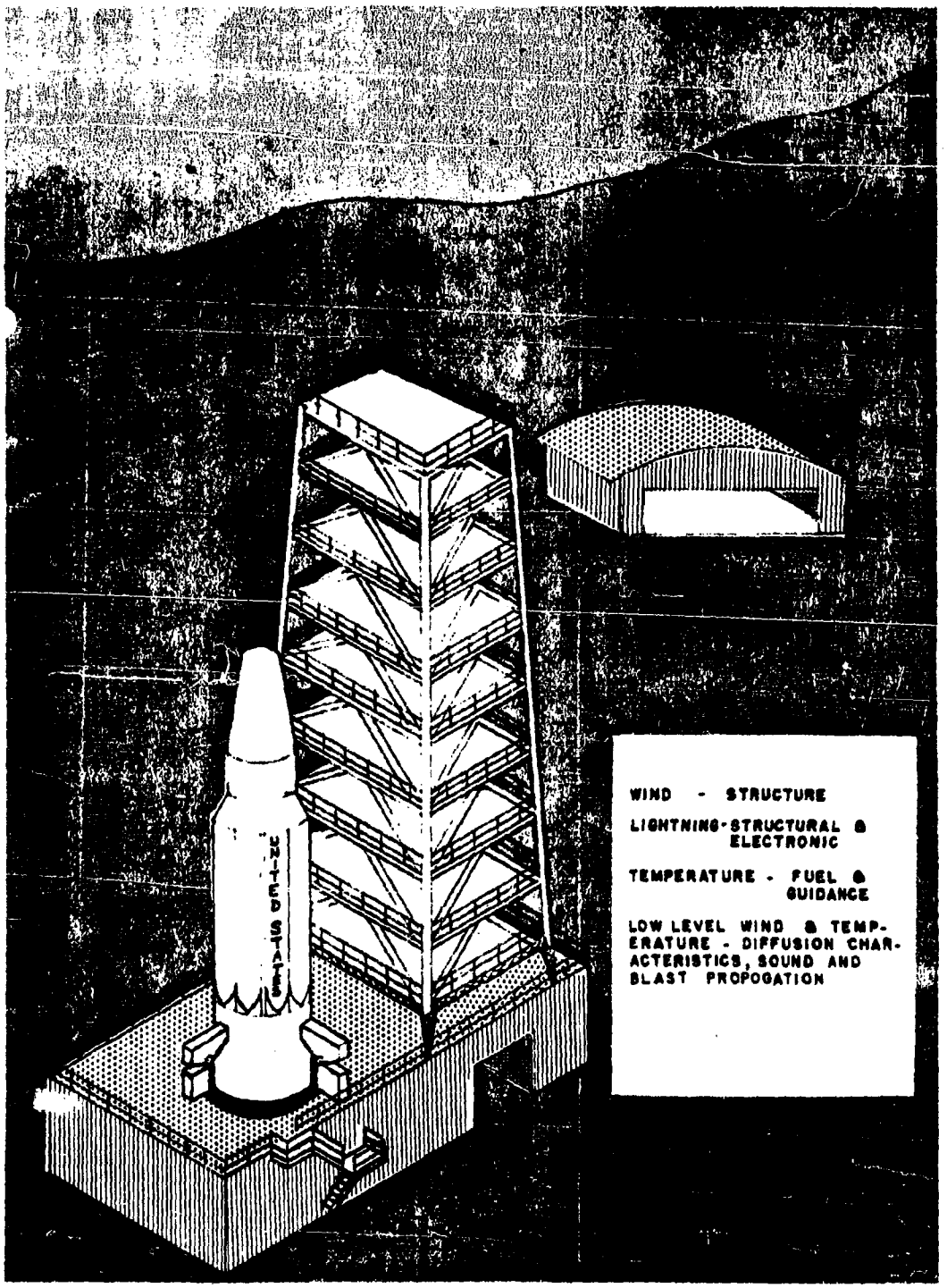
UNITED STATES
WIND - STRUCTURE
LIGHTNING - STRUCTURAL & ELECTRONIC
TEMPERATURE - FUEL & GUIDANCE
LOW LEVEL WIND & TEMPERATURE - DIFFUSION CHARACTERISTICS, SOUND AND BLAST PROPOGATION

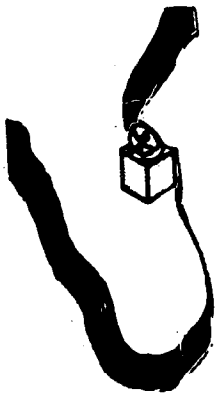

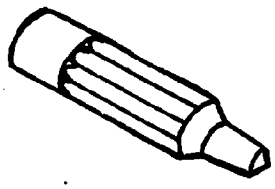

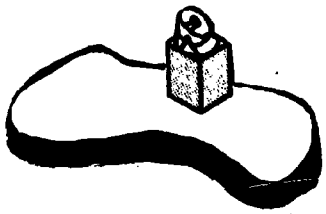

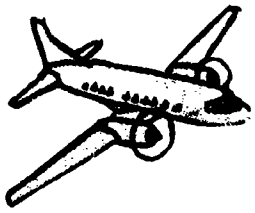

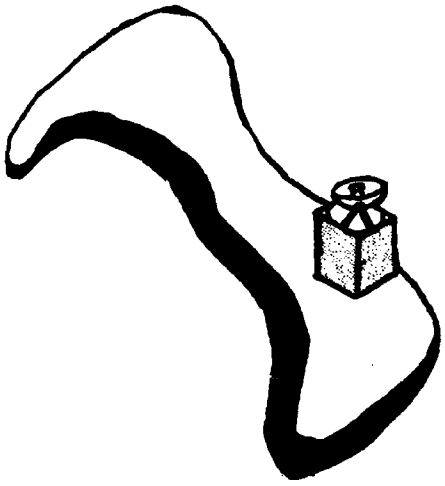

HUMIDITY - TRACKING

CLOUD / VISIBILITY - TELEMETRY AIRCRAFT, AND OPTICAL COVERAGE

WIND	STRUCTURE, CONTROL/GUIDANCE
DENSITY	STRUCTURE, CONTROL/GUIDANCE AND THRUST.
CLOUD & VISIBILITY	RANGE SAFETY AND OPTICAL COVERAGE.
TEMPERATURE	THRUST/DRAG.
HUMIDITY	TRACKING ACCURACIES

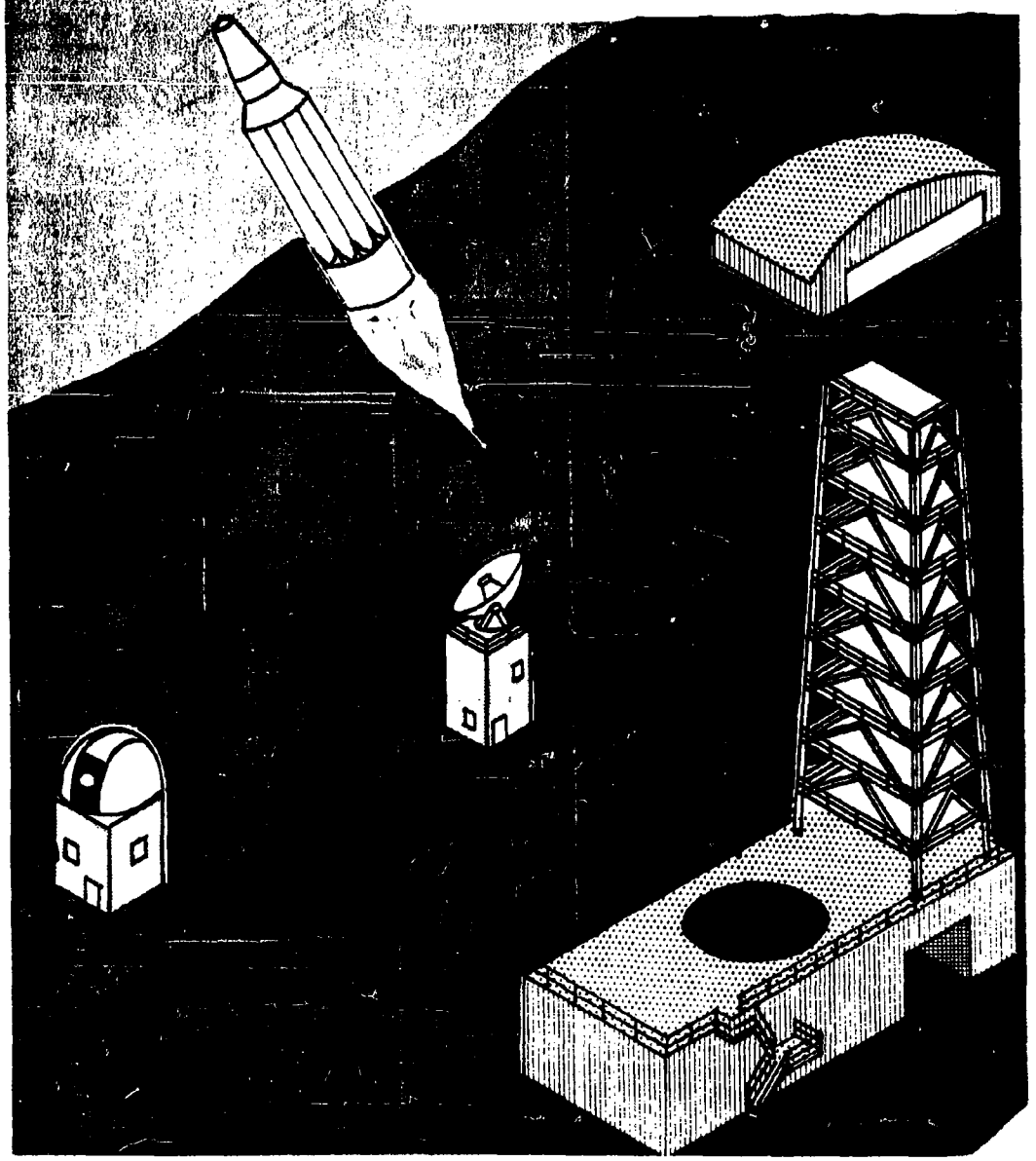

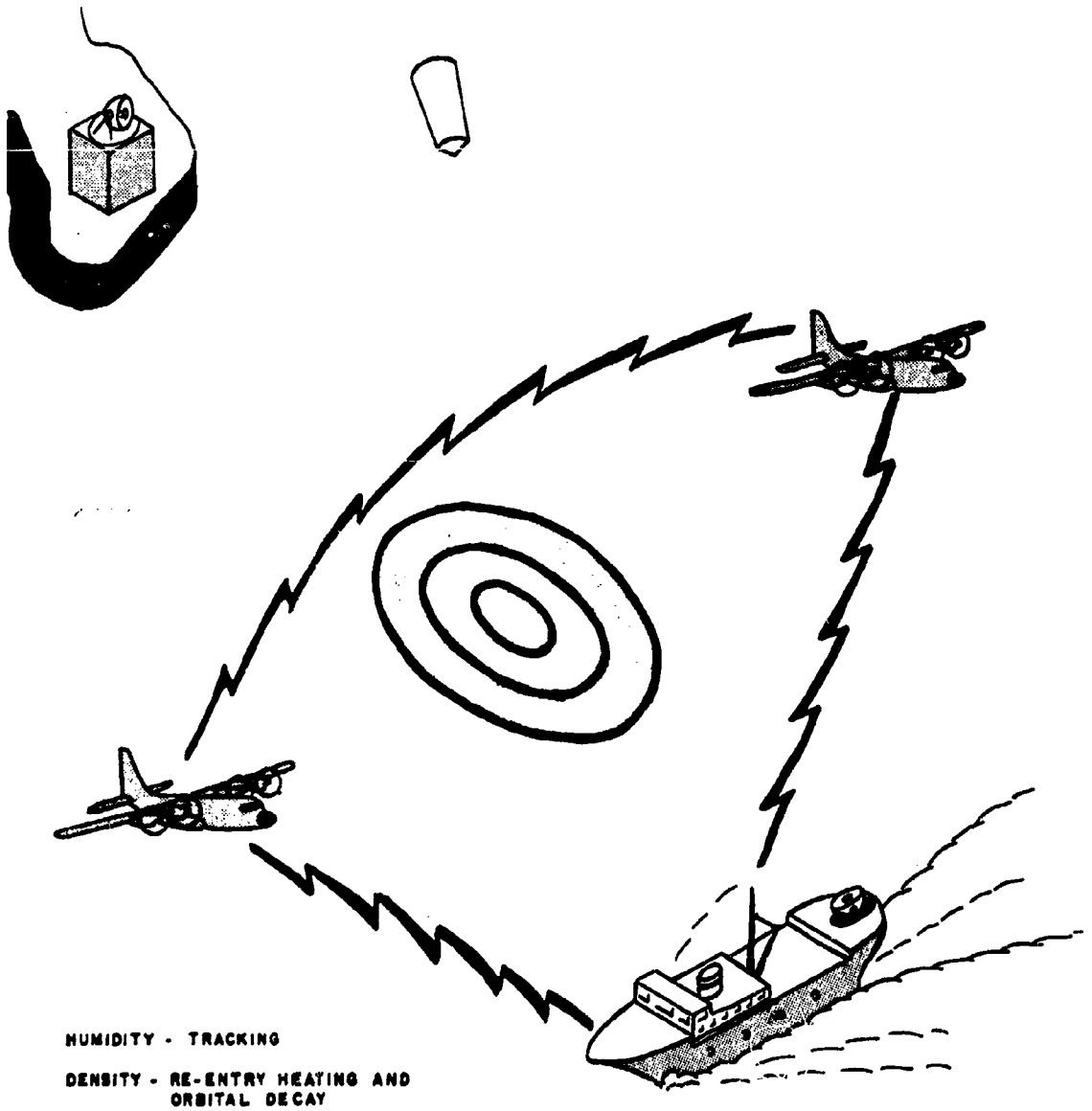

HUMIDITY - TRACKING

DENSITY - RE-ENTRY HEATING AND ORBITAL DECAY

CLOUD / VISIBILITY - TELEMETRY AIRCRAFT AND OPTICAL COVERAGE

STATE OF SEA - RECOVERY OPERATIONS

WEATHER FUNCTIONS

ON THE

ATLANTIC MISSILE RANGE

AFMTC REG 105-1

(55→63)

CONSULTANT SERVICES
ALL FORECASTS
PAFB WEATHER STATION
MONITOR CONTRACTOR

(≈150)

ALL AMR OBSERVATIONS
INSTRUMENTATION
MET DATA REDUCTION

PLANNING & DEVELOPMENT
SUPPLY
MAINTENANCE

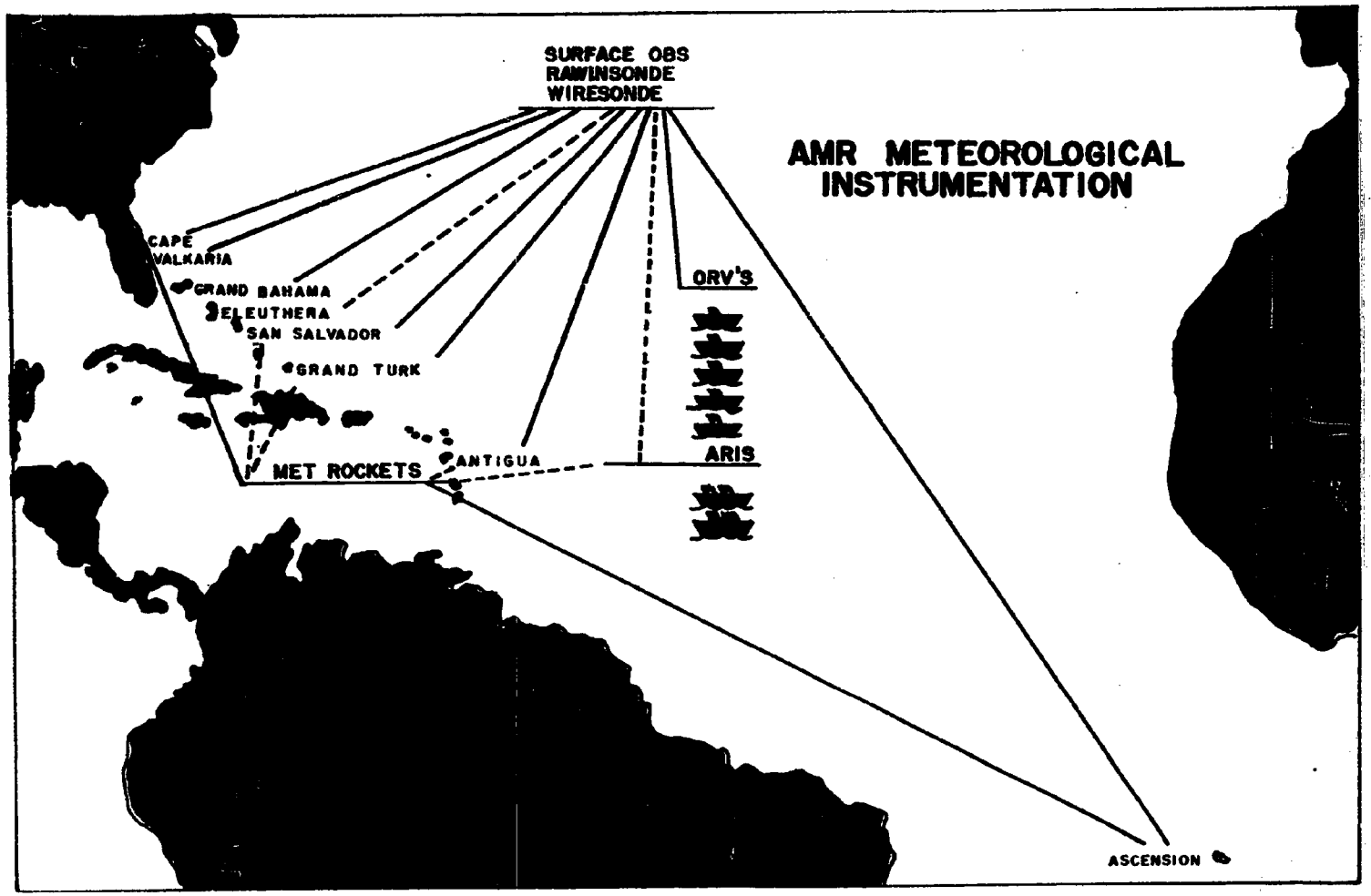
SURFACE OBS
RAWINSONDE
WIRESONDE
AMR METEOROLOGICAL
INSTRUMENTATION
CAPE
CANAVERAL
GRAND BAHAMA
ELEUTHERA
SAN SALVADOR
GRAND TURK
ORV'S
ARIS
MET ROCKETS
ANTIGUA
ASCENSION

RAWINSONDE RUN
CAPE CANAVERAL MTA, FLA.
1705Z 31 JAN 1963
ASCENT NBR 0142

ALT FT.	WDIR	WKTS	TEMP	DEW PT	PRES	RH	AB HUM	DEN	IR	VS
16	240	8	24.0	14.5	1021.3	54	11.95	1190.1	336	678
1000	269	10	20.0	12.4	986.8	60	10.58	1165.9	322	667
2000	278	13	17.9	11.0	952.4	65	9.73	1138.3	311	664
3000	289	17	16.1	10.0	919.0	66	9.18	1101.2	300	662
4000	299	18	14.8	9.2	886.6	69	8.75	1067.4	291	661
5000	300	13	13.5	6.6	855.3	62	7.35	1034.9	278	659
6000	290	11	12.1	5.8	824.9	65	6.97	1003.1	466	658
7000	292	15	9.6	4.4	795.3	70	6.42	975.9	257	655
8000	291	19	6.9	2.6	766.5	73	5.71	949.7	247	652
9000	288	19	4.8	- .5	738.6	67	4.58	922.7	234	649
10000	291	19	2.8	- 4.3	711.5	59	3.50	895.8	221	647
11000	298	19	1.2	- 8.8	685.1	47	2.50	868.2	209	645
12000	292	17	.0	-22.3	659.6	21	1.08	840.3	194	643
13000	288	19	- 1.2	-30.1	635.0	8	.39	813.3	183	642
14000	296	23	- 2.6	99.9	611.0	99	99.99	786.8	175	640
15000	301	27	- 4.1	99.9	588.0	99	99.99	761.5	169	638
16000	298	29	- 4.9	99.9	565.7	99	99.99	734.8	163	637
17000	292	29	- 6.7	99.9	544.1	99	99.99	711.4	158	635
18000	284	29	- 8.7	99.9	523.3	99	99.99	689.4	153	633
19000	281	34	-10.4	99.9	503.0	99	99.99	666.9	148	631
20000	280	38	-12.5	99.9	483.4	99	99.99	646.2	143	629

	CAPE		GRAND BAHAMA		SAN SALVADOR		ANTIGUA		ASCENSION		ORV		TOTALS
	TIME	OUTPUT	TIME	OUTPUT	TIME	OUTPUT	TIME	OUTPUT	TIME	OUTPUT	TIME	OUTPUT	
SURFACE OBSERVATIONS	NEAREST SYNOPTIC OBSERVATION BEFORE & AFTER LAUNCH										HOURLY FROM T-6	*	3 COPIES
	T-0	*	T-0	*	T-0	*	IMPACT	*	IMPACT	*	IMPACT & T+20	*	
UPPER AIR OBSERVATIONS	NEAREST SYNOPTIC OBSERVATION BEFORE & AFTER LAUNCH 5 TABS, 3 CARD DECKS, & 1 MULTIMAT FOR EACH STATION												50 TAB COPIES 30 CARD DECKS 10 MULTIMATS
	T-0	3 TABS 4 CARDS 1 MAT	T-0	3 TABS 4 CARDS 1 MAT	T-0	3 TABS 4 CARDS 1 MAT	IMPACT	3 TABS 4 CARDS 1 MAT	IMPACT	3 TABS 4 CARDS 1 MAT	IMPACT	3 TABS 4 CARDS 1 MAT	18 TAB COPIES 24 CARD DECKS 6 MULTIMATS
MET ROCKET DATA	T+120	3 TABS 1 MAT							T+150	3 TABS 1 MAT			6 TAB COPIES 2 MULTIMATS

DEADLINE: QUICK LOOK T+7 HRS
FINAL DISTRIBUTION T+12 HRS

* SURFACE OBSERVATIONS ARE MANUALLY REDUCED TO A SINGLE CHRONOLOGICAL LISTING BY GEOGRAPHICAL LOCATION.

SUB TOTALS	
23 SURFACE OBS	3 COPIES
16 UPPER AIR OBS	68 TAB COPIES 54 CARD DECKS 16 MULTIMATS
2 MET ROCKETS	8 TAB COPIES 2 MULTIMATS
GRAND TOTALS	3 COPIES SFC OBS 74 TAB COPIES 54 CARD DECKS 18 MULTIMATS

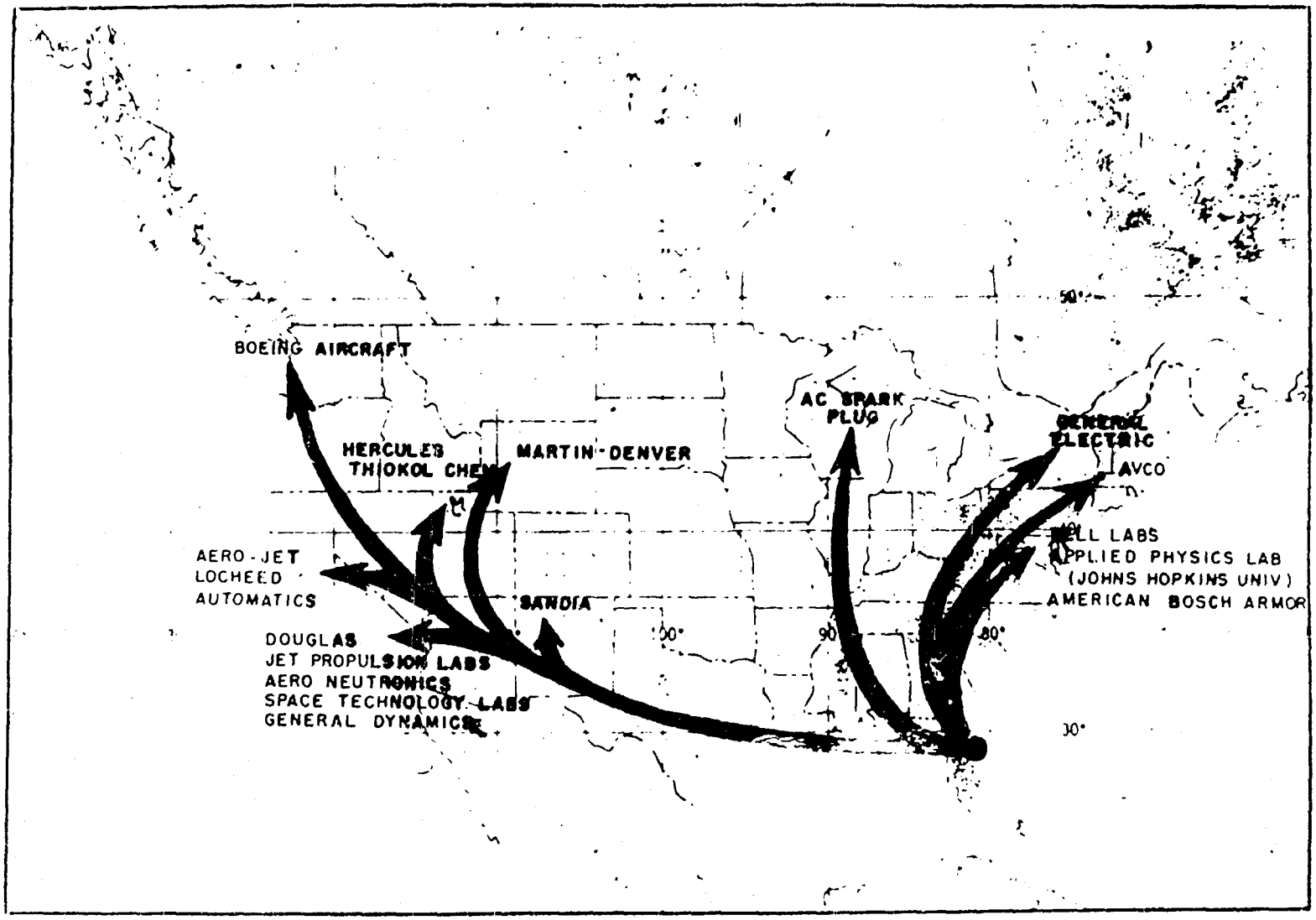
BOEING AIRCRAFT
HERCULES
THIOKOL CHEM
MARTIN-DENVER
AC SPARK PLUG
GENERAL ELECTRIC
AVCO
AERO-JET
LOCHEED
AUTOMATICS
SANDIA
DOUGLAS
JET PROPULSION LABS
AERO NEUTRONICS
SPACE TECHNOLOGY LABS
GENERAL DYNAMICS
LL LABS
PPLIED PHYSICS LAB
(JOHNS HOPKINS UNIV)
AMERICAN BOSCH ARMOR
50°
90°
80°
30°

CALIBRATION SATELLITE

by

ARMANDO MANCINI
Air Force Cambridge Research Laboratories

D. C. BROWN
D. Brown Associates, Inc.

Presented at the
Fourth Joint AFMTC/Range User Data Conference
26 - 28 February 1963
Orlando Air Force Base Conference Facility
Orlando, Florida

Geodesy and Gravity Branch
Terrestrial Sciences Laboratory
Air Force Cambridge Research Laboratories

CALIBRATION SATELLITE

FEBRUARY 1962

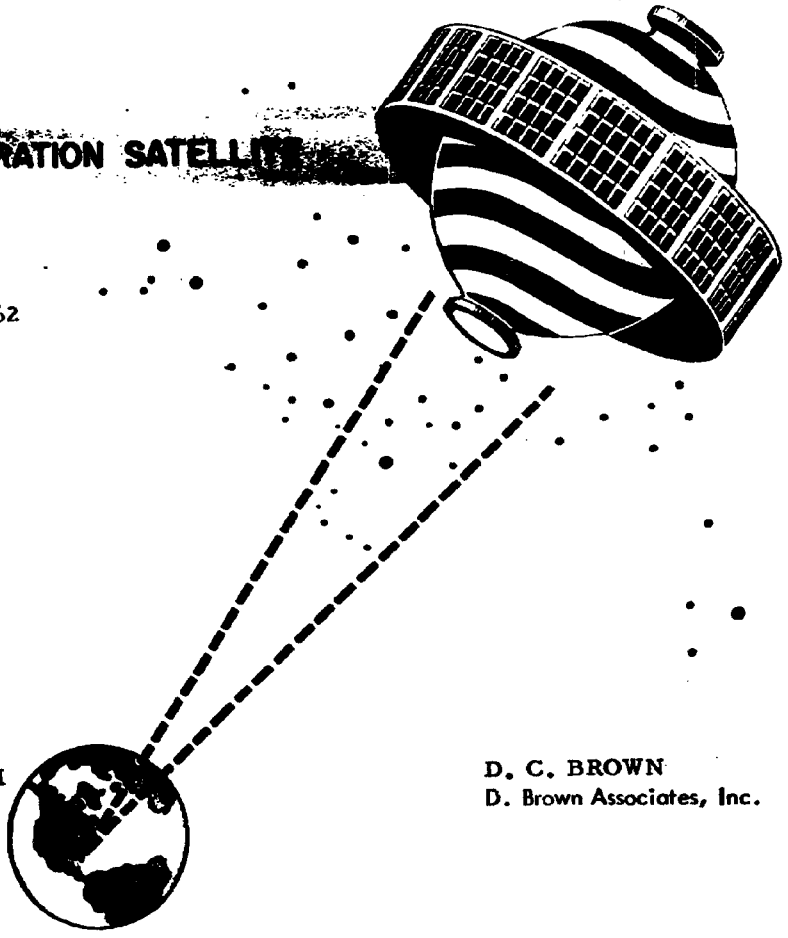

ARMANDO MANCINI
Air Force Cambridge
Research Laboratories

D. C. BROWN
D. Brown Associates, Inc.

Introduction:

Our interest in calibrating range instrumentation involves the development of a system which can serve as a calibration tool for all DOD missile test ranges. This system must have a general application such that it is not closely tied to the relative distribution of the tracking net; it will serve to calibrate several electronic systems at the same time; and is capable of checking system performance over the ranges and velocities for which the equipment was developed and will be operating. We would hope that when the tool is built and tested, the ranges would utilize it not only for their immediate calibration needs, but use it also to maintain and improve the calibration parameters. Perhaps as system performances improve, such a satellite or satellites can serve as a standard in space such that the electronic systems can use it as a pre and post calibration device during actual missile tests much the same way that the optical sy[illegible] uses the stars.

Missile Application:

Before we discuss some preliminary aspects of the satellite calibration concept, let us briefly consider the possibility of using missiles to accomplish the same task. Since the interests of this group are related to the AMR, we will restrict our remarks mostly to this range. As indicated previously, there are two MISTRAM Systems on the Range, one at Valkaria and the other on Eleuthera. It would be reasonably easy to design a series of missile shots between the two MISTRAM stations shown in Figure 1 carrying a MISTRAM transponder to perform the calibration. These stations are sufficiently close such that one trajectory can produce equally valuable observations for each site. It is not known exactly how many shots would be required, but it appears that six trajectories well distributed in azimuth and altitude would be a conservative estimate.

Let us now enlarge the picture and consider the GLOTRAC System. We note from Figure 2 that these sensors extend further down-range and cover a much wider area than MISTRAM. Based purely on the relative distribution of this network, it is obvious that a GLOTRAC calibration would require many more missile shots. Even if a combined MISTRAM-GLOTRAC calibration is assumed, the addition of Bermuda and Cherry Point would add at least three trajectories to the initial six, in order to satisfy the northerly azimuth direction of these stations. If we go beyond MISTRAM and GLOTRAC and incorporate C-band radar sites extending to South Africa, the rocket concept soon reaches an impractical number of missiles and an unreasonable amount of work.

S[illegible]llite Application:

Inasmuch as satellite calibration calls for very precise predictions, the utilization of such objects generally raises doubts as to the accuracy of orbit calculations. This is a natural reaction in view of the fact orbital work involves the use of a model and this particular model is far from perfect at the present time. Although this is a serious factor for normal orbit updating over a two or three day period, the effect of the error can be completely minimized by the application of very short arcs.

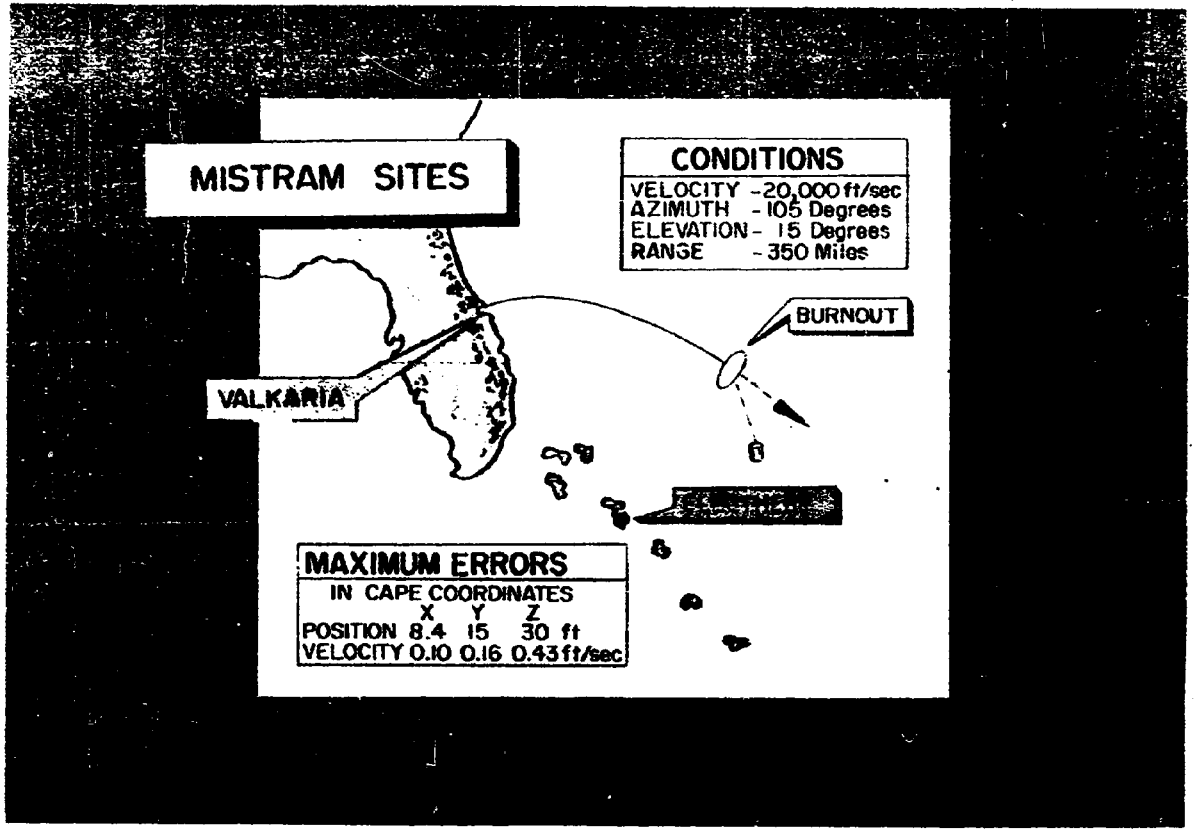
MISTRAM SITES
CONDITIONS
VELOCITY - 20,000 ft/sec
AZIMUTH - 105 Degrees
ELEVATION - 15 Degrees
RANGE - 350 Miles
BURNOUT
VALKARIA
MAXIMUM ERRORS
IN CAPE COORDINATES
X Y Z
POSITION 8.4 15 30 ft
VELOCITY 0.10 0.16 0.43 ft/sec

FIGURE 1

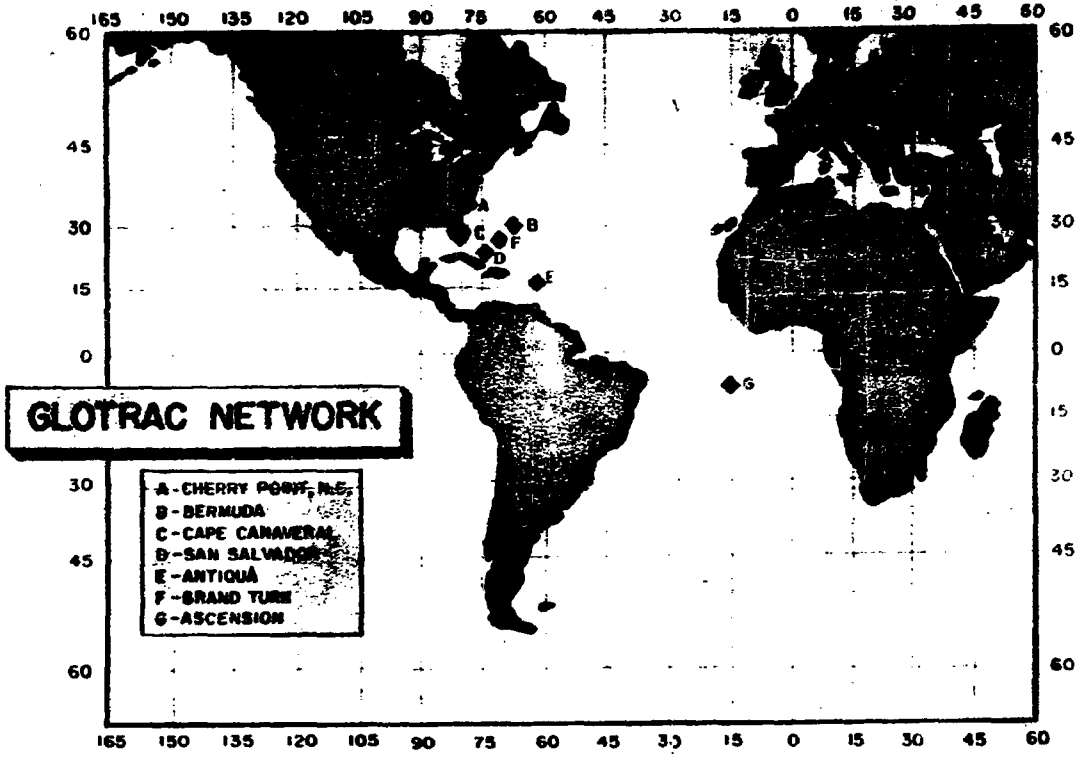
GLOTRAC NETWORK
A - CHERRY POINT, N.C.
B - BERMUDA
C - CAPE CANAVERAL
D - SAN SALVADOR
E - ANTIGUA
F - GRAND TURK
G - ASCENSION
165 150 135 120 105 90 75 60 45 30 15 0 15 30 45 60
60 45 30 15 0 15 30 45 60

FIGURE 2

As a rule, the model for satellite predictions should account for the following perturbations.

a. Those created by the gravitational field, i.e. the potential expression should carry at least the first five zonal terms, the pair of sectorial (degree two-order two), and the pair of tesseral harmonics of degree four-order one.

b. Those due to atmospheric drag accounted for by integrating step by step along the orbit instead of making an average correction over one revolution.

c. Those due to solar radiation pressure; allowing for perigee in sunlight or darkness, and

d. Perturbations due to the attraction of the sun and moon.

In short arc applications, only the first factor becomes significant. The other perturbations can be minimized by selecting appropriate altitudes such that the mechanical effect due to drag and the gravitational effect from the sun and moon are essentially zero. Solar radiation can be circumvented by using a satellite with a small area-to-mass ration (less than 1 cm^2/gm) and to some degree by fabricating the satellite in a spherical form.

The expression in Figure 3 represents the only source of satellite perturbation which must be applied for short arcs on the order of 3000 or 4000 nm. The first part $(\frac{U}{r})$ denotes the two body term, the second term represents the latitude dependent factors (zonal harmonics) and the last term defines the tesseral harmonics which depend both on latitude and longitude. The P_{nm}'s are conventional associated Legendre functions, ϕ is the geocentric latitude, J_{nm} K_{nm} are coefficients, a_e is the radius of the earth and r is the geocentric radius to the satellite. Values for the zonal and tesseral coefficients have been derived from satellites and terrestrial gravity data by many sources. Presently there are good estimates for the zonal terms up to J_6 and few tesseral terms such as given in Figure 3. Other high-order coefficients are also available, but in most cases the uncertainties in these values are still rather large.

Short Arc Orbital Prediction:

It is now of interest to establish just how much of the potential expression can be truncated for typical MISTRAM or GLOTRAC calibration. In order to perform this investigation, it was assumed that the inclination of the satellite was 40 degrees, the altitude was 400 nautical miles, the eccentricity approximately zero, the weight of the satellite approximately 350 pounds, and the diameter of the satellite approximately one meter. These assumptions are consistent with the criteria given earlier to minimize orbital perturbations (other than the effect of U) and also to provide a maximum number of observations by selecting an inclination which follows the general trend of the tracking sites.

The results of this study are tabulated in Figure 4. The first four columns in this figure show the time since epoch and the corresponding space position of the satellite when all five zonal terms

THE EARTH'S GRAVITATIONAL POTENTIAL

$$U = \frac{\mu}{r}\left\{1 - \sum_{n=2}^{\infty}\left(\frac{a_e}{r}\right)^n\left[J_n P_n(\sin\phi) + \sum_{m=1}^{n}\left(J_{nm}\cos m\lambda + K_{nm}\sin m\lambda\right)P_{nm}(\sin\phi)\right]\right\}$$

$J_2 = (1082.3 \pm 0.2) \times 10^{-6}$

$J_3 = (-2.3 \pm 0.1) \times 10^{-6}$

$J_4 = (-1.8 \pm 0.2) \times 10^{-6}$

$J_5 = (-0.3 \pm 0.2) \times 10^{-6}$

$J_{22} = (-0.06 \pm 0.19) \times 10^{-6}$

$K_{22} = (2.24 \pm 0.19) \times 10^{-6}$

$J_{41} = (0.25 \pm 0.04) \times 10^{-6}$

$K_{41} = (0.06 \pm 0.03) \times 10^{-6}$

FIGURE 3

EFFECT OF ZONAL HARMONICS AND DRAG

Time*	Position in Meters**			CHANGE IN POSITION IN METERS DUE TO														Drag		
				$J_5 = 0$			$J_5 = J_4 = 0$			$J_5 = J_4 = J_3 = 0$			$J_5 = J_4 = J_3 = J_2 = 0$							
	X	Y	Z	ΔX	ΔY	ΔZ	ΔX	ΔY	ΔZ	ΔX	ΔY	ΔZ	ΔX	ΔY	ΔZ	ΔX	ΔY	ΔZ	ΔX	ΔY	ΔZ
1	-5,858,953.8	-1,141,429.3	3,971,378.6	0	0	0	.1	0	0	.1	0	.1	0	0	0						
4	-5,813,648.5	-2,380,860.7	3,472,729.3	.1	0	0	.7	.1	0	1.1	.5	.6	115.8								
6	-5,439,825.3	-3,697,530.8	2,623,007.6	.1	.1	.1	2.6	.8	.4	3.4	1.2	1.1	202.2								
12	-4,731,200.7	-5,174,372.9	1,611,418.1	.2	.2	.2	5.0	1.9	1.8	8.5	4.0	3.8	0								
16	-3,732,008.4	-6,133,463.3	500,597.7	.2	.2	.2	7.9	3.0	3.8	15.6	8.3										

* The period of 16 minutes represents 4000 N. M. segment of the orbit

** Using Five Zonal Harmonics J_2, J_3, J_4, J_5

FIGURE 4

are taken into account. The subsequent columns show the deviation from the X, Y, Z coordinates of the satellite as the J_5 , J_4, J_3, and J_2 terms are set to zero. The last three columns show the effect due to drag. A 4000 nm segment of the orbit (16 minutes) was selected in order to establish the error in the predictions as the satellite traveled from Valkaria to Ascension.

It can be concluded from this table that terms on the order of J_4 or larger must be carried in the prediction process. Although the deviations offer 16 minutes for $J_5 = J_4 = 0$ are 7.3m, 3.0m, and 3.8m in X, Y, and Z, these errors can be reduced by fitting an ellipse with the epoch at 8 minutes instead of zero minutes and distributing the error up and down range. Obviously, the arc required for the MISTRAM calibration would probably be on the order of 6 minutes and for that period of time the main term ($\frac{U}{r}$) and the second zonal (J_2) are the only terms required. The same type of analysis can be made in regard to the tesseral harmonics. It is very likely that the $J_{nm} K_{nm}$ terms where $(n, m) \leq 3$ must also be employed, but these should constitute the extent of the model.

Observations from Satellite Passes:

So far we have assumed that exact orbital elements are known at some instant that the satellite approaches the calibration area and with these elements we have generated an ephemeris as the satellite travels down range. Actually, in real operations the reverse is true; i.e. only approximate elements are known during the approach phase and the observations made over the calibration area are used to make a least squares adjustment of the elements. This being the case, it becomes obvious that the observation program including station distribution, observation geometry, redundancy in observation, type of equipments and their accuracies, etc., are all extremely important to this problem. We have not completed a thorough analysis of all these factors, but we can show you the wide variation of observations made possible by using a satellite.

Figure 5 shows a typical satellite coverage for part of the AMR. The right ascension of the node of the orbit and the right ascension of the sun were selected such that the down range passes occur at night and the south to north passes occur during the day. A station centrally located in the area of this diagram can observe 45 of the 105 passes over a period of seven days. Moreover, half of these passes can be observed optically as well as electronically. This figure definitely points out the geometric variations and long period sampling of observation for the satellite over the missile concept. In addition, this observation pattern remains essentially unchanged for other areas under the arc (40° N to 40° S for i = 40° and over all longitude) and if the life of the satellite is assumed to be six months to one year, the coverage becomes absolutely saturated with good passes.

Let us now examine in more detail the type of observation available from these passes. Figure 6 and Figure 7 represent 'the heavy lined' path (pass number 35) shown in Figure 5 as seen first from Valkaria and then as seen from Valkaria and Eleuthera. We can note from these diagrams that these orbits provide excellent geometry, long data sampling periods, large variations in range measurements, almost complete overlap in observations, and optimum conditions for optical measurements. The optical observations in the former diagram occur between t = 5 minutes and t = 10 minutes and in the latter figure between the two shaded

CALIBRATION PASS COVERAGE FOR AMR

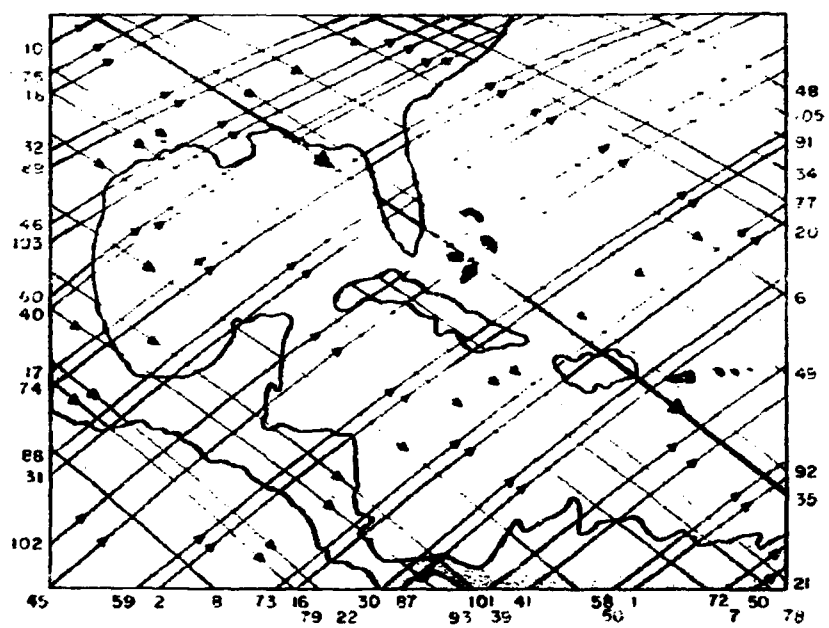

FIGURE 5

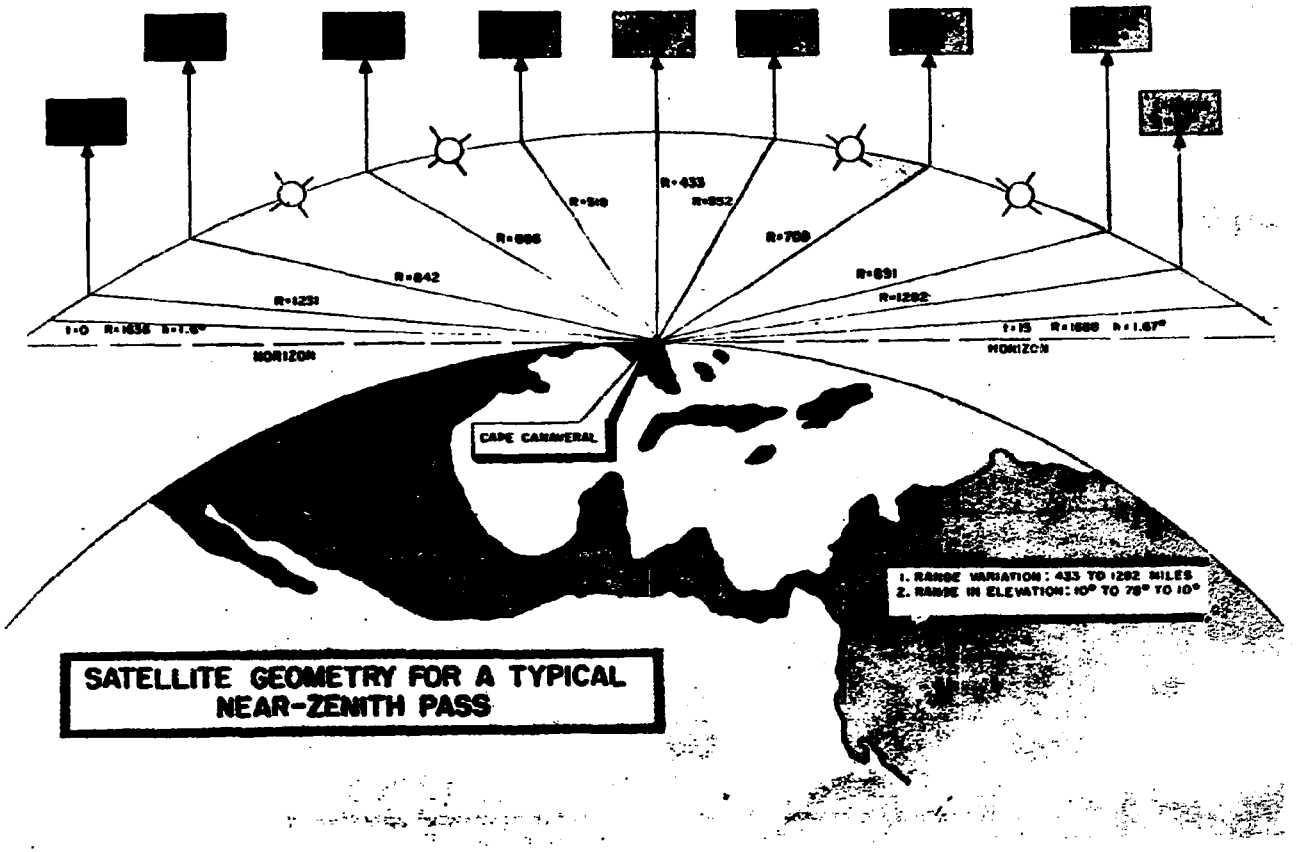
R=433
R=852
R=709
R=891
R=1282
R=842
R=1231
HORIZON
HORIZON
CAPE CANAVERAL
1. RANGE VARIATION: 433 TO 1282 MILES
2. RANGE IN ELEVATION: 10° TO 78° TO 10°
SATELLITE GEOMETRY FOR A TYPICAL NEAR-ZENITH PASS

FIGURE 6

COMMON OBSERVATIONS
BETWEEN OPTICAL AND ELECTRONIC MEASUREMENTS

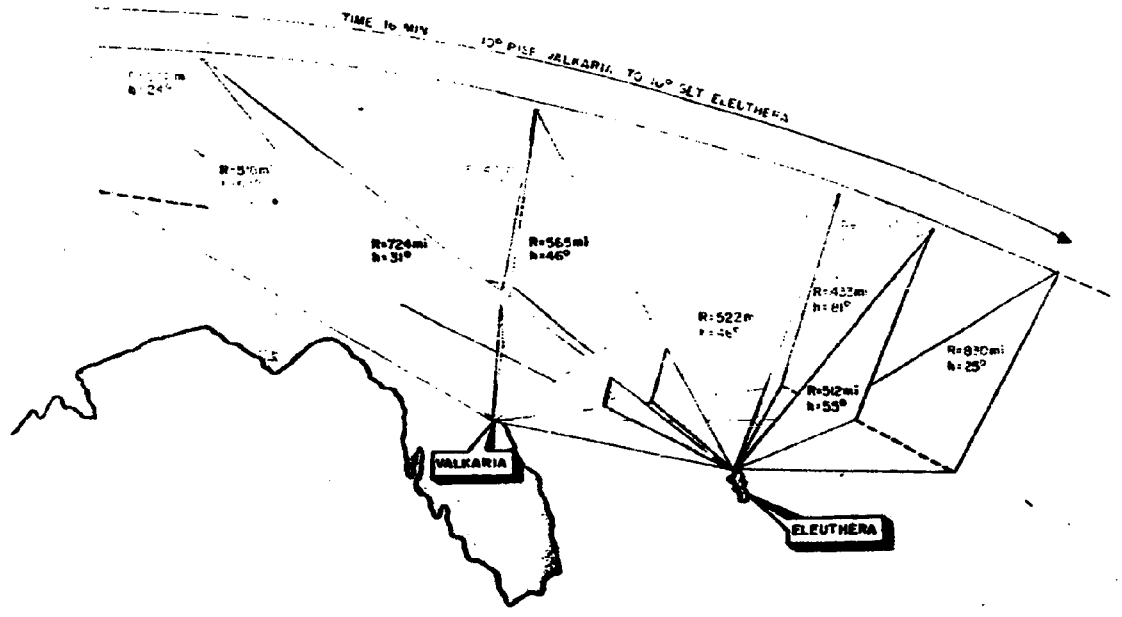

FIGURE 7

planes (from h = 31° elevation to h = 55° elevation from Eleuthera). This interval also represents that portion of the orbit where simultaneous optical observations can be made from both stations. The electronic overlap occurs between h = 24° for Valkaria and h = 25° at Eleuthera with the minimum observed angles at these times being 10° for the opposite site. The 10° rise angle at Valkaria and 10° set at Eleuthera represents the 16 minute arc discussed earlier for which gravitational perturbations were analyzed.

The near zenith pass was taken as an example for two reasons: (a) it represents the arc most affected by the U expression (other arcs would be considerably shorter in length) and (b) it shows a wide range of distances which are very essential in isolating MISTRAM error sources. The example also shows that the satellite passes either maximize one effect and minimize the others. If we refer to Figure 5 again, we can see that passes such as number 8, 18, 48, 92 and other near the corners have exactly the reverse effect as (a) and (b) above, while others closer to the center have a tendency to equalize both factors. As will be shown later, the observation redundancy provided by the satellite proves very significant in deriving the error coefficients.

Satellite Instrumentation:

The experiment payload will be limited to the most important electronic AMR missile-ranging transponders -- MISTRAM, GLOTRAC and DPN-66 -- plus a high performance flashing beacon to provide the needed optical data. (Figure 8)

The electronic ranging systems will be operated 3 times daily on the average, and 4 times daily as a maximum. An "operation" will entail a 5-minute warm-up plus a 10 to 14 minute period available for use. This utilization frequency is in keeping with the data acquisition requirements as well as with the distribution of the GLOTRAC, optical, DPN-66 ground stations and the more limited distribution of MISTRAM. The optical system should furnish at least 30 bursts daily. A single burst will consist of 4 flashes minimum, to provide assured identification when photographed against the star background and to maintain accuracy in optical data. Each of these systems will be tied to individual power supply.

The light and all three ranging transponders must be capable of being operated both simultaneously as well as in any sequence so as to permit using the satellite in any one of the several tracking modes. This required flexibility in operation will necessitate an extensive memory and logic system as well as an accurate (good to at least 0.3 milliseconds) clock. The resulting capability to operate with only infrequent injection of commands means that only a single ground injection station will be needed, but an additional back-up station will be provided in the event of memory failure and to provide a manual override for all systems.

Telemetry will be provided to gather the usual operational data as well as to give assurance checks on the operation of transponders and the light.

Stabilization will be required, as undoubtedly will be de-spin. The closer the axis can be stabilized to point downward toward the earth's center, the better will be utilization of high-gain, narrow-beam antennas and light optics. Magnetic stabilization is presently good to 3 degrees, but this may not be sufficiently accurate for antenna orientation required for MISTRAM.

RANGE CALIBRATION SATELLITE BLOCK DIAGRAM

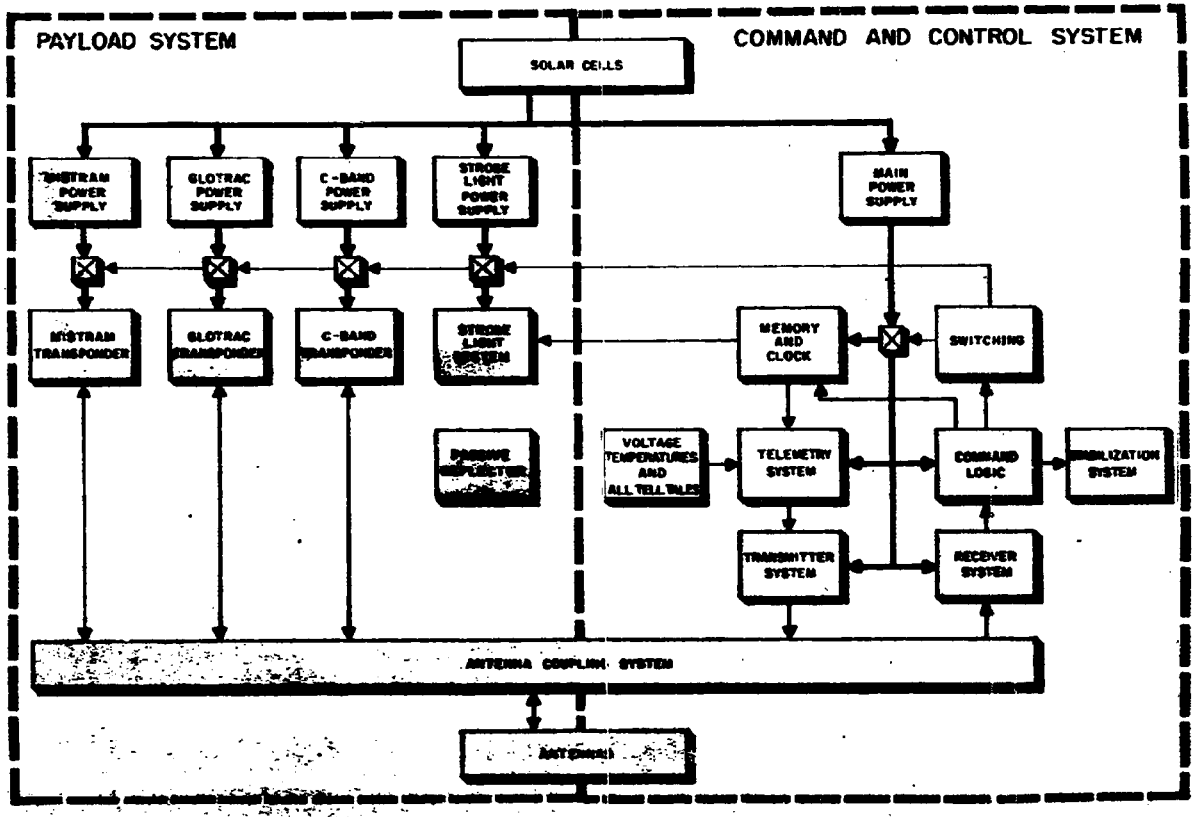

FIGURE 8

Obviously the minimum weight is desired for the satellite, but the practical philosophy will be adopted by using the lightest known and proven components, many of which have been proven during other programs. No attempt will be made to engage in extensive development of new components to wring out the last bit of weight-saving. This reflects the desire to limit costs and get the program going without development-induced delays. A preliminary estimate of satellite weight is shown in Table 1.

Summary:

Before I ask Mr. Brown to make the second part of this presentation, I would like to stress that the missile tracking systems represent a considerable investment of Government funds and are scheduled to play major roles in our missile and space programs. These systems and in particular MISTRAM, also represent the state-of-the-art knowledge in the electronic field in which every practical design refinement was utilized to achieve maximum accuracy. We believe that it is absolutely essential that the capability of these equipments be fully evaluated, improved, and maintained over the years, and we further believe that the satellite concept is the only practical tool to achieve this goal.

TABLE 1
AMR CALIBRATION SATELLITE
PRELIMINARY WEIGHT BUDGET

		Weight in Pounds		
		Min.	Max.	Estimated Attainable
A.	Experiment Payload (Gov't Furn. Equip.)			
	1. Mistram (transponder only)	12.0	16.5	14.0
	2. Glotrac (transponder only)	5.5	7.0	7.0
	3. DPN-66 (transponder only)	8.8	10.5	10.5
	4. Electronic Flash Heads & Controls (2 flash heads, trigger & charging circuitry, capacitors, sequence controller)	30.0	50.0	40.0
B.	Supporting Payload			
	1. Structure (body, solar blades and hinges, thermal insulation, balance weights)	40.0	80.0	70.0
	2. Power Supply (Separate batteries for light transponder and other electronics, solar cells, isolators & regulators)	40.0	95.0	60.0
	3. Stabilization (De-spin, attitude set & stabilizer)	6.0 (magnetic)	30.0	15.0
	4. Command, Logic, Switching, Memory & Clock (Memory, 100% redundant receivers commutator, clock, alternate command system)	25.0	45.0	35.0
	5. Telemetry (Commutator & transmitter)	10.0	15.0	13.0
	6. Antennas (Single system, looking downward only)	2.0	8.0	6.0
	7. Cabling & Harnesses (RF, power distribution & special flashing light cables)	15.0	30.0	20.0
	8. Payload Accessories (Vehicle adapters & misc. interface elements)	5.0	10.0	8.0
	TOTAL	199.3	397.0	298.5

MISTRAM Regression Simulation

Mr. Mancini has shown that the satellite approach to the calibration of tracking systems is attractive from the standpoints of geometry, frequency of suitable passes, global applicability, and operational as well as reductional feasibility. It remains to be demonstrated whether or not a significantly worthwhile calibration can be achieved through satellite observations. A study has recently been initiated to investigate this matter. We shall present some of the preliminary results of this study. The specific problem to be considered here is that of calibrating MISTRAM by means of satellite observations. In order to calibrate any system it is necessary to derive an error model for each channel of observations. The error model adopted for MISTRAM is presented in Figure 10. Each of the unknown parameters of the error model (the a^is) has the specific physical interpretation indicated in Figure 10. We do not consider the proposed error model to be necessarily exhaustive; it is altogether possible that additional terms may be justified by a more thorough systems analysis than that which we have had an opportunity to make thus far. It should be noted that any required corrections which can be made perfectly for all practical purposes are not included in the error model; relativistic corrections and propagation time delays fall in this category. While time does not permit presentation of the derivation of the error model, several remarks are in order. First, the error models for P, Q and R are not necessarily independent, inasmuch as certain of the error parameters may be rigidly interrelated. For instance, the frequency drift coefficients a_3, a_{10}, a_{19} may logically be considered to be equal to each other; the same is true of the timing bias parameters a_5, a_{12} and a_{21}. The frequency bias a_4 may be regarded as being implicit in the parameters a_{11} and a_{21} which also serve to account for first order refractive effects in P and Q. In addition to rigid constraints, certain statistical constraints may be placed on some of the parameters. For instance, the first and second order refraction parameters in the P error model should be very nearly the same as the corresponding parameters in the Q error model. Such knowledge may be exploited by regarding the differences between these parameters as having means of zero and variances of specified magnitude. Similar statistical constraints may be placed on individual error parameters. This makes it possible to exploit a priori knowledge of the likely range of variation of a given parameter to constrain the parameter to lie in probability within specified statistical bounds.

Because certain of the parameters of the P, Q, R error models are interrelated, the parameters of all three error models must be determined simultaneously in a single multiple regression. In order to obtain specific numerical results, we assumed that MISTRAM observed three successive passes of a satellite in a circular orbit, 400 nm high and inclined 40°. Figure 11 indicates the geometry of the passes and the interval of coverage assumed for each pass. The central pass (pass 0) was taken to go, directly over Cape Canaveral. Although MISTRAM can provide P, Q, R data at a rate of up to 20 samples per second, a sampling rate of only one point per five seconds was assumed in the regression. This was done in recognition of the possibility that a significant degree of serial correlation might possibly exist in the observational channels. Since a low sampling rate would be more likely to yield a set of nearly independent observations than would a high sampling rate, the dangers inherent in neglecting serial correlation in a regression analyses are generally minimized if the regression utilizes a low sampling

$$\Delta R = a_1 + a_2 t + a_3 tR + a_4 R + a_5 \dot{R} + a_6 \csc E + a_7 \csc^3 E$$

(Phase Bias; 1st Order Phase Drift; 1st Order Freq. Drift; Frequency Bias; Timing Bias; 1st Order Refraction; 2nd Order Refraction)

$$\Delta P = a_8 + a_9 t + a_{10} tP + a_{11} P + a_{12} \dot{P} + a_{13} P \cot^2 E + a_{14} \lambda_p + a_{15} \mu_p + a_{16} \nu_p$$

(Phase Bias; 1st Order Phase Drift; 1st Order Freq. Drift; Freq. Bias + 1st Order Refrac.; Timing Bias; 2nd Order Refraction; X Survey Error; Y Survey Error; Z Survey Error)

$$\Delta Q = a_{17} + a_{18} t + a_{19} tQ + a_{20} Q + a_{21} \dot{Q} + a_{22} Q \cot^2 E + a_{23} \lambda_Q + a_{24} \mu_Q + a_{25} \nu_Q$$

$$\lambda_p = (X - X_p)/R_p, \quad \mu_p = (Y - Y_p)/R_p, \quad \nu_p = (Z - Z_p)/R_p, \quad R_p = [(X - X_p)^2 + (Y - Y_p)^2 + (Z - Z_p)^2]^{\frac{1}{2}}$$

Possible Constraints:

$a_3 = a_{10} = a_{19}$, $\quad a_{11} = a_4 + \tilde{a}_{11}$, $\quad a_{11} - a_{20} = \theta_1$; $\mu(\theta_1) = 0$, var $\theta_1 = \sigma^2_{\theta_1}$

$a_5 = a_{12} = a_{21}$, $\quad a_{20} = a_4 + \tilde{a}_{20}$, $\quad a_{13} - a_{22} = \theta_2$; $\mu(\theta_2) = 0$, var $\theta_2 = \sigma^2_{\theta_2}$

FIGURE 10

rate. ...tic... the esulti...g est...es ... ...cu...cy ...re l...y to be cons...tive, rather than ov...optimi...ic, it the ...mplin... rate ...ffic...ently lov... c...re seria... ...ependence.

F...urpo...es of the egre...ion s...ulat... the errors in ...cessive values of P, Q, R sample... ...ery 5 se...onds ...ere c...sume... to b... in...ependent with ...tandard deviation... of $\sigma_P = \sigma_Q = 0.3$ f... $\sigma_R = 0.4$ ft.

Nume... Results:

P... al resul...s o... the MIS RAN regre...ion analysis for t... passes of Figure 11 are summarized in Tab... ..., 3 and 4. In orde... o in...re that the regression wo...ld be determinant, we constrained the adj...ment by ...pecify...ng a ...riori standard deviations for ...ch of the parameters as indicated in the f... ...res. Re...ressic...s wa... ...per...ormed on individual pass...s, as well as on the combined data fr... all three succe...sive p...sses. For comparative purpo...es a regression was also performed on ...a c... be expe...cted fr...m a highly loftec trajectory of a ro...ket launched from Cape Canaveral; the flig... ...ine was taken as running due east (90° azimuth) and apogee was taken as 700 nm and the imp... poir... a... 120 miles downrange. Points of the rocke... trajectory below an altitude of 50 nm ... e excluc...ed fr...m the regres...ion so that drag would not be a serious factor in free flight orbital ...uctio...s.

... but a few exceptions the error parameters resulting from regression based on satellite ...a...es... well det...rmined and well separated. The exceptions are a_{11} (first order refraction) and a_4 (Y survey error) in the P error model and a_{20} (first order refraction) and a_{24} (Y survey error) in the Q error model. The covariance matrix of the regression parameters shows that a_{11} and a_4 ... very highly correlated. The same is true of a_{20} and a_{24}. The reason for this stems from the fact that when the range R is large compared with the lengths of the P and Q baselines, (b_P and b_Q respectively), one has very nearly $P \cong b_P \lambda_P$, $Q = b_Q \lambda_Q$ inasmuch as the X and Y axes coinc...de approximately with the P and Q baselines respectively. Accordingly in the error models the coefficients of a_{11} and a_4 as well as those of a_{20} and a_{24} are essentially constant multiples of each other no matter what the geometry (as long as $R >> b_P, b_Q$). Thus the separation of first order refraction and baseline lengths is not feasible from either satellite or rocket observation. In order to obrain a sharp determination of either of these parameters, it is necessary to specify the other.

... ofted trajectory yields results comparable to those of the satellite passes with the exceptio... ...at first and second orde... refra...tion (a_6, a_7) in the range error model are poorly de...erm...ed. This ...ay be attributed to the fact that the elevation angles of the lofted trajectory re...ativ... to MISTRA N never become sufficiently low to exercise the coefficients of a_6 and a_7 adequ...ely, for on...y points outside ...he effective atmosphere (h > 50 nm in this case) were carried. It ...olle...s ...at a lofted trajectory m...st impact rather far down range (at least 500 to 600 nm) if it ... to rec... to a sh...rp determinatio... of re...raction pa...amete... for range.

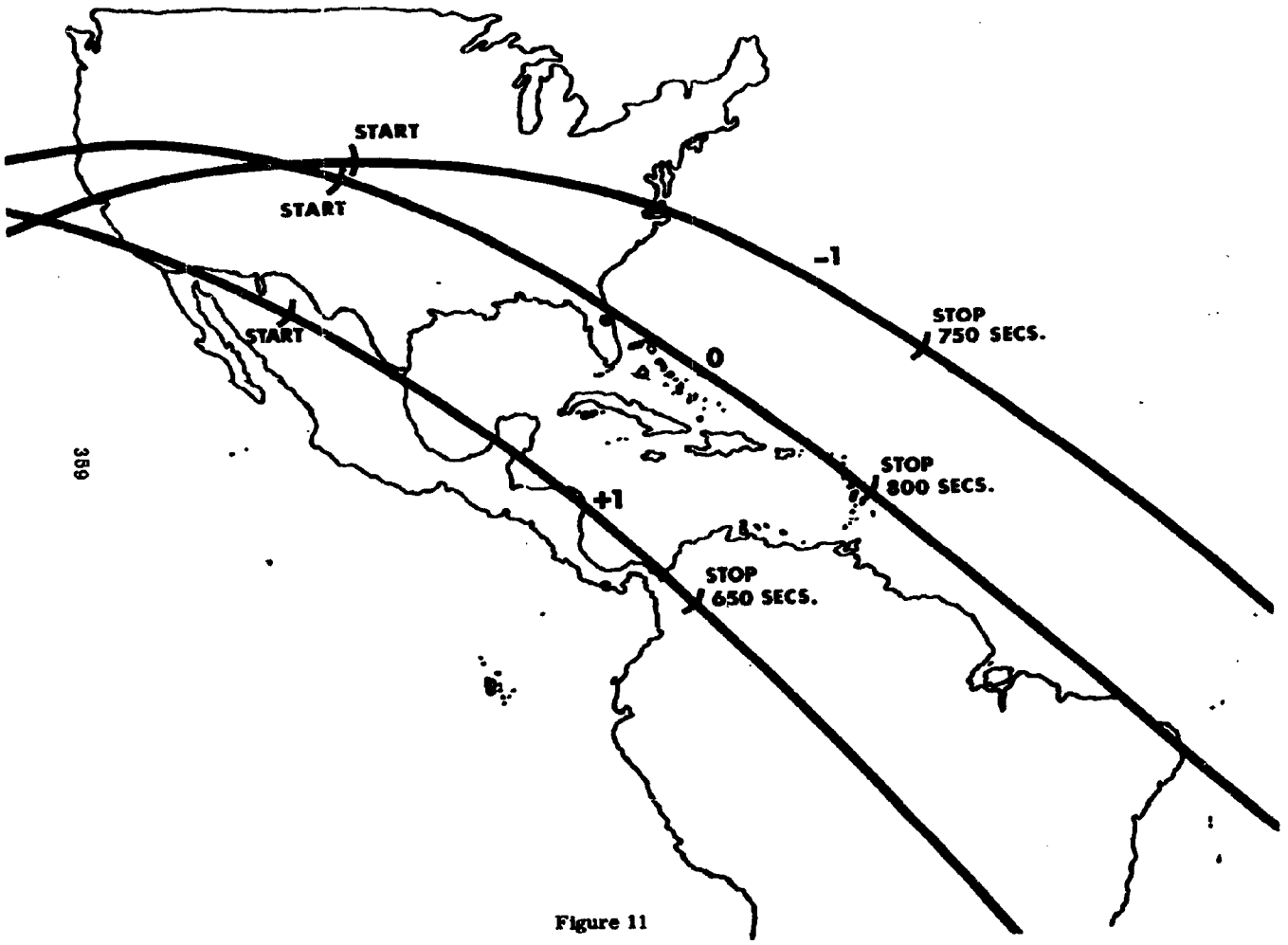
START
START
START
-1
STOP
750 SECS.
0
STOP
800 SECS.
+1
STOP
650 SECS.

Figure 11

TABLE 2

$$\Delta R = a_1 + a_2 t + a_3 tR + a_4 t + a_5 \dot{R} + a_6 \csc E + a_7 \csc^3 E$$

	A PRIORI	SAT. PASS -1	SAT. PASS 0	SAT. PASS +1	SAT. PASS -1, 0, +1	LOFTED TRAJECTORY
σ_{a_1}	10 ft.	4.40	0.14	7.88	0.12	0.82
σ_{a_2}	0.1 ft/sec	0.0076	0.0032	0.014	0.00024	0.0018
σ_{a_3}	1×10^{-8} sec^{-1}	0.054×10^{-8}	0.027×10^{-8}	0.094×10^{-8}	0.0035×10^{-8}	0.0097×10^{-8}
σ_{a_4}	1×10^{-5}	0.032×10^{-5}	0.0057×10^{-5}	0.054×10^{-5}	0.0039×10^{-5}	0.0051×10^{-5}
σ_{a_5}	1×10^{-3} sec	0.055×10^{-3}	0.019×10^{-3}	0.100×10^{-3}	0.0017×10^{-3}	0.083×10^{-3}
σ_{a_6}	1.0 ft.	0.060	0.052	0.111	0.032	0.35
σ_{a_7}	0.002 ft.	0.00010	0.00011	0.00022	0.00006	0.00198

RESULTS OF REGRESSION SIMULATION: R ERROR MODEL

TABLE 3

$$\Delta P = a_8 + a_9 t + a_{10} tP + a_{11} P + a_{12} \dot{P} + a_{13} P \cot^2 E + a_{14} \lambda_p + a_{15} \mu_p + a_{16} \nu_p$$

	A PRIORI	PASS -1	PASS 0	PASS +1	PASSES -1, 0, +1	LOFTED TRAJECTORY
σ_{a_8}	0.1 ft.	0.051	0.026	0.064	0.0047	0.038
σ_{a_9}	5×10^{-4} ft/sec	0.81×10^{-4}	0.48×10^{-4}	0.90×10^{-4}	0.055×10^{-4}	0.135×10^{-4}
$\sigma_{a_{10}}$	1×10^{-7} sec^{-1}	0.10×10^{-7}	0.12×10^{-7}	0.12×10^{-7}	0.011×10^{-7}	0.089×10^{-7}
$\sigma_{a_{11}}$	1×10^{-5}	0.63×10^{-5}	0.66×10^{-5}	0.80×10^{-5}	0.49×10^{-5}	0.88×10^{-5}
$\sigma_{a_{12}}$	1×10^{-3} sec	0.055×10^{-3}	0.019×10^{-3}	0.100×10^{-3}	0.0017×10^{-3}	0.083×10^{-3}
$\sigma_{a_{13}}$	2×10^{-7}	0.068×10^{-7}	0.092×10^{-7}	0.100×10^{-7}	0.0032×10^{-6}	0.177×10^{-6}
$\sigma_{a_{14}}$	0.05 ft.	0.046	0.042	0.043	0.042	0.0498
$\sigma_{a_{15}}$	0.05 ft.	0.041	0.047	0.043	0.014	0.035
$\sigma_{a_{16}}$	0.05 ft.	0.046	0.029	0.0499	0.0080	0.038
		n = 155	n = 165	n = 155	n = 495	n = 235

RESULTS OF REGRESSION SIMULATION: P ERROR MODEL

(NOTE: If $R \gg b_p$, $P \cong b_p \lambda_p$)

TABLE 4

$$\Delta Q = a_{17} + a_{18}t + a_{19}tQ + a_{20}Q + a_{21}\dot{Q} + a_{22}Q\cot^2 E + a_{23}\lambda Q + a_{24}\mu_Q + a_{25}\nu_Q$$

	A PRIORI	SAT. PASS -1	SAT. PASS 0	SAT. PASS +1	SAT. PASS -1, 0, +1	LOFTED TRAJECTORY
$\sigma_{a_{17}}$	0.1 ft.	0.048	0.026	0.066	0.0047	0.036
$\sigma_{a_{18}}$	5×10^{-4} ft/sec	0.68×10^{-4}	0.48×10^{-4}	1.40×10^{-4}	0.057×10^{-4}	0.110×10^{-4}
$\sigma_{a_{19}}$	1×10^{-7} sec^{-1}	0.110×10^{-7}	0.092×10^{-7}	0.100×10^{-7}	0.0087×10^{-7}	0.340×10^{-7}
$\sigma_{a_{20}}$	1×10^{-3}	0.76×10^{-5}	0.56×10^{-5}	0.60×10^{-5}	0.45×10^{-5}	0.58×10^{-5}
$\sigma_{a_{21}}$	1×10^{-3} sec	0.055×10^{-3}	0.019×10^{-3}	0.100×10^{-3}	0.0017×10^{-3}	0.177×10^{-6}
$\sigma_{a_{22}}$	2×10^{-7}	0.068×10^{-7}	0.071×10^{-7}	0.120×10^{-7}	0.031×10^{-7}	2.00×10^{-7}
$\sigma_{a_{23}}$	0.05 ft.	0.033	0.044	0.046	0.014	0.048
$\sigma_{a_{24}}$	0.05 ft.	0.049	0.048	0.045	0.043	0.045
$\sigma_{a_{25}}$	0.05 ft.	0.0495	0.029	0.048	0.0076	0.038
		n = 155	n = 165	n = 155	n = 495	n = 235

RESULTS OF REGRESSION SIMULATION: Q ERROR MODEL

(NOTE: If $R \gg b_Q$, $Q \cong b_Q \mu_Q$)

Propagation of Regression Covariance Matrix Through Sample Trajectory:

The significance of the results listed in Tables 2, 3 and 4 can be ascertained by propagating the covariance matrices of the error parameters resulting from satellite regression through various trajectories of interest. Table 5 indicates the results of propagating the covariance matrix resulting from satellite pass 0 through the lofted trajectory described above. Sigma R, Sigma P, Sigma Q in this figure denote the standard deviations in R, P, and Q attributable to the errors remaining in the calibrated error parameters. We find that these standard deviations have generally been suppressed to a level of 1/3 to 1/10 that of postulated noise in the respective channels. This demonstrates that a calibration resulting from a single pass of a satellite can successfully suppress systematic error to insignificance in comparison with the random error. This is the ultimate objective of calibration.

Conclusions

Although the results obtained thus far are of a preliminary nature, they do strongly indicate that satellite techniques can lead to an effective calibration of tracking instrumentation. In further work the assumption that the short arc orbit is perfectly known will be abandoned in favor of the more realistic assumption that the osculating orbital elements are subject to error. The determination of the covariance matrix of the osculating elements and the propagation of this through the regression to determine the error parameters must be accomplished in order to obtain definitive results. On the other hand, it should be appreciated that had an unsatisfactory regression been obtained under the assumption of a perfectly known orbit, the entire concept of a calibration satellite could have been dismissed without further investigation. The highly favorable results obtained thus far indicate that the calibration satellite clearly warrants an exhaustive investigation of the theoretical, operational, logistical, reductional and economic aspects of a possible full scale future program. Such an investigation is now well underway under the sponsorship of Electronic Systems Division of the Air Force

TABLE 5

T (Sec)	SIGMA R ft.	SIGMA P ft.	SIGMA Q ft.
150.00	.1573187	.0053253	.0030654
200.00	.1485915	.0050784	.0030246
250.00	.1340646	.0048021	.0030275
300.00	.1092174	.0044765	.0030160
349.99	.0837006	.0041630	.0030070
399.99	.0610131	.0038788	.0030114
449.99	.0435491	.0036343	.0030321
499.99	.0353083	.0034433	.0030704
549.99	.0374892	.0033327	.0031262
599.99	.0446640	.0033940	.0031983
	(0.5)	(0.03)	(0.03)

ASSUMED RMS NOISE LEVELS

SOME NUMERICAL CHARACTERISTICS OF AN ERROR MODEL BEST ESTIMATE OF TRAJECTORY

by:

D. H. Parks

RCA-Missile Test Project

PAFB, Florida

Presented at:

FOURTH JOINT AFMTC-RANGE USER DATA CONFERENCE

Orlando Air Force Base, Florida

26-28 February 1963

SOME NUMERICAL CHARACTERISTICS OF AN ERROR MODEL BEST ESTIMATE OF TRAJECTORY

Abstract

Certain numerical characteristics which have exhibited themselves in the results from several simulated and real "Best Estimate of Trajectory" reductions are discussed. Emphasis has been placed upon the effects of various error model assumptions upon a BET. In addition, the effects of weighting the observations and of applying certain a priori knowledge to the solution are considered.

1. Introduction

This paper has been preceded by two others on the same general topic delivered at the Joint AFMTC - Range User Conferences of 1961 and 1962. The first paper (1) discussed the philosophical basis of the error model approach to a "Best Estimate of Trajectory," or BET, and outlined the data processing procedures deemed necessary for the implementation of such an approach. The second paper (2) provided a history of BET computer program development as of that time and described plans for future modifications. Due to the rapidly expanding nature of the BET problem, the scope of this presentation has been limited to only one of its aspects - certain numerical characteristics which have become evident in the results of many computer runs over the past few years. Some of the examples were chosen randomly and some were chosen because they emphasized certain characteristics. In order to give the numerical results meaning to those unfamiliar with the BET concept certain basic assumptions of the error model BET will first be outlined.

2. The Formulation of an Error Model

Before any measurement can be of use in a trajectory computation, the condition equation relating it to the trajectory parameters must first be formulated. Until the inception of the error model approach, this simply entailed the formulation of a geometric or dynamic relationship between the measurement and the trajectory parameters. The equations were then solved for the trajectory parameters by a unique solution if only three measurements were available or by a weighted least squares adjustment (3) if more than the necessary minimum of three measurements were available. By-products of the least squares adjustment were estimates of covariance in the estimated trajectory parameters and residual errors (residuals) formed by differencing the measurements with their adjusted values:

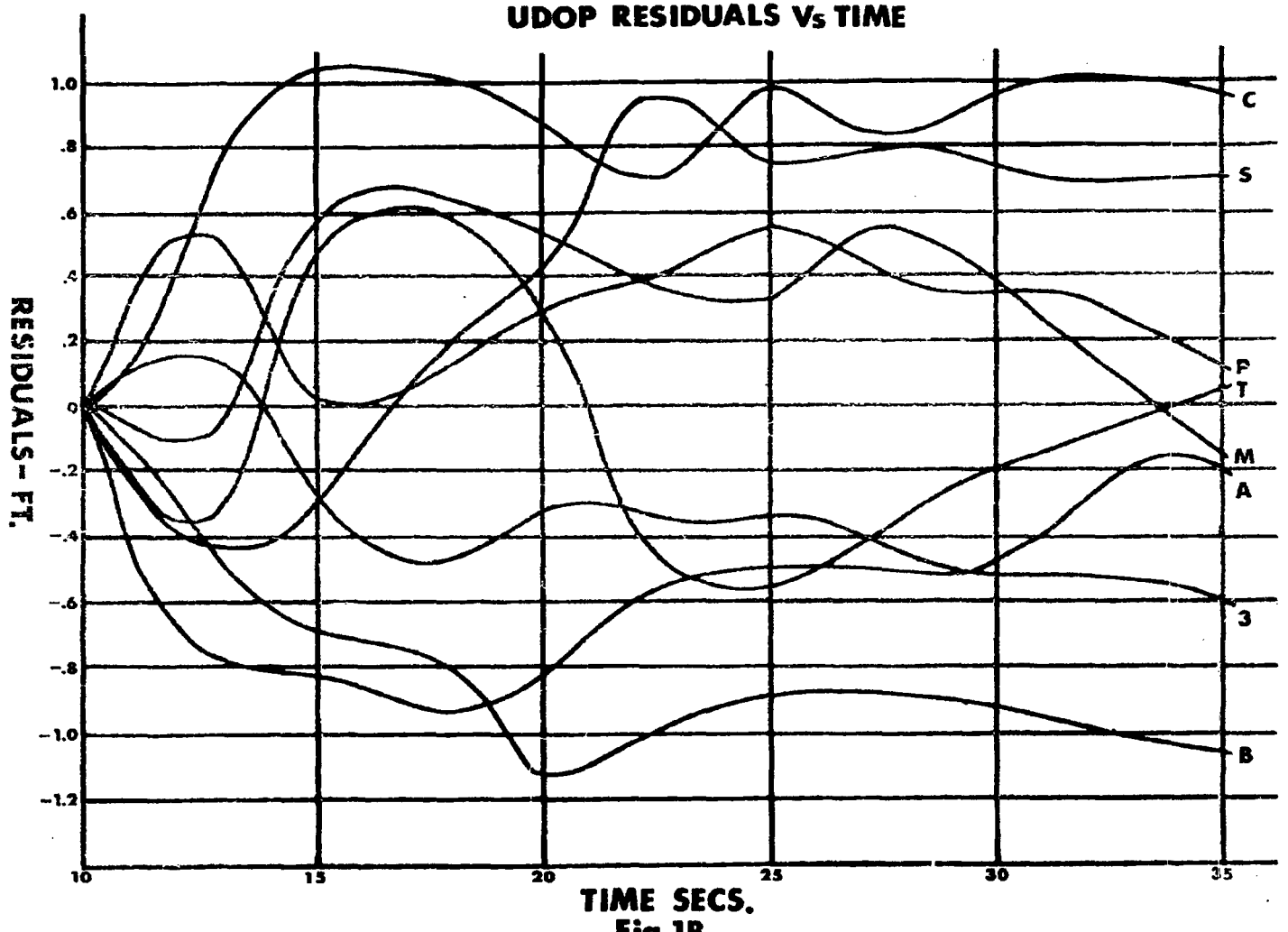
UDOP RESIDUALS Vs TIME
RESIDUALS- FT.
1.0
.8
.6
.4
.2
0
-.2
-.4
-.6
-.8
-1.0
-1.2
10
15
20
25
30
35
TIME SECS.
C
S
P
T
M
A
3
B
Fig.1B

GE MOD III Minus Rereferenced AZUSA Mark II

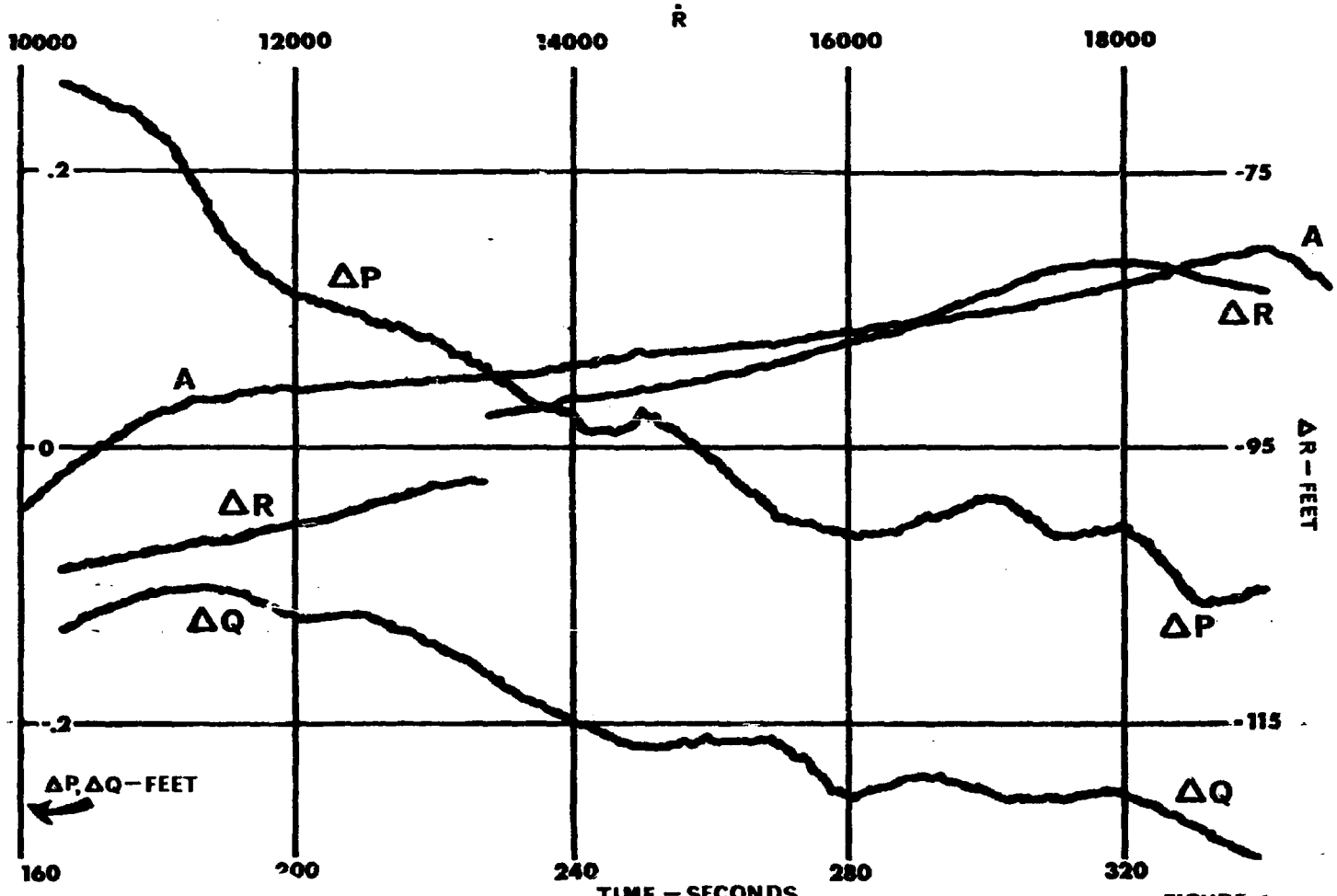

FIGURE 2

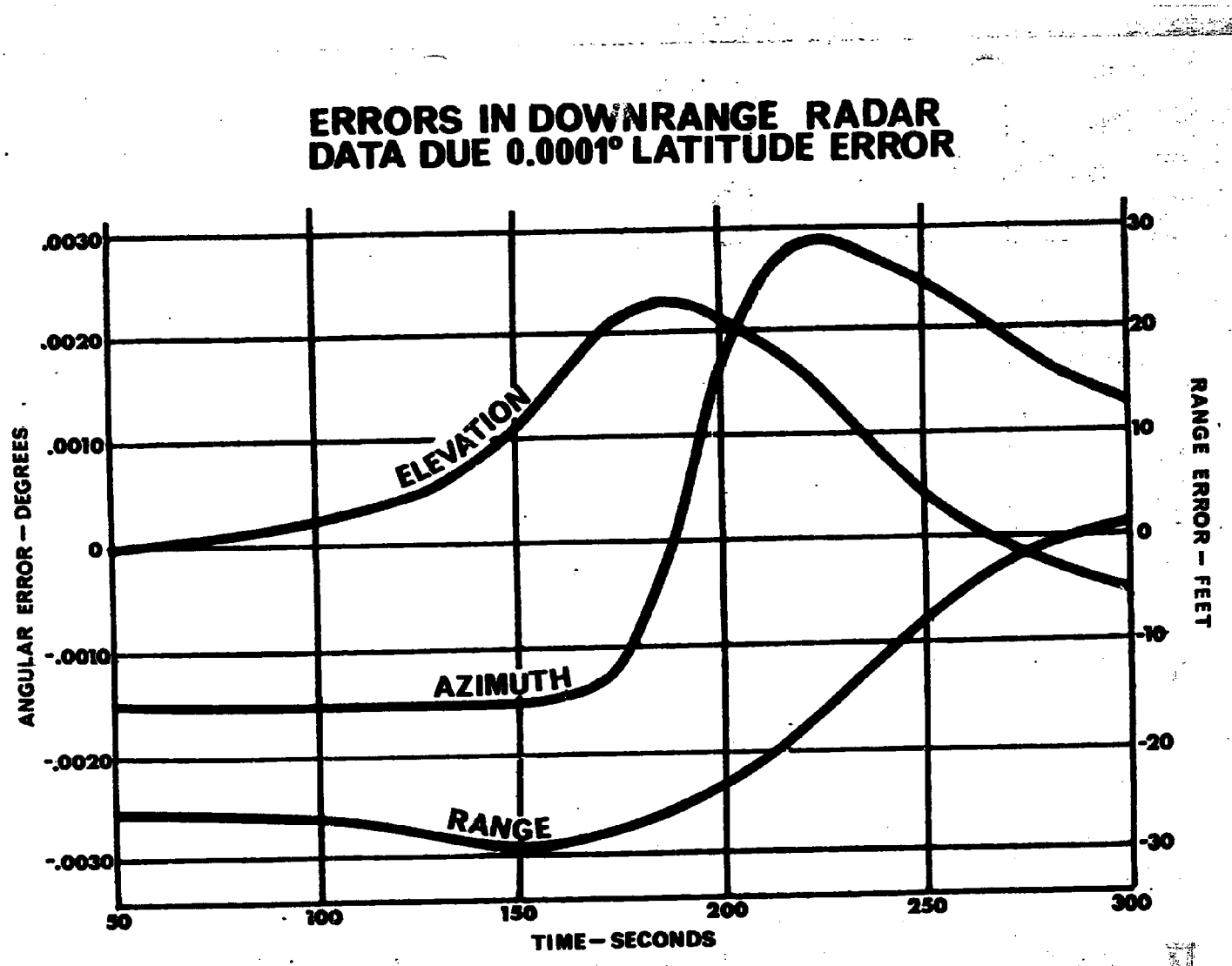
ERRORS IN DOWNRANGE RADAR
DATA DUE 0.0001° LATITUDE ERROR
ANGULAR ERROR – DEGREES
.0030
.0020
.0010
0
-.0010
-.0020
-.0030
ELEVATION
AZIMUTH
RANGE
50
100
150
200
250
300
TIME – SECONDS
RANGE ERROR – FEET
30
20
10
0
-10
-20
-30

FIGURE 3A

$$V = m - f(x,y,z)$$

where

V is the residual,

m is the measurement, and

f(x,y,z) is the least squares estimate of missile position in some arbitrary coordinate system. Similar residuals existed for the velocity equations.

A common characteristic noted in the residuals was that for a system possessing high precision (low noise content) the residuals usually exhibited trends (high serial correlation) over long intervals of a trajectory. Such trends may be noted in Figure 1A, which is a graph of residuals from a typical UDOP (a UHF Doppler tracking system) reduction. Measurements from four UDOP sites were involved in the least squares adjustment.

In one of the earliest uses of an error model at AMR, it was assumed that such trends in the residuals from Doppler data were due mainly to systematic errors in the calibration process. At that time (1957), the existing Doppler system, known as DOVAP, was usually calibrated or "tied in" early in a trajectory with theodolite data. The persistence of trends in the residuals thus led rather naturally to the tie-in point as the source of systematic error and the inclusion of the tie-in point in each condition equation as an unknown. An analytical solution (4) existed at the time and was programmed for the Cape 704 Computer. Later a more straightforward solution (5) was derived and programmed for the FLAC Computer. Data from several Redstone and Thor flights were processed using the two techniques although, for reasons mentioned later in this paper, no resulting trajectory was ever published.

The DOVAP tie-in point solutions closely resemble the constant bias error model BET (an obvious defect of the tie-in point method is the inclusion of the random error at the time of tie-in as a systematic error throughout the trajectory). In the constant bias error model type of BET a constant term is added to each condition equation as an unknown. The basic assumptions here again are that the system is poorly calibrated, that the calibration error is the major part of the total systematic error and that the systematic error remains constant throughout the reduction. Some justification for such an error model exists in that comparisons of Ballistic Camera data with electronic tracking data from aircraft calibration tests often show a fairly constant bias over long stretches of the aircraft's flight path. The existence of such a constant bias may also be justified in many cases from an engineering standpoint if the equipment design is such as to prohibit large drifts.

After transforming the trajectory coordinates as indicated by one system into a second system's natural coordinates (LMR, PQR, AER, etc.), comparisons often indicate a drift between the transformed data of the first system and the measured data of the

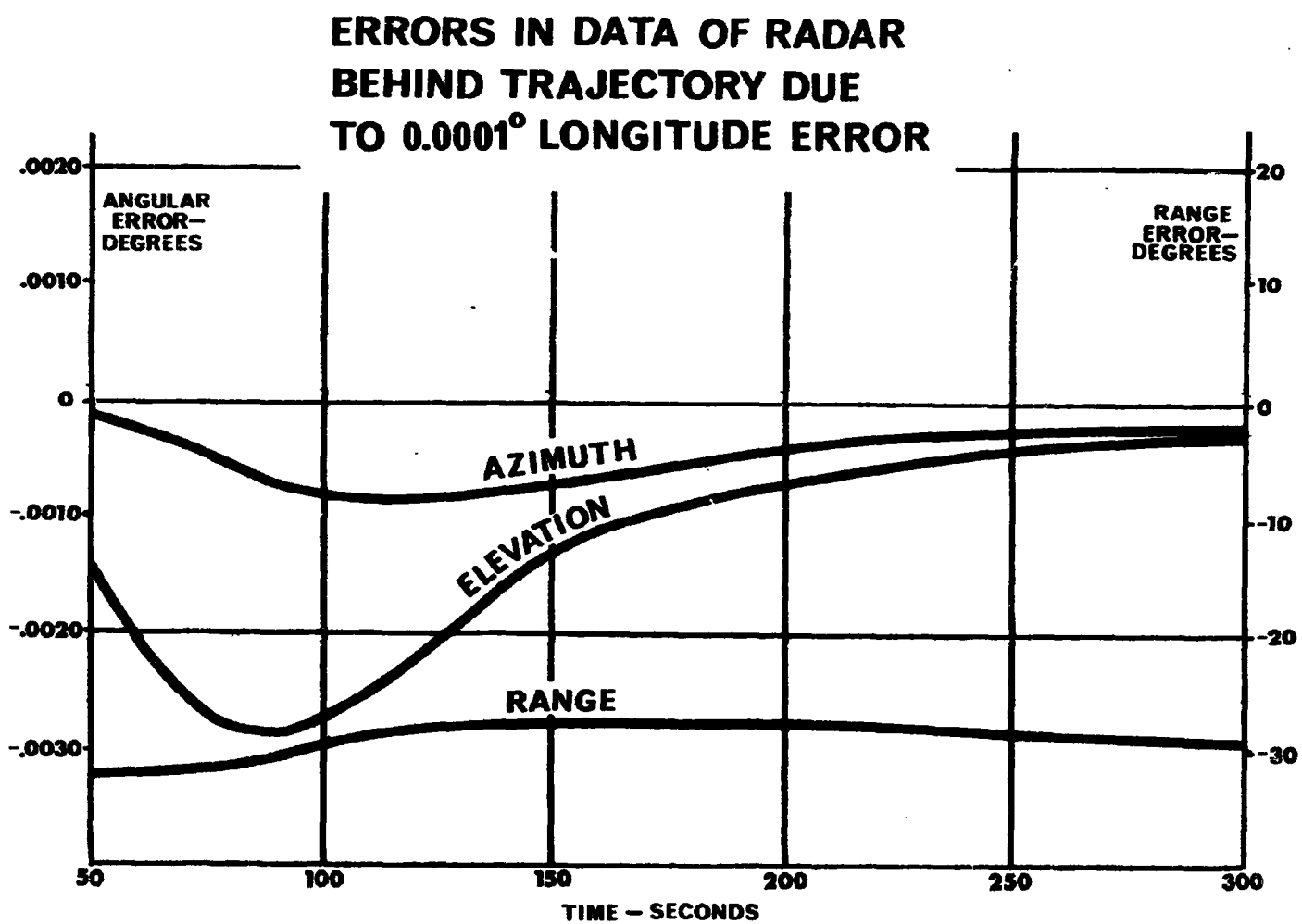
ERRORS IN DATA OF RADAR
BEHIND TRAJECTORY DUE
TO 0.0001° LONGITUDE ERROR
.0020
.0010
0
-.0010
-.0020
-.0030
ANGULAR
ERROR—
DEGREES
RANGE
ERROR—
DEGREES
20
10
0
-10
-20
-30
AZIMUTH
ELEVATION
RANGE
50
100
150
200
250
300
TIME — SECONDS

FIGURE 3B

second system. Figure 2 shows the differences between transformed AZUSA LMR data and GE MOD III measured PQR data on a recent test. Such differences can often be approximated closely over long portions of a trajectory by a low degree polynomial, with time as the independent variable (it should be understood, however, that the drifts in the differences do not necessarily imply a drift error in either system, since a constant bias in one system could transform into a drift relative to the other system). The existing BET routine, BETY2, assumes a polynomial of the first degree (systematic error = a + bt) as its error model. The physical basis for such an error model lies in the fact that measurement errors due to such factors as timing bias and survey bias can often be approximated by a low degree polynomial. Figure 3 shows the effects of a 0.0001° (approximately 36 feet) error in location of the site on the measurements of two radars over a typical ICBM trajectory. Note that the errors for the radar located behind the trajectory can be approximated more closely by a linear error model than the errors for a radar located along the trajectory such as at Grand Bahama Island.

In formulating an error model, one has a choice of using an expression in which errors are implicitly expressed or one in which the errors are explicitly expressed. A polynomial represents the implicit case in which no attempt is made to assign the cause of an error to a particular source such as calibration, survey, timing, reference frequency drift, refraction, etc. Even errors due to unknown sources, when finally detected, can often be described by a low degree polynomial. A good case can also be made for the application of an explicit error model in which actual physical quantities may be evaluated. One great advantage of such an approach lies in the fact that certain errors may be in common to several of the different measuring devices. Thus, all the UDOP measurements from one complex might be assigned the same timing bias due to a timing error at the recording site or the same survey error terms due to an error in the location of the involved survey net. Decreasing the number of error model terms in such a manner should result in a much better convergence of the solution. Disadvantages of such an approach will be discussed later.

3. The Assigning of Weights

Another basic assumption involved in determining a BET is that the covariance matrix of the observations is known. This requires, in the case of an error model BET, an estimate of the precision with which the condition equation fits the physical situation. The assumption made in the existing BET reduction program is that the condition equation, including the error model terms, fits the physical situation except for the total noise content of the data. Estimates of total noise in the observations are used to weight the observations during the least squares adjustment. Investigations are now being made concerning the possibility of including serial correlation terms in the

weight matrices. At the present time, the need for autocorrelation considerations is being partially avoided by choosing data samples far enough apart so that serial independence can be assumed for all data entering into the error model coefficient determination.

4. Additional Assumptions

An argument can be made that in utilizing only the measurement data from a particular test in determining that test's trajectory, a large body of useful knowledge gained from past experience is ignored. The existing BET routine is capable of making use of such a priori knowledge of the behavior of the error model coefficients by treating this knowledge as quasi-measurement data with known variance. This a priori knowledge can be derived from past ballistic camera comparisons, calibrations made using calibration towers, engineering specifications, etc. Similarly, knowledge of certain trajectory points may be entered into the computer routine as quasi-measurement data with associated covariance matrices. Such data, called "control data," are usually furnished by optical systems whose basic measurements have not been assigned an error model in the reduction. Both types of quasi-measurements enter into the least squares adjustment and affect, in varying degrees, the determination of the error model coefficients. A newer version of the BET routine will incorporate integrated guidance data as quasi-measurement data with a polynomial in time error model.

There are, of course, other constraints which could be placed upon the data. The error model terms could be adjusted further in free flight by determining a post-burnout position-velocity vector which, when numerically integrated down the trajectory, would give a least squares fit to the data (and a best estimate of impact). Additional quasi-measurement equations could be used in relating various error model coefficients. The position data could be constrained to equal the integrated velocity data.

5. Certain Effects of the Error Model Assumptions on the Error Model BET

It was previously mentioned that no trajectories using the DOVAP tie-in point solutions were ever published. The principal reason for not publishing the trajectories was that, although the trends in the residuals became less obvious in most cases, the computed tie-in points often took on values which differed unreasonably from points determined by the optical tracking systems. Although the tie-in point solutions were eventually discarded, many of the characteristics which later appeared in BET computations were evident in the tie-in point computations. It was found that convergence of the solution was poor unless data samples over a long portion of the trajectory were used and that

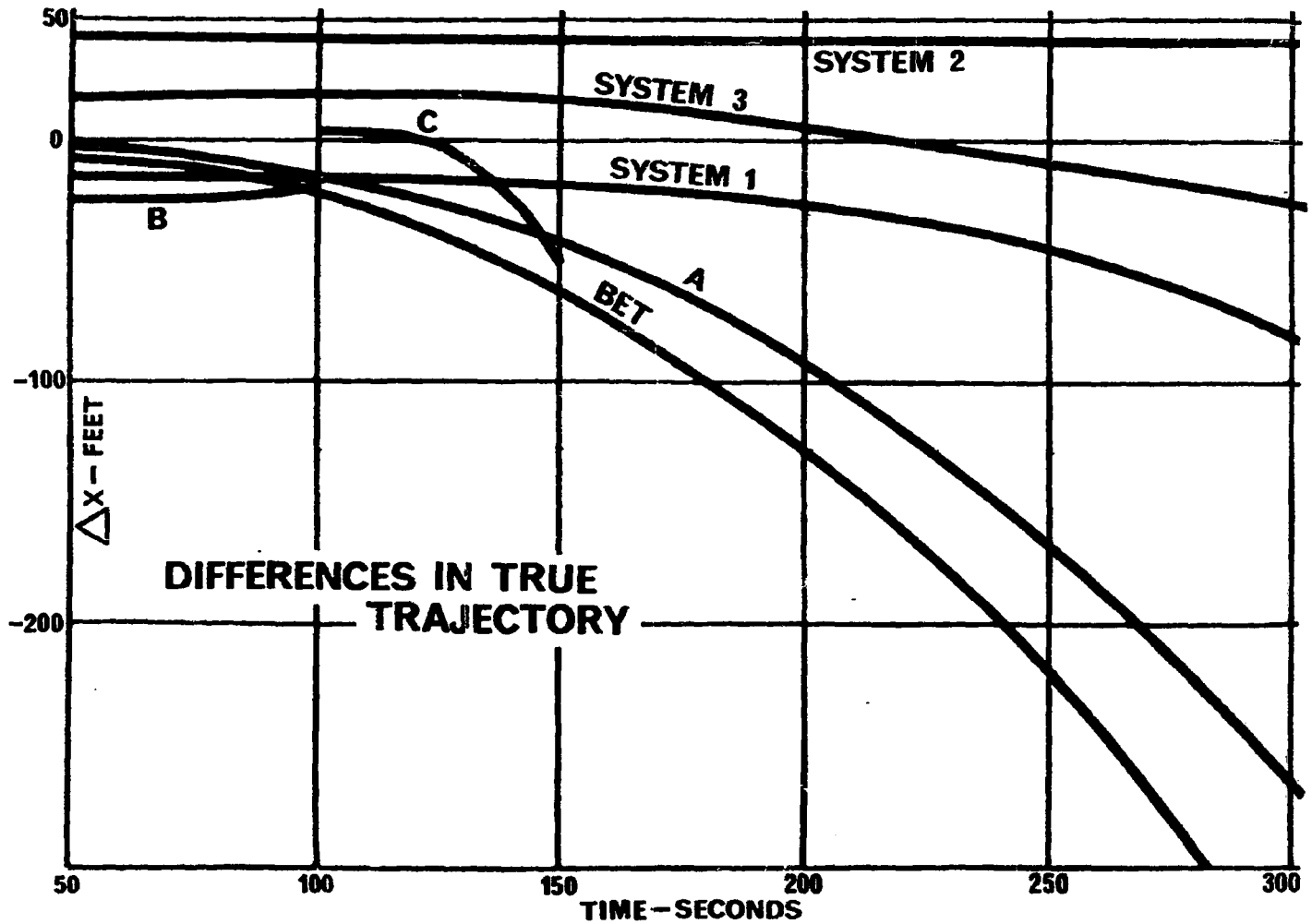
50
0
-100
-200
SYSTEM 2
SYSTEM 3
C
SYSTEM 1
B
A
BET
ΔX - FEET
DIFFERENCES IN TRUE
TRAJECTORY
50
100
150
200
250
300
TIME - SECONDS

FIGURE 5A

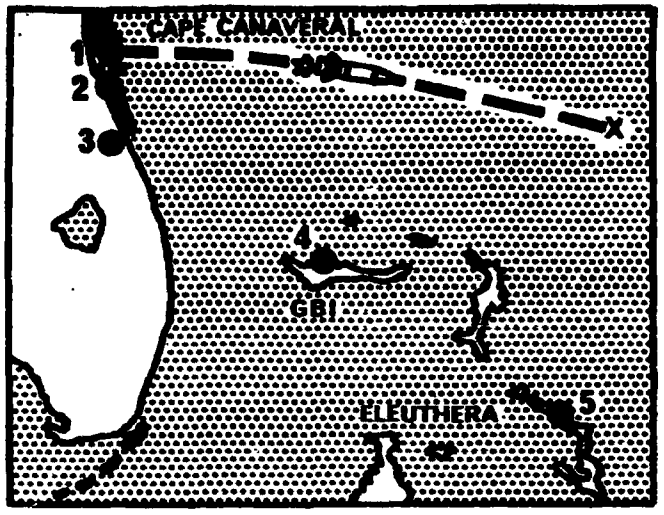

FIGURE 4A

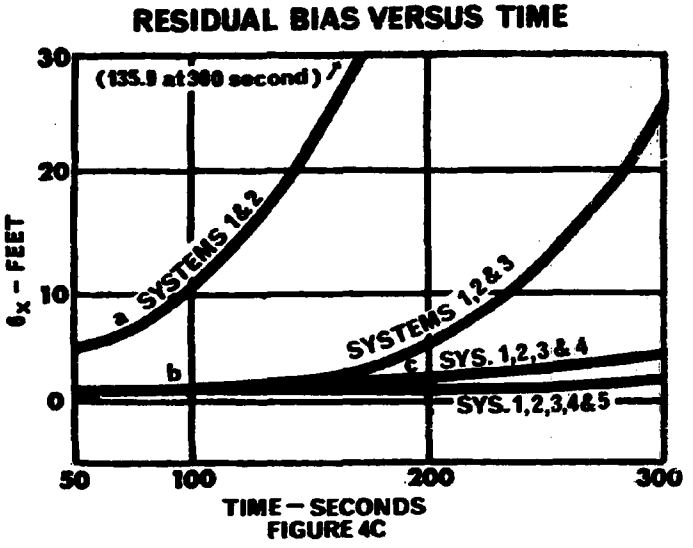

FIGURE 4C

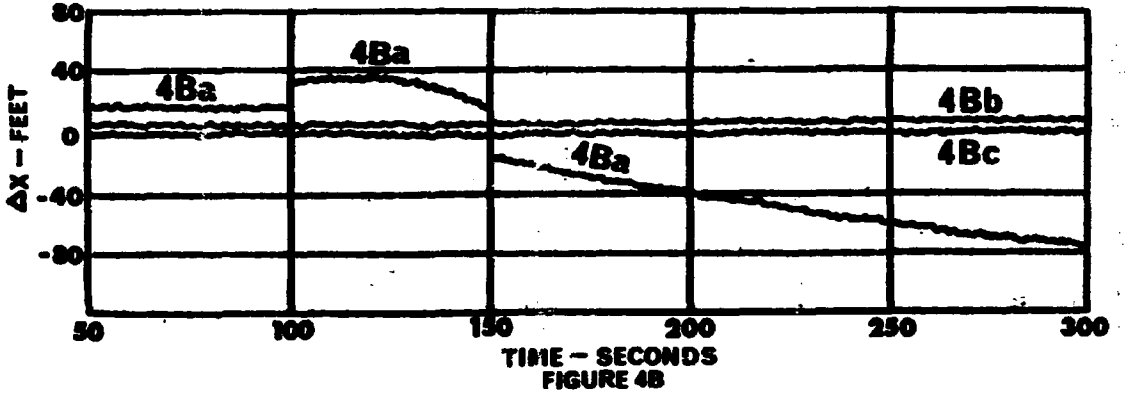

FIGURE 4B

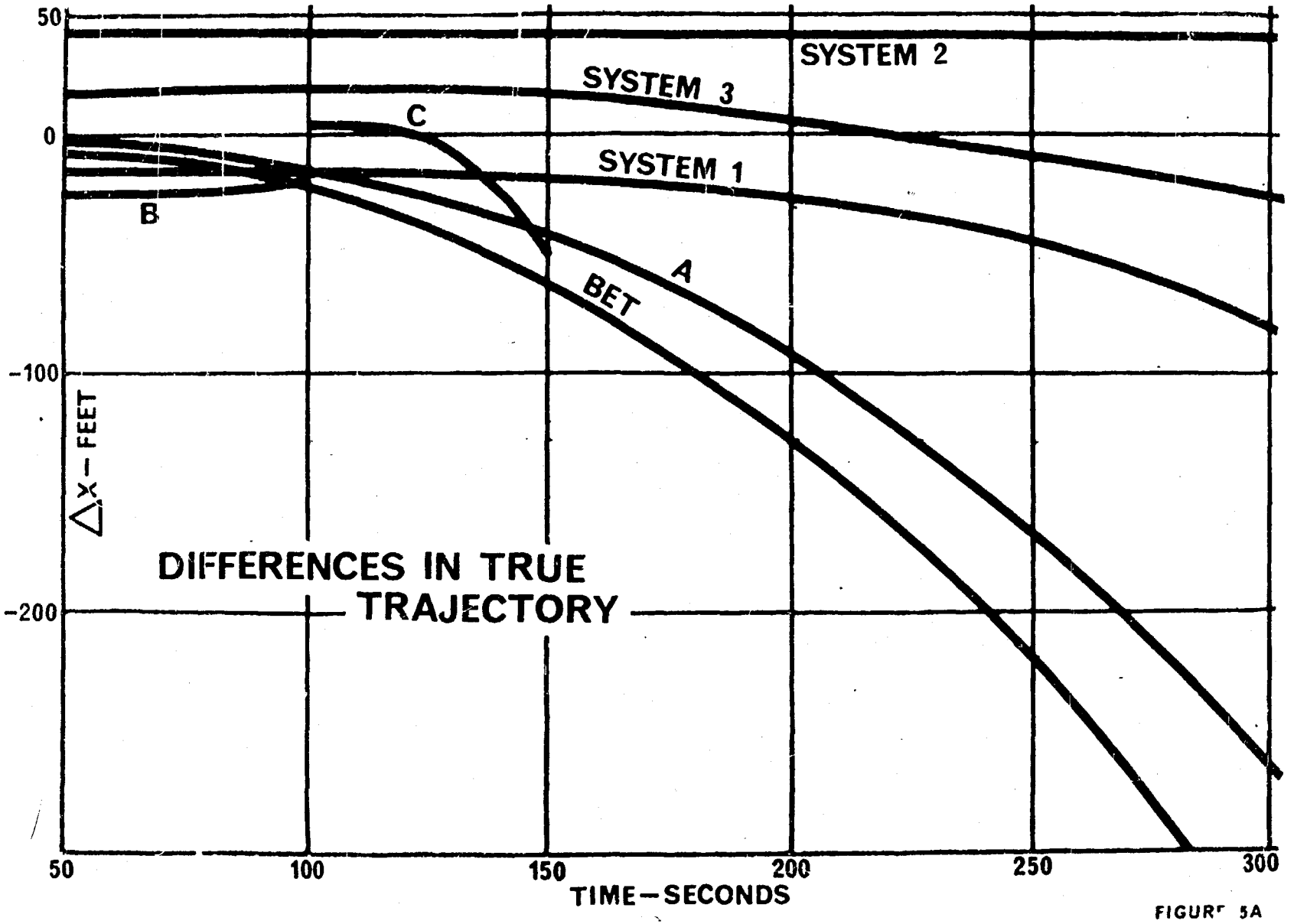
50
0
-100
-200
SYSTEM 2
SYSTEM 3
C
SYSTEM 1
B
A
BET
ΔX – FEET
DIFFERENCES IN TRUE TRAJECTORY
50
100
150
200
250
300
TIME – SECONDS

FIGURE 5A

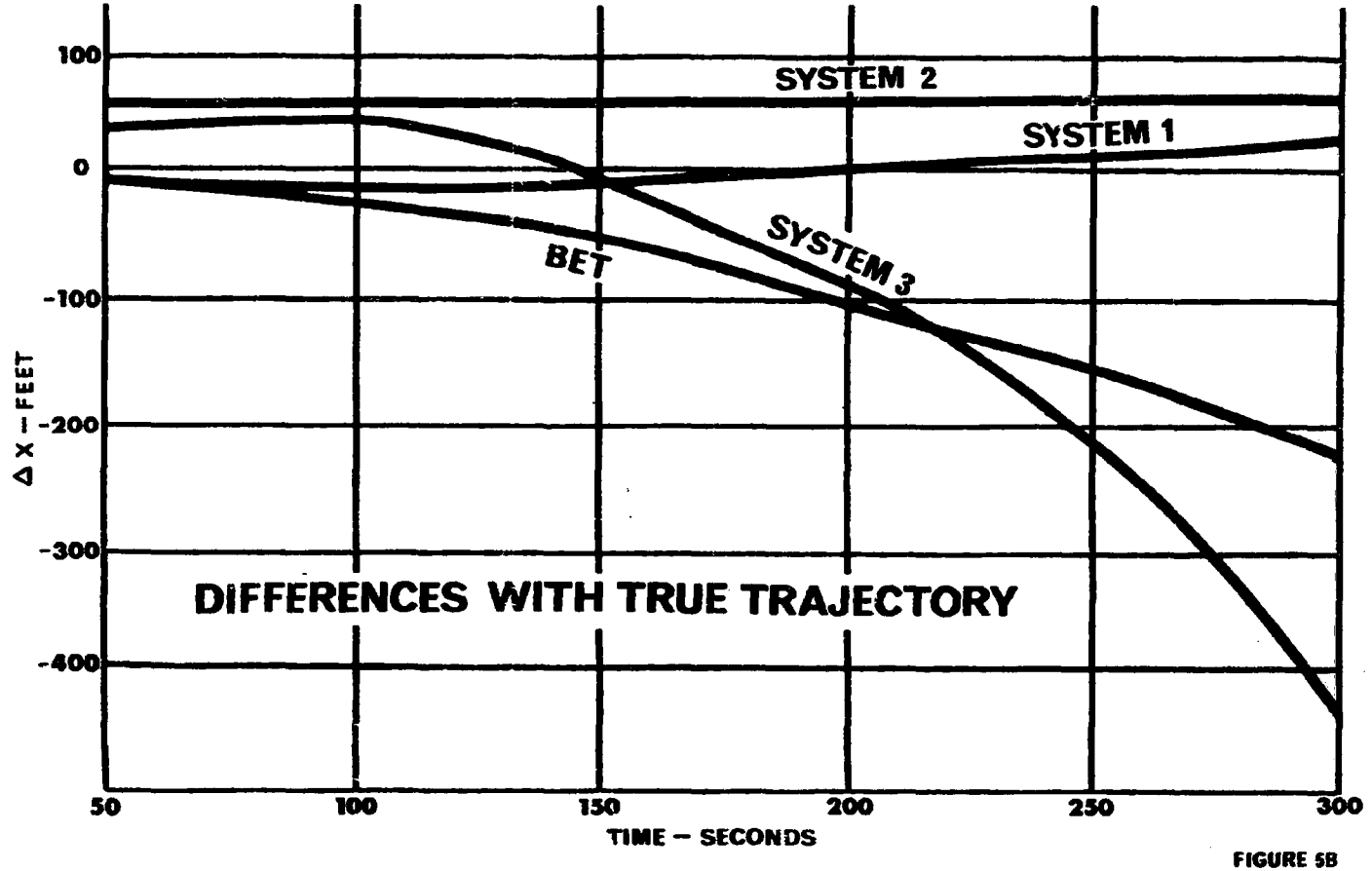
100
0
-100
-200
-300
-400
ΔX – FEET
SYSTEM 2
SYSTEM 1
SYSTEM 3
BET
DIFFERENCES WITH TRUE TRAJECTORY
50
100
150
200
250
300
TIME – SECONDS

FIGURE 5B

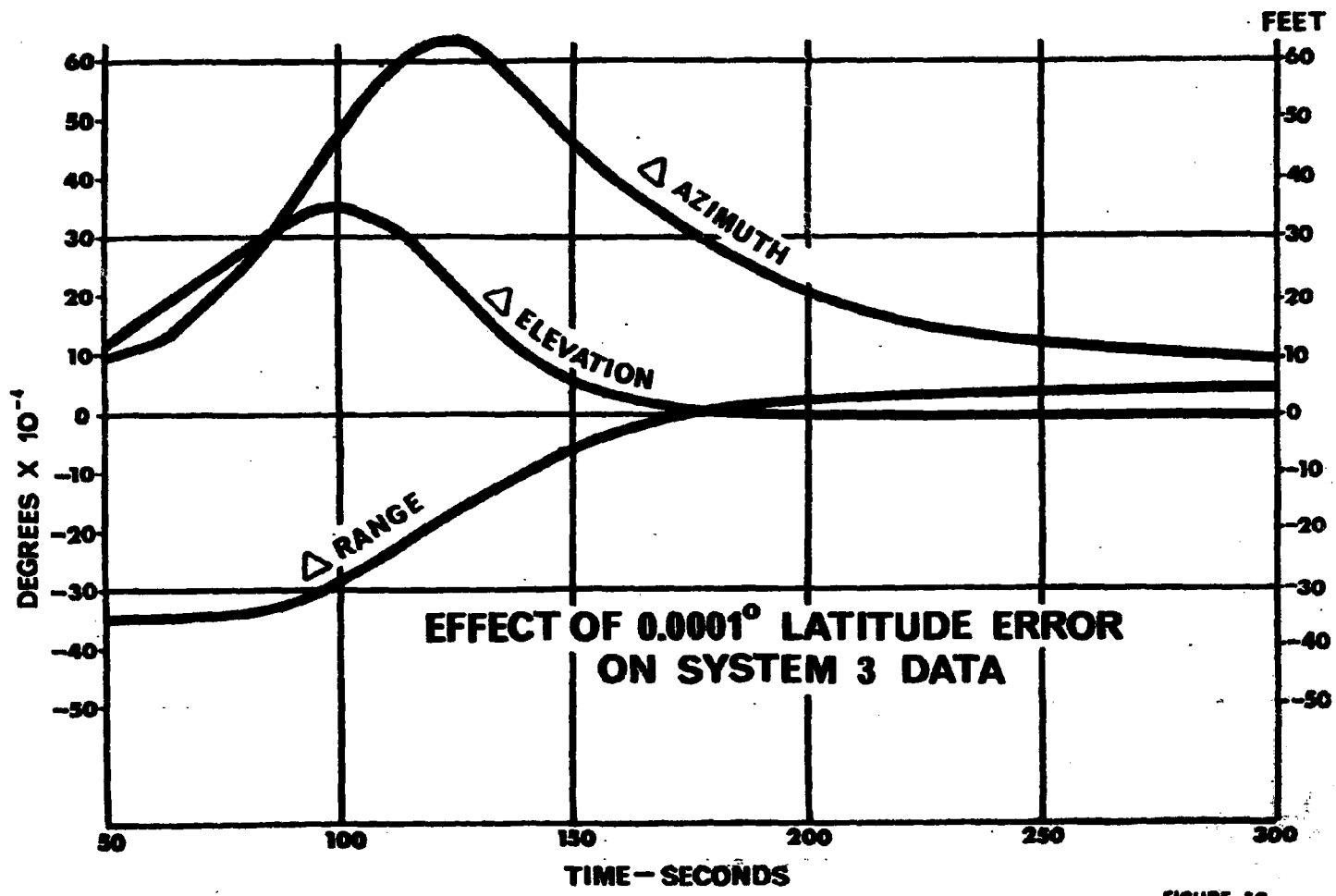
FEET
60
50
40
30
20
10
0
-10
-20
-30
-40
-50
Δ AZIMUTH
Δ ELEVATION
Δ RANGE
DEGREES X 10⁻⁴
EFFECT OF 0.0001° LATITUDE ERROR
ON SYSTEM 3 DATA
50
100
150
200
250
300
TIME – SECONDS

FIGURE 5C

indicated by propagation of the covariance matrix of error model coefficients into the Cartesian trajectory coordinates. This is shown in Figure 4C for the above linear error model solution. Note that the estimate of residual bias decreases significantly as the number of stations is increased (curve a to curve b) and even more significantly as the geometry is expanded to include a Downrange system (curve b to curve c).

Two cases which show vividly the possible effects of erroneous error model assumptions are shown in Figures 5A and 5B. Here, only the first three systems involved in the preceding theoretical case were used. In the first case, a survey error of 0.0001° (approximately 36 feet) was applied to the latitude of the third system in addition to its linear error. The effect of this survey error on the system's measurements is shown in curve 5C. A least squares solution for the trajectory was then made, assuming only the linear error model. The differences in Figure 5A show that the BET estimate (again x only) was far worse during the late portion of the trajectory than any of the individual erroneous trajectories. In the second example, constant biases were applied to the true values of the first two systems and a linear error was applied to each measurement of the third system. A constant bias error model was then assumed for each measurement involved in the least squares adjustment. Note that again the BET was not as good as two of the individual trajectories.

These two cases are good illustrations of a rule which has made itself evident in BET data from many tests. In these two cases the relative values of the measurements changed rapidly during the first 100 seconds of the reduction due to the missile's trajectory being within the station configuration (in order of magnitude). In the later portion of the trajectory the relative values of the measurements changed only gradually. This resulted in the familiar GDOP (Geometric Dilution of Precision) effect upon the error model coefficient determination. The least squares solution automatically biased the determination to give the best estimate of systematic error (and trajectory) in the region of good geometry. The effect of the erroneous error model was in these two cases greatly magnified later in the trajectory. This is similar in concept to evaluating a poorly fitting polynomial at a great distance beyond the span of data used in determining the polynomial coefficients. The evaluation may be close to the true value at the midpoint but the errors may become tremendous at a time far beyond the span. The effect of having the best geometry very early in the trajectory is especially detrimental when the point of track of any system is uncertain. An error of a few feet in the tracking point can be interpreted as an angular error of several hundred microradians in one of the instruments. This may result in only a small trajectory error early in the flight but will become greatly magnified later.

Returning to Figure 5C, we see that the survey error resulted in measurement errors that were approximately linear in time over several intervals. BETs were computed over several fifty-

AZUSA Data Minus Rereferenced UDOP Data

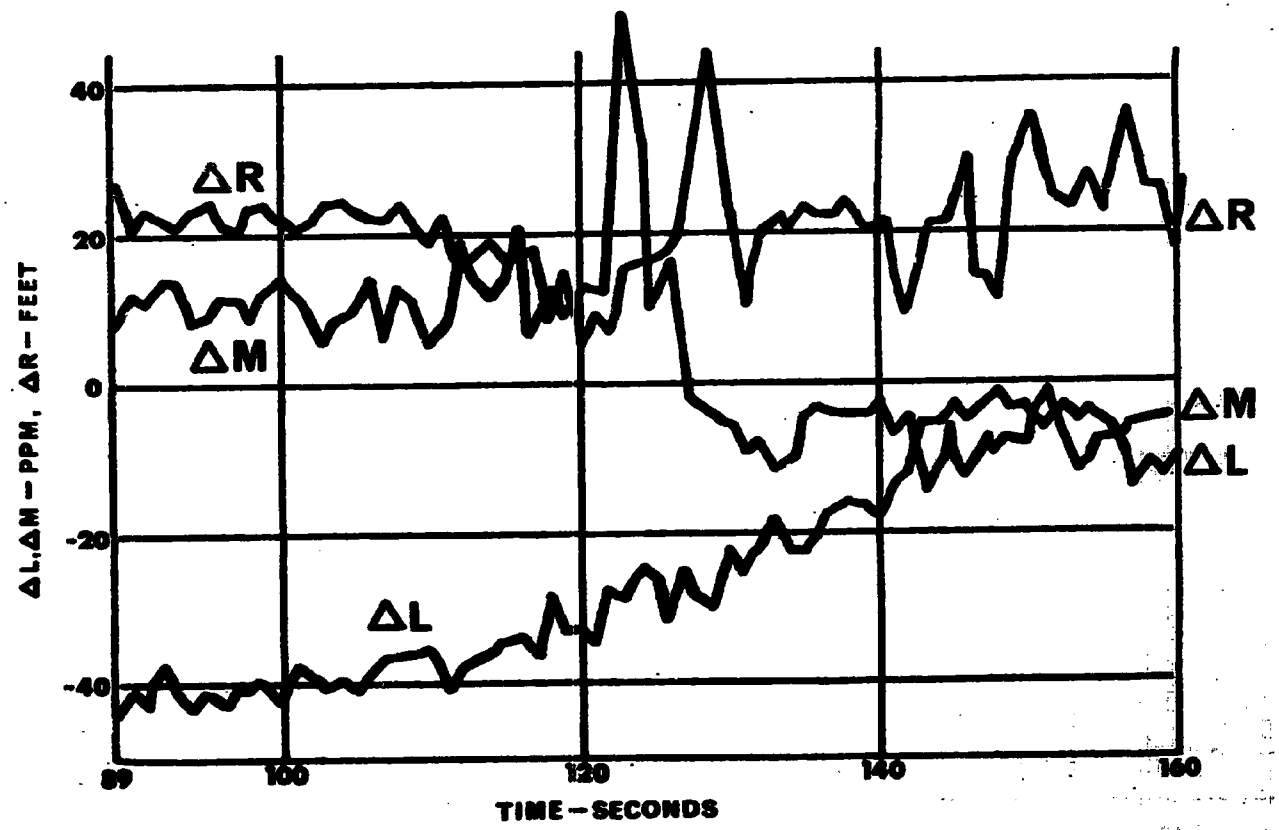

FIGURE 6A

89–160 SECONDS – Constant Bias Error Model

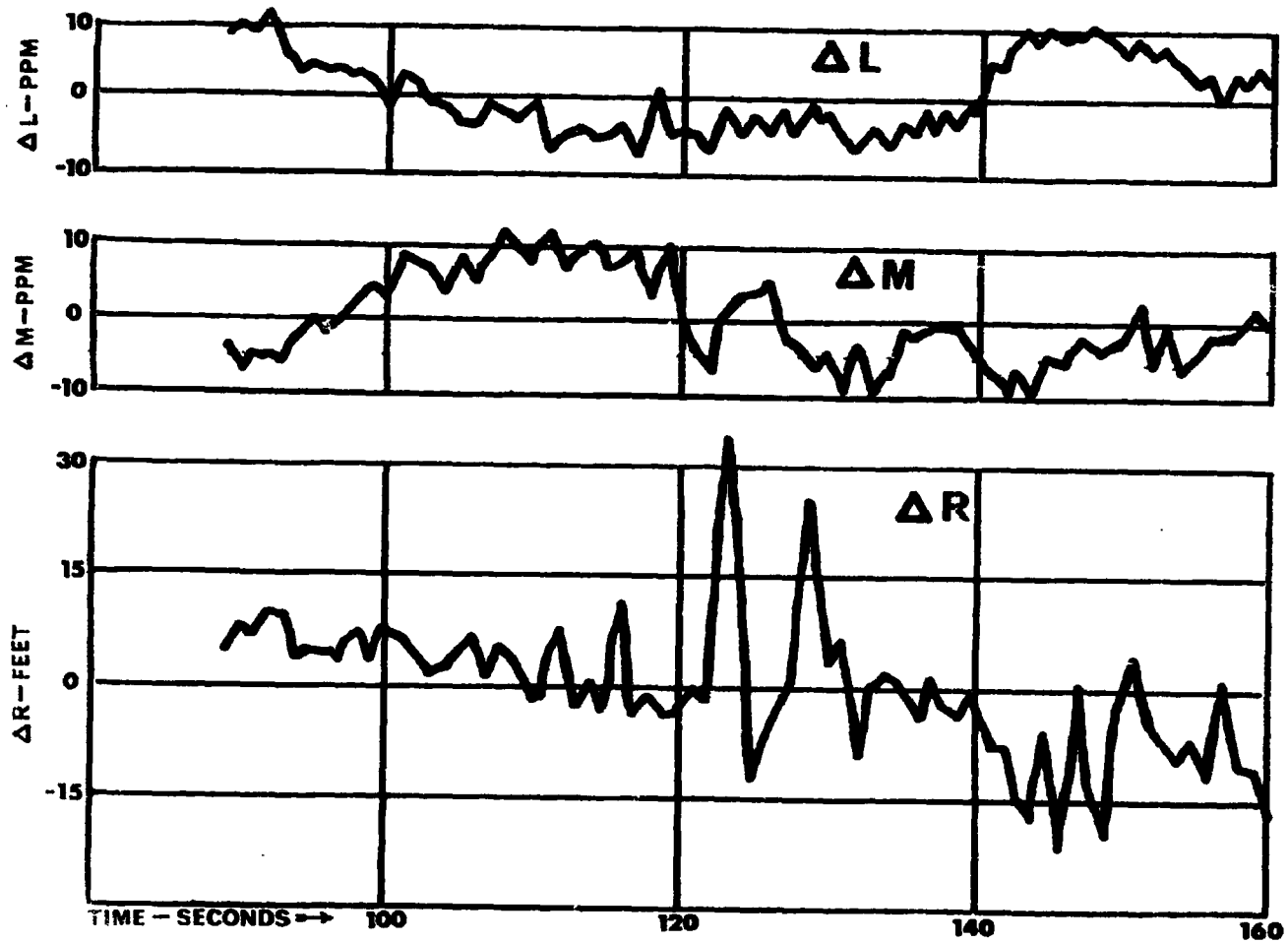

fig. 6B

second intervals of the trajectory, The results (x coordinates only) of the two 50-second intervals which had convergent solutions are shown in Figure 5A, curves B and C. The residuals of both solutions were very random but the estimates of residual bias indicated by the covariance matrices were so large as to exceed any reasonable accuracy requirements. This breaking up of the trajectory into several pieces has been suggested as a means of avoiding multi-term error models but, with the instrumentation data available on a typical test at AMR, this usually results in near indeterminacy.

One additional example shows the effects of an erroneous error model upon the bias adjustment for a recent Minuteman. Figure 6A shows the differences between AZUSA LMR measurements and the same data as indicated by the Downrange UDOP system. Note that the drift between the two systems appears to be fairly linear in all parameters only in the range 89-119 seconds. A constant bias error model BET was first computed using the data from 89 to 175 seconds. This resulted in the following bias estimates for each system and the associated estimates of standard deviation:

AZUSA		UDOP	
L =	.22 ppm	Range Difference 1 =	- .915 feet
M =	16.22 ppm	Range Difference 2 =	- 4.999 feet
R =	-20.53 feet	Range Sum =	46.46 feet
σ_L =	1.75 ppm	σ_{D1} =	.23 feet
σ_M =	1.73 ppm	σ_{D2} =	.34 feet
σ_R =	1.10 feet	σ_{RS} =	2.54 feet

As can be seen in Figure 6B, obvious trends still remained in the residuals from this reduction. The trajectory was then recomputed using the area from 89 seconds to 119 seconds only, using a higher sampling rate to improve convergence. The estimates of the bias estimates with their associated standard deviations were then as follows:

AZUSA		UDOP	
L =	27.03 ppm	Range Difference 1 =	- .892 feet
M =	- 8.81 ppm	Range Difference 2 =	- 2.066 feet
R =	- 10.98 feet	Range Sum =	7.68 feet
σ_L =	3.33 ppm	σ_{D1} =	.29 feet
σ_M =	1.80 ppm	σ_{D2} =	.56 feet
σ_R =	2.89 feet	σ_{RS} =	7.56 feet

The AZUSA residuals, shown in 6C have now taken on the appearance of randomness. The UDOP residuals, not shown, also appeared random. Because of the size and trends of the residuals in the 89-160 second reduction we must conclude that we have a poor estimate of the true systematic errors and that the associated

89–119 SECONDS – Constant Bias Erro. Model

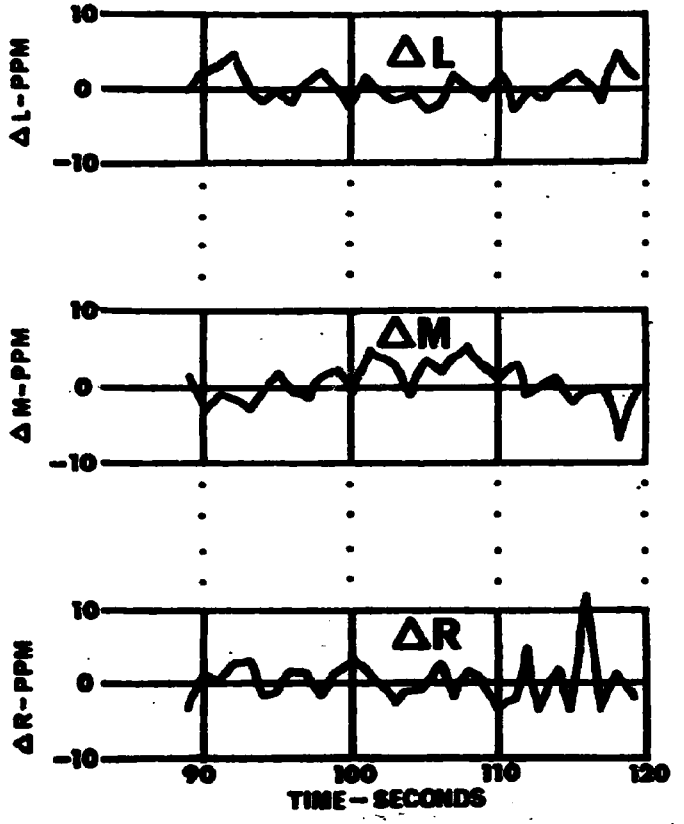

FIGURE 8C

estimates of error in the error model coefficients are much too small. On the other hand, based upon internal consistency only, the 89-119 second reduction gave a reasonable estimate of the instrumentation biases. The higher sampling rate in the 89-119 second reduction appeared justified because the total noise content of Minuteman data is derived mainly from the higher frequencies, thus allowing serial independence of data samples to be assumed over relatively small time lags. On this basis the estimates of standard deviation in the error model coefficients also appear realistic. A study of critical times on this test indicates that the unrealistic estimates derived in the 89-160 second reduction were due mainly to discontinuities in the AZUSA data because of the interference effects of the third stage flame.

Many of the problems encountered with the existing BET routine appear to stem from an assumption which was considered intuitively obvious. The assumption has manifested itself in statements taking the average form: "Given a sufficiently overdetermined set of trajectory observations, the estimate of trajectory can be improved by including certain persistent bias terms as unknown parameters. Even the application of the simplest error model, such as a constant bias, will improve the trajectory estimate." That this statement is not necessarily true is pointed out by the previous numerical examples. Additional examples follow.

Data from continuous wave tracking systems often contain discontinuities which result in a true error model of square wave or step function shape. Application of a polynomial type error model over the entire trajectory could result here in large estimates of rate error whereas between the actual discontinuities the true rate errors might well be negligible. Unfortunately, breaking such a trajectory into several portions with independent error models would, in many cases, result in near indeterminacy because of poor geometry.

An analogy from polynomial curve fitting might be of interest here. It is well known that application of too low a degree polynomial to a set of data which has a large degree polynomial trend can result in a large bias which might cancel any improvement due to noise reduction. In actual practice it does little good to smooth through burnouts or ignitions, the unsmoothed data, for CW systems in particular, being in most cases closer to the true values than the smoothed data.

Recently, much impetus has been given to the development of explicit type error models using actual physical quantities as unknowns rather than polynomial type error models in which the errors are implicitly expressed. Lest one believe that this is the ultimate panacea for our error model BET problems, let us return to Figure 3B. This graph shows the effective measurement error in some radar measurements due to survey error. Note that the error in the range measurement for the radar behind the

trajectory is approximately constant. Thus, if a range measuring station behind the trajectory were assigned an error model which contained both calibration and survey error terms, and the noise content of the data were of such magnitude as to account for the differences between the two assumptions, it would be impossible to separate the two sources of error without recourse to additional knowledge. Similarly, elevation and azimuth errors can be explained in particular cases by calibration, survey and timing errors independently.

The effect of a timing error upon a measurement can be expressed as a function of measurement rate. We can see in Figure 2, curve A, the difference between AZUSA range and GE MOD III as a function of range rate. It appears that the assumptions of a relative timing error of about two milliseconds could, except for the change of trend at the end of the trajectory, account for the drift between the two ranges. Unfortunately, no timing errors of such magnitude in the two systems appeared physically possible.

It is important to note the word "relative" in the above paragraph. The BET Solution is based upon considerations of internal consistency of the data. It is obvious that only relative timing errors can be removed by the BET since internal consistency can be maintained by adding the same arbitrary timing error to each system's data. Similarly, errors in longitude can only be corrected relatively since the same arbitrary longitude error could be added to each instrument's position without affecting the internal consistency of the data. Advantage can be taken of this situation by assuming one system's timing and location as the standard. Because of the resulting decrease in the number of unknowns, the solution normally converges faster when this is done. The effect of this assumption on the trajectory is not very detrimental because a small timing bias or survey bias existing in common at all sites normally results in only a small displacement of the trajectory in the desired coordinate system.

6. Effects of the Weighting and a Priori Estimates on the Error Model BET

The total noise estimates used in weighting the measurement data have been, in most cases, computed using a varying lag variate difference technique. The physical basis for using such a technique is mentioned in (6). The most detrimental effect of poor weighting appears to be that it may cause the BET to be noisier than trajectories computed by one or more of the individual systems. If the error model fits the physical situation (as in the previously used hypothetical ICBM case), erroneous weighting does not have a great effect upon the determination of error model coefficients although the associated estimates of covariance become erroneous as do the covariance estimates of the trajectory coordinates. One example of the effect of a

change of weight upon the BET is given in Figure 5A, curve A. Here the estimate of the standard deviation of the noise in the System 3 data was doubled (thus decreasing its weight). Note that the trajectory moved much closer to the true trajectory at the beginning, where System 3 was at a relatively great distance from the missile, but again diverged far from the true trajectory as System 3's geometric contribution to the solution became more significant. The effect upon the estimates of systematic error in Systems 1 and 2 was to bring them much closer to their known values.

The effects of the a priori quasi-measurement data on the BET results depend largely upon the amount of overdetermination existing. Thus, if we have enough overdetermination to give us an estimate of error in the computed error model coefficients of one part per million in direction cosine, the additional a priori quasi-measurements with a standard deviation estimate of twenty parts per million will have little effect on the BET results. The use of a priori estimate in a BET reduction does not rest upon very firm ground. The effect of the estimates can be varied drastically by simply changing the sampling rate if this is warranted by having independent samples. The estimates can be weighted in such a way as to enforce one system over another if this should be desired. The effect of the a priori estimates is especially significant in cases where near undeterminacy exists (as in the case described in Figure 5A, curve C). On most BETs published so far, because of the questionable validity of their application, the estimates of variance in the quasi-measurement data have been made so large that the overdetermination due to the actual trajectory measurements has been the overwhelming factor. In effect, the error model coefficients have been treated as complete unknowns.

7. Conclusion

The findings discussed in this presentation might be summarized by repeating an old axiom: Beware of the intuitively obvious. The intuitively obvious in this case was that, given a sufficiently overdetermined set of observations, the application of any simple error model (such as a constant bias) would lead to an improved estimate of trajectory.

The preceding examples have shown that this is not necessarily true. Most of the early analysis on the BET problem was based upon hypothetical error models which fitted the simulated data exactly. The application at AMR of the method to actual rather than simulated data has brought into display the many possible limitations of the method. These include:

(a) The fact that increasing the number of terms in the error model can cause a swift approach toward indeterminacy. Thus, in going from the constant bias

error model to the linear error model, the estimates of residual bias can in many cases increase by one or two orders of magnitude.

(b) The fact that as we increase the number of terms in the error model, the effect of the remaining small errors on the trajectory becomes accentuated. This is a direct consequence of (a).

(c) The fact that different physical errors can have the same effects upon the internal consistency of the data and thus cannot be separately determined by the BET error model solution.

(d) The fact that error model coefficients determined mainly by the geometry over one portion of the trajectory often prove detrimental when applied to another portion of the trajectory.

Much analysis remains to be done concerning the effects of erroneous error model assumptions on a BET, and much of our knowledge of BET limitations gained so far has been the result of chance encounters during data processing. The tone of this presentation may have appeared pessimistic but this was completely unintended. As in many other fields, the study of failures and limitations is a necessary step toward a better understanding and toward further progress. Despite all of the negative aspects stressed here, one fully compensating positive fact cannot be denied: Given a realistic error model with a good geometric distribution of tracking stations over the trajectory in question, the error model BET method will truly provide a "Best Estimate of Trajectory."

8. References

(1) Pepple, R.J., "Best Estimate of Trajectory," Second Joint AFMTC-Range User Data Conference.

(2) Lasman, Lonnie L., "Improvements in the Estimation of Trajectory Determination," Third Joint AFMTC-Range User Data Conference.

(3) Brown, Duane C., "A Treatment of Analytical Photogrammetry with Emphasis on Ballistic Camera Applications," RCA Data Reduction Technical Report No. 39, 1957.

(4) Guard, K., "A Technique for the Determination of a DOVAP Starting-Point," WSPD, New Mexico, Technical Memorandum 428, 1957.

(5) Willmann, James B., "A Least Squares Solution for DOVAP Position and Tie-in Point Considering Refraction," RCA Data Reduction Technical Report. No. 42, February 1958.

(6) Pavley, Richard F., "A Unified Approach to Data Smoothing," Third Joint AFMTC-Range User Conference.

(7) Lasman, Lonnie L., "Best Estimate of Trajectory, BETY2," RCA Mathematical Services TM-62-7.

APPENDIX I

LIST OF ATTENDEES

ATTENDEES

Abercrombie, J.	NASA	Cocoa Beach, Fla.
Aein, J. M.	I. D. A.	Washington, D. C.
Aichele, D. G.	Marshall Spc Flt Ctr	Huntsville, Ala.
Alexander, J. C.	PMR	Pt. Mugu, Calif.
Anderson, B. E., Jr.	STL	Cocoa Beach, Fla.
Anderson, J. M.	STL	Cocoa Beach, Fla.
Arbuthnot, G. L.	STL	Cocoa Beach, Fla.
Ariail, F. P. Lt	DWLT	PAFB
Aumann, C. R.	RCA	PAFB
Autery, R. M.	N. American Avia.	Columbus, Ohio
Bagg, J. L.	Aerospace	PAFB
Bailey, G. W.	Aerospace	El Segundo, Calif.
Bain, R. A.	STL	Redondo Bch, Calif.
Barnett, F. Q.	MTOER	PAFB
Barton, D. K.	RCA	Moorestown, N. J.
Bedard, P. E.	STL	Cocoa Beach, Fla.
Bishop, E.	NASA	Cocoa Beach, Fla.
Bergeson, J. E.	Boeing	Seattle, Wash.
Blanchard, R. W.	NASA	Cocoa Beach, Fla.
Boland, L. W.	WSMR	New Mexico
Boyd, E. W.	Hercules Pwdr Co	Magna, Utah
Briner, D. M.	STL	Redondo Bch, Calif.
Brinkman, W.	RCA	PAFB
Brown, D. C.	D. Brown Associates	Melbourne, Fla.
Brown, J. E.	Douglas Acft	Cp. Canaveral, Fla.
Brown, R. A.	RCA	PAFB
Bruns, R. H.	NASA	Cocoa Beach, Fla.
Bryant, D. J.	STL	Cocoa Beach, Fla.
Bryant, R. P.	RCA	PAFB
Buckley, R. C.	Wolf R&D Corp	Cocoa Beach, Fla.
Bullard, E. E.	Boeing	Cocoa Beach, Fla.
Burkett, S. B., Jr.	PAWA	PAFB
Butcher, L. E.	JPL	Cp. Canaveral, Fla.
Campbell, A. T.	AVCO	Wilmington, Dela.
Cancio, P.	GE	
Canty, F. G.	Martin Co	Orlando, Fla.
Carman, R. A.	RCA	PAFB
Carr, R.	NASA	Houston, Texas
Carroll, C. L., Jr.	PAWA	PAFB
Ceely, W. W.	Boeing	Seattle, Wash.
Chaloupka, B. C.	Martin Co	Denver, Colo.
Chase, D. G.	L. B. Hanscom Fld.	Mass.

Cerar, P. V.	ARMA	Garden City, N.Y.
Chen, B. S.	PAWA	PAFB
Choiniere, L. E.	AVCO	Wilmington, Mass.
Christ, O. J. W.	RCA	PAFB
Christen, G. L.	Chrysler Corp	Melbourne, Fla.
Clark, Billy V. Capt	DWLT	PAFB
Clark, G. D.	RCA	PAFB
Clifton, H. W.	Martin Co	Cocoa, Fla.
Cockerham, F.	RCA	PAFB
Collins, L. B.	RCA	PAFB
Congdon, T. W.	GE	Pittsfield, Mass.
Connor, A. H. Capt	BSD	Horton AFB, Calif.
Connor, M. G.	Thiokol Chem Corp	Brigham City, Utah
Cooper, W. T.	Martin Co	Cocoa, Fla.
Cornell, K, Lt	MTOER	PAFB
Craft, R. H.	Marshall Spc Flt Ctr	Huntsville, Ala.
Davenport, F. S.	PAWA	PAFB
Davidson, T. F.	Acoustica	Cocoa Beach, Fla.
Dawson, J. E.	Martin Co	Cocoa Beach, Fla.
Deal, W. K. Jr.	Hercules Pwder Co	Magna, Utah
Dean, A. E.	MartinCo	Cocoa Beach, Fla.
Decino, A.	Aerospace	PAFB
Deily. W. H.	Boeing	New Orleans, La.
Dickson, E. L.	NASA	Houston, Texas
Dickson, W. H.	Lockheed	PAFB
Donovan, M. A., Jr.	Chrysler Corp	New Orleans, La.
Downey, N. J.	Martin Co	Denver, Colo.
Drew, E. O.	RCA	PAFB
Drucker, A. N.	STL	Calif.
Dryden, W. A.	RCA	PAFB
Edson, J. R.	Boeing	Seattle, Wash.
Ellis, G. W.	GE	PAFB
England, H. T.	WECO	PAFB
Fagen, B. W., Maj	APCS	OAFB
Farnsworth, G. D.	Thiokol Chem Corp	Brigham City, Utah
Fatig, B.	RCA	PAFB
Feldman, S.	GE	PAFB
Ferguson, C. R.	PAWA	PAFB
Fields, M. H.	PMR	Pt. Mugu, Calif.
Finkle, J. F., Capt	MTOER	PAFB
Finley, C. J., Capt	APCS	OAFB
Flater, J. F.	Martin Co	Denver, Colo.
Franklin, M. R.	NASA	Houston, Texas
Flickinger, B. L.	RCA	PAFB
Flowers, L. H.	RCA	PAFB

Friebertshauser, George O.	Aerospace	PAFB
Frohme, K. R.	Martin Co	Orlando, Fla.
Gabler, R. T.	Rand Corp	Santa Monica, Calif.
Gandy, W. F.	Martin Co	Cocoa Beach, Fla.
Garrett, J. R.	RCA	PAFB
Geist, J. H.	DWTMS	PAFB
Gennery, D. B.	RCA	PAFB
Giraud, C. E., Lt/Col	APCS	OAFB
Glass, B.	D. Brown Assoc.	Melbourne, Fla.
Gleason, G. W.	Martin Co.	Denver, Colo.
Gleason, W. E.	ARMA	Orlando, Fla.
Goad, Granville G.	Martin Co	Cocoa Beach, Fla.
Godke, D. P.	RCA	PAFB
Goff, H. C.	GE	PAFB
Gott, A. H.	Aerospace	San Bernardino, Calif.
Grunenfelder, A. C.	NASA	Cocoa Beach, Fla.
Gunar, Murray		
Gwinn, R. T.	NASA	Cocoa Beach, Fla.
Hagin, E. J., Maj.	MTDR	PAFB
Hain, J. L.	Bendix	Baltimore, Md.
Haltinner, E. J.	Hercules Pwdr Co	Magna, Utah
Harden, E. A.	RCA	PAFB
Hamilton, S. G., Jr.	Aerospace	PAFB
Hanson, N. L.	RCA	PAFB
Harding, J. D.	Martin Co	Cocoa Beach, Fla.
Hatch, M.	RCA	PAFB
Hatcher, E. T.	RCA	Moorestown, N.J.
Hekimian, K. K.	AVCO	Wilmington, Mass.
Held, G.	STL	Redondo Beach, Calif.
Heller, D. W.	Martin Co	Cocoa Beach, Fla.
Henriksen, O. M.	ARMA	Cp. Canaveral, Fla.
Hereford, W. V.	Sandia	Albuquerque, N. M.
Herrington, A. H.	IBM	Cocoa Beach, Fla.
Hedman, E. L.	RCA	PAFB
Hess, G. K., Jr.	MTGS	PAFB
Hicks, H. C.	GE	
Hickey, J. R.	STL	Cp. Canaveral, Fla.
Hinds, N. F.	NASA	PAFB
Hlavaty, E. M.	MTQXP	PAFB
Hoffman-Heyden, A. E.	RCA	PAFB
Holzman, R. E.	JPL	Pasadena, Calif.
Hood, R.	AC Spark Plug	Milwaukee, Wisc.
Howell, G. K.	Hercules Pwdr Co	Magna, Utah
Huber, H. J.	Aerospace	PAFB
Hyde, W. L.	Sandia	Cp, Canaveral, Fla.

Incerto, D. J.	NASA	Houston, Texas
Jaenke, M. G.	AFMDC	Holloman AFB, N. M.
Jamieson, J. N.	RCA	PAFB
Jelen, G. W.	NASA	Cocoa Beach, Fla.
Jones, N. C.	Martin Co	Cocoa Beach, Fla.
Juliana, W. J.	GE	Pittsfield, Mass.
Jacobs, C.	RCA	PAFB
Kahler, H. R.	Wolf R&D Corp	West Concord, Mass.
Kaiser, J.	I. D. A.	Washington, D. C.
Keenan, R. V.	STL	Redondo Beach, Calif.
Keene, L. F.	NASA	Cocoa Beach, Fla.
Keller, R. L.	Autonetics	Anaheim, Calif.
Kerr, S. V.	RCA	PAFB
Kershner, W. S.	AVCO	PAFB
Keys, R. R., Capt	Aerospace Research	Washington, D. C.
Knight, T. J.	GE	
Korpal, J. W.	Lockheed	PAFB
Kotecki, V. D., Jr.	Douglas Aircraft	Santa Monica, Calif.
Krivanich, M. A.	MTDR	PAFB
Lake, W. M., Maj	MTOER	PAFB
Lanckton, A. H.	RADC	Bedford, Mass.
La Plante, E. J.	GE	PAFB
Lasman, L. L.	RCA	PAFB
Leonard, D. L.	MTOER	PAFB
Layman, E. R.		
LeDuc, A. L.	RCA	PAFB
Levy, H. N., Jr.	JPL	Pasadena, Calif
Lindstrom, G. M.	STL	Calif.
Lindemann, N. L.	RCA	PAFB
Lippke, B. R.	Aerospace	PAFB
Little, P. R.	STL	Cocoa Beach, Fla.
Lucchesi, G. A., Lt Col	APCS	OAFB
Lutowski, N.	MTOER	PAFB
Luzietti, J. L.	NASA	Cocoa Beach, Fla.
McCall, W. L.	Autonetics	Cp. Canaveral, Fla.
McCollough, R. R.	Martin Co	Denver, Colo.
McCombie, H. E.	Hercules Pwder Co.	Bacchus, Utah
McCormack, P. J	IBM	Cocoa Beach, Fla.
McDonald, F. W., Jr.	Autonetics	Anaheim. Calif.
Mallinckrodt, A. J.	Comm Res Labs	Santa Ana, Calif.
Mallory, N. D.	RCA	PAFB
Mancini, A.	AFCRL	Hanscom Fld, Mass.
Manges, R. E.	Thiokol	Bringham City, Utah
Mann, M. E., Jr.		
Manning, W. H., Jr.	MTGSS	PAFB

Martin, C. F.	PAWA	PAFB
Martin, K. W.	GE	Philadelphia, Pa.
Martin, M. A.	GE	PAFB
Masch. H. D.	RCA	PAFB
Mayo, J. M.	RCA	San Bernardino, Calif.
Merkle, R. A.	Aerospace	PAFB
Mertens, L. A.	RCA	Cocoa Beach, Fla.
Mitchell, R. W.	STL	Cocoa Beach, Fla.
Moody, R. H.	STL	PAFB
Morrissey, G. E., Capt	MTOEC	Cp. Canaveral, Fla.
Moss, H. D.	JPL	Whippany, N. J.
Motley, C. H.	Bell Tel Lab	Cocoa Beach, Fla.
Moyer, R. W.	Martin Co	Milwaukee, Wisc.
Murrin, Francis E.	AC Spark Plug Div	Huntsville, Ala.
Naumcheff, M.	NASA	Cocoa Beach, Fla.
Neal, D. A.	STL	Magna, Utah
Neal, W. C.	Hercules Pwdr Co	OAFB
Needham, P. E., Capt	APCS	PAFB
Nelson, B. B.	GE	PAFB
Nelson, D. M.	Aerospace	PAFB
Nersesian, R. R.	MTQMA	PAFB
Nicol, D. A.	RCA	Milwaukee, Wisc.
Nobles, R. O.	AC Spark Plug Div	PAFB
Norman, R. L.	MTQDD	PAFB
Norowich, V. R.	MTGSS	Pt. Canaveral, Fla.
Nosby, L. J.	AC Spark Plug Div	PAFB
O'Connor, E. A., Jr., Lt	DWTM	PAFB
O'Connor, J. J.	RCA	Downey, Calif.
Oliver, C. F.	Autonetics	Vandenberg AFB, Calif.
Ollikala, E. E.	ARMA	
Page, E. N.	STL	PAFB
Parks, D. H.	RCA	PAFB
Parks, J. E.	PAWA	PAFB
Painter, J. T.	RCA	PAFB
Pearce, C. E., Maj	MTGS	
Peer, R. R.		PAFB
Pepple, R.	RCA	PAFB
Perkins, C. E.	RCA	
Pickover, H.	STL	
Pinder, P. H., Jr.	MTQP	PAFB
Pinter, P. N.	STL	Calif.
Powell, W.	MTQXP	PAFB
Price, W. A.	RCA	PAFB
Principe, V. P.	PAWA	PAFB
Radcliffe, F. R.	GE	PAFB
Randolph, C. R.	Aerospace	Los Angeles, Calif.

Randolph, J. P.	JPL	Silver Spring, Md.
Rasque, D. E.	Autonetics	Downey, Calif.
Redmond, J. A.	Boeing	Cocoa Beach, Fla.
Reif, K.	RCA	PAFB
Reuyl, J. S.	JPL	Calif.
Rivett, J. E.	Chrysler Corp	Detroit, Mich.
Roberts, H. A.	RCA	PAFB
Rollins, J.	RCA	PAFB
Romo, P. E., Lt Col	MTQFW	PAFB
Rosenfield, G. H.	RCA	PAFB
Roy, A. J.	RCA	PAFB
Rudy, L. E.	NASA	Cocoa Beach, Fla.
Rutherford, D. E.	DWTM	PAFB
Rutkowski, P. T.	N. American Avia	Downey, Calif.
Sanders, Alfred	AC Spark Plug Div	Pt. Canaveral, Fla.
Sanders, M. A.	Chrysler Corp	Melbourne, Fla.
Schmyser, C. F.	Sangamo Elec Co	Springfield, Ill.
Schulze, G. H.	RCA	PAFB
Scott, C. R.	Aerospace	PAFB
Sellers, R. E.	Martin Co	Cocoa Beach, Fla.
Shaifer, R. H.	AFCRL	Hanscom Fld, Mass.
Sheldon, L. L., Capt	MTQMA	Cp. Canaveral, Fla.
Shirley, R. C.	STL	Redondo Beach, Calif.
Shook, G. R.	N. American Avia	Downey, Calif.
Short, W. T.	MTOEC	PAFB
Silvestre, H.	JPL	Pasadena, Calif.
Sjogren, W. L.	Burroughs Corp	Pt. Canaveral, Fla.
Smith, D. P.	Martin Co	Denver, Colo.
Smith, M. R.	Douglas Acft Co	Santa Monica, Calif.
Smith, V. J.	Autonetics	Calif.
Snapper, J.	Martin Co	Cocoa Beach, Fla.
Snell, B. J.	APCS	OAFB
St. Clair, J. H., Capt	N. American Avia	Downey, Calif.
Steagall, W. F.	APL	Silver Spring, Md.
Strauss, W. C.	Martin Co	Cocoa Beach, Fla.
Strickland, D. M.	RCA	PAFB
Tabeling, R. H.	NASA	Cocoa Beach, Fla.
Taiani, Angelo J.	PGVM	Eglin AFB, Fla.
Taylor, W. C., Jr.	Wolf R&D Corp	Mass.
Tear, R. T.	Sangamo Elec Co	Springfield, Ill.
Thomas, T. R.	PMR	Pt. Mugu, Calif.
Thorne, C. J.	Lockheed	Sunnyvale, Calif.
Tice, L. T., Jr.	AVCO	Wilmington, Mass.
Trimble, W. J., Jr.	AVCO	Wilmington, Mass.
Vancor, E.		

Vergenz, G. R.	Martin Co	Orlando, Fla.
Ward, A. B.	RCA	PAFB
Watson, E. B., Jr.	FTFSE-2	Edwards AFB, Calif.
Weller, R. K.	RCA	PAFB
Wells, J. L., Jr.	NASA	Houston, Texas
Wiles, J. H.	Lockheed	Cocoa Beach, Fla.
Williams, J. H.	NASA	Cocoa Beach, Fla.
Williams, P. E.	Lockheed	Sunnyvale, Calif.
Williams, T. T.	RCA	PAFB
Winn, S.	N. American Avia	Downey, Calif.
Wynn, J. B.	FBM Proj Off	PAFB
Yeager, M. R.	Martin Co	Orlando, Fla.
Young, R. D.	Martin Co	Cocoa Beach, Fla.
Zgurich, E. E.	Martin Co	Orlando, Fla.
Zimmerman, R., Jr.	RCA	PAFB
Zirm, R. R.	US Naval Res Lab	Washington, D.C.

UNCLASSIFIED

UNCLASSIFIED